Radio Resource Scheduling in Homogeneous Coordinated Multi-Point Joint Transmission of Future Mobile Networks

Shyam Babu Mahato

Department of Computer Science & Technology

University of Bedfordshire

Luton, United Kingdom

A thesis submitted to the University of Bedfordshire, in partial fulfilment of the requirements for the degree of

Doctor of Philosophy (PhD)

21st June 2013

"For as high as the heavens are above the earth, so great is his love for those who fear him" - Psalm 103:11

Abstract

The demand of mobile users with high data-rate services continues to increase. To satisfy the needs of such mobile users, operators must continue to enhance their existing networks. The radio interface is a well-known bottleneck because the radio spectrum is limited and therefore expensive. Efficient use of the radio spectrum is, therefore, very important. To utilise the spectrum efficiently, any of the channels can be used simultaneously in any of the cells as long as interference generated by the base stations using the same channels is below an acceptable level. In cellular networks based on Orthogonal Frequency Division Multiple Access (OFDMA), inter-cell interference reduces the performance of the link throughput to users close to the cell edge. To improve the performance of cell-edge users, a technique called Coordinated Multi-Point (CoMP) transmission is being researched for use in the next generation of cellular networks. For a network to benefit from CoMP, its utilisation of resources should be scheduled efficiently.

The thesis focuses on the resource scheduling algorithm development for CoMP joint transmission scheme in OFDMA-based cellular networks. In addition to the algorithm, the thesis provides an analytical framework for the performance evaluation of the CoMP technique. From the system level simulation results, it has been shown that the proposed resource scheduling based on a joint maximum throughput provides higher spectral efficiency compared with a joint proportional fairness scheduling algorithm under different traffic loads in the network and under different criteria of making cell-edge decision.

A hybrid model combining the analytical and simulation approaches has been developed to evaluate the average system throughput. It has been found that the results of the hybrid model are in line with the simulation based results. The benefit of the model is that the throughput of any possible call state in the system can be evaluated.

Two empirical path loss models in an indoor-to-outdoor environment of a residential area have been developed based on the measurement data at carrier frequencies 900 MHz and 2 GHz. The models can be used as analytical expressions to estimate the level of interference by a femtocell to a macrocell user in link-level simulations.

Declaration

I, Shyam Babu Mahato, declare that the thesis entitled *Radio Resource Scheduling in Homogeneous Coordinated Multi-Point Joint Transmission of Future Mobile Networks* and the work presented in the thesis are my own, and have been generated by me as the result of my own original research. It is being submitted for the degree of *Doctor of Philosophy (PhD)* at the University of Bedfordshire.

I confirm that:

- it has not been submitted before for any degree or examination in any other University;
- this work has been done in candidature for a research degree at this University.

Name of candidate: Shyam Babu Mahato Signature:

Date: 21st June 2013

Acknowledgements

First of all, I would like to thank my saviour Lord Jesus Christ for choosing me from many and listening to my goal. I would like to thank Professor Jie Zhang, for an opportunity he gave me to join his research group, formerly known as Centre for Wireless Network Design (CWiND) under the Institute for Research in Applicable Computing (IRAC). Without the support of bursaries and studentship, I would never have expected to start my PhD study. I thank Prof. Zhang and the University of Bedfordshire for believing in me and providing bursaries and studentship to support my study. I will always be grateful for them.

I would like to thank my Director of Studies Professor Ben Allen, the Head of Centre for Wireless Research (CWR) under IRAC, for supervising, encouraging, guiding, commenting and supporting me all through my study. His continuous encouragement and moral support have uplifted my potential towards the completion of my goal. Without his supervision, I would not have completed my goal. I also thank Dr. Enji Liu for her supervision and providing useful feedback.

I would like to acknowledge and thank my colleague Dr. David Lopez Perez for his valuable time and consistent guidance all through to understand the functionality of the tool our colleagues had developed during their research. I would like to thank my colleague Dr. Alvaro Valcarce for providing the measurement data he had obtained during his PhD study, and also for introducing and guiding new software. I would like to thank Dr. Andres Alayon Glazunov for his encouragement and guidance during the early stage of my research. I would like to thank my colleagues Dr. Guillaume de la Roche, Dr. Alvaro Valcarce, Dr. Hui Song, Dr. Akos Ladanyi, Dr. Zhihua Lai, Dr. Ebenezer Amusa

for their friendship, guidance, useful suggestions and sharing of experiences. I also thank Mr. Malcom Foster for his friendly social talk and English corrections. I would like to thank Dr. David Gunton for his valuable feedback and proofreading comments. I would like to extend my acknowledgement and thank all our friends of CWR in Room D109 for having friendly discussion.

Let me express my gratitude to my parents, brother and sister for their love and caring all through my childhood. I am standing here because of their love and guidance. Let me acknowledge and give thanks from the bottom of my heart to my father-in-law, mother-in-law and brother-in-law for their continuous prayer and love. Their enthusiasm to know my progress has always been encouraging for me.

Finally, let me express my feeling of thanks and love from the bottom of my heart to my caring wife Mrs. Ritu Daniel Mahato and my 16 months old son Master Arpit Mahato for their love, caring, smile and sacrifices in various ways to support my study. Without their love and sacrifice, I would not have completed my research. Arpit's smile has acted as a relief medicine for tiredness after coming home from the University. I really wish I could somehow pay back the sacrifices my wife and son offered to my study.

Publications

Conferences

1. **Shyam B. Mahato**, Ben Allen, Enjie Liu, Jie Zhang, "Performance Evaluation of Maximum Throughput Based Scheduling of OFDMA LTE Networks", in *Wireless Advanced (WiAd), IEEE 8th*, London, UK, pp. 1-5, 25-27 June, 2012.
2. Zhu Xiao, Peng Wang, Xu Zhang, **Shyam Mahato**, Lei Chen, Jie Zhang, "Incentive Mechanism for Uplink Interference Avoidance in Two-Tier Macro-Femto Networks", in *Vehicular Technology Conference (VTC Spring), IEEE 75th*, Yokohama, Japan, pp. 1-6, 6-9 May, 2012.
3. **Shyam B. Mahato**, Jie Zhang, "Overview of Coordinated Multi-Point (CoMP) Transmission in Heterogeneous Network", in *Computer Communications and Networks (ICCCN), Proc. of IEEE 20th*, Maui, Hawaii, p. 1595, July 31-Aug 4, 2011.

Posters

1. **Shyam Mahato**, Ben Allen, "Indoor-to-Outdoor Path Loss Modelling in Femtocell Networks", in *Colloquium on Innovation in Computing, University of Bedfordshire*, Luton, UK, 23 Mar, 2013.
2. **Shyam B. Mahato**, Ben Allen, Enjie Liu, Jie Zhang, "Resource Scheduling of Coordinated Multi-Point Joint Transmission in LTE-Advanced Networks", in *University of Bedfordshire Conference 2012*, Luton, UK, 3-4 July, 2012.

Contents

Abbreviations

1G	1st Generation
2G	2nd Generation
3G	3rd Generation
3GPP	3rd Generation Partnership Project
4G	4th Generation
5G	5th Generation
BLER	Block Error Rate
BR	Bedroom
BS	Base Station
CBF	Coordinated Beamforming
CCS	CoMP Cooperating Set
CCU	Cell-Centre User
CDMA	Code Division Multiple Access
CEU	Cell-Edge User
CFR	Cooperative Frequency Reuse
CoMP	Coordinated Multi-Point
CQI	Channel Quality Indicator
CSI	Channel State Information
CW	Continuous Wave
dB	Decibel
dBi	Decibel Isotropic
dBm	Decibel Milliwatts
eNB	enhanced-NodeB

ETSI	European Telecommunications Standards Institute
FDMA	Frequency Division Multiple Access
FFA	Fixed Frequency Allocation
FFR	Fractional Frequency Reuse
FlexFAP	Flexible Frequency Allocation Plan
FP7	Seventh Framework Programme
FR	Frequency Reuse
FRS	Frequency Reuse Scheme
FTP	File Transfer Protocol
Gbps	Gigabits per second
GHz	Giga Hertz
GPS	Global Positioning System
GSM	Global System for Mobile Communication
HTTP	Hyper Text Transfer Protocol
i.i.d.	independent and identically distributed
ICI	Inter-Cell Interference
ID	Identity
IMT	International Mobile Telecommunications
IMT-2000	International Mobile Telecommunications-2000
IMT-A	International Mobile Telecommunications (IMT)-Advanced
ISD	Inter-Site Distance
ITU	International Telecommunications Union
ITU-R	International Telecommunications Union (ITU) - Radiocommunication Sector
JMT	Joint Maximum Throughput

JPF	Joint Proportional Fairness
JT	Joint Transmission
kbps	Kilobits per second
kHz	Kilo Hertz
KPI	Key Performance Indicator
LOS	Line-Of-Sight
LR	Livingroom
LTE	Long-Term Evolution
LTE-A	Long-Term Evolution (LTE)-Advanced
M2M	Machine-to-Machine
MAC	Medium Access Control
Mbps	Megabits per second
MCS	Modulation and Coding Scheme
METIS	Mobile and Wireless communications Enablers for the Twenty-twenty (2020) Information Society
MHz	Mega Hertz
MIMO	Multi-Input Multi-Output
MRMSE	Minimum Root Mean Square Error
ms	milliseconds
MSC	Mobile Switching Centre
MT	Maximum Throughput
MU	Mobile Unit
NLOS	Non-Line-Of-Sight (LOS)
NTT	Nippon Telephone and Telegraph
OFDM	Orthogonal Frequency Division Multiplexing

OFDMA	Orthogonal Frequency Division Multiple Access
PDF	Probability Density Function
PF	Proportional Fair
PFR	Partial Frequency Reuse
PSTN	Public Switched Telephone Network
QAM	Quadrature Amplitude Modulation
QoS	Quality of Service
RAB	Radio Access Bearer
RAN	Radio Access Network
RAN1	RAN Working Group 1
RB	Resource Block
Rel	Release
RMSE	Root Mean Square Error
RR	Russell Rise
RRH	Remote Radio Head
RRM	Radio Resource Management
RS	Reference Signal
RSRP	Reference Signal Received Power
SC	Stockwood Crescent
SFR	Soft Frequency Reuse
SINR	Signal-to-Interference plus Noise Ratio
SLS	System Level Simulation
SMS	Short Messaging Service
SVD	Singular Value Decomposition
TDMA	Time Division Multiple Access

UE	User Equipment
UMTS	Universal Mobile Telecommunications System
WCDMA	Wideband CDMA
WiFi	Wireless Fidility
X2	eNB to eNB interface

List of Symbols

A	Offered traffic in cell m
A_H	Attenuation offset of antenna's horizontal radiation pattern
A_V	Attenuation offset of antenna's vertical radiation pattern
$A_{h,max}$	Maximum attenuation of the antenna's horizontal radiation pattern
$A_{v,max}$	Maximum attenuation of the antenna's vertical radiation pattern
B	System bandwidth
$BR_{u,r}$	Bit-rate of user u in subchannel r
B_{ccu}	Bandwidth for CCUs
B_{ceu}	Bandwidth for CEUs
C	Number of CoMP clusters in the system
CR_k	Coding rate of MCS k
D	Site-to-site distance
G^m	Normalisation constant
G_{tx}	Isotropic gain of a sectorial transmit antenna
H	Number of hexagon sites (eNBs) in the system
$I_{u,r}^{m,i}$	Interference power received by user u connected to cell m in subchannel r from its neighbour cell i
K	Number of modulation and coding scheme
M	Number of cells in the system
N	Cardinality of set Ω_u^m
N_k	Number of constellation points in MCS k
N_r	Number of sub-carriers in subchannel r
O_r	Number of OFDM symbols in subchannel r

P_n	Pilot power from the neighbour cell
P_s	Pilot power from the serving cell
P_{edge}	Relative Reference Signal Received Power (RSRP) threshold value for cell-edge decision
R	Number of resource blocks in each cell
$RSRP_u^{m,i}$	RSRP from cell i to user u connected to cell m
R_h	Radius of a regular hexagon
$S_{u,r}^m$	Signal power received by user u on subchannel r from cell m
T^m	Throughput of cell m
T_u^m	Throughput of user u connected to cell m
$T_{u,r}^m$	Throughput of user u in subchannel r connected to cell m
T^{sys}	System's throughput
U^m	Maximum number of users in cell m
$X_{\mathfrak{u}}^m(t)$	Random variable relating to the number of calls of type-$\mathfrak{u}$ user in cell m at time t
Ω_u^m	CCS of cells for user u connected to cell m
α_r^m	Allocation indicator of RB r in cell m
$\boldsymbol{n}$	Vector representing the number of users in the system
$\varepsilon(\gamma_{u,r}^m, k)$	BLER suffered by user u on subchannel r and is a function of SINR and MCS
$\eta_{r,k}$	RAB efficiency in subchannel r for MCS k
γ_u^m	SINR of Pilot signal of user u connected to cell m
$\gamma_{u,r}^m$	SINR of user u in subchannel r connected to cell m
γ_{edge}	Absolute SINR threshold boundary value for cell-edge decision
λ_u^m	Mean arrival rate of user u in cell m
λ_{hu}^m	Mean arrival rate of handoff user u in cell m

λ_{nu}^{m}	Mean arrival rate of new user u in cell m
$\mathcal{C}$	Set of CCS clusters in the system
$\mathcal{H}$	Set of hexagon sites (eNBs) in the system
$\mathcal{K}$	Set of MCSs
$\mathcal{M}$	Set of cells in the system
$\mathcal{RSRP}_{u}^{m}$	Set of RSRPs of user u connected to cell m
$\mathcal{R}$	Set of resource blocks in each cell
$\mathcal{S}$	State space of users in the system
$\mathcal{T}_{ceu}^{c}$	Set of throughput of CEUs in cluster c
$\mathcal{T}_{ccu}^{m}$	Set of throughput of CCUs in cell m
$\mathcal{U}^{m}$	Set of users in cell m
$\mathcal{U}_{ccu}^{m}$	Set of CCUs in cell m
$\mathcal{U}_{ceu}^{m}$	Set of CEUs in cell m
$\mathfrak{U}$	Number of user class types
$\mathfrak{u}$	A class of user type
μ_{u}^{m}	Mean service rate $(1/h_{u}^{m})$ of user u in cell m
$\overline{\Omega_{u}^{m}}$	Set of interfering cells for user u connected to cell m
ϕ	Angle of arrival in the azimuth plane between a user and a cell
ρ	Channel utilisation factor
ρ_a	Auto-correlation coefficient
σ	Thermal noise density which is additive white Gaussian noise
τ	Duration of a subframe in ms
θ	Angle of arrival in the vertical plane between a user and a cell
θ^{h}	Angle of arrival in the vertical plane from the antenna located at the base station h

θ_{3dB}	Half power beam width of the vertical antenna radiation pattern
θ_{etilt}	Electrical tilt angle, i.e., an angle between the antenna horizon and the main beam direction
$\tilde{T}_u^m$	Average throughput of user u connected to cell m
ξ_u^m	Shadow fading between user u and cell m
ζ_u^m	Fast fading gain between user u and cell m
d	Distance of a user from its serving cell
d_u^m	Distance between user u and cell m
$d_u^{m,h}(d, \theta')$	Distance of user u connected to cell m from base station h
d_{cor}	Decorrelation distance
d_{edge}	Absolute distance threshold value for cell-edge decision
d_{min}	The minimum distance a user can be located from the base station
g_u^m	Channel gain between user u and cell m
$g_{tx}^m(\theta, \phi)$	Transmit antenna gain from cell m to a user located at (θ, ϕ)
$g_{u,rx}$	Receive antenna gain of user u
h_b	Height of a transmit (enhanced-NodeB (eNB)) antenna
h_u	Height of a receiver (User Equipment (UE)) antenna
l_u^m	Path loss of user u from cell m
l_{cab}	Signal loss due to cable
l_{eqp}	Signal loss due to equipment
l_{fast}	Signal loss due to fast fading
l_{sh}	Signal loss due to shadowing
$n_{\mathfrak{u}}^m$	Number of users of type-$\mathfrak{u}$ in cell m
$p_{u,r}^m$	Transmit power for user u on RB r from cell m
r	An index to represent a general resource block (subchannel)

r_g	Number of subchannels reserved for handoff traffic
t_u^m	Mean holding time of user u in cell m
u	An index to represent a general user
$\boldsymbol{\pi}^m(\boldsymbol{n}^m)$	Steady state probability of the cell m in the state $\boldsymbol{n}^m$
$\boldsymbol{\pi}(\boldsymbol{n})$	Steady state probability of the system in the state space $\boldsymbol{n}$
$\boldsymbol{n}^m$	Vector representing the number of users in the cell m

List of Figures

List of Tables

List of Algorithms

Chapter 1:

Introduction

This chapter presents a brief introduction to the evolution of cellular networks and discusses how Inter-Cell Interference (ICI) is becoming a major problem for cellular providers as their networks evolve. The chapter provides basic information behind the principle of Orthogonal Frequency Division Multiple Access (OFDMA) transmission technology and discusses the scenario of the ICI problem and possible solutions in brief. Finally, it describes the motivation, research methodology and structure of the thesis.

1.1 Evolution of Mobile Cellular Networks

A cellular network is a radio network distributed over a large geographical area consisting of a number of cells with each cell[a] served by at least one fixed-location transceiver, known as a cell site or Base Station (BS). The basic structure of a cellular network is depicted in Fig. 1.1. A cellular network consists of Mobile Units (MUs)[b], BSs, and a Mobile Switching Centre (MSC). The MUs are linked to a BS via an interface called radio interface. The BS serves as a bridge between all MUs in the cell and connects to the MSC via microwave links, telephone lines or optical fibers. The MSC is a gateway

[a] A cell and a sector have the same meaning in this thesis. Usually, a cell was represented by a hexagon area and by the introduction of sectorial antennas, part of the cell was represented by a sector. But with the introduction of small power nodes, also known as small cells, the concept of sector is replaced into a cell.

[b] A Mobile Unit (MU), a User Equipment (UE) and a user have the same meaning in this thesis.

between different parts of the cellular network and a fixed Public Switched Telephone Network (PSTN).

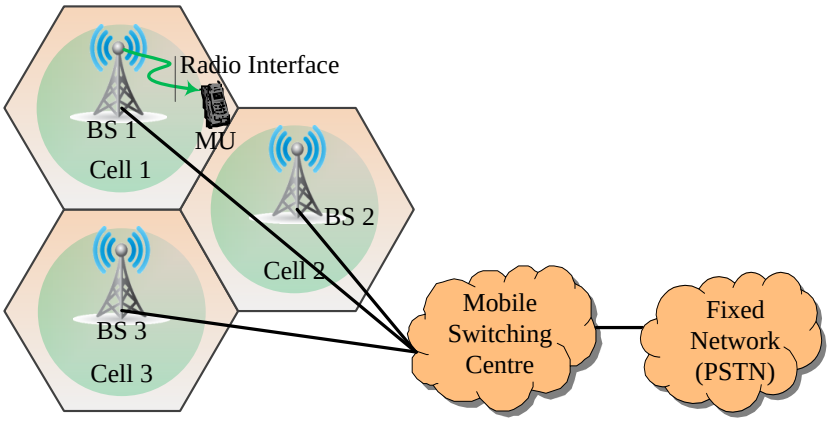

Figure 1.1: Basic structure of a cellular network

1st Generation

In 1970s, Bell Laboratories developed the cellular concept and from then the era of wireless mobile communication was born [1]. In the early stage of mobile communications, around the 1980s, cellular networks were referred to as 1st Generation (1G) cellular systems [2, 3]. 1G cellular systems were analog in nature and Frequency Division Multiple Access (FDMA) radio system was the air-interface technology. The purpose of 1G cellular networks was to provide voice only. The first cellular system in the world was operated in Japan by Nippon Telephone and Telegraph (NTT) in 1979. 1G systems offered handover with limited roaming and within the same network. Global mobile subscribers grew at a rate of 40% annually and the number of subscribers worldwide reached approximately 10 million by 1990 [1, 4]. Interference was not a major problem and the only focus was how to provide a basic voice service.

2nd Generation

As the number of cellular subscribers grew and there was a need for an increased network capacity, digital systems were invented. In the early 1990s, digital Time Division Multiple Access (TDMA) and Code Division Multiple Access (CDMA) air interface technologies were used in cellular networks to accommodate more cellular phone subscribers. These digital systems were known as 2nd Generation (2G) cellular systems. In addition to the voice service, 2G systems introduced basic data services with limited capacity such as Short Messaging Service (SMS) with a speed of 9.6 Kilobits per second (kbps) data and removed the barrier of international roaming from 1G systems. The Global System for Mobile Communication (GSM) is an example of 2G cellular systems developed by the European Telecommunications Standards Institute (ETSI) based on TDMA air interface technology [5]. By late 2001, mobile subscribers of GSM systems exceeded over 500 millions worldwide and GSM had become the world's leading 2G standard [6]. Owing to the large number of cell sites deployed for coverage and capacity expansion, interference became a problem for cellular providers. The problem of interference was resolved by optimising antenna azimuth/tilt and introducing the "frequency reuse" concept in the frequency plan [7].

3rd Generation

As the use of 2G phones in daily activities became more popular, it became clear that the demand for data services, such as access to the Internet, was growing. The demand for higher capacity, faster data rates, and better Quality of Service (QoS) drove the cellular networks towards the evolution of 3rd Generation (3G) cellular systems. During mid-1995, the ITU formulated a plan to implement a global frequency band in the 2000 Mega Hertz (MHz)

range that would support a single standard for all countries throughout the world and provide high speed data services when compared with 2G. The plan was called International Mobile Telecommunications-2000 (IMT-2000) [**?**]. In 1998, the 3rd Generation Partnership Project (3GPP) standardisation body was established to develop a 3G mobile system based on the evolved GSM core networks but with a new air interface technology [8]. Universal Mobile Telecommunications System (UMTS) is a 3G mobile cellular technology developed by 3GPP with Wideband CDMA (WCDMA) as the air interface technology and which requires a minimum spectrum allocation of 5 MHz. In 2001, the first commercial network of a 3G system was launched in Japan based on WCDMA [8]. Some of the applications of 3G systems are mobile television, video conferencing, telemedicine and location-based services.

4th Generation

The ever-increasing growth of mobile broadband users had triggered researchers to come up with a comprehensive new transmission technology that satisfied the growing demand of high speed mobile broadband. In October 2007, a consensus was reached by the ITU community to expand the IMT-2000 3G radio interface family with an OFDMA technology and to establish IMT-Advanced (IMT-A) as the name for the systems beyond IMT-2000, also called the 4th Generation (4G) system [9, 10]. In 2008, the ITU set the requirements of the 4G system [11]; and one of the main requirements was that the downlink data rate should be at least 1 Gigabits per second (Gbps), and the uplink should be at least 500 Megabits per second (Mbps). Long-Term Evolution (LTE) is a standard developed by the 3GPP standardisation body. It is based on OFDMA and was first defined in the technical standard as Release (Rel)-8. One of the main requirements of LTE is that it should provide at least 100 Mbps in the downlink and 50 Mbps in the uplink and operate within a 20 MHz

bandwidth. LTE is considered as 3.9th Generation (3.9G) technology.

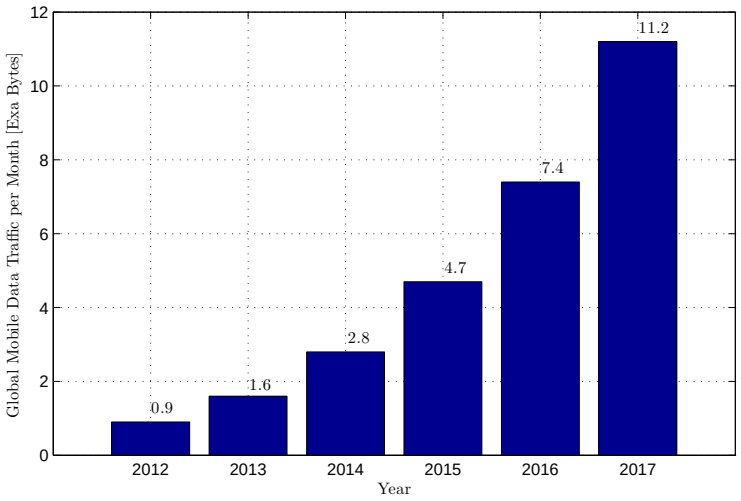

Figure 1.2: Mobile data traffic prediction from 2012 to 2017

According to Cisco, it is predicted that the overall mobile data traffic is expected to grow at a compound annual rate of 66 % from 2012 to 2017, reaching 11.2 Exa Bytes per month by 2017, as shown in Fig. 1.2 [12], and that by the end of 2013 the number of mobile-connected devices will exceed the number of people on earth [12]. Furthermore, in 2017, 4G mobile will be 10 % of connections, but 45 % of the total traffic and will generate 8 times more traffic on average than non-4G connections [12]. To satisfy these requirements, vendors and operators are working on the development of a new standard called LTE-Advanced (LTE-A) [13]. LTE-A is an evolution of LTE technology; it is also known as 4G, and is referred to in the technical standard as Rel-11 where the standardisation of LTE-A is on going.

5th Generation

According to the traffic prediction of mobile data, as shown in Fig. 1.2, it seems that the demand of high data rate of mobile service is increasing exponentially.

In the future, in addition to the high data rate demand, the introduction of large-scale of communicating devices, such as smartphones, tablets, electric metres, machine-to-machine communication, will put many diverse requirements on the network in terms of, for example, latency, battery consumption, device cost and reliability [14]. The 5th Generation (5G) technology is to provide the solution to these diverse requirements and is currently well underway in research. In November 2012, the first large-scale international project on 5G called Mobile and Wireless communications Enablers for the Twenty-twenty (2020) Information Society (METIS) was established under the Seventh Framework Programme (FP7) for research and development by the European Commission [15]. In October 2012, the University of Surrey, UK, secured £35 million for a new 5G research centre to offer testing facilities to mobile operators keen to develop a standard that uses less energy and radio spectrum whilst delivering faster than current 4G data rate [16, 17]. 5G technology is considered to be the future mobile technology for 2020 and beyond. The METIS project is developing technical solutions in order to provide a system which supports [15]:

- 1000 times more mobile data volume per area,
- 10 to a 100 times more number of connected devices,
- 10 to a 100 times more user data rate,
- 10 times longer battery life for low power massive Machine-to-Machine (M2M) communication, and
- 5 times reduced End-to-End latency.

In order to meet the above challenges, the following technology components are being researched:

- Radio Links: The advanced transmission technologies, including the use of new transmission waveforms and new approaches to multiple ac-

cess, Medium Access Control (MAC) and Radio Resource Management (RRM) are under investigation.

- Multi-node/Multi-antenna Transmission: Multi-hop communications, advanced inter-node coordination and cooperation schemes, and massive antenna configurations, i.e., Multi-Input Multi-Output (MIMO), are under investigation.
- Network Dimension: Novel approaches for efficient interference management, including traffic demand and mobility management, in dense heterogeneous deployments are under investigation.
- Spectrum Usage: The extension of spectrum-band-of-operation, as well as the operation in a new spectrum band is under investigation.

1.2 Fundamentals of OFDMA: The LTE perspective

OFDMA is the multi-carrier transmission technique adopted by 3GPP in 4G cellular networks [18]. For OFDMA-based networks, user data is divided and modulated onto a large number of narrow band subcarriers in the frequency domain, and each of them is modulated by low rate data [19]. The subcarriers are orthogonal to each other, meaning that cross-talk between the sub-carriers is eliminated and inter-carrier guard bands are not required. The orthogonality among the subcarriers prevents inter-subcarrier interference because the subcarrier's spectrum has nulls located at the centre frequencies of adjacent subcarriers [19] as shown in Fig. 1.3. A group of consecutive subcarriers is known as a *subchannel*. Moreover, the time domain is split into consecutive frames that are in turn divided into time slots called *Orthogonal Frequency Division Multiplexing (OFDM) symbols*. As a multiple access technique, OF-

DMA offers the possibility of enhancing the spectral efficiency of networks by assigning distinct OFDM symbols or subchannels to distinct users, thus taking advantage of their diverse time and frequency channel conditions as compared to TDMA and FDMA techniques.

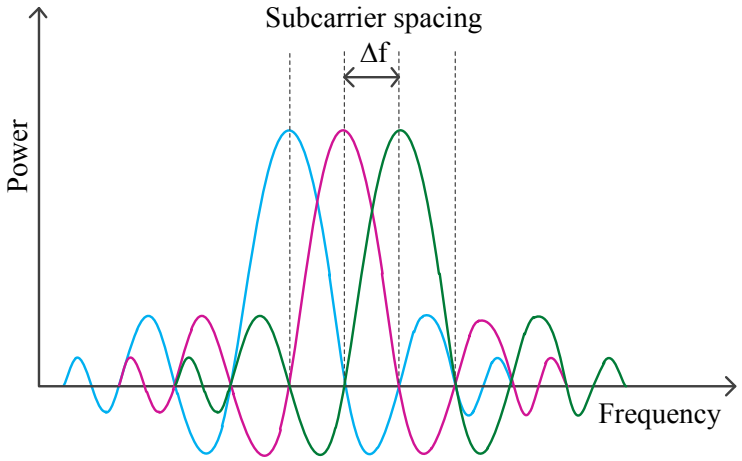

Figure 1.3: OFDM orthogonal subcarriers modulating rectangular pulses

For LTE, downlink transmission is based on OFDMA. Figure 1.4 shows a frequency-time radio resource grid. In the frequency domain, the radio spectrum is divided into a number of narrow subcarriers of 15 Kilo Hertz (kHz)[c] spacing. In the time domain, a frame of 10 milliseconds (ms) duration is divided into 10 subframes of 1 ms each. Each subframe is further divided into 2 time slots of 0.5 ms each. Each time slot then consists of 6 or 7 OFDM symbols depending on the length of cyclic prefix (normal or extended cyclic prefix) [19]. A grid of 1 subcarrier (15 kHz) in the frequency domain and 1 OFDM symbol (0.5 ms) in the time domain is known as 1 *resource element*, while a grid of 12 adjacent subcarriers ($12 \times 15 = 180$ kHz) and 1 OFDM symbol (0.5 ms) is known as 1 *Resource Block (RB)*. Hence, an RB is a rect-

[c]In addition to 15 kHz subcarrier spacing, a reduced subcarrier spacing of 7.5 kHz with twice OFDM symbol time is also defined for LTE which targets Multicast-Broadcast Single-Frequency Network (MBSFN)-based multicast/broadcast transmissions [20].

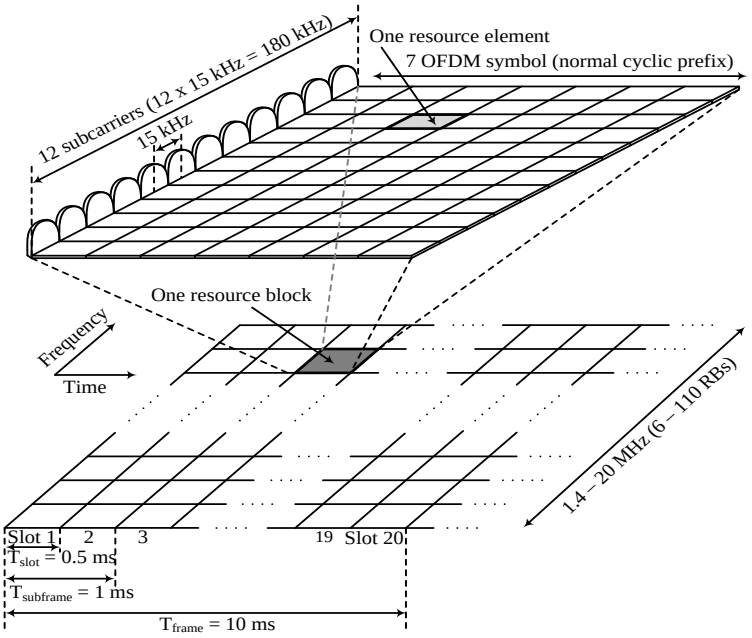

Figure 1.4: Physical layer structure of LTE (3GPP Release 8)

angular block of resource elements, which spans 12 adjacent subcarriers in the frequency domain and 7 OFDM symbols in the time domain (180 kHz $\times$ 0.5 ms). In LTE, an RB is also known as a *subchannel*, and from now on we refer to an RB as a subchannel. Depending on the transmission bandwidth, a downlink carrier comprises a variable number of subchannels in the frequency domain. The minimum bandwidth of 1.4 MHz corresponds to 6 RBs, while the maximum one of 20 MHz corresponds to 110 RBs. The assignment of subchannels to users is carried out by the MAC scheduler, and it is performed on a subframe-by-subframe basis, i.e., each 1 ms. The scheduler decides which users are allowed to transmit on which subchannel. It should be noted that the minimum resource scheduling unit[d] that the scheduler can assign to a user is comprised of 2 consecutive RBs and thus spans an entire subframe.

[d]From now on, when we refer to an RB, we refer to this minimum scheduling unit of 2 consecutive RBs, spanning 1 ms.

1.3 Inter-Cell Interference

In OFDMA-based cellular networks, intra-cell interference is cancelled out by the orthogonality of OFDM subcarriers. Then the main problem of interference comes from neighbouring cells. The problem of ICI occurs if two or more cells use the same radio spectrum. In LTE and LTE-A systems, the radio spectra are utilised efficiently by employing a frequency reuse of 1, meaning each set of available radio spectra are being used in each cell which in turn causes the cell-edge performance to heavily degrade. Figure 1.5 shows a scenario of the ICI problem in a homogeneous and a heterogeneous network. A network containing only a high power macro eNB is termed a *homogeneous network* and is shown in Fig. 1.5(a); while a network containing nodes with transmit powers, such as a combination of macro nodes and low power nodes (e.g., Remote Radio Head (RRH), microcell, picocell, femtocell, etc.), is termed a *heterogeneous network* and is shown in Fig. 1.5(b). As shown in Fig. 1.5(a), UE 1 is in the area of Cell 1 near the boundary with Cell 2 and Cell 3. This UE receives interference signals from the neighbouring cells 2 and 3 if the subchannel used by it is utilised in these two neighbouring cells. On the other hand, in Fig. 1.5(b), UE 1 is in the area of Picocell 1 but at the same time it receives ICI from its neighbours Picocell 2 and Macrocell 1. Similarly, in Macrocell 2, UE 2 is served mainly by Macrocell 2 but at the same time it receives ICI from the small power nodes called Femtocell 1 and Picocell 3. The ICI creates a severe problem for the performance of UE, especially to the cell-edge UE. This causes their data throughput to degrade, coverage to shrink and the system capacity to decrease.

The ICI is inevitable in OFDMA-based networks and degrades the UE performance. There are three main methods of ICI mitigation which have been considered [21–25]:

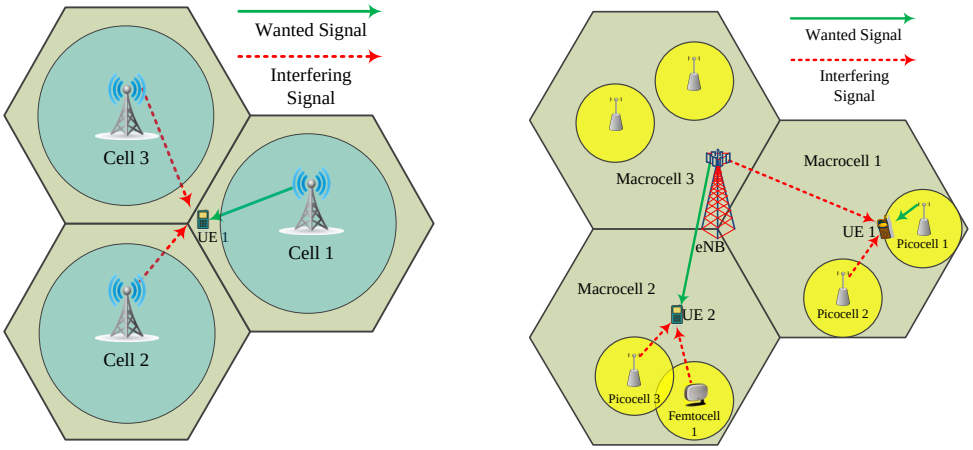

(a) Homogeneous network (b) Heterogeneous network

Figure 1.5: Inter-cell interference problem

- *ICI randomisation* by frequency hoping,
- *ICI cancellation* through receiver processing,
- *ICI coordination (or avoidance)* by restrictions imposed in resource usage in terms of frequency partitioning and power control.

In LTE and LTE-A system, 3GPP has mainly focused on ICI coordination and considered different schemes to coordinate interference [24, 26]. There are four approaches to degrade the infulence of ICI in a coordinated method [27]:

- reduce transmission power
- stop transmission
- reduce interferences by using directional gain
- combine interference (network collaborative MIMO)

The first two approaches do not seem preferable. In these approaches, the cell-edge efficiency of the serving cell may be improved, but the efficiency of the adjacent cell, which contributes the ICI reduction, degrades because their

cell-edge users are unable to receive power [27]. Hence, the last two approaches seem more suitable for improving cell-edge efficiency without (or with little) degradation of efficiency of the adjacent cells. In these last two approaches, interference is either avoided by generating directional beamforming or treated by combining. These are the techniques considered as Coordinated Multi-Point (CoMP) Transmission and Reception in Rel-11 of LTE-A by 3GPP. In order to enhance the cell-edge performance, CoMP techniques have been investigated which are considered as in Rel-10 an extension of ICI coordination to the spatial domain [28, 29].

1.4 Focus of Thesis

The main focus of the thesis is the development of a novel resource allocation algorithm together with an analytical model for data throughput evaluation in CoMP joint transmission mode of LTE-A networks.

1.4.1 Aim and Objectives

The main objectives of the thesis are:

1. To review current approaches of resource scheduling in CoMP joint transmission in cellular networks, and to discuss their capability to satisfy the needs of cell-edge users.
2. To propose and evaluate the performance of a novel algorithm for resource scheduling technique in CoMP joint transmission.
3. To develop analytical models for throughput evaluation of cellular networks with and without CoMP joint transmission.
4. To develop empirical path loss models in an indoor-to-outdoor scenario of Femtocell networks.

1.4.2 Motivation of Thesis

On the one hand, operators are in a stage of enhancing their existing networks to satisfy the needs of growing high data speed mobile services. On the other hand, radio interface is a well known bottleneck because the radio spectrum is limited and therefore expensive. This situation has led to the spectrum attracting a very high price. For example, according to Ofcom, a telecom regulatory body in the UK, Everything Everywhere Ltd paid £ 588,876,000 (£ 589 million) for 2×5 MHz spectrum from 800 MHz band and 2×35 MHz spectrum from 2.6 GHz band, while, Vodafone Ltd paid £ 790,761,000 (£ 791 million) for 2×10 MHz spectrum from 800 MHz band, 2×20 MHz spectrum from 2.6 GHz band and 1×25 MHz spectrum from 2.6 GHz band [30]. Hence, from the view of cost saving and the scarcity of the radio spectrum, operators are forced to use their available radio spectrum highly effectively in their upgraded networks. If the same spectrum is re-used in each cellular network, major interference occurs and degrades the performance of networks, which is unsatisfactory to customers, especially those located nearby a cell-edge boundary. To satisfy the needs of customers, interference should be avoided, and the CoMP joint transmission technique is a solution to avoid interference, especially for users located near a cell-edge boundary. Consequently, it is a 'hot-topic' in the field of next generation of mobile networks. To benefit from the implementation of CoMP, the radio spectrum should be utilised in a smart and efficient manners, which is the motivation of the thesis.

1.4.3 Research Methodology

In order to evaluate the performance of the developed resource scheduling algorithm, simulation and analysis methods are utilised.

Simulation Methods

An event-driven System Level Simulation (SLS) has been developed to evaluate the performance of the developed resource allocation algorithm in CoMP joint transmission. This tool is written in `C++` with the CoMP transmission fully integrated.

Analytical Methods

To boost the results of simulation, an analytical model has been developed for the evaluation of the system throughput under CoMP joint transmission.

Hybrid Methods

This method combines the approach of both simulation and analysis. The performance of a network by a hybrid method was compared with a simulation approach and an analytical approach.

Measurements

Empirical path loss models for indoor-to-outdoor environments in a residential area have been developed based on a measurement campaign.

1.4.4 Validation and Verification

The implementation of a scheduling algorithm in a simulator has been validated by checking simulation results against numerical examples. The results of the developed resource scheduling were verified by comparing them with published results. Details of validation are covered in the relevant sections of the thesis.

1.4.5 Structure of Thesis & Key Original Contributions

The structure of the thesis is shown in Fig. 1.6 and is described in brief as follows:

- In Chapter 2, the literature of the CoMP technique and ICI coordination in CoMP joint transmission scheme by resource scheduling are reviewed.
- In Chapter 3, a novel resource scheduling algorithm based on the joint maximum throughput is proposed. To evaluate the performance of the scheduling algorithm, a system-level simulator tool is developed and the chapter describes the methodology utilised for modelling the network performance into the tool.

  Contribution: A novel resource scheduling algorithm based on the maximum throughput under CoMP joint transmission scheme has been developed.
- Chapter 4 presents a complete dynamic analytical model developed for throughput evaluation in CoMP joint transmission during the research.

  Contribution: A complete dynamic analytical model was developed for performance evaluation of CoMP joint transmission scheme.
- In Chapter 5, the performance of the CoMP scheduling algorithm in intra-site deployment was evaluated under various traffic loads, different criteria of cell-edge decision and users under static and mobile conditions.

  Contribution: Performance of intra-site CoMP joint transmission scheme has been evaluated for different criteria of cell-edge decision.
- In Chapter 6, the performance of the CoMP scheduling algorithm in inter-site deployment has been evaluated under various traffic loads, dif-

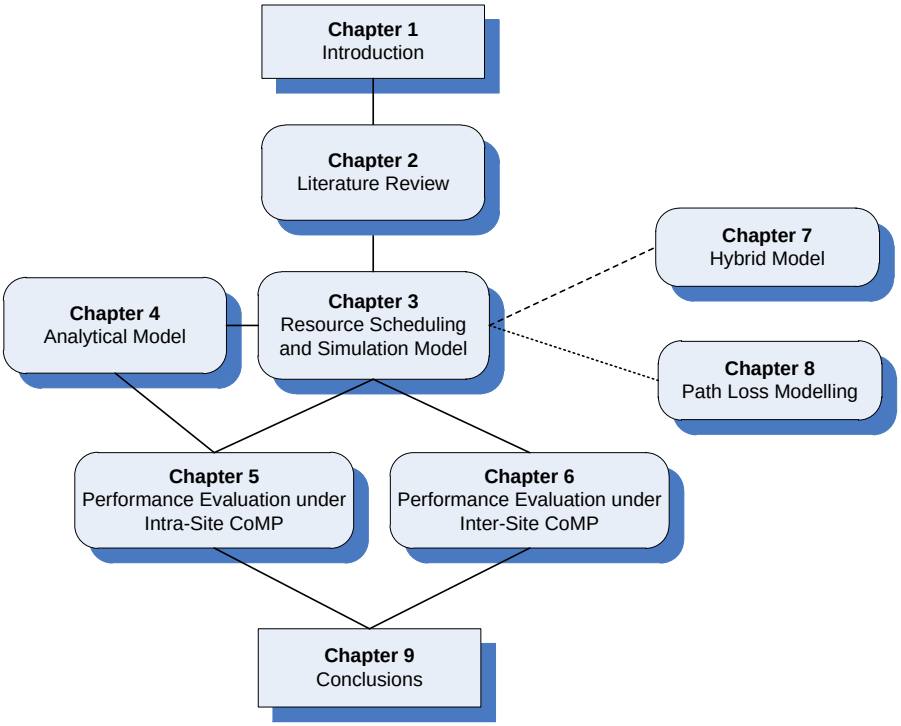

Figure 1.6: Overview of the thesis structure

ferent criteria of cell-edge decision and users under static and mobile condition.

Contribution: Performance of inter-site CoMP joint transmission scheme has been evaluated for different criteria of cell-edge decision.

- Chapter 7 evaluates the performance of an OFDMA-based network under a Non-CoMP scenario by a Hybrid model of simulation and analysis.

  Contribution: A novel hybrid model of simulation and analysis has been developed for the OFDMA-based system throughput evaluation from a user's point of view.

- In Chapter 8, empirical path loss models in an indoor-to-outdoor scenario have been modelled based on the data from a previous measurement campaign.

Contributions: Two empirical path loss models in an indoor-to-outdoor environment were derived.

- Chapter 9 provides conclusions, discusses limitations and proposes future work.

Chapter 2:

Literature Review

In the previous chapter, the problem of Inter-Cell Interference (ICI) was discussed. It was shown that ICI affects the performance of UE located at the cell edge if the neighbouring cells use the same frequencies. To benefit from the implementation of CoMP transmission, radio resources should be carefully scheduled. In this chapter, a literature review of current trends in ICI solutions by resource scheduling in Non-CoMP and CoMP transmission will be discussed.

2.1 Inter-Cell Interference Solution by Frequency Reuse

A Frequency Reuse Scheme (FRS) indicates how often an available frequency spectrum is reused in a cellular network. The simplest scheme to allocate frequencies in a cellular network is to use a reuse factor 1, i.e., to allocate all the available radio subchannels to each cell, thus leading to high system capacity. However, a frequency reuse of 1 leads to high inter-cell interference, especially to UE located near by the cell-edge boundary. A tree diagram of the frequency reuse scheme is depicted in Fig. 2.1 and the concept of each scheme is described in the following subsections.

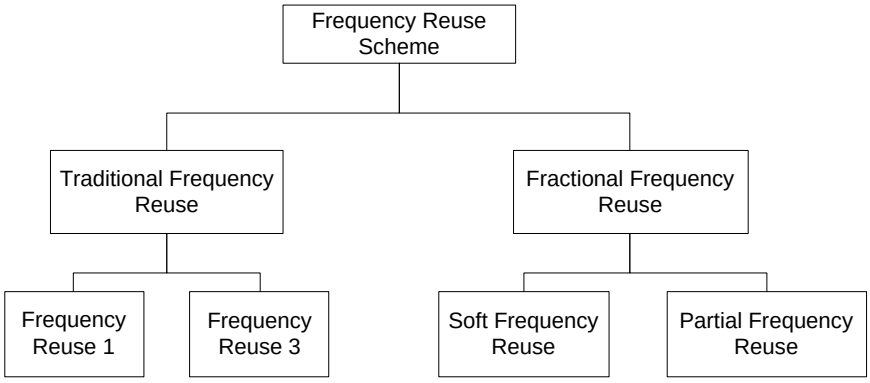

Figure 2.1: Tree diagram of frequency reuse scheme

2.1.1 Traditional Frequency Reuse Scheme

Traditionally, in early digital mobile networks such as in GSM, ICI was handled by the classical clustering technique, for example, a frequency reuse of 3 [21, 31]. Figure 2.2 demonstrates two ways of implementing FRS, where the total transmit power per cell transmitter remains constant in both cases [21]. In Fig. 2.2(a), each cell uses all the available frequencies without imposing any restriction on the frequency resource usage or power allocation. In this scheme, a Frequency Reuse (FR) 1 is achieved and the available spectrum is efficiently utilised, but with the highest level of ICI in the neighbouring cells.

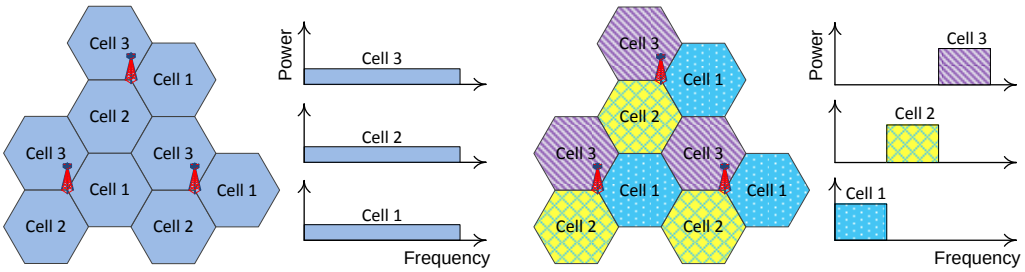

(a) Frequency reuse 1 (b) Frequency reuse 3

Figure 2.2: Frequency reuse scheme

On the other hand, as shown in Fig. 2.2(b), if all the available frequency

spectrum is divided into three equal sub-bands and each cell is given a sub-band which is orthogonal to the neighbouring cells' sub-bands, then FR 3 is obtained. FR 3 reduces ICI but this scheme results in a system capacity loss due to the spectrum partition because only one third of the available frequency resources are used in each cell. Consequently, a network designer would ideally use FR 1 but would need an effective means of mitigating ICI.

2.1.2 Fractional Frequency Reuse

In the recent years, Fractional Frequency Reuse (FFR) schemes have attracted the attention of researchers [32–38]. The motivation behind FFR lies in the fact that UE in the cell-centre region are more robust against ICI due to the relatively low path loss from the serving eNB, and hence can tolerate higher reuse. On the other hand, UE in the cell-edge region are more prone to ICI. Therefore, it makes sense to use different degrees of reuse factor for Cell-Centre Users (CCUs) and Cell-Edge Users (CEUs). Figure 2.3 illustrates two variants of FFR: Soft Frequency Reuse (SFR) and Partial Frequency Reuse (PFR).

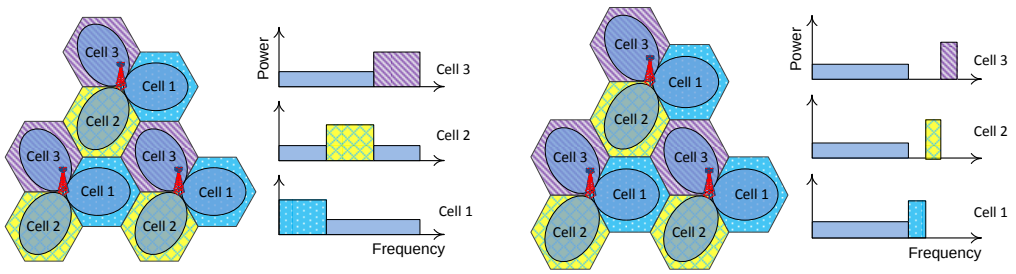

(a) Soft frequency reuse (b) Partial frequency reuse

Figure 2.3: Fractional frequency scheme

Soft Frequency Reuse

Figure 2.3(a) illustrates the concept of SFR [21, 32, 38]. In SFR, the cell is divided into cell-centre and cell-edge zones, and accordingly, the available frequency spectrum is divided into these two zones. The cell-centre zone uses 2/3 of the available spectrum, while the cell-edge zone uses 1/3 of the available spectrum which is orthogonal to those in the neighbouring cells. The higher transmission power is used in the cell-edge zone, while the lower power is used in the cell-centre zone, as shown in Fig. 2.3(a). The cell-edge zone can be used in the cell-centre region as well, so long as it is not occupied by CEUs, but the cell-centre zone is available only to CCUs.

Partial Frequency Reuse

Contrary to SFR, the idea of a PFR scheme is to further divide the cell-edge zone into three sub-zones and use only one sub-zone in a cell for CEUs [21,32,33]. To illustrate this, let us assume that the available system bandwidth is B which is divided into a cell-centre band B_{ccu} and a cell-edge band B_{ceu}. The band B_{ccu} is used with a reuse factor of 1, and the band B_{ceu} is used with a reuse factor of 3. The effective frequency reuse factor is given by $B/(B_{ccu} + (B_{ceu}/3))$ [21].

Although ICI can be minimised by a frequency reuse scheme, there is a system capacity loss from the spectrum efficiency point of view, because the frequency in a cell-centre zone may be under-utilised but not be able to be used by CEUs as well as not being flexible among CCUs and CEUs.

2.2 Coordinated Multi-Point Transmission

In recent years, researchers and industries have been working on an alternative solution of the ICI problem called the CoMP technique [39–49]. The CoMP

transmission is a technique in LTE-A to improve cell-edge data throughput and/or system capacity by either turning ICI into a useful signal or avoiding ICI using directional beamforming in a coordinated way [29]. In 3GPP Radio Access Network (RAN) meeting #50 [39], a revised CoMP study item was agreed for Rel-11. In 3GPP RAN Working Group 1 (RAN1) meeting #63bis [40], a CoMP study item was initiated. Currently, the standardisation work of CoMP performance is ongoing; it was expected to freeze by the end of year 2012 [44] but has been delayed to June 2013 [45]. The complete standardisation work of CoMP is expected to freeze by the end of 2013 [45].

The main idea of CoMP is as follows. When a UE is at a cell-edge region, it may receive signals from multiple cell sites separated geographically. If these signals are coordinated somehow, then the downlink performance can be increased significantly by either turning ICI into a useful signal using a joint transmission technique or avoiding ICI using a beamforming technique. Figure 2.4 shows the ICI coordination technique in CoMP transmission by interference combining (Fig. 2.4(a)) and directional beamforming (Fig. 2.4(b)). The coordination information such as resource scheduling and Channel State Information (CSI) is shared among the coordinated cells over the eNB to eNB interface (X2) or optical fiber, whichever is feasible.

2.3 CoMP Categories

In the downlink, CoMP transmission can be divided into two main categories [46–50]: Joint Transmission (JT) and Coordinated Beamforming (CBF). This thesis is focused on the JT CoMP category.

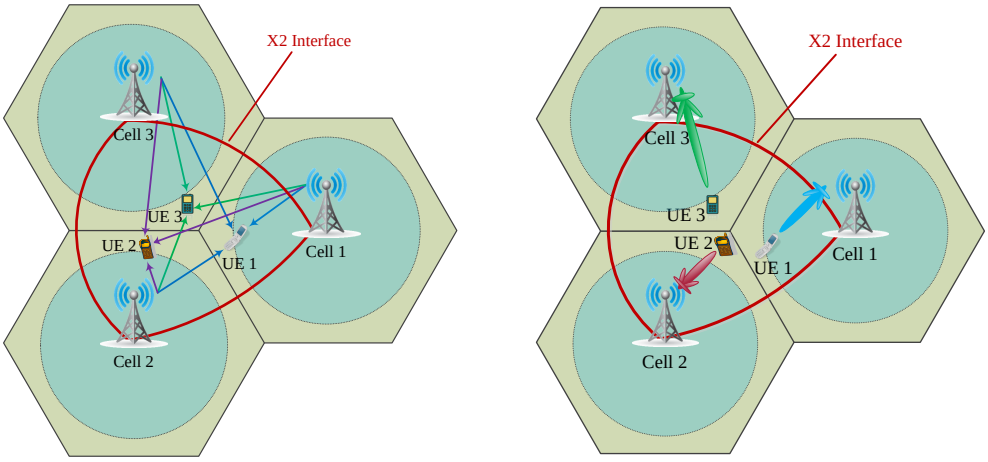

(a) Interference combining (b) Coordinated beamforming

Figure 2.4: Inter-cell interference coordination in CoMP transmission

2.3.1 Joint Transmission

For a JT scheme, a signal destined for a UE or multiple UE is transmitted from multiple transmission points simultaneously, either coherently or non-coherently [48–50]. Figure 2.4(a) shows an example of the JT technique where each coordinated cell serves a particular UE simultaneously, based on the scheduled information shared via the X2 interface. On the one hand, the radio spectra from multiple transmission points are reserved to serve a particular UE, which is a major disadvantage in terms of the efficient use of spectrum. On the other hand, it provides significant performance gains since multiple transmission points serve the same UE and the ICI is turned into a useful signal. The JT approach has the disadvantage of putting higher requirements on the coordination links and on the backhaul because:

- user data needs to be made available at multiple coordinated transmission points.
- the amount of data to be exchanged over the coordination links is also

large, e.g., channel knowledge and computed transmission weights.

2.3.2 Coordinated Beamforming

For the CBF scheme, a signal destined for a UE or multiple UE is transmitted from a single transmission point while the scheduling decisions and/or generated beamforming are coordinated among multiple coordinating points [48, 49, 51, 52]. Figure 2.4(b) shows an example of coordinated beamforming. Each coordinated cell shares its scheduling information with each other via an X2 interface and generates directional beamforming to serve its particular UE, based on the decision of the shared scheduled information, and avoids the interference with the other coordinated cells. It is an advantage that the requirements on the coordination links and on the backhaul are significantly reduced because:

- only information on scheduling decision and/or generated beams needs to be coordinated,
- user data does not need to be made available at the coordinated transmission points, since there is only one serving transmission point for a particular UE.

2.4 CoMP Implementation Challenges

Before receiving the performance gain by CoMP, many implementation challenges have to be considered. Some of the challenges are described here.

2.4.1 CoMP Deployment Scenario

In 3GPP RAN#63bis meeting [40], an agreement of four deployment scenarios of CoMP were reached for evaluation purposes and work was divided into two

phases [41–43]:

- Phase 1: Homogeneous network
- Phase 2: Heterogeneous network

CoMP in Homogeneous Deployment

A conventional network containing high power macro eNB is termed as a homogeneous network. The following two scenarios of homogeneous deployment for CoMP evaluation considered by 3GPP are:

- Scenario 1: Homogeneous networks with intra-site CoMP
- Scenario 2: Homogeneous networks with high transmit power RRHs (inter-site CoMP)

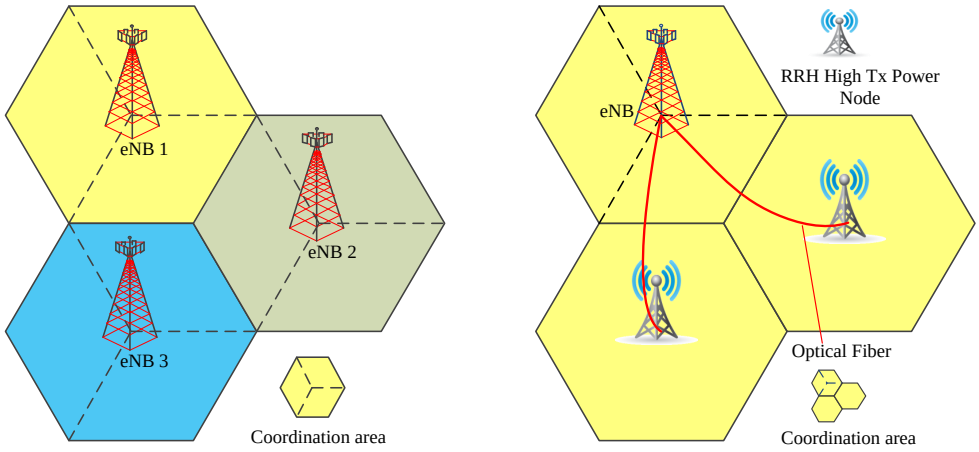

(a) Scenario 1 (b) Scenario 2

Figure 2.5: CoMP homogeneous deployment

Figure 2.5 illustrates CoMP deployment in homogeneous networks [43]. In the intra-site CoMP deployment of a homogeneous network (Scenario 1) as shown in Fig. 2.5(a), the coordination area is among the cells of their own

eNB. In such a deployment, where all the coordinating cells are co-located, cells do not require any interface, due to which the performance of CoMP would be faster than that of inter-site CoMP deployment. Whereas, in the case of inter-site CoMP deployment of a homogeneous network (Scenario 2) as shown in Fig. 2.5(b), the distributed RRHs are connected to their eNB via optical fiber.

CoMP in Heterogeneous Deployment

A network which contains nodes with different levels of transmit power, such as a combination of a macro node and low power nodes (e.g., RRH, microcell, picocell and femtocell) are termed as a heterogeneous network. The following two scenarios of heterogeneous deployment for CoMP evaluation considered by 3GPP are:

- Scenario 3: Heterogeneous networks with low transmit power RRHs within the cell coverage but having different cell Identitys (IDs) than macrocell
- Scenario 4: Heterogeneous networks with low transmit power RRHs within the cell coverage having same cell IDs as macrocell

Figure 2.6(a) shows a heterogeneous deployment scenario of low power nodes (e.g., picocell, femtocell) within a cell having different cell IDs than the cell. The coordination among the low power nodes and the cell can be done through optical fiber. Figure 2.6(b) depicts Scenario 4 where each of the low power nodes have the same cell IDs as that of the cell (e.g., RRH, relay).

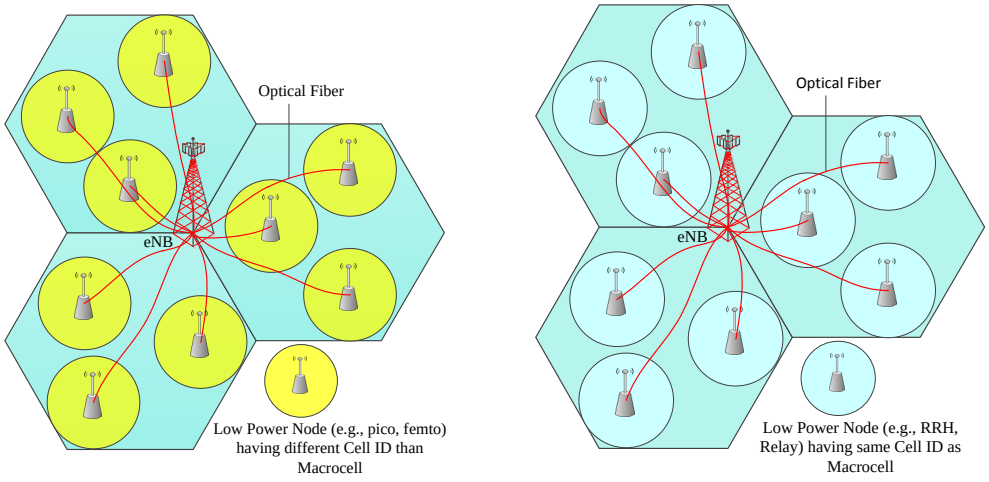

(a) Scenario 3 (b) Scenario 4

Figure 2.6: CoMP heterogeneous deployment

2.4.2 CoMP Cooperating Set Formation

CoMP Cooperating Set (CCS)[a] is a set of cells which take part in the coordination of scheduling and data transmission to UE. One of the main problems is how to determine a CCS for a UE to achieve the maximum throughput performance. The CCS of cells can be formed in three different ways [53–58]:

- eNB-centric
- UE-centric
- Hybrid-approach

eNB-centric

In a network-centric approach, the formation of a CCS is made in a static way, which means, the cells in the CCS remain the same for a particular UE although there might be a best cell outside of the CCS to serve this UE. It is

[a]In this thesis, a CoMP Cooperating Set (CCS) is also known as a cluster.

easy to implement but it will cause a large performance degradation especially to UE near the boundary of a cluster [55].

UE-centric

In a UE-centric approach, each UE will choose a small number of cells in order to benefit the most from their cooperation. On the one hand, scheduling of UE will be a challenging task since the CCS is chosen in a dynamic way and if UE are in mobility, then this imposes a further task of maintaining the measurement list since UE suddenly change their cells. On the other hand, this approach will provide more gain by enabling the diversity of choosing the best cells in a dynamic way according to the measurement data.

Hybrid-approach

Taking into account both performance and complexity, a hybrid approach would be more suitable. This will alleviate the boundary problems among CCSs.

2.4.3 CoMP Measurement Set Determination

A measurement set is a set of cells about which the CSI related to their link to the User Equipment (UE) is measured using a Reference Signal (RS). There are two ways to determine the measurement set [59]: *UE-based* and *eNB-based*. The CoMP cooperating set can be itself a measurement set or part of a measurement set for a particular UE.

UE-based

The UE determines the CoMP measurement set by comparing the RSRP of each neighbouring cell in RRM measurement with a predefined threshold set

by the eNB. Additional cells are added to the measurement set if the RSRP of a candidate cell is $\Delta_{threshold}$ Decibel (dB) lower than that of the serving cell [60, 61], i.e.,

$$RSRP_{serving} - RSRP_{candidate} \leq \Delta_{threshold}. \tag{2.1}$$

eNB-based

The eNB determines the CoMP measurement set based on the RSRP report from UE. In this case, eNB needs to inform UE about their CoMP measurement set. Then UE will perform the CSI measurement task based on the configure measurement list and feedback the CSI to their serving eNB.

In a heterogeneous network, maintaining the CoMP measurement set would be a challenging task because the cells in the set would be changing frequently if UE are in mobility.

2.4.4 CoMP Multi-Cell Synchronisation

To benefit from CoMP efficiently, all cells in the cooperating set need to synchronise. Otherwise, instead of a gain, CoMP imposes more interference. Timing errors due to different propagation delays from the individual eNBs to the UE would results in loss of orthogonality at the receiver [62]. In the case of a heterogeneous CoMP deployment as in Scenario 4 (Fig. 2.6(b)), where all the cooperating cells have the same cell ID, it would be a challenge to address the case of different transmit antennas at the macrocell and RRH.

2.4.5 CoMP Feedback and Backhaul

The efficient CoMP schemes that can tolerate high latency and low capacity backhaul can make CoMP even more appealing in practice. However, in general the capacity of an inter-eNB link and the associated latency for information

exchange often limits the effectiveness of CoMP schemes [63–66]. The CoMP schemes require an exchange of information among cooperating sets such as scheduling decisions related to time/frequency resources, the CSI from multiple cells and the user data. In homogeneous networks, such information can be exchanged over an X2 interface (inter-eNB link) or over an optical fiber (eNB-RRH link) among cooperating sets. But in heterogeneous networks such as a combination of macrocells and femtocells, there is no such interface because femtocells are directly connected to the internet broadband. It would be a challenge to do CoMP in such a heterogeneous network.

2.4.6 CoMP Mobility Management

The mobility of users in a network imposes major challenges in a CoMP scheme. For example, in a heterogeneous network, a cell's coverage range is small such as in the case of a femtocell or a picocell. In such an environment, the mobility of UE imposes a burden of maintaining the CCS in CoMP since UE will be frequently reporting a better RSRP signal to their serving cells and CoMP CCS needs to update accordingly. Hence, taking account of mobility, one should have to think carefully which CoMP schemes would be suitable in such a environment. The detail of the handover mechanism under the CoMP transmission scheme can be found in [67, 68].

2.4.7 CoMP Scheduling

The process of allocation of radio resources in terms of time, frequency and power to UE in cellular networks is termed *scheduling*. The performance of a network depends on how efficiently the available resources are allocated to the UE. Depending on the network deployment strategies, two types of scheduling in CoMP are feasible [69, 70]:

- Centralised Scheduling
- Distributed Scheduling

Centralised Scheduling

In centralised scheduling, as shown in Fig. 2.7, one of the cooperating cells (usually the serving cell) acts as a master cell which performs the scheduling process based on the Channel State Information (CSI) received from the UE and shares the scheduling information with the transmission points in the CCS via an X2 interface [71]. This type of scheduling is more suitable for a deployment scenario where a low latency and a high capacity interface among the transmission points is available such as an X2 interface between eNBs. But, nowadays, distributed networks (such as RRHs, Relay) are under consideration and in such a deployment we cannot have an X2 interface everywhere. In such a distributed network, distributed scheduling would be more suitable.

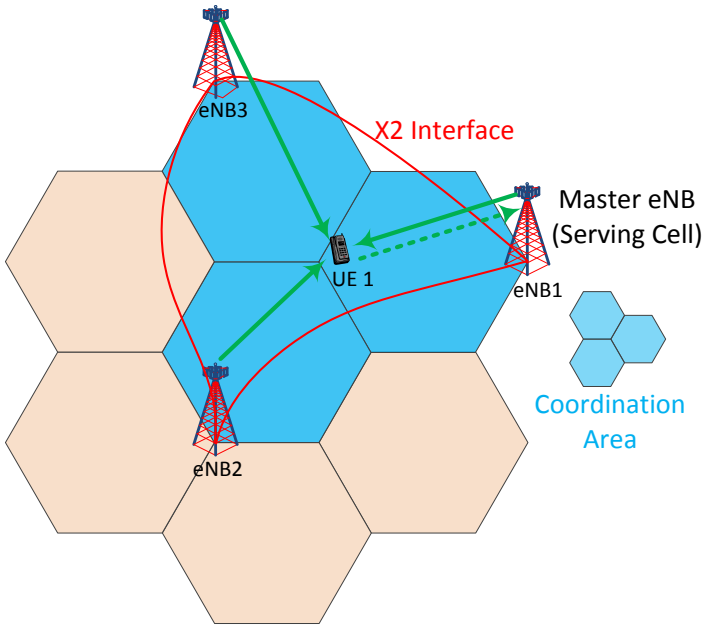

Figure 2.7: CoMP centralised scheduling

Distributed Scheduling

In distributed scheduling, the scheduling process is done independently and smartly by transmission points based on the CSI received from their cooperating eNBs. In this type of scheduling, usually a small amount of coordination information exchange is needed across the cooperating points. This type of scheduling is more suitable for heterogeneous deployments where we do not need an X2 interface. But in the case of a heterogeneous deployment having femtocells, it is a challenging task to do CoMP scheduling because femtocells can appear randomly.

2.4.8 Drawbacks of CoMP

The following are the downside of CoMP techniques:

- The radio spectrum from the cooperating cells are reserved to serve the neighbour CEUs, and hence the cooperating cells can not serve more users because of the lack of spectrum.
- The user data needs to be made available at the multiple coordinated transmission points in a joint transmission scheme which leads to overhead in the backhaul.
- The amount of data to be exchanged over coordination links is also large, e.g., the channel knowledge and the computed transmission weights. Therefore, synchronisation among the cooperating cells is a major concern.
- The coordinated beamforming CoMP technique provides less throughput gain compared with the joint transmission technique.

2.5 Inter-Cell Interference Solution by Scheduling in CoMP Transmission

2.5.1 Fixed Frequency Allocation

In [72], a fixed resource allocation plan was presented based on frequency partition. In the Fixed Frequency Allocation (FFA) scheme, the whole available frequency bandwidth in a cell is divided into two sets, as shown in Fig. 2.8, namely the CoMP Frequency Zone set to serve only the CEUs and Non-CoMP Frequency Zone set to serve only the CCUs. The size of the CoMP Frequency Zone is the same in each cell. This scheme suffers from throughput loss due to the lack of flexibility between different cells. Also, there might be a case where the resources in the CoMP Frequency Zone are left unused if there are not many CEUs.

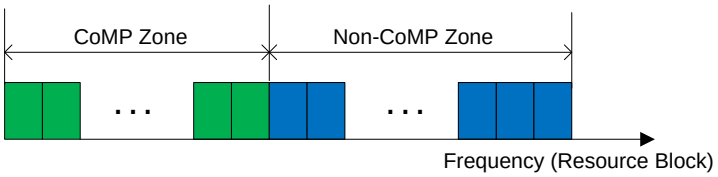

Figure 2.8: Fixed frequency allocation of CoMP

2.5.2 Flexible Frequency Allocation Plan

To further improve the system performance, a Flexible Frequency Allocation Plan (FlexFAP) has been presented in [73]. In the FlexFAP scheme, each cell has its particular CoMP frequency zone based on the proportional relationship of the sum of CEUs and the total users. The ratio of a CoMP frequency zone is calculated as [73]:

$$f_{CoMP} = \frac{N_{CEUs}}{N_{CEUs} + N_{CCUs}}\beta, \tag{2.2}$$

where N_{CEUs} and N_{CCUs} represent the number of cell-edge and cell-centre users, respectively, f_{CoMP} represents the CoMP frequency band partition ratio and β represents a scaling factor to adjust the size of the allocated frequency band to the CEUs. The cells which have more CEUs need to be allocated more CoMP frequency resource and vice versa. Once there is a frequency zone partition, some of the resources must be assigned to a fixed transmission mode and this causes performance loss of the system.

2.5.3 Cooperative Frequency Reuse

In [74], a Cooperative Frequency Reuse (CFR) scheme has been proposed based on the partition of the cell-edge region. The cell-edge area of each cell is divided into six cell-edge zones as shown in Fig. 2.9. In each cell, all frequency resources are divided into two sets, say G and F. The resources in set G are used for the CCUs, while the resources in set F are used for CEUs. Set F is further divided into three subsets, say F_1, F_2 and F_3. The subset F_i is used to serve the neighboring CEUs of Cell i in CCS with cooperation, while the subset F_j and F_k are used to serve their own CEUs in cooperation with Cell j and Cell k, respectively, $\forall i, j, k \in \{1, 2, 3 \| i \neq j \neq k\}$, as illustrated in the Fig. 2.9.

As shown in Fig. 2.9, UE 1 of Cell 1 is at the cell-edge boundary with Cell 3, while UE 2 of Cell 2 is at the cell-edge boundary with Cell 1. Cell 1 will serve the neighboring CEU of Cell 2, i.e., UE 2 with frequency subset F_1, while its own CEU, i.e., UE 1, which is at the boundary with Cell 3, will be served with frequency subset F_3.

Practically, the partition of a cell area is not feasible since the coverage area does not have any regular shape. Also, we may not know the channel quality of each of the frequency resources in the subsets in advance, which leads unfair to the CCUs and CEUs. In addition, there is no flexibility among

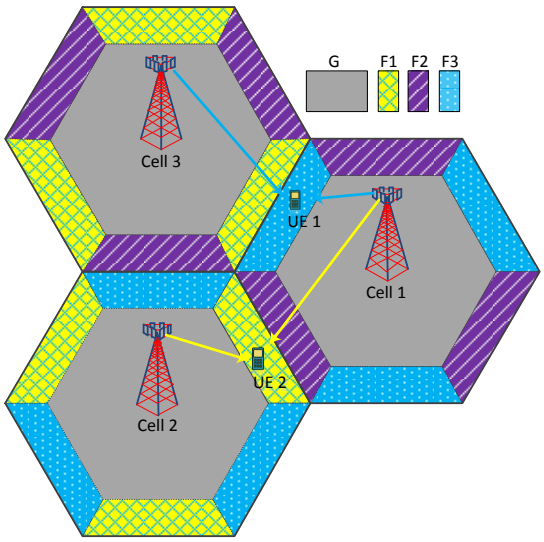

Figure 2.9: Cooperative frequency reuse

the frequency subsets and we can not guarantee that all the frequency resources in the subsets will be fully utilised.

2.5.4 Joint Proportional Fairness Allocation

To further improve the system performance and maintain the fairness of resource allocation among CEUs and CCUs without partition of frequency, a Joint Proportional Fairness (JPF) allocation scheme has been presented in [75]. The JPF scheme provides frequency diversity gain by enabling equal opportunities for both CEUs and CCUs to transmit in every time-frequency resource. The algorithm provides proportional fairness when all of the UE are experiencing the same channel conditions, which is generally not possible in real systems [76]. Also, to maximise revenue, service providers may prefer to maximise total cell throughput.

2.5.5 Proposed Joint Maximum Throughput Allocation

The FR is a traditional technique to avoid ICI by using different frequency bands in one cell compared to other neighbour cells as described in earlier sections. That is, the total available frequency band (the total number of RBs in the context of LTE) is divided into different groups and each group is restricted in terms of by defined types of users, such as CCUs or CEUs in a cell. Although, the FR technique provides high users' throughput by avoiding the ICI problem, it reduces the overall throughput of the cell or system. This is because only part of the total frequency spectrum is available to be used by the cell. For example, suppose the available frequency spectrum is 10 MHz, which means there are 50 RBs. In the case of FR3, a cell can have only $50/3 \approx 17$ RBs to be used by users in the cell. Let us say, $R_1 = \{1, 2, 3, \ldots, 16, 17\}$ is the set of RBs available in Cell 1, $R_2 = \{18, 19, 20, \ldots, 33, 34\}$ for Cell 2 and $R_3 = \{35, 36, 37, \ldots, 49, 50\}$ for Cell 3. Now, if we further restrict some part of the RBs to be assigned only for CEUs or CCUs, the following issues arise from the perspective of efficient use of the spectrum:

- The spectrum is not being efficiently utilised in each cell, because only 1/3 is available in each cell.
- The spectrum is divided in groups in advance to be assigned in each cell without knowing the channel quality of each sub-carrier or an RB, which may not be the best spectrum group suitable for the cell.
- Under CoMP scenario, there is no flexibility of the spectrum to be used among the CCUs and the CEUs. That is, each user is restricted to use the RB from the defined set.
- Also, in order to serve a CEU under CoMP transmission technique, each cooperating cell must have common RBs to transmit data together for a user.

It is well-known that the radio spectrum is a limited resource and is, therefore, very expensive. The cellular service providers definitely want to utilise their available spectrum more efficiently satisfying the high data rate demands of their customers. Hence, considering the efficient utilisation of the limited frequency spectrum, this thesis has considered FR1. That is, all the available spectrum (i.e., 50 RBs) are available in each cell and both the CCUs and the CEUs have equal chance to use any RBs.

By inheriting the idea of fairness among CEUs and CCUs from JPF allocation scheme in [75] without partition of available resources, a novel Joint Maximum Throughput (JMT) allocation algorithm based on the maximum throughput is proposed. In this algorithm, users are scheduled based on the joint maximum throughput. The CEUs are scheduled as CoMP transmission mode, whereas CCUs are as Non-CoMP transmission mode. The algorithm is described in detail in Chapter 3.

Chapter 3:

Resource Scheduling and Modelling of a Dynamic System Level Simulator

In Chapter 2, a literature review of interference avoidance techniques in Non-CoMP and CoMP transmission schemes was discussed. Based on that review, a novel resource scheduling algorithm called JMT was introduced.

In this chapter, the proposed resource scheduling algorithm will be discussed and the design of a network simulator will be described. In order to evaluate the performance of CoMP transmission, an event-driven dynamic System Level Simulation (SLS) tool was used. The features of CoMP transmission were implemented using this tool. The tool models the downlink communication of OFDMA based networks, i.e., LTE. Here, a general overview and methodology of modelling the network performance in this dynamic SLS tool are described.

3.1 Network Notations

For the sake of clarity of the resource allocation algorithm and the modelling of a dynamic SLS tool, let us introduce some general notations. Note that these notations will be subsequently used in the following chapters through out the thesis. Let

- M be the number of cells in a network,
- $\mathcal{M} = \{1, 2, \ldots, i, \ldots, j, \ldots, m, \ldots, M\}$ be the set of all cells in the network,
- U^m be the maximum number of users in cell m,
- $\mathcal{U}^m = \{1, 2, \ldots, u, \ldots, U^m\}$ be the set of all users in cell m,
- $\mathcal{U}^m_{ccu}$ be the set of all CCUs in cell m,
- $\mathcal{U}^m_{ceu}$ be the set of all CEUs in cell m,
- R be the number of RBs in a cell,
- $\mathcal{R} = \{1, 2, \ldots, r, \ldots, R\}$ be the set of RBs in a cell,
- K be the number of Modulation and Coding Schemes (MCSs),
- $\mathcal{K} = \{1, 2, \ldots, k, \ldots, K\}$ be the set of MCSs as shown in Table 3.1 [77,78],
- C be the number of CoMP clusters in the network, i.e., the number of cooperating sets,
- $\mathcal{C} = \{1, 2, \ldots, c, \ldots, C\}$ be the set of CoMP clusters in the network,
- Ω^m_u be the CCS of user u connected to cell m, where $\Omega^m_u \in \mathcal{C}$ and $\Omega^m_u \subset \mathcal{M}$,
- N be the cardinality of the set Ω^m_u, i.e., $N = \|\Omega^m_u\|$ be the number of cooperating cells in the set Ω^m_u,
- $\overline{\Omega^m_u} = \mathcal{M} - \Omega^m_u$ be the set of interfering cells for user u connected to cell m,
- γ^m_u be the Pilot SINR of user u connected to cell m,
- γ_{edge} be the SINR threshold for cell-edge user decision,
- $\mathcal{RSRP}^m_u$ be the set of RSRPs of user u connected to cell m,
- $RSRP^{m,i}_u$ be the RSRP from cell i to user u connected to cell m,
- $T^m_{u,r}$ be the throughput of user u in subchannel r connected to cell m,

- $\tilde{T}_u^m$ be the average throughput of user u connected to cell m,
- $\mathcal{T}_{ccu}^m$ be the set of throughput of CCUs in cell m,
- $\mathcal{T}_{ceu}^c$ be the set of throughput of CEUs in cluster c,
- λ_u^m be the mean call arrival rate of user u in cell m,
- t_u^m be the mean call holding time of user u in cell m,
- μ_u^m be the mean service rate $(1/t_u^m)$ of user u in cell m,
- $p_{u,r}^m$ be the transmit power for user u on subchannel r from cell m,
- $g_{tx}^m(\theta, \phi)$ be the transmit antenna gain from cell m to the user situated at angles of (θ, ϕ), where θ and ϕ are polar and azimuth angles respectively,
- $g_{u,rx}$ be the receive antenna gain of user u,
- α_r^m be the subchannel, r, allocation indicator in cell m,

3.2 Resource Scheduling Algorithm

The process of allocation of radio resources such as frequency, time and power to UE in cellular networks is termed as *scheduling*. Four types of resource scheduling algorithms are implemented and compared in Non-CoMP and CoMP transmission schemes.

3.2.1 Proposed Joint Maximum Throughput Based Scheduling under CoMP Transmission

By inheriting the idea of fairness among CEUs and CCUs from JPF allocation scheme in [75] without partition of available resources, a novel JMT scheduling algorithm based on the maximum throughput is proposed. In this algorithm, users are scheduled based on the joint maximum throughput. CEUs are scheduled as CoMP transmission mode, whereas, CCUs as Non-CoMP transmission

mode. The flowchart of the proposed algorithm is shown in Fig. 3.1 and the algorithm is described in detail in Algorithm 1.

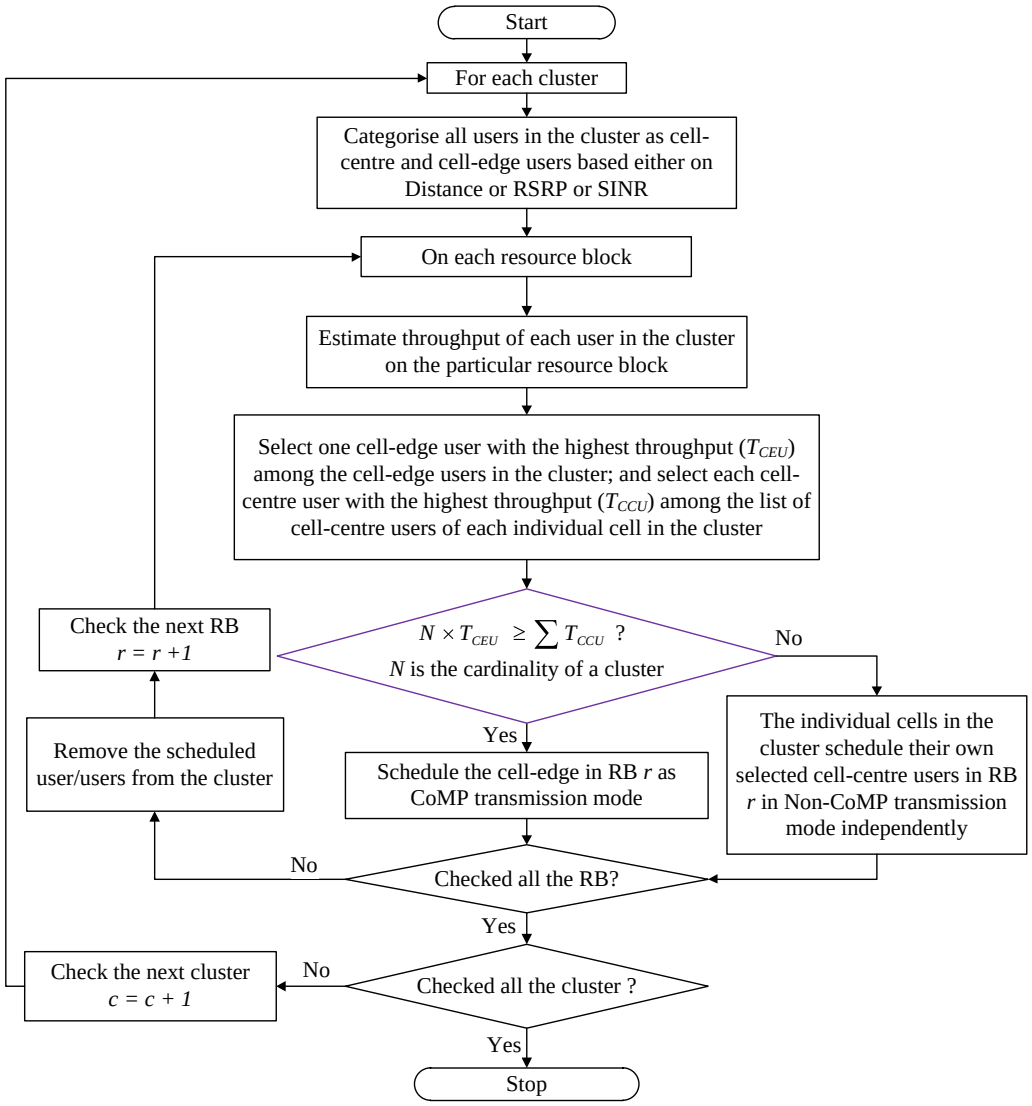

Figure 3.1: Flowchart of the proposed JMT scheduling

Algorithm 1 Proposed JMT based scheduling algorithm under CoMP transmission

1: **for** a cluster $c \in \mathcal{C}$ **do**,

2: categorise all UE of cell $m \in c$ as CCUs and CEUs as follows

- if the cell-edge decision is based on the pilot absolute SINR:

$$\mathcal{U}_{ccu}^{m} = \{u : \gamma_u^m > \gamma_{th}\} \quad \text{and} \quad \mathcal{U}_{ceu}^{m} = \{u : \gamma_u^m \leq \gamma_{th}\},$$

- if the cell-edge decision is based on the pilot relative RSRP:

$$\mathcal{U}_{ccu}^{m} = \{u : P_s - P_n > P_{edge}\} \quad \text{and} \quad \mathcal{U}_{ceu}^{m} = \{u : P_s - P_n \leq P_{edge}\},$$

- if the cell-edge decision is based on the absolute distance:

$$\mathcal{U}_{ccu}^{m} = \{u : d_u^m < d_{edge}\} \quad \text{and} \quad \mathcal{U}_{ceu}^{m} = \{u : d_u^m \geq d_{edge}\}.$$

3: **for** a subchannel $r \in \mathcal{R}$ **do**,

4: initialize the sets: $\mathcal{T}_{ccu}^{m} \leftarrow \emptyset$ and $\mathcal{T}_{ceu}^{c} \leftarrow \emptyset$, $\forall m \in c$.

5: estimate the throughput, $T_{u,r}^{m}$, of each CCU u in the cluster c on the subchannel r and store as

$$\mathcal{T}_{ccu}^{m} \leftarrow \mathcal{T}_{ccu}^{m} \cup \left\{T_{u,r}^{m}\right\}, \quad \forall u \in \mathcal{U}_{ccu}^{m} \text{ and } \forall m \in c.$$

6: estimate the throughput, $T_{u,r}^{m}$, of each CEU u in the cluster c on the subchannel r and store as

$$\mathcal{T}_{ceu}^{c} \leftarrow \mathcal{T}_{ceu}^{c} \cup \left\{T_{u,r}^{m}\right\}, \quad \forall u \in \mathcal{U}_{ceu}^{m} \text{ and } \forall m \in c.$$

7: choose one best CCU from each cell in the cluster c as

$$\left\{T_{u,r}^{m}\right\} \leftarrow \max(\mathcal{T}_{ccu}^{m}), \quad \forall m \in c, u \in \mathcal{U}_{ccu}^{m}.$$

8: choose one best CEU from the cluster c as

$$T_{u,r}^{i} \leftarrow \max(\mathcal{T}_{ceu}^{c}), \quad i \in c, u \in \mathcal{U}_{ceu}^{i}.$$

Algorithm 1 Proposed JMT based scheduling algorithm under CoMP transmission (continued)

if $N \cdot T^i_{u,r} \geq \sum_{m \in c, u \in \mathcal{U}^m_{ccu}} T^m_{u,r}$, where $N = \|c\|$ **then**

schedule CEU u from cell i on subchannel r under CoMP transmission mode, where all cells in cluster c serve this user.

remove the scheduled UE from the set as

$$\mathcal{U}^i_{ceu} \leftarrow \mathcal{U}^i_{ceu} - \{u\},$$

else

each cell in cluster c schedules its own CCU u on the subchannel r independently under Non-CoMP transmission scheme.

remove the scheduled UE from the sets as

$$\mathcal{U}^m_{ccu} \leftarrow \mathcal{U}^m_{ccu} - \{u\}, \quad \forall m \in c.$$

end if

remove the scheduled subchannel r from the set as

$$\mathcal{R} \leftarrow \mathcal{R} - \{r\}.$$

if $\mathcal{R} \neq \emptyset$ **then**

repeat from step 3 for the remaining UE in the cluster c.

else

repeat from step 1 for remaining clusters in the system.

end if

end for ▷ end for subchannel loop

end for ▷ end for cluster loop

3.2.2 Proportional Fair Based Scheduling under Non-CoMP Transmission

The Proportional Fair (PF) scheduling algorithm is a well-known algorithm and widely used in cellular networks. According to the PF algorithm [76, 79–81], a subchannel in a cell is assigned to a UE which provides the highest proportional throughput weight compared with other UE in the cell. That is, the PF algorithm assigns subchannel r to UE u in cell m at scheduling instant t as [76, 79, 81]

$$\{u, r\} \leftarrow \arg \max_{1 \leq u \leq U^m} \left\{ \frac{T^m_{u,r}(t)}{\tilde{T}^m_u(t-1)} \right\}, \tag{3.1}$$

where $T^m_{u,r}(t)$ is the instantaneous throughput of UE u on subchannel r at the current scheduling instant t and $\tilde{T}^m_u(t-1)$ is the past average throughput of the UE. The average throughput is updated following exponential weighted moving average of the instantaneous data rate as [76, 81]

$$\tilde{T}^m_u(t) = \begin{cases} \left(1 - \frac{1}{t_a}\right) \tilde{T}^m_u(t-1) + \frac{1}{t_a} T^m_{u,r}(t), & \text{if } u \text{ is scheduled} \\ \left(1 - \frac{1}{t_a}\right) \tilde{T}^m_u(t-1), & \text{otherwise} \end{cases}, \tag{3.2}$$

where $t_a = 10$ is a time-constant window size. The implementation of the Non-CoMP algorithm PF is shown in Algorithm 2 in Appendix A.

3.2.3 Maximum Throughput Based Scheduling under Non-CoMP Transmission

The Maximum Throughput (MT) scheduling algorithm operates directly proportional to the supported throughput [82]. The algorithm provides the maximum total cell throuhgput by maximising the subchannel throughput. According to the MT algorithm, a subchannel r is assigned to a UE u which provides the maximum throughput as [82]

$$\{u, r\} \leftarrow \arg \max_{1 \leq u \leq U^m} \left\{ T^m_{u,r}(t) \right\}, \tag{3.3}$$

where $T^m_{u,r}(t)$ is the instantaneous throughput of UE u on subchannel r at the scheduling instant t. Since the throughput maps with the SINR, this scheduler is equivalent to a maximum SINR scheduler. The implementation of the Non-CoMP algorithm MT is shown in Algorithm 3 in Appendix A.

3.3 Simulation Assumptions

Without the loss of generality, the following assumptions are made in order to assess the functionality of an OFDMA based network:

1. There is always data available to be transmitted to all users. That is, a full buffer based traffic model is employed in order to simulate the downlink traffic of users [83].
2. Inter-Cell Interference (ICI) will occur only when several users are allocated to the same subchannel at the same time in different cells [84].
3. The coherence bandwidth of a channel is larger than the subchannel bandwidth, hence the fading of all subcarriers within a subchannel due to multipath is constant and flat [84].

These assumptions are widely used to evaluate the system level performance of a network [84, 85].

3.4 Traffic Behaviour Model

In the tool, users are generated in two different ways as described below:

1. Fixed: A fixed number of users are uniformly distributed within the coverage area of each cell and stay in the network until the end of the simulation. This type of traffic generation is used to evaluate the performance of data services, where we can consider that there is always a fixed number of busy users [84].

2. Poisson process: Users in a cell m are generated uniformly according to a homogeneous Poisson process with the mean arrival rate, λ_u^m, and the mean holding time, $1/\mu_u^m$. The inter-arrival time between users and the mean holding time of a user are exponentially distributed random variables with a probability density function given by [84]

$$f(t;\eta) = \eta e^{-\eta t}, \tag{3.4}$$

where η is the rate parameter such as λ_u^m for the arrival rate and μ_u^m for the holding time. This type of traffic generation is used to evaluate the performance of voice services, where calls in the network are coming and going according to a random process.

Two different ways of computing user load in a cell has been generated. In the Fixed case, the total number of generated users in the whole network remains the same until the end of the simulation period. This type of user load in a network has been considered to evaluate the performance of the algorithm when the traffic load is not fluctuating, i.e., the traffic in the network is stable. In the Poisson case, users are generated uniformly according to a homogeneous Poisson process with a mean arrival rate; and stay in the network until a mean holding time. Both the inter-arrival time between users and the mean holding time of a user are exponentially distributed. This type of user load in a network has been considered to evaluate the performance of the algorithm when the traffic load is fluctuating, i.e., the traffic in the network is varying. In both cases, the performance is evaluated by session based simulation. The actual packet is not generated. Instead, it is considered that a user transmits data during a session time. A full buffer of traffic is considered, which means there is always data available for the user to transmit during the session time.

The following are some of the traffic models which are used to capture the major Internet traffic applications such as video and Web browsing:

- Best effort File Transfer Protocol (FTP) traffic model
- Web browsing Hyper Text Transfer Protocol (HTTP) traffic model
- Video streaming traffic model

The detail information of these traffic models are described in Appendix C.

3.5 User Location Modelling

The prediction of a user's location during an arrival in a cell is modelled based on two parameters: the angle from the antenna's boresight to the line joining the cell-site and the user, and the distance of the user from the cell-site. As illustrated in Fig. 3.2, the dotted arrows indicate the antenna's boresight in each cell. An angle in the clock-wise direction from the antenna's boresight represents a positive angle, while the counter-clockwise direction is a negative angle. Hence, the maximum angle from the antenna's boresight of a user in a cell is ± 60 degrees. Let us suppose ϕ is a random variable of an angle in the range from 0 to 59 degrees. We use a uniformly distributed random variable between 0 and 1 to select which side of the antenna's boresight a user is located. If the selected number is ≤ 0.5, we suppose it is counter-clockwise from the antenna's boresight, and clock-wise if the number is > 0.5. The distance of this user from the centre of the cell-site is also estimated using a uniformly distributed random variable in the range d_{min} to d, where d is the half of the inter-site distance and d_{min} (35 m) is chosen as the minimum distance between the user and the base station to avoid the near-field effect from the base station. A snapshot of user distribution in the network in the steady state considering users mobility obtained by simulation is shown in Fig. 3.3.

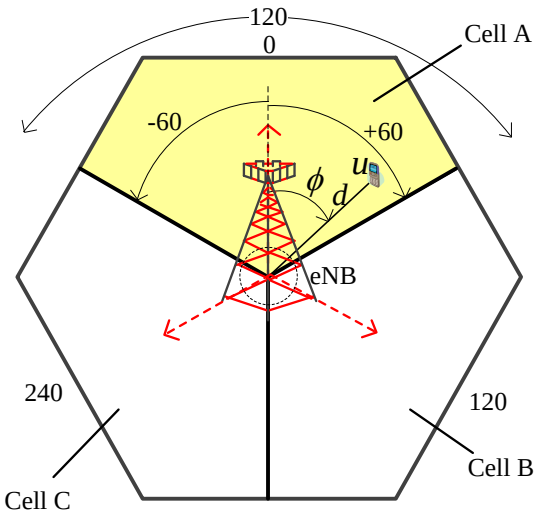

Figure 3.2: Prediction of user's location during arrival

3.6 User Mobility Modelling

A user at one location may be categorised as a CCU, while at an other location it would be a CEU. The category of a user as a CCU or a CEU directly affects on the performance of a CoMP technique. Therefore, to articulate the performance of the proposed algorithm considering every possible location inside a cell area, the user's location should be changed. Hence, the motivation behind the mobility of a user considered in this thesis is just to evaluate the performance of CoMP at every possible location inside a cell and therefore, intra-site mobility is considered. The intra-site mobility situation appears in real scenarios because sometimes users move but are still under the coverage of the current serving cell. But if we consider inter-cell mobility, then a handover algorithm under a CoMP scenario is needed. Because at the cell-edge boundary users might be under service as CoMP mode, receiving signals from more than once cell. To successfully handover the ongoing service to the neighbour cell or cells, we need a handover algorithm under a CoMP scenario. Since the

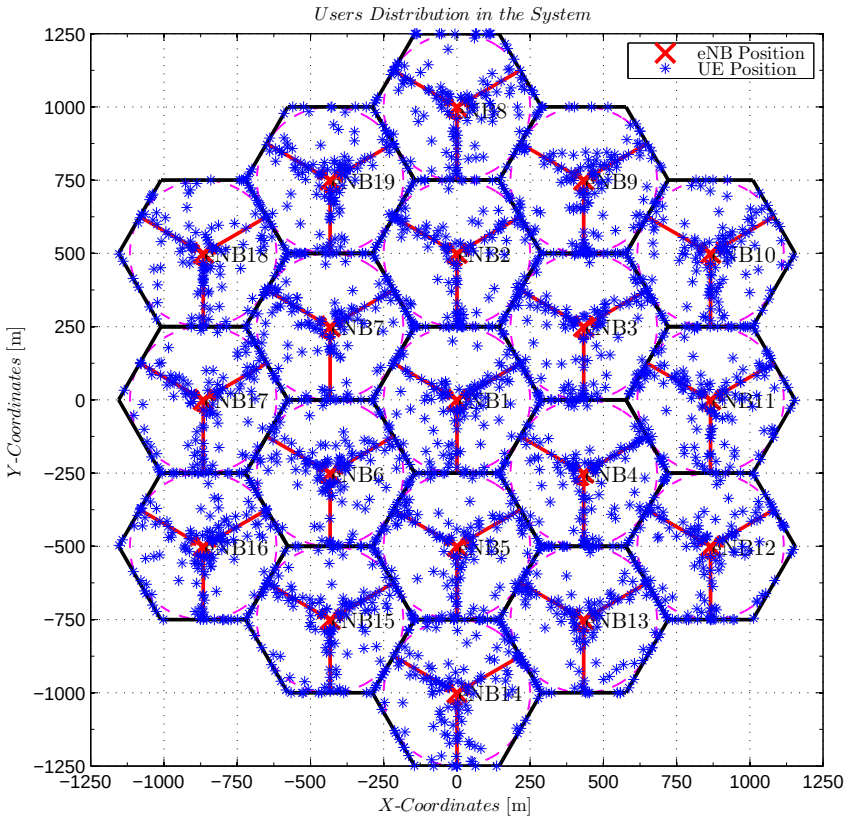

Figure 3.3: A snapshot of users distribution in the system in the steady state obtained from simulation

handover is out of scope of this thesis, hence intra-site mobility is considered. If we consider inter-site mobility, the proposed algorithm has noting to do with mobility because after successful of handover the user will be under the influence of a new cluster and the new cluster will take care of the scheduling process.

User movement within a cell has been modelled as a random direction [86]. That means, users from the current position move to a new position with a defined speed along a random direction, and this random direction is taken with reference to the vertical direction (Y-axis) in the two-dimensional plane. The movement of users is restricted within their serving cells, which means that

inter-cell movement of users is not allowed, since a handover technique is not considered, which is out of scope of this thesis. The purpose of user movement is to consider the effect of distance variation in the receivers' signal strength. To check whether a user has travelled beyond a confined cell boundary or below the minimum distance, we compare its new distance from the base station with the minimum and maximum distance a user can be inside a cell away from its base station as well as the azimuth angle of the user in reference to the antenna's boresight.

After using geometrical analysis and considering different possibilities of user locations, as shown in Fig. 3.4, it can be generalised that the azimuth angle (ϕ) of a user from the vertical plane of the serving base station antenna's boresight within the cell can be expressed as

$$\phi = \frac{\pi}{2} - \beta - m, \tag{3.5}$$

where β is the bearing angle of an antenna's boresight from the north direction as clockwise in the spherical coordinates (i.e., from Y-axis as clockwise in two-dimensional plane) and m is the slope of the line between the user's position and the base station with reference to the X-axis as counter-clockwise, which are given as

$$\beta = \begin{cases} 0, & \text{Bearing angle for Cell A} \\ \frac{2\pi}{3}, & \text{Bearing angle for Cell B} \\ \frac{4\pi}{3}, & \text{Bearing angle for Cell C} \end{cases}, \tag{3.6}$$

and

$$m = \begin{cases} \pi \pm m, & \text{if } m \text{ is negative value in case of } \beta = 0 \\ \pm m, & \text{in case of } \beta = \frac{2\pi}{3} \\ -\pi \pm m, & \text{in case of } \beta = \frac{4\pi}{3} \end{cases}. \tag{3.7}$$

To clarify, let us take examples of a user's movement within a cell as shown in Fig. 3.4. Suppose a user u is located at position $P_1(x_1, y_1)$ in Cell A at an instant of time t_1 seconds. The azimuth angle (ϕ) of this user from the

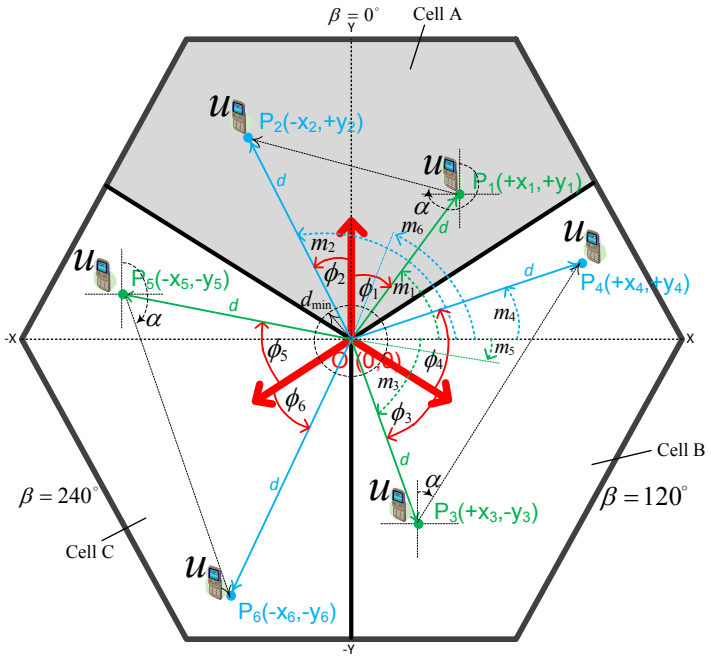

Figure 3.4: User mobility modelling

antenna's boresight direction is ϕ_1. According to the convention of ϕ angle with reference to the antenna's boresight, the angle ϕ_1 is in a clockwise direction and hence its value should be positive. By using trigonometric analysis, the slope of the line between the user at position P_1 and the base station located at origin O with reference to the X-axis in a counter-clockwise direction is $m_1 = \tan^{-1}(y_1/x_1)$ radians. Hence, the azimuth angle of the user u located at position P_1 from the antenna's boresight direction is $\phi_1 = \pi/2 - m_1$ radians, which can also be evaluated directly from Eq. 3.5. Since the slope of the user at position P_1 has a positive value and the bearing angle of Cell A is 0, using Eq. 3.5 we can obtain $\phi_1 = \pi/2 - 0 - m_1 = \pi/2 - m_1$.

Now suppose that the user u from the current position P_1 moves along any random direction between 0 and 360 degrees with an average speed of v m/sec. Suppose α is a uniformly distributed random number between 0 and 360 degrees, and the user u moves to a new position $P_2(x_2, y_2)$ in a time interval

$\Delta t = t_2 - t_1$. Then, the new coordinates of the user u can be written as

$$x_2 = x_1 + (\Delta t \cdot v)\cos(\pi/2 - \alpha),$$
$$y_2 = y_1 + (\Delta t \cdot v)\sin(\pi/2 - \alpha). \tag{3.8}$$

The slope of the line between the new position P_2 and the base station with reference to the X-axis is $m_2 = \tan^{-1}(y_2/x_2)$ radians. Therefore, the azimuth angle of the user u at the new location P_2 from the antenna's boresight direction is $\phi_1 = \pi/2 - m_2$ radians. Note that the value of m_2 in this case will be either negative or above $\pi/2$. Hence, the value of ϕ_2 in this case will be negative which is in line with the convention of an azimuth angle since the new position P_2 is counter-clockwise from the antenna's boresight.

Now let us consider the case of Cell B. A user u is currently at position P_3 at a time instant t_3 seconds. The slope of the line OP_3 with reference to the X-axis is $m_3 = \tan^{-1}(y_3/x_3)$. For a numerical example, let us suppose $m_3 = -70$ degrees in this case. Then, using Eq. (3.5), the azimuth angle $\phi_3 = \pi/2 - \beta - m_3 = 90 - 120 - (-70) = 40$ degrees which is right as the user is clockwise from the antenna's boresight. Now the user moves to a new position P_4 in the time interval $\Delta t = t_4 - t_3$. Then, the new coordinates of the user at position P_4 can be written as

$$x_4 = x_3 + (\Delta t \cdot v)\cos(\pi/2 - \alpha),$$
$$y_4 = y_3 + (\Delta t \cdot v)\sin(\pi/2 - \alpha). \tag{3.9}$$

The slope of the line OP_4 with reference to the X-axis is $m_4 = \tan^{-1}(y_4/x_4)$ radians. For a numerical example, let us suppose $m_4 = 20$ degrees in this case. Therefore, using Eq. (3.5), the azimuth angle $\phi_4 = \pi/2 - \beta - m_4 = 90 - 120 - (20) = -50$ degrees which is right as the user is counter-clockwise from the antenna's boresight.

In a similar way, we can check the azimuth angle of users inside Cell C. Now once we obtain the user's azimuth angle, we are able to decide whether

the user has travelled within the cell or outside the cell by checking the user's azimuth angle in the range of -60 to $+60$ degrees. If the user's azimuth angle falls within this range, then the user is still inside the cell, otherwise it has travelled outside the cell and hence we need to restrict the user to stay at the boundary or return back from the boundary. However, there is a possibility that the user has travelled below the minimum distance (d_{min}) or beyond the maximum distance ($D/2$ and R_h). If this happens, we restrict the user either to stay on the limit distance or return back within the cell.

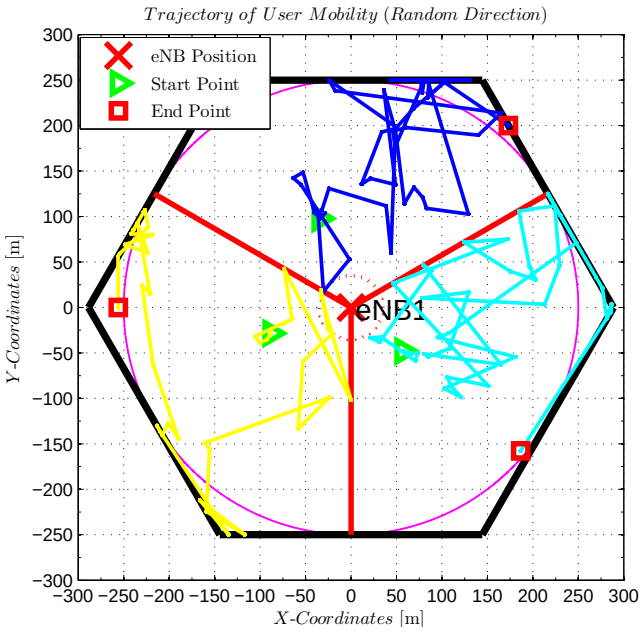

Figure 3.5: A snapshot of trajectory for user movement within a cell according to random direction mobility model

A snapshot of users movement within their respective serving cells obtained by simulation is shown in Fig. 3.5. For illustration purpose of the trajectory path of a user's mobility, the snapshot has been obtained by simulation of one user in each cell for a period of 1 hour. The average speed of user movement was considered as 3 km/h. The inter-log time of user movement was taken as an exponential distribution with the mean time of 60 s. That is, the time to

take log of the user movement is exponentially distributed with a mean time of 60 s.

3.7 Antenna Radiation Pattern Model

The antenna radiation pattern for the sectorial antennas follows according to the model proposed in the 3GPP standard [29] as:

- horizontal antenna pattern:

$$A_H(\phi) = -\min\left[12\left(\frac{\phi}{\phi_{3dB}}\right)^2, A_{h,max}\right], \phi_{3dB} = 70^\circ, A_{h,max} = 25 \text{ dB}, \tag{3.10}$$

- vertical antenna pattern:

$$A_V(\theta) = -\min\left[12\left(\frac{\theta - \theta_{etilt}}{\theta_{3dB}}\right)^2, A_{v,max}\right], \theta_{3dB} = 10^\circ, A_{v,max} = 20 \text{ dB}, \tag{3.11}$$

- 3D antenna pattern:

$$A(\phi, \theta) = -\min\{-\left[A_H(\phi) + A_V(\theta)\right], A_{h,max}\}, \tag{3.12}$$

where A_H and A_V represent the attenuation offsets introduced by the horizontal and vertical antenna patterns with respect to maximum antenna gain, respectively. ϕ and θ represent the angles in the horizontal and the vertical plane, respectively, between a cell and a user; θ_{etilt} is the electrical tilt angle, i.e., the angle between the axis of the radiation of the main lobe of the the vertical antenna pattern and the horizontal plane; θ_{3dB} represents the half power antenna beam width; and $A_{h,max}$ and $A_{v,max}$ represent the maximum offset of the pattern in the horizontal and the vertical plane respectively.

3.8 Channel Model

The medium between the transmit and receive antennas is known as the *channel*. The characteristics of a radio signal change as it travels from the transmitter antenna to the receiver antenna and depend upon parameters such as distance between these two antennas, propagation scenario (e.g., outdoor-to-outdoor, outdoor-to-indoor, indoor-to-indoor, etc.) and the surrounding environment (e.g., buildings, trees, etc). The received signal can be estimated if we have a suitable model of the medium. This model of the medium is called a *channel model*. The radio channel propagation is typically modelled as the combination of three main effects: mean path loss, shadowing generally characterised as log-normal [87,88] and fading typically taken as Rayleigh [89].

3.8.1 Path Loss Model

Path loss is the distance-dependent mean attenuation of a signal as it propagates through space. A suitable model of path loss depends on parameters such as the type of environment (e.g., macrocell, microcell, indoor, etc.), the propagation medium (e.g., outdoor-to-outdoor, outdoor-to-indoor, indoor-to-indoor, etc.), the carrier frequency and distance. The path loss model recommended by 3GPP [29] for outdoor macrocells at a carrier frequency of 2 Giga Hertz (GHz) is given as

$$(l_u^m)_{dB} \quad = \quad 128.1 + 37.6 \log_{10}(d_u^m), \tag{3.13}$$

where l_u^m is the path loss in dB from macrocell m to user u and d_u^m is the distance in kilometres from macrocell m to user u.

3.8.2 Shadow Fading Model

In reality, clutter from objects such as buildings, trees, terrain conditions along the path of a signal differs for every path, and consequently signal attenuation varies from path to path. Shadow fading is used to model fluctuations in the path loss due to such obstacles between a mobile and a base station [87]. Shadow fading is also known as *slow fading* [90]. The effect of shadowing is commonly approximated by a log-normal distribution [90,91]. Accordingly, the shadow fading in the path between a BS and a UE can be *a priori* modelled using a log-normal random variable, $l_{sh} \sim \mathcal{N}(\mu, \sigma)$, where μ and σ are the mean and a standard deviation in dB, respectively. However, the modelling of shadow fading when considering the change of a user's position is more intricate due to spatial auto-correlation between paths. The shadow fading process is auto-correlated in space, meaning that a moving UE may see similar shadow fading attenuations from the same BS at different but nearby locations.

Auto-Correlation

A widely adopted auto-correlation model for shadow fading is the Gudmundson model [90], which defines the auto-correlation coefficient as follows

$$\rho_a(\Delta x) = \exp\left(-\frac{|\Delta x|}{d_{cor}} \ln 2\right), \tag{3.14}$$

where d_{cor} is the decorrelation distance (which is defined as the distance at which the correlation coefficient ρ_a falls to 0.5 [92]), and Δx is the distance between two positions.

The auto-correlation of shadow fading can be implemented as follows. If l^1_{sh} is the log-normal component, $\mathcal{N}(\mu, \sigma)$, in dB at position P_1, and l^2_{sh} is the log-normal component in dB at position P_2, which is Δx away from P_1, then l^2_{sh} can be modeled as a normally distributed random variable, l_{sh}, in dB with

a mean μ' and a standard deviation σ' as [92]

$$l_{sh} = l_{sh}^2 \sim \mathcal{N}(\mu\prime, \sigma\prime), \tag{3.15a}$$

$$\mu' = \rho_a(\Delta x) l_{sh}^1, \tag{3.15b}$$

$$\sigma' = \sqrt{(1-\rho_a^2(\Delta x))\sigma^2}. \tag{3.15c}$$

3.8.3 Multipath Fading Model

Owing to the presence of obstacles such as trees, buildings, terrain conditions, etc. between the path of a base station and a mobile station, multiple versions of the transmitted signal travel along different paths to reach the receiver, which cause rapid fluctuation in the received signal arising from the relative phase shifts. The fluctuation of the received signal due to the multi-path components is known as *fast fading* since the received signal varies rapidly. The fast fading gain between a base station and a UE is usually modelled as Rayleigh distribution [89]. Define ζ_u^m a random variable with a zero mean and σ standard deviation which follows Rayleigh distribution of path loss l_u^m. According to Rayleigh distribution, the fast fading gain of path loss l_u^m between a cell m and a UE u can be written as [89]

$$l_{fast} = \zeta_u^m = \frac{l_u^m}{\sigma^2} e^{-\frac{(l_u^m)^2}{2\sigma^2}}. \tag{3.16}$$

3.9 Signal Strength Model

Let us assume that uniform and equal transmission power is distributed on each sub-carrier. Assuming that all sub-carriers within an RB experience similar channel conditions, the strength of the carrier signal received by user u from

its serving cell m in subchannel r is modelled as [84]

$$\begin{aligned} S_{u,r}^{m} &= \sum_{m\in\Omega_u^m} \frac{p_{u,r}^{m} g_{tx}^{m}(\theta,\phi) g_{u,rx}}{l_u^m l_{sh} l_{fast} l_{eqp} l_{cab}} = \sum_{m\in\Omega_u^m} \frac{p_{u,r}^{m}}{l_{eqp} l_{cab}} \left[\frac{g_{tx}^{m}(\theta,\phi) g_{u,rx}}{l_u^m l_{sh} l_{fast}}\right], \\ &= \sum_{m\in\Omega_u^m} \frac{p_{u,r}^{m}}{l_{eqp} l_{cab}} g_u^m, \end{aligned} \tag{3.17}$$

where $S_{u,r}^{m}$ is the received power, $g_u^m = [g_{tx}^{m}(\theta,\phi) g_{u,rx}/(l_u^m l_{sh} l_{fast})]$ is the channel gain between user u and cell m, Ω_u^m is the set of cooperative cells for user u, $p_{u,r}^{m}$ is the transmit power in subchannel r from cell m, $g_{tx}^{m}(\theta,\phi)$ is the transmit antenna gain from cell m to user u situated at angles of (θ, ϕ) where θ and ϕ are the angles in the vertical and azimuth planes respectively from antenna's boresight, $g_{u,rx}$ is the receive antenna gain of user u, l_u^m is the path loss between user u and cell m, l_{sh} is the shadowing loss, l_{fast} is the fast fading loss, l_{eqp} and l_{cab} are the equipment and cable losses respectively.

3.10 Interference Model

If neighbour cells are serving their users in the same subchannels at the same time, inter-cell interference occurs. The strength of the interference received by user u, which is connected to cell m on subchannel r, from its neighbouring cell i is modelled as [84]

$$\begin{aligned} I_{u,r}^{m,i} &= \frac{p_{u,r}^{i} g_{tx}^{i}(\theta,\phi) g_{u,rx}}{l_u^i l_{eqp} l_{cab} l_{sh}} \alpha_r^i = \frac{p_{u,r}^{i}}{l_{eqp} l_{cab}} \left[\frac{g_{tx}^{i}(\theta,\phi) g_{u,rx}}{l_u^i l_{sh} l_{fast}}\right] \alpha_r^i, \\ &= \frac{p_{u,r}^{i}}{l_{eqp} l_{cab}} g_u^i \alpha_r^i, \end{aligned} \tag{3.18}$$

where $I_{u,r}^{m,i}$ is the interference received by user u on subchannel r from its neighbour cell i, and α_r^i is the subchannel allocation indicator given by

$$\alpha_r^i = \begin{cases} 1, & \text{if the subchannel } r \text{ is used in the cell } i \\ 0, & \text{otherwise} \end{cases}. \tag{3.19}$$

3.11 Signal Quality Model

The signal quality in terms of SINR for user u in subchannel r connected to cell m is modelled as [84]

$$\gamma_{u,r}^{m} = \frac{\sum_{m \in \Omega_u^m} \frac{p_{u,r}^{m}}{l_{eqp} l_{cab}} g_u^m}{\sum_{i \in \overline{\Omega_u^m}, i \neq m} \frac{p_{u,r}^{i}}{l_{eqp} l_{cab}} g_u^i \alpha_r^i + \sigma^2}, \tag{3.20}$$

where $\gamma_{u,r}^{m}$ is the SINR of user u in subchannel r connected to cell m and σ is the background thermal noise density which is additive white Gaussian noise.

3.12 Channel Quality Indicators

The quality of a signal received by a UE depends on the channel quality from the serving cell, the level of interference from other cells, and the noise level. For the downlink data transmissions, the eNB typically selects a modulation scheme and code rate depending on a prediction of the downlink channel conditions. An important input to this selection process is the Channel Quality Indicator (CQI) feedback transmitted by the UE in the uplink. CQI feedback is an indication of the data rate which can be supported by the channel, taking into account the SINR. In LTE-A, the UE can be configured to report CQIs to assist the eNB in selecting an appropriate MCS to use for the downlink transmissions. The CQI reports are derived from the downlink received signal quality, typically based on measurements of the downlink RS from the serving cell. The UE feed back regularly CQIs of each subchannel to its server to assess channel status, which is an input in making decision of scheduling resources.

3.13 Radio Access Bearer Efficiency Model

The Radio Access Bearer (RAB) is the entity responsible for transporting radio frames of an application over the radio access of a network. From the received CQI, the eNB selects a suitable MCS for each user, provided that the SINR satisfies the threshold for the MCS. The higher the SINR, the higher the order of MCS is used, satisfying the SINR threshold value required to achieve this MCS, and thereby providing a higher bit rate. The RAB efficiency (defined in 3GPP 36.213 in Table 7.2.3-1 [77]) is shown in Table 3.1.

Table 3.1: Modulation and coding schemes

MCS No.	Modulation Type	Code Rate	SINR Threshold (dB)	RAB Efficiency (bits/symbol)
k_1	QPSK	1/12	-6.5	0.15
k_2	QPSK	1/9	-4.0	0.23
k_3	QPSK	1/6	-2.6	0.38
k_4	QPSK	1/3	-1.0	0.60
k_5	QPSK	1/2	-1.0	0.88
k_6	QPSK	3/5	-3.0	1.18
k_7	16QAM	1/3	6.6	1.48
k_8	16QAM	1/2	10.0	1.91
k_9	16QAM	3/5	11.4	2.41
k_{10}	64QAM	1/2	11.8	2.73
k_{11}	64QAM	1/2	13.0	3.32
k_{12}	64QAM	3/5	13.8	3.90
k_{13}	64QAM	3/4	15.6	4.52
k_{14}	64QAM	5/6	16.8	5.12
k_{15}	64QAM	11/12	17.6	5.55

3.14 Bit Rate Model

Once an MCS is selected, the bit-rate of user u over the subchannel r is modelled as as [93]

$$BR_{u,r} = \eta_{r,k} \frac{N_r O_r}{\tau}, \tag{3.21}$$

where $BR_{u,r}$ is the bit-rate (bits/sec), $\eta_{r,k}$ is the RAB efficiency of the subchannel r on the selected MCS k, N_r is the number of sub-carriers in the subchannel r, O_r is the number of OFDM data symbols in the subchannel r in τ duration of a subframe.

3.15 Throughput Model

Once the bit-rate is known, the throughput of user u connected to cell m on the subchannel r can be modelled as [94]

$$T_{u,r}^{m} = BR_{u,r} \left(1 - \varepsilon \left(\gamma_{u,r}^{m}, k\right)\right), \tag{3.22}$$

where $T_{u,r}^{m}$ represents throughput of the user u in subchannel r connected to the cell m, $\varepsilon(\gamma_{u,r}^{m}, k)$ represents the Block Error Rate (BLER) suffered by the user u over the subchannel r connected to the cell m, which is a function of both its SINR, $\gamma_{u,r}^{m}$, and MCS, k.

3.16 Cell-Edge User Model

Users in a cell can be categorised into CEUs and CCUs. The decision of a user category is modelled in three different ways: distance from its respective serving cell centre and compared with the threshold distance, the pilot SINR received from its respective serving cell and compared with the threshold SINR, and the difference between the two strongest pilot RSRPs and compared with

the RSRP threshold. Accordingly, a UE u is a CEU if it satisfies the following relation

$$\text{for distance based cell-edge decision:} \quad d_u^m \geq d_{edge}, \tag{3.23a}$$

$$\text{for SINR based cell-edge decision:} \quad \gamma_u^m \leq \gamma_{edge}, \tag{3.23b}$$

$$\text{for RSRP based cell-edge decision:} \quad P_s - P_n \leq P_{edge}, \tag{3.23c}$$

where d_u^m is the distance of the UE u from its serving cell m; d_{edge} is the threshold distance; γ_u^m is the pilot SINR of user u connected to cell m; γ_{edge} is the SINR threshold; $P_s - P_n$ is the difference between the two strongest pilot RSRP signals where P_s and P_n are the pilot power from the serving cell and the strongest neighbour cell, respectively; and P_{edge} is the RSRP threshold.

3.17 User Status Flow Model

A general overview of the simulation model is shown in flowchart Fig. 3.6. The status of users in the system is modelled as described below. A user passes through the following stages before success:

- Blocked/No Resource: if all resources are already occupied.
- No Coverage: the user has the resource but the received signal strength is less than the required receiver sensitivity.
- No RAB: if the user's SINR does not satisfy the minimum required SINR to get a particular MCS.

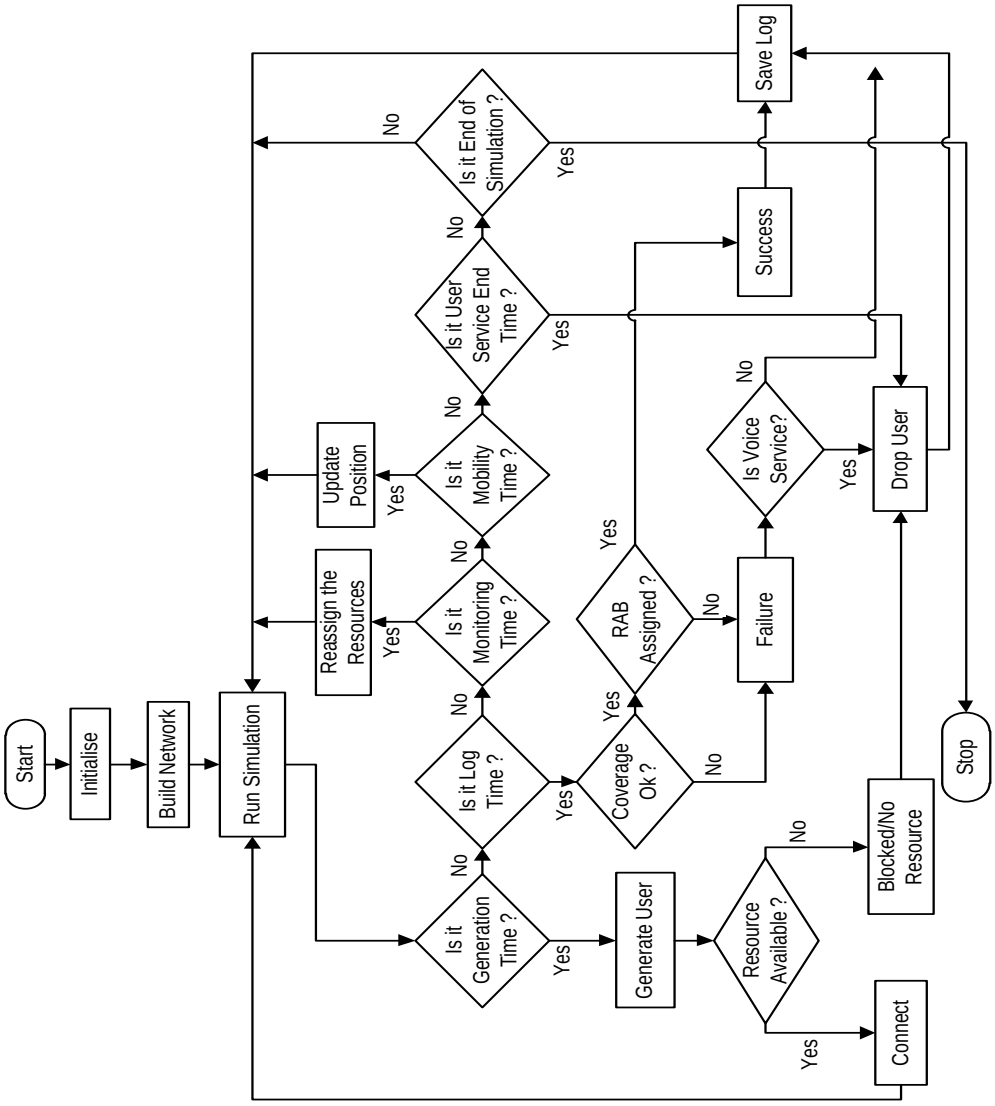

Figure 3.6: User status flow diagram

Chapter 4:

Analytical Model: A Complete Dynamic Analytical Model

In Chapter 3, a novel resource scheduling algorithm was discussed together with the design of an event-driven dynamic network simulator. The simulator models the downlink communication of OFDMA based networks, i.e., LTE-A. A general overview and methodology for modelling the network performance in this dynamic System Level Simulation (SLS) tool was described.

In this chapter, a complete dynamic analytical model for the throughput evaluation is developed. An analytical model can be used as a tool to estimate the performance of a network in CoMP transmission in terms of throughput, which is useful in dimensioning the network by a network designer.

4.1 Network Notations

In addition to the notations used in the previous chapter, let us introduce some further notations as follows. Let

- H be the number of hexagonal sites (eNBs) in the system, that is, the number of BSs.
- $\mathcal{H} = \{1, 2, \ldots, h, \ldots, H\}$ be the set of hexagonal sites.
- d be the distance of a user from its serving base station.
- $d_u^{m,h}(d, \theta')$ be the distance of user u connected to cell m from a neighbour base station h, where θ' is the angle made by the line joining the base

station to a user with a vertical direction in 2D XY-plane.

- d_{edge} be the distance of a user from its serving cell beyond which the user is categorised as a CEU.
- $A = \lambda_u^m/\mu_u^m$ is the offered traffic by user u in cell m, where λ_u^m and μ_u^m are the user arrival and service rate, respectively.
- $\rho = A^m/R$ is the channel utilisation factor, i.e., the offered voice traffic per subchannel in cell m.
- $\mathfrak{U}$ is the number of user class types, i.e., voice, video streaming, etc.
- $n_{\mathfrak{u}}^m$ is the number of users of type-$\mathfrak{u}$ in cell m.
- $X_{\mathfrak{u}}^m(t)$ denotes a random variable relating to the number of users of type-$\mathfrak{u}$[a] user in cell m at time t.
- The cell residence time of a user type-$\mathfrak{u}$ in cell m is exponentially distributed with the mean $1/r_u^m$.
- λ_{nu}^m and λ_{hu}^m are the mean arrival rates of a new user and of a handoff user, respectively, in cell m.

4.2 Analytical Assumptions

The following assumptions are made in order to evaluate the performance of the system analytically without the loss of generality.

- $H = 19$ hexagonal base station sites (eNBs) placed at the center of each hexagon.
- Each base station site is divided into tri-sector cells and co-located at the base station.
- Consider the high interference scenario, that is, each cell is fully loaded.

[a]Note that $\mathfrak{u}$ and u are different variables, $\mathfrak{u}$ represents the type of user (e.g., voice, video, etc.), whereas u as an index to represent a general user.

4.3 Steady State Distribution and Blocking Probabilities

Let us assume that new users are generated in cell m according to a Poisson random process with the mean arrival rate λ_{nu}^m and the requested call connection time is exponentially distributed with the mean $\mu_u^m = 1/t_u^m$. Both the inter-arrival time $(1/\lambda_u^m)$ and the mean holding time (t_u^m) are exponentially independent and identically distributed (i.i.d.) random variables [95–97].

4.3.1 Steady State Distribution

In a cellular network, the handoff traffic is considered more important than new arriving traffic, because the forced termination of an ongoing call is considered less desirable than the blocking of a new call [98–100]. The priority schemes of how to handle the handoff traffic depend on the network designer [101]. A popular scheme is the *guard channel scheme* [97, 98, 100, 101], where a fixed number of subchannels in a given cell are reserved for handoff traffic. For example, in a cell with R subchannels, r_g subchannels are reserved for handoff traffic. The state of the cell m at time t can be written as [102]

$$\boldsymbol{X}^m(t) = (X_1^m(t), \ldots, X_{\mathfrak{u}}^m(t), \ldots, X_{\mathfrak{U}}^m(t)), \tag{4.1}$$

where $X_{\mathfrak{u}}^m(t)$ is the arbitrary number of users of type-$\mathfrak{u}$ class in cell m at time t. The state of the system at time t is $\boldsymbol{X}(t) = (\boldsymbol{X}^1(t), \ldots, \boldsymbol{X}^m(t), \ldots, \boldsymbol{X}^M(t))$ with state space

$$\mathcal{S} = \{(\boldsymbol{n}^1, \ldots, \boldsymbol{n}^m, \ldots, \boldsymbol{n}^M) : \boldsymbol{n}^m = (n_1^m, \ldots, n_{\mathfrak{U}}^m)\}, \tag{4.2}$$

where $\mathcal{S}$ is the state space of users in the system, $0 \leq \sum_{\mathfrak{u}=1}^{\mathfrak{U}} n_{\mathfrak{u}}^m \leq U^m$ and $\boldsymbol{n}$= $(\boldsymbol{n}^1, \ldots, \boldsymbol{n}^m, \ldots, \boldsymbol{n}^M)$ is the number of users in the system. The statistically

stationary distribution of users in the system is given by [97, 102]

$$\begin{aligned}\boldsymbol{\pi}(\boldsymbol{n}) &= \Pr_{t\to\infty}(\boldsymbol{X}(t)=\boldsymbol{n}) \\ &= \Pr_{t\to\infty}(\boldsymbol{X}^1(t)=\boldsymbol{n}^1,\ldots,\boldsymbol{X}^m(t)=\boldsymbol{n}^m,\ldots,\boldsymbol{X}^M(t)=\boldsymbol{n}^M) \\ &= \prod_{m=1}^{M}\boldsymbol{\pi}^m(\boldsymbol{n}^m),\quad \boldsymbol{n}^m\in\mathcal{S}, \end{aligned} \tag{4.3}$$

and

$$\boldsymbol{\pi}^m(\boldsymbol{n}^m) = \frac{1}{G^m}\prod_{\mathfrak{u}=1}^{\mathfrak{U}}\prod_{l=1}^{n_{\mathfrak{u}}^m}\frac{\lambda_{\mathfrak{u}}^m}{l\mu_{\mathfrak{u}}^m},\quad m=1,\ldots,M, \tag{4.4}$$

where $\boldsymbol{\pi}(\boldsymbol{n})$ is the probability of the system in a state $\boldsymbol{n}$, $\boldsymbol{\pi}^m(\boldsymbol{n}^m)$ is the probability of the cell m in state $\boldsymbol{n}^m$, G^m is the normalisation constant chosen such that the sum of the probabilities of all the possible states in any cell m is 1, and the sum of the product of probabilities of all the possible configurations in the system is 1. That is,

$$\sum_{\boldsymbol{n}^m=0}^{U^m}\boldsymbol{\pi}^m(\boldsymbol{n}^m)=1, \tag{4.5}$$

and

$$\sum_{\boldsymbol{n}^m\in\mathcal{S}}\prod_{m=1}^{M}\boldsymbol{\pi}^m(\boldsymbol{n}^m)=1. \tag{4.6}$$

The normalisation constant is given by [97, 102]

$$G^m = \sum_{0\le\sum_{\mathfrak{u}=1}^{\mathfrak{U}}n_{\mathfrak{u}}^m\le U^m}\prod_{\mathfrak{u}=1}^{\mathfrak{U}}\prod_{l=1}^{n_{\mathfrak{u}}^m}\frac{\lambda_{\mathfrak{u}}^m}{l\mu_{\mathfrak{u}}^m},\quad m=1,\ldots,M, \tag{4.7}$$

where

$$\lambda_{\mathfrak{u}}^m = \lambda_{n\mathfrak{u}}^m 1[l<R-r_g]+\lambda_{h\mathfrak{u}}^m,\quad l=0,1,\ldots,R, \tag{4.8}$$

$$\mu_{\mathfrak{u}}^m = \left(\frac{1}{t_{\mathfrak{u}}^m}+\frac{1}{r_{\mathfrak{u}}^m}\right), \tag{4.9}$$

in which $1[l<R-r_g]$ is the indicator function taking the value 1, if the available subchannel is $l<R-r_g$, where r_g is the number of reserved subchannels for handoff traffic.

Based on the above equations, we can compute the probability of cell m, $\boldsymbol{\pi}^m(\boldsymbol{n}^m)$, being in a particular state and the probability of the system, $\boldsymbol{\pi}(\boldsymbol{n})$, in a specific state $\boldsymbol{n} = (\boldsymbol{n}^1, \ldots, \boldsymbol{n}^m, \ldots, \boldsymbol{n}^M) \in \mathcal{S}$ of the system, as illustrated in an example in Appendix B.

4.3.2 Blocking Probability

If all subchannels are occupied when a call arrives, then the arriving call can not be completed and is blocked. According to the guard channel scheme, a new call in a cell m will be assigned a subchannel if and only if the call occupies less than $R - r_g$ subchannels and that at least one subchannel is available [97]. Otherwise, the call is blocked with the blocking probability [95]

$$\mathbb{P}_B = A^{R-r_g} \frac{\displaystyle\sum_{k=0}^{r_g} \frac{A_1^k}{(k+R-r_g)!}}{\displaystyle\sum_{n=0}^{R-r_g-1} \frac{A^n}{n!} + \sum_{n=R-r_g}^{R} \frac{A^{R-r_g}}{n!} A_1^{n-(R-r_g)}}, \tag{4.10}$$

where $A = \lambda/\mu = (\lambda_{n\mathrm{u}}^m + \lambda_{h\mathrm{u}}^m) + /(1/t_{\mathrm{u}}^m + 1/r_{\mathrm{u}}^m)$ is the total offered traffic in cell m, $A_1 = \lambda_{h\mathrm{u}}^m/(1/t_{\mathrm{u}}^m + 1/r_{\mathrm{u}}^m)$ is the handoff traffic. Although the guard channel scheme properly handles the ongoing handover traffic, but from a spectral efficiency point of view it losses the system capacity because new call can not be accepted even though there are free subchannels in the reserved list. Hence, if the is no reserved subchannels in a cell, i.e., $r_g = 0$, the blocking probability Eq. (4.10) reduces to

$$\mathbb{P}_B = \frac{\dfrac{A^R}{R!}}{\displaystyle\sum_{r=0}^{R} \frac{A^r}{r!}}, \tag{4.11}$$

which is the classical *Erlang-B* loss formula [103,104]. The average arrival rate of served calls in cell m is given by [104]

$$\lambda^m = (\lambda_{n\mathrm{u}}^m + \lambda_{h\mathrm{u}}^m)\,(1 - \mathbb{P}_B)\,. \tag{4.12}$$

The average number of active calls in cell m can be estimated as [104]

$$E[n^m] = \frac{\lambda^m}{\mu^m_{\mathfrak{u}}} = \frac{(\lambda^m_{n\mathfrak{u}} + \lambda^m_{h\mathfrak{u}})}{\mu^m_{\mathfrak{u}}} (1 - \mathbb{P}_B) . \tag{4.13}$$

4.4 Probability of Interference

In the steady state of the system, $(\boldsymbol{n} = (\boldsymbol{n}^1, \ldots, \boldsymbol{n}^m, \ldots, \boldsymbol{n}^M))$, the number of type-$\mathfrak{u}$ class calls in cell m is $n^m_{\mathfrak{u}}$. The subchannel r $(1 \leq r \leq R)$ is allocated to call u $(1 \leq u \leq \sum_{u=1}^{U^m})$ in cell m $(1 \leq m \leq M)$. Consider that

- There are $\boldsymbol{n}^m = (n^m_1, \ldots, n^m_{\mathfrak{u}}, \ldots, n^m_{\mathfrak{U}}) = U^m$ calls in cell m and we have to allocate resources from R subchannels so that $U^m = \sum_{\mathfrak{u}=1}^{\mathfrak{U}} n^m_{\mathfrak{u}} \leq R$.
- The probability that the subchannel r is allocated to call u is $1/R$.
- If a random allocation of subchannel is applied, then the number of possibilities (which subchannel is allocated to which calls) that the subchannels are assigned among the calls in cell m is $R!/(R - U^m)!$.
- The number of possibilities that the subchannel r is allocated to a particular call u in cell m is

$$\frac{R!}{(R - U^m)!}/R = \frac{(R-1)!}{(R - U^m)!}.$$

In the system state $\boldsymbol{n}$, the maximum number of possible interfering cells is $s(\boldsymbol{n})$, where, $s(\boldsymbol{n}) = \sum_{m=1}^{M} \mathbf{I}_{>\mathbf{0}}(U^m)$, $s(\boldsymbol{n}) \leq M$ and $\mathbf{I}_{>\mathbf{0}}$ is the indicator function given by

$$\mathbf{I}_{>\mathbf{0}}(U^m) = \begin{cases} 1 & \text{if } U^m > 0 \quad \text{(i.e., there are calls in cell m)} \\ 0 & \text{if } U^m = 0 \quad \text{(i.e., there is no call in cell m)} \end{cases} . \tag{4.14}$$

The number of interfering possibilities is equivalent to a k-combination of $s(\boldsymbol{n})$ elements, which is equal to $\binom{s(\boldsymbol{n})}{k}$. Therefore, the probability, p_k, that k number of calls are allocated subchannel r in $s(\boldsymbol{n})$ cells (thus suffer interference) is

$$p_k = \binom{s(\boldsymbol{n})}{k} \left(\frac{1}{R}\right)^k \left(1 - \frac{1}{R}\right)^{s(\boldsymbol{n})-k} . \tag{4.15}$$

The probability that the call u in cell m has interference from other $k-1$ calls is expressed as

$$p_k \boldsymbol{\pi}(\boldsymbol{n}). \tag{4.16}$$

4.5 User's Location and Distance Modelling

The user's location in a cell has a direct impact on its performance because the power attenuation has the direct relationship with the distance between the transmitter and the receiver. Also, to estimate the average signal strength or interference power received by a user, we need a relationship of distance between the user's location and the base station. We first evaluate the probability density function of a user's distance within a serving cell from the centre of its base station. After knowing the probabilistic distance a user can be away from the base station within a cell, we evaluate the distance of this user from the remaining base stations in the network.

4.5.1 Probability Density Function of User Distance from the Centre within a Hexagon

Let us model the arbitrary position of a user within a cell. To model the location of a user within a cell, we first find the probability distribution of a random distance of the user from the centre of the base station in a regular hexagon cell. As shown in Fig. 4.1(a), a base station consists of three cells: Cell A, Cell B and Cell C. Each cell's area is equally divided into four triangles and they are symmetric to each other. For example, the area covered by Cell A (i.e., area OABCDE) is four times the area of a triangle OAB. Hence, the distance distribution of a user from the centre of the base station to an arbitrary position inside the hexagon is equivalent to that from the centre to anywhere inside one of the equilateral triangles, i.e., OAB. There are two possibilities

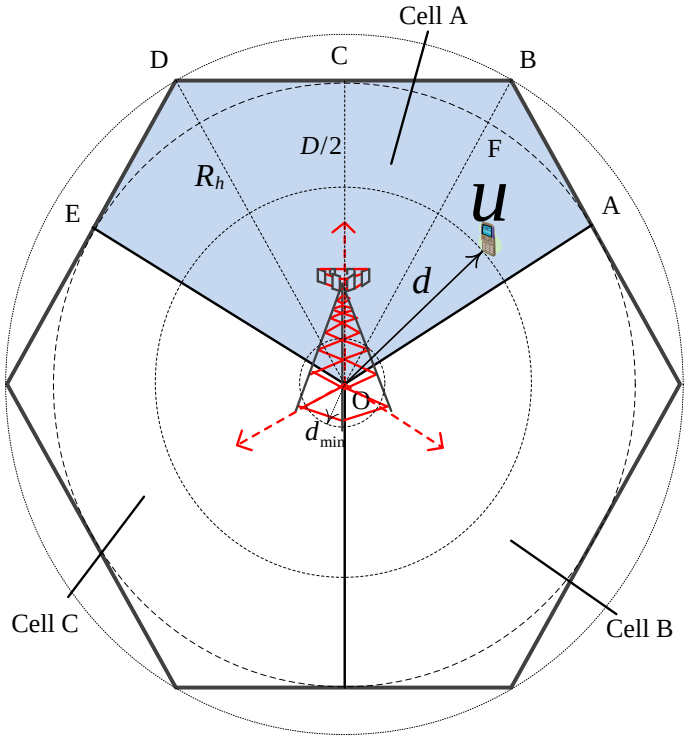

(a) User's position in a cell

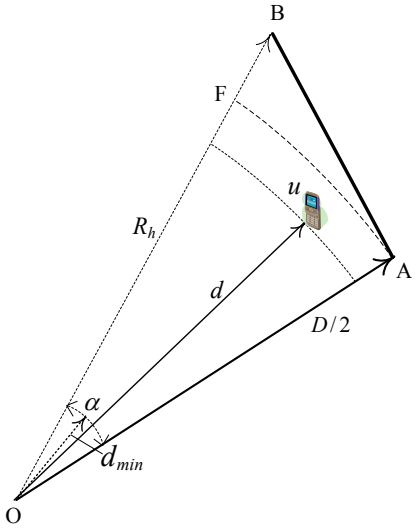

(b) $d_{min} \leq d \leq \frac{D}{2}$

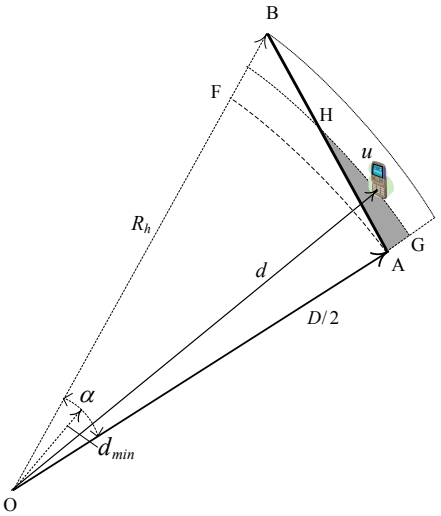

(c) $\frac{D}{2} \leq d \leq R_h$

Figure 4.1: Random distance of a user in a cell from the centre of a hexagon

that the user can be: either inside the area OAF or inside the area ABF. Hence, we need to find the probability of distance distribution in these two areas separately depending on the distance [b] as follows.

Case 1: $d_{min} \leq d \leq \frac{D}{2}$

In this case, the user's possible location will be within the area OAF (see Fig. 4.1(b)). The probability of the user's distance distribution in the area OAF is given by

$$\begin{aligned}
\mathbb{F}\left[d_{min} \leq d \leq \frac{D}{2}\right] &= \frac{\text{Area by arc length } \alpha(d-d_{min}) \text{ with the centre}}{\text{Area of triangle OAB } - \text{Area by arc length } \alpha d_{min}}, \\
&= \frac{\pi(d^2-d_{min}^2)/12}{\frac{3\sqrt{3}R_h^2/2}{12} - \frac{\pi d_{min}^2}{12}} = \frac{\pi(d^2-d_{min}^2)}{\frac{3\sqrt{3}R_h^2}{2} - \pi d_{min}^2}, \\
&= \frac{2\pi}{\sqrt{3}}\left(\frac{d^2-d_{min}^2}{D^2 - \frac{2\pi}{\sqrt{3}}d_{min}^2}\right), \qquad (4.17)
\end{aligned}$$

where R_h is the radius of a regular hexagon, $D = \sqrt{3}R_h$ is the inter-site (eNB-to-eNB) distance and d_{min} is the minimum distance a user can be located from its base station.

Case 2: $\frac{D}{2} \leq d \leq R_h$

In this case, the user's possible location will be within the area ABF (see Fig. 4.1(c)). As the distance, d, of the user's location increases from $D/2$ to R_h, there is a possibility that the user may be located outside the cell. For example, the user is located in the area AGH (i.e., shaded area in Fig. 4.1(c)), which is outside of the cell. Hence, we need to subtract the area AGH in the probability estimation. Then, the probability of the user's distance distribution

[b] Note that the user is not located in the near distance d_{min} from the base station. Hence, we need to subtract the area made by an arc length, αd_{min}, with the centre.

in the area ABF is given by

$$\begin{aligned}\mathbb{F}\left[\frac{D}{2} \leq d \leq R_h\right] &= \frac{\text{Possible area inside ABF}}{\text{Area of } \triangle\text{OAB} - \text{Area by arc length } \alpha d_{min}}, \\ &= \frac{\text{Area by } \alpha(d - \frac{D}{2}) - \text{Area of AGH}}{\text{Area of } \triangle\text{OAB} - \text{Area by arc } \alpha d_{min}}. \end{aligned} \tag{4.18}$$

By inspecting Fig. 4.1(c) and using geometrical analysis, the area of AGH can be obtained as

$$\text{Area of AGH} = \frac{1}{2}\left(d^2 \cos^{-1}\left(\frac{\sqrt{3}R_h}{2d}\right) - \frac{\sqrt{3}}{2}R_h\sqrt{d^2 - \frac{3R_h^2}{4}}\right). \tag{4.19}$$

The area made by an arc of length, αd, with the centre of the hexagon (Fig. 4.1(c)) is given by

$$\begin{aligned}\text{Area by arc length } \alpha d &= \frac{1}{2}d^2\alpha = \frac{1}{2}d^2 \cos^{-1}\left(\frac{\text{OA}}{\text{OB}}\right), \\ &= \frac{1}{2}d^2 \cos^{-1}\left(\frac{D/2}{R_h}\right), \\ &= \frac{\pi d^2}{12}. \end{aligned} \tag{4.20}$$

Similarly, the area of OAF, i.e., the area made by an arc of length, $\alpha D/2$, with the centre of the hexagon (Fig. 4.1(c)) is given by

$$\text{Area by arc length } \alpha D/2 = \frac{\pi(D/2)^2}{12}. \tag{4.21}$$

The area made by an arc of length, αd_{min}, with the centre of the hexagon (Fig. 4.1(c)) is given by

$$\text{Area by arc length } \alpha d_{min} = \frac{\pi d_{min}^2}{12}. \tag{4.22}$$

And, the area of $\triangle$ OAB is given by

$$\text{Area of } \triangle\text{OAB} = \frac{3\sqrt{3}R_h^2}{2}/12. \tag{4.23}$$

By substituting Eqs. (4.19), (4.20), (4.21), (4.22) and (4.23) in Eq. (4.18), the probability of distance distribution can be obtained as

$$\begin{aligned}\mathbb{F}\left[\frac{D}{2} \leq d \leq R_h\right] &= \frac{\pi d^2 - \pi(\frac{D}{2})^2 - 6\left(d^2 \cos^{-1}\left(\frac{\sqrt{3}R_h}{2d}\right) - \frac{\sqrt{3}}{2}R_h\sqrt{d^2 - \frac{3R_h^2}{4}}\right)}{\frac{3\sqrt{3}R_h^2}{2} - \pi d_{min}^2}, \\ &= \frac{\pi\left(d^2 - (\frac{D}{2})^2\right) - 6\left(d^2 \cos^{-1}\left(\frac{D}{2d}\right) - \frac{D}{2}\sqrt{d^2 - \frac{D^2}{4}}\right)}{\frac{\sqrt{3}}{2}D^2 - \pi d_{min}^2}. \end{aligned} \tag{4.24}$$

Now, by taking the derivative of $\mathbb{F}$, the probability density function of the random distance of a user from the centre within a hexagon can be obtained as

$$f(d) = \frac{\frac{4}{\sqrt{3}}}{D^2 - \frac{2\pi}{\sqrt{3}}d_{min}^2} \begin{cases} \pi d, & d_{min} \leq d \leq \frac{D}{2} \\ \pi d - 6d\cos^{-1}\left(\frac{D}{2d}\right), & \frac{D}{2} \leq d \leq R_h \\ 0, & \text{otherwise} \end{cases} . \quad (4.25)$$

Verification: To verify the above probability density function, let us compare with the one derived in [105]. In [105], the side of a regular hexagon is considered a unit length and the minimum distance is not considered. Therefore, if the side length of a regular hexagon is 1 unit, i.e., $R_h = 1 \Rightarrow D = \sqrt{3}$, and $d_{min} = 0$, then Eq. (4.25) reduces to

$$\begin{aligned} f(d) &= \frac{4d}{\sqrt{3}} \begin{cases} \frac{\pi}{3}, & \text{for } 0 \leq d \leq \frac{\sqrt{3}}{2} \\ \frac{\pi - 6\cos^{-1}\left(\frac{\sqrt{3}}{2d}\right)}{3}, & \text{for } \frac{\sqrt{3}}{2} \leq d \leq 1 \\ 0, & \text{otherwise} \end{cases}, \\ &= \frac{4d}{\sqrt{3}} \begin{cases} \frac{\pi}{3}, & \text{for } 0 \leq d \leq \frac{\sqrt{3}}{2} \\ \frac{\pi}{3} - 2\cos^{-1}\left(\frac{\sqrt{3}}{2d}\right), & \text{for } \frac{\sqrt{3}}{2} \leq d \leq 1 \\ 0, & \text{otherwise} \end{cases}, \quad (4.26) \end{aligned}$$

which is equal to the expression derived in [105].

The expected value of the probabilistic distance, x (note that we have used variable x instead of distance variable d to avoid writing dd in the integral), of a user within the serving cell from its base station can be estimated as

$$\begin{aligned} E[x] &= \int_{x=d_{min}}^{\frac{D}{2}} xf(x)dx + \int_{x=\frac{D}{2}}^{R_h} xf(x)dx, \\ &= K_c \left[\int_{x=d_{min}}^{\frac{D}{2}} \pi x^2 dx + \int_{x=\frac{D}{2}}^{R_h} x\left(\pi x - 6x\cos^{-1}\left(\frac{D}{2x}\right)\right)dx \right], \\ &= K_c \left[\pi \int_{x=d_{min}}^{\frac{D}{2}} x^2 dx + \pi \int_{x=\frac{D}{2}}^{R_h} x^2 - 6\int_{x=\frac{D}{2}}^{R_h} x^2 \cos^{-1}\left(\frac{D}{2x}\right)dx \right], \\ &= K_c \left[\pi I_1 + \pi I_2 - 6I_3\right], \quad (4.27) \end{aligned}$$

where

$$K_c = \frac{\frac{4}{\sqrt{3}}}{D^2 - \frac{2\pi}{\sqrt{3}} d_{min}^2} \text{ is a constant,} \tag{4.28}$$

$$I_1 = \int_{x=d_{min}}^{\frac{D}{2}} x^2 dx = \frac{1}{24}\left(D^3 - 8d_{min}^3\right), \tag{4.29}$$

$$I_2 = \int_{x=\frac{D}{2}}^{R_h} x^2 dx = \frac{1}{24}\left(8R_h^3 - D^3\right) = \frac{1}{216}\left(8\sqrt{3} - 9\right) D^3, \tag{4.30}$$

$$\begin{aligned} I_3 &= \int_{x=\frac{D}{2}}^{R_h} x^2 \cos^{-1}\left(\frac{D}{2x}\right) dx, \\ &= \frac{1}{48}\left[-2Dx^2\sqrt{4 - \frac{D^2}{x^2}} - D^3 \ln\left(x\left(\sqrt{4 - \frac{D^2}{x^2}} + 2\right)\right) + 16x^3 \cos^{-1}\left(\frac{D}{2x}\right)\right]\Bigg|_{x=\frac{D}{2}}^{\frac{D}{\sqrt{3}}}, \\ &= \frac{D^3}{48}\left(-\frac{2}{3} + \ln\left(\frac{1}{\sqrt{3}}\right) + \frac{8\pi}{9\sqrt{3}}\right). \end{aligned} \tag{4.31}$$

By substituting Eqs. (4.29), (4.30) and (4.31) in Eq. (4.27) and after re-arranging, Eq. (4.27) reduces to

$$E[d] = K_c\left(\frac{D^3}{12} - \frac{\pi}{3} d_{min}^3 + \frac{D^3}{8}\ln(\sqrt{3})\right). \tag{4.32}$$

Hence, by knowing the Inter-Site Distance (ISD), D, of base stations and the minimum distance, d_{min}, a user can be away from the serving base station, we can easily calculate the expected distance of the user within the serving cell from its base station using the above Eqs. (4.32) and (4.28). For example, consider D= **500** m and d_{min}= **35** m, then the expected distance of a user can be calculated as

$$\begin{aligned} E[d] &= \frac{\frac{4}{\sqrt{3}}}{500^2 - \frac{2\pi}{\sqrt{3}} 35^2}\left(\frac{500^3}{12} - \frac{\pi}{3} 35^3 + \frac{500^3}{8}\ln(\sqrt{3})\right), \\ &= \textbf{178.26} \text{ m.} \end{aligned}$$

4.5.2 User's Distance Modelling from Neighbour Base Stations

After knowing the probabilistic distance a user can be away from the base station within a serving cell, let us now model the distance of this user from the other base stations in the network. As shown in Fig. 4.2, we focus on a UE which is in the central base station. The reason behind selecting the central base station is that it is located symmetrically to the surrounding base stations. Therefore, UE in the central base station will receive a similar interference level from every direction. The naming convention of the base stations matters in the following expressions for user distance modelling. Starting from the central site, the sequence of the naming of sites follows in a clockwise direction from a vertical direction. Define θ' as the angle from the vertical direction clockwise to the line joining the user position with the serving base station. And ϕ' is the angle from the vertical direction in a clockwise sense to the line joining the serving base station with the interfering base station. Note that the convention of the angles θ' and ϕ' defined here are not the same angles as defined in the antenna radiation pattern in the previous chapter. These angles are the angles only in the horizontal x-y plane from specific references (as shown in Fig. 4.2); whereas the angles θ and ϕ in the antenna radiation pattern are the polar and the azimuth angles, respectively, in the spherical coordinates (as shown in Fig. 4.3). The distance of a user u in the central base station site is $d_u^1 = d$ and D is the site-to-site distance. By inspecting Fig. 4.2 and using geometrical analysis, the distance of a user u in the central base station[c] from the eNB h in the network can be expressed in general as

$$d_u^{m,h}(d, \theta') = \sqrt{aD^2 + d^2 + bDd\cos(\phi' - \theta')}, \tag{4.33}$$

[c]Note that the location of cells in a hexagon site is considered at the same location as the base station, which means all the cells in a hexagon site are co-located.

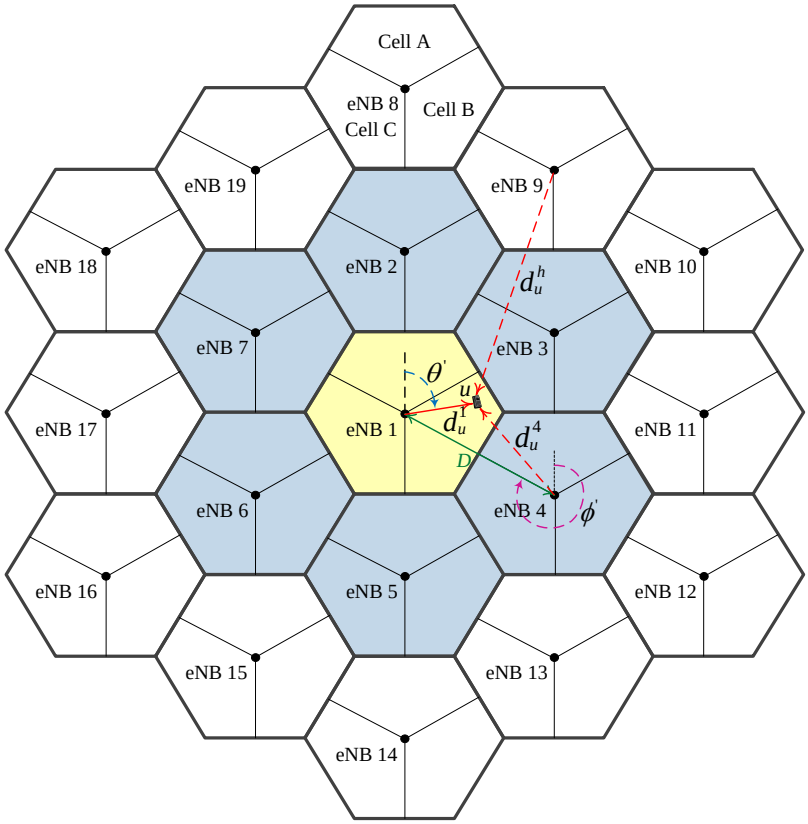

Figure 4.2: System model for analytical evaluation

where

$$\phi' = \frac{\pi}{3}(h+1) + \kappa\frac{\pi}{6}(h+4), \tag{4.34a}$$

$$\kappa = \begin{cases} 0, & \text{for inner tier, i.e., } 2 \leq h \leq 7 \\ 1, & \text{for outer tier, i.e., } 8 \leq h \leq 19 \end{cases}, \tag{4.34b}$$

$$a = \begin{cases} 1, & \text{for } 2 \leq h \leq 7 \\ 4, & \text{for h is even in } 8 \leq h \leq 19 \\ 3, & \text{for h is odd in } 8 \leq h \leq 19 \end{cases}, \tag{4.34c}$$

and

$$b = \begin{cases} 2, & \text{for } 2 \leq h \leq 7 \\ 4, & \text{for h is even in } 8 \leq h \leq 19 \\ 3\sqrt{3}, & \text{for h is odd in } 8 \leq h \leq 19 \end{cases}. \tag{4.34d}$$

Hence, using Eq. (4.33), we can easily estimate the distance of a user in a cell from the other cells in the network. Note that the user distance (Eq. (4.33)) from the other base stations in the network is dependent on the distance, d, of the user, u, from its serving base station and the angle θ'. For simplicity, we will use $d_u^{m,h}$ instead of $d_u^{m,h}(d, \theta')$.

The expected distance of the user from the other base stations can be expressed as

$$\begin{aligned} E[d_u^{m,h}] &= E[\sqrt{aD^2 + d^2 + bDd\cos(\phi' - \theta')}], \\ &= \sqrt{aD^2 + (E[d])^2 + bDE[d]E[\cos(\phi' - \theta')]}, \end{aligned} \tag{4.35}$$

where $E[d]$ represents the expected value of a random distance variable d and $E[\cos(\phi' - \theta')]$ represents the expected value of a random angle variable θ'. Note that the angle variable ϕ' is a constant value for a specific base station h and can be calculated using Eq. (4.34a). The expected value $E[d]$ is estimated in the previous section in Eq. (4.32) and is given as

$$E[d] = K_c \left(\frac{D^3}{12} - \frac{\pi}{3} d_{min}^3 + \frac{D^3}{8} \ln(\sqrt{3}) \right), \tag{4.36}$$

where

$$K_c = \frac{\frac{4}{\sqrt{3}}}{D^2 - \frac{2\pi}{\sqrt{3}} d_{min}^2}. \tag{4.37}$$

To estimate the expected value of $\cos(\phi' - \theta')$, where θ' is a random variable, we need to find the probability density function of θ'. The probability density of the random angle variable θ' can be written as

$$f(\theta') = \frac{\theta'}{2\pi}. \tag{4.38}$$

Let us consider the user u to be inside the area of Cell A of eNB 1. Then the possible angle of the user from the antenna boresight in the 2D plane will be from $-\pi/3$ to $+\pi/3$. Therefore, the expected value of $\cos(\phi' - \theta')$ can be

written as

$$\begin{aligned} E[\cos(\phi' - \theta')] &= \int_{\theta'=-\frac{\pi}{3}}^{+\frac{\pi}{3}} \cos(\phi' - \theta') f(\theta') d\theta', \\ &= \frac{1}{2\pi} \int_{\theta'=-\frac{\pi}{3}}^{+\frac{\pi}{3}} \theta' \cos(\phi' - \theta') d\theta', \\ &= \frac{1}{2\pi} \left[\cos(\phi' - \theta') - \theta' \sin(\phi' - \theta')\right] |_{\theta'=-\frac{\pi}{3}}^{+\frac{\pi}{3}}, \\ &= \frac{1}{2\pi} \left(\sqrt{3} - \frac{\pi}{3}\right) \sin(\phi'). \end{aligned} \tag{4.39}$$

Hence, by using Eqs. (4.35) to (4.39) and Eqs. (4.34a) to (4.34d), we can estimate the average distance of a user u in Cell A of eNB 1 from the other eNBs in the system. Once we know these distances, we can estimate the path loss to the user from each of the eNBs. Table 4.1 shows the expected distance of a user u in Cell A of eNB 1 from the other eNBs in the network.

4.6 Antenna Radiation Pattern Modelling

The antenna radiation pattern for the sectorial antennas follows according to the model proposed in the 3GPP standard [29]. The vertical radiation pattern offset from the sectorial antennas of eNB h to the user u situated at distance $d_u^{m,h}$ is modelled as [29]

$$A_V(\theta^h) = -\min\left[12\left(\frac{\theta^h - \theta_{etilt}}{\theta_{3dB}}\right)^2, A_{v,max}\right], \tag{4.40}$$

where θ^h represents the angle of arrival of the vertical radiation from the antenna located at the base station h, $\theta_{etilt} = 15^\circ$ is the electrical tilt angle, i.e., the angle between the antenna horizon and the axis of the main lobe of the the vertical antenna pattern, $\theta_{3dB} = 10^\circ$ represents the half power antenna vertical beam width, and $A_{v,max} = 20$ dB represents the maximum offset of the pattern in the vertical plane.

By inspecting Fig. 4.3 and using geometrical analysis, ϕ^h can expressed, in

Table 4.1: Expected distance of a user located in the central base station area from the neighbour base stations

Tier	eNB Index h	Constant			ϕ' [radians]	$E[\cos(\phi' - \theta')]$	eNB to User Distance, d_u^h [m]
		κ	a	b			
First Tier	1	-	-	-	-	-	178.26
	2	0	1	2	3.14	0.00	530.83
	3	0	1	2	4.19	-0.09	514.73
	4	0	1	2	5.24	-0.09	514.73
	5	0	1	2	6.28	0.00	530.83
	6	0	1	2	7.33	0.09	546.45
	7	0	1	2	8.38	0.09	546.45
Second Tier	8	1	4	4	15.71	0.00	1015.76
	9	1	3	$3\sqrt{3}$	17.28	-1.08	784.67
	10	1	4	4	18.85	0.00	1015.76
	11	1	3	$3\sqrt{3}$	20.42	1.08	973.58
	12	1	4	4	21.99	0.00	1015.76
	13	1	3	$3\sqrt{3}$	23.56	-1.08	784.67
	14	1	4	4	25.13	0.00	1015.76
	15	1	3	$3\sqrt{3}$	26.70	1.08	973.58
	16	1	4	4	28.27	0.00	1015.76
	17	1	3	$3\sqrt{3}$	29.85	-1.08	784.67
	18	1	4	4	31.42	0.00	1015.76
	19	1	3	$3\sqrt{3}$	32.99	1.08	973.58

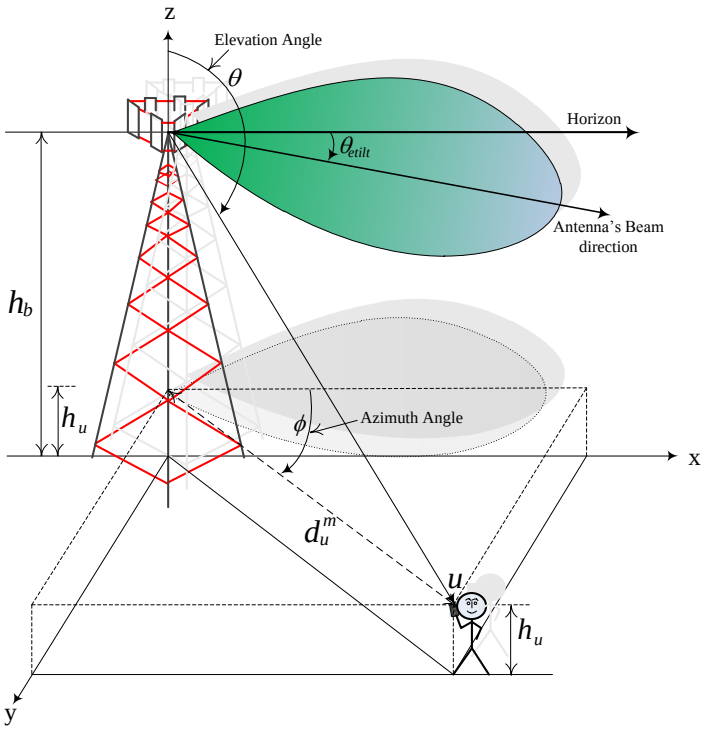

Figure 4.3: Illustration of the polar angle, θ, and the azimuth angle, ϕ, in the antenna radiation pattern model

general, as

$$\theta^h = \pi - \tan^{-1}\left(\frac{d_u^{m,h}}{h_b - h_u}\right) = 180 - \frac{180}{\pi}\tan^{-1}\left(\frac{d_u^{m,h}}{h_b - h_u}\right), \quad \text{(degrees)} \quad (4.41)$$

where d is the distance of the user u from the serving cell m, $d_u^{m,h}$ is the distance of the user u from the base station h, h_b is the height of the base station and h_u is the height of the UE. Substituting Eq. (4.41) in Eq. (4.40), the vertical offset antenna gain can be expressed as

$$A_V(\theta^h) = -\min\left[12\left(\frac{180 - \frac{180}{\pi}\tan^{-1}\left(\frac{d_u^{m,h}}{h_b - h_u}\right) - \theta_{etilt}}{\theta_{3dB}}\right)^2, A_{v,max}\right] \quad (4.42)$$

The net transmit antenna gain from the sectorial antenna located at the base station h can be written as

$$g_{tx}^m(\theta, \phi) = G_{tx} + A_V(\theta^h), \qquad \text{[dB]} \quad (4.43)$$

where $G_{tx} = 18$ dBi is the isotropic gain of the sectorial transmit antenna. Hence, by knowing the distance of a user from any eNBs, we can estimate the net transmit antenna gain analytically from the respective antenna at the eNB using the above expressions. Table 4.2 shows analytically the expected vertical antenna gain by a user u in Cell A of eNB 1 from the other eNBs in the network.

Table 4.2: Expected antenna gain received by a user located in the central base station area from the neighbour base station antennas

Tier	eNB Index, h	eNB to User Distance, d_u^h [m]	θ^h [deg]	$\theta^h - \theta_{etilt}$ [deg]	Vertical Offset $A_V(\theta^h)$ [dB]	Net Antenna Gain $g_{tx}^m = G_{tx} + A_V(\theta^h)$ [dB]
First Tier	1	178.26	9.71	-5.29	-5.26	12.74
	2	530.83	3.29	-11.71	-12.16	5.84
	3	340.15	5.12	-9.88	-10.68	7.32
	4	340.15	5.12	-9.88	-10.68	7.32
	5	530.83	3.29	-11.71	-12.16	5.84
	6	669.22	2.61	-12.39	-12.65	5.35
	7	669.22	2.61	-12.39	-12.65	5.35
Second Tier	8	1015.76	1.72	-13.28	-13.26	4.74
	9	784.67	2.23	-12.77	-12.92	5.08
	10	1015.76	1.72	-13.28	-13.26	4.74
	11	973.58	1.79	-13.21	-13.21	4.79
	12	1015.76	1.72	-13.28	-13.26	4.74
	13	784.67	2.23	-12.77	-12.92	5.08
	14	1015.76	1.72	-13.28	-13.26	4.74
	15	973.58	1.79	-13.21	-13.21	4.79
	16	1015.76	1.72	-13.28	-13.26	4.74
	17	784.67	2.23	-12.77	-12.92	5.08
	18	1015.76	1.72	-13.28	-13.26	4.74
	19	973.58	1.79	-13.21	-13.21	4.79

4.7 Channel Modelling

The radio channel propagation is typically modelled as the combination of three main effects: mean path loss; shadowing generally characterised by a log-normal distribution function [87, 88]; and fading which is often modelled by a Rayleigh probability distribution function [89].

4.7.1 Path Loss Modelling

The path loss between a UE u from a cell m can be modelled as

$$l_u^m = C(d_u^{m,h}(d,\theta'))^\eta, \tag{4.44}$$

where $C = 10^{12.81}$ is a constant and $\eta = 3.76$ is the path loss exponent at 2 GHz carrier frequency; $d_u^{m,h}(d,\theta')$ is the distance in kilometres between the considered UE u and the neighbour base station h which is a function of d and θ'.

4.7.2 Shadow Fading Modelling

Define ξ_u^m to be a Normal random variable with a zero mean and σ standard deviation representing the shadowing effect of the path loss l_u^m. According to the log-normal distribution, the shadowing fading gain of path loss l_u^m between a cell m and a UE u can be written as [106]

$$l_{sh} = 10^{\frac{\xi_u^m}{10}}, \tag{4.45a}$$

$$\xi_u^m = \frac{1}{\sigma\sqrt{2\pi}} e^{-\frac{1}{2}\left(\frac{L_u^m-\mu}{\sigma}\right)^2}. \tag{4.45b}$$

Finally, the channel gain between the cell m and the UE u can be written as

$$g_u^m = \frac{g_{tx}^m(\theta,\phi)g_{u,rx}}{l_u^m l_{sh}} = \frac{g_{tx}^m(\theta,\phi)g_{u,rx}}{C(d_u^{m,h}(d,\theta'))^\eta 10^{\frac{\xi_u^m}{10}}}. \tag{4.46a}$$

4.8 Signal Quality Modelling

The Signal-to-Interference plus Noise Ratio (SINR) is a key performance metric to evaluate the performance of a network. The signal quality model in terms of SINR as obtained in Eq. (3.20) from Chapter 3 is written as

$$\gamma_{u,r}^{m} = \frac{\sum\limits_{m\in\Omega_u^m} \frac{p_{u,r}^{m}}{l_{eqp}l_{cab}} g_u^m}{\sum\limits_{i\in\overline{\Omega_u^m}, i\neq m} \frac{p_{u,r}^{i}}{l_{eqp}l_{cab}} g_u^i \alpha_r^i + \sigma^2}, \tag{4.47}$$

where $g_u^m = g_{tx}^m(\theta,\phi)\, g_{u,rx} / (l_u^m l_{sh})$ and $g_u^i = g_{tx}^i(\theta,\phi)\, g_{u,rx} / (l_u^i l_{sh})$ are the channel gains of user u from cells m and i respectively. Ω_u^m is the set of cooperative cells for user u. $p_{u,r}^m$ and $p_{u,r}^i$ are the transmit power in subchannel r from cells m and i respectively. $g_{tx}^m(\theta,\phi)$ and $g_{tx}^i(\theta,\phi)$ are the transmit antenna gains from cells m and i, respectively, to the user u situated at angles of $(\theta,\ \phi)$, where θ and ϕ are the angles in the vertical and the azimuth planes respectively. $g_{u,rx}$ is the receive antenna gain of UE u. l_u^m and l_u^i are the mean path loss of user u from cells m and i respectively. l_{sh} is the shadowing loss. l_{eqp} and l_{cab} are the equipment and cable losses respectively. α_r^i is the subchannel allocation indicator and σ is the background thermal noise density which is additive white Gaussian noise.

Assume that the uniform and equal transmit power is distributed on each sub-carrier; and all sub-carriers within a subchannel (RB) experience similar channel conditions. We can drop out the subscript of subchannel, i.e., r without loss of generality. Also, assume that the network is fully loaded. That is, all subchannels in all cells are utilised ($\alpha_r^i = 1$), which in turn contribute interference to each other and the network will be considered as an *interference-limited* network. In such a scenario, thermal noise can be neglected compared to high interference. The assumption of interference-limited communication is very realistic in urban wireless environments. Considering

the above analysis, the expression of SINR in Eq. (4.47) can be simplified as

$$\gamma_u^m \simeq \frac{\sum_{m\in\Omega_u^m} g_u^m}{\sum_{i\in\overline{\Omega_u^m}, i\neq m} g_u^i}, \tag{4.48}$$

The γ_u^m can be written in the form

$$\gamma_u^m = \frac{X}{Y}, \tag{4.49}$$

where

$$X = \sum_{m\in\Omega_u^m} g_u^m = \sum_{m\in\Omega_u^m} \frac{g_{tx}^m(\theta,\phi)}{\left(d_u^{m,h}(d,\theta')\right)^{\eta} 10^{\frac{\xi_u^m}{10}}}, \tag{4.50}$$

$$Y = \sum_{i\in\overline{\Omega_u^m}, i\neq m} g_u^i = \sum_{i\in\overline{\Omega_u^m}, i\neq m} \frac{g_{tx}^i(\theta,\phi)}{\left(d_u^{i,h}(d,\theta')\right)^{\eta} 10^{\frac{\xi_u^i}{10}}}. \tag{4.51}$$

Note that in a Rayleigh/Rayleigh fading environment, γ_u^m is a complex random variable with what would appear to be a very complex distribution, since it is the ratio of an exponential random variable (or sum of exponential random variables in the case of cell-edge users) to a sum of exponential random variables with different mean values.

Let us derive the Probability Density Function (PDF) of X. Here, X is the sum of the log-normal random variable which can be approximated by a the log-normal distribution [107]. The mean and variance of X can be obtained as [106, 108]

$$E[X] = \sum_{m\in\Omega_u^m} f^m \left\{ \mu_S + 10\log_{10}\left(\frac{g_{tx}^m(\theta,\phi)}{d_u^{m,h}(d,\theta')^{\eta}}\right), \sigma_S \right\}, \tag{4.52}$$

$$Var[X] = \sum_{m\in\Omega_u^m} g^m \left\{ \mu_S + 10\log_{10}\left(\frac{g_{tx}^m(\theta,\phi)}{d_u^{m,h}(d,\theta')^{\eta}}\right), \sigma_S \right\}, \tag{4.53}$$

where μ_S and σ_S are the mean and the standard deviation in dB value of log-normally distributed random variable $S_m = 10^{\frac{\xi_u^m}{10}}$. Typically, the value of

$\mu_S = 0$ dB and the value of σ_S is in the range of 6-10 dB. Also, the functions, $f^m\{a,b\}$ and $g^m\{a,b\}$ in Eq. (4.52) and Eq. (4.53) are defined as [106, 108]

$$f^m\{a,b\} = \exp\left(\beta a + \frac{\beta^2 b^2}{2}\right), \tag{4.54}$$

$$g^m\{a,b\} = \exp\left(2\beta a + \beta^2 b^2\right)\left(\exp\left(\beta^2 b^2\right) - 1\right), \tag{4.55}$$

where $\beta = \ln(10)/10$. The mean and the standard deviation in dB value of log-normal random variable X, $10\log_{10} X$, can be computed as [106, 108]

$$m_x = \frac{1}{\beta}\ln(E[X]) - \frac{1}{2}\beta\sigma_x^2, \tag{4.56}$$

$$\sigma_x^2 = \frac{1}{\beta^2}\ln\left(1 + \frac{Var[X]}{(E[X])^2}\right). \tag{4.57}$$

In a similar way, we can derive the PDF of Y. Here, Y is also the sum of log-normal random variable which can be approximated by a log-normal distribution whole mean and variance can be obtained as

$$E[Y] = \sum_{i\in\overline{\Omega_u^m}, i\neq m} f^i\left\{\mu_I + 10\log_{10}\left(\frac{g_{tx}^i(\theta,\phi)}{\left(d_u^{i,h}(d,\theta')\right)^\eta}\right), \sigma_I\right\}, \tag{4.58}$$

$$Var[Y] = \sum_{i\in\overline{\Omega_u^m}, i\neq m} g^i\left\{\mu_I + 10\log_{10}\left(\frac{g_{tx}^i(\theta,\phi)}{\left(d_u^{i,h}(d,\theta')\right)^\eta}\right), \sigma_I\right\}, \tag{4.59}$$

where μ_I and σ_I are the mean and the standard deviation in dB value of log-normally distributed random variables $I_i = 10^{\frac{\xi_u^i}{10}}$. Also, the functions, $f^i\{a,b\}$ and $g^i\{a,b\}$ in Eq. (4.58) and Eq. (4.59) are defined as

$$f^i\{a,b\} = \exp\left(\beta a + \frac{\beta^2 b^2}{2}\right), \tag{4.60}$$

$$g^i\{a,b\} = \exp\left(2\beta a + \beta^2 b^2\right)\left(\exp\left(\beta^2 b^2\right) - 1\right), \tag{4.61}$$

where $\beta = \ln(10)/10$. The mean and the standard deviation in dB value of log-normal random variable Y, $10\log_{10} Y$, can be computed by

$$m_y = \frac{1}{\beta}\ln(E[Y]) - \frac{1}{2}\beta\sigma_y^2, \tag{4.62}$$

$$\sigma_y^2 = \frac{1}{\beta^2}\ln\left(1 + \frac{Var[Y]}{(E[Y])^2}\right). \tag{4.63}$$

Since X is a log-normally distributed random variable with the mean dB value m_x and the standard deviation dB value σ_x, and that Y is also a log-normally distributed random variable with the mean dB value m_y and the standard deviation dB value σ_y, we can say that X/Y is a log-normal random variable with the following mean dB value and variance dB value [108]:

$$E[\gamma_u^m] = E\left[10\log_{10}\frac{X}{Y}\right] = m_x - m_y, \quad \text{[dB]} \tag{4.64}$$

$$Var[\gamma_u^m] = Var\left[10\log_{10}\frac{X}{Y}\right] = \sigma_x^2 + \sigma_y^2. \quad \text{[dB]} \tag{4.65}$$

Numerically: Now, let us calculate the expected SINR $E[\gamma_u^m]$ numerically. From Eqs. (4.52) and (4.54), we have

$$\begin{aligned} a &= \mu_S + 10\log_{10}\left(\frac{g_{tx}^m(\theta,\phi)}{\left(d_u^{m,h}(d,\theta')\right)^\eta}\right), \\ &= \mu_S + 10\log_{10}(g_{tx}^m(\theta,\phi)) - 10\eta\log_{10}\left(d_u^{m,h}(d,\theta')\right), \\ &= \mu_S + \left(E[g_{tx}^m]\right)_{dB} - \eta\left(E[d_u^h]\right)_{dB}, \end{aligned} \tag{4.66}$$

$$b = \sigma_S, \tag{4.67}$$

where $\mu_S = 0$ dB is the mean of the shadowing fading, $\sigma_S = 8$ dB is the standard deviation of the shadow fading, $E[g_{tx}^m]$ is the expected antenna gain in dB from cell m, $\eta = 3.76$ is the path loss exponent and $E[d_u^h]$ is the expected distance in kilometers between the user u and the cell m of eNB h. The estimation of functions $f^m\{a,b\}$ of Eq. (4.52) and $g^m\{a,b\}$ of Eq. (4.53) are calculated from each eNB and are shown in Table 4.3. For intra-site CoMP scenario, all cells belonging to a eNB serve as cooperating cells. In our case, there are three cooperating cells in each eNB and the location of each serving cell are co-located. Hence, we can modify the notation of Eq. (4.52) by adding an eNB location index. Then, the expected value $E[X]$ is calculated as

$$\begin{aligned} E[X] &= \sum_{m\in\Omega_u^m} f^{m,h}\{a,b\} = f^{1,1}\{a,b\} + f^{2,1}\{a,b\} + f^{3,1}\{a,b\}, \\ &= 3\times f^1\{a,b\} = 3\times 67122, \\ &= 201366. \end{aligned}$$

Similarly, the expected value $Var[X]$ from Eq. (4.53) can be calculated as

$$\begin{aligned} Var[X] &= \sum_{m \in \Omega_u^m} g^{m,h}\{a,b\} = g^{1,1}\{a,b\} + g^{2,1}\{a,b\} + g^{3,1}\{a,b\}, \\ &= 3 \times g^{1}\{a,b\} = 3 \times (1295.8 \times 10^8), \\ &= 38874 \times 10^7. \end{aligned}$$

In our scenario, the signal received from cells of other than the central eNB are treated as an interfering signal. Hence, using Eq. (4.58) and adding the eNB location index, we can calculate the expected value $E[Y]$ as

$$\begin{aligned} E[Y] &= \sum_{i \in \overline{\Omega_u^m}, i \neq m} f^{i,h}\{a,b\} = 3\sum_{h=2}^{19} f^{h}\{a,b\}, \\ &= 12883. \end{aligned}$$

Similarly, using Eq. (4.59) and adding the eNB location index, we can calculate the expected value $Var[Y]$ as

$$\begin{aligned} Var[Y] &= \sum_{i \in \overline{\Omega_u^m}, i \neq m} g^{i,h}\{a,b\} = 3\sum_{h=2}^{19} g^{h}\{a,b\}, \\ &= 50790 \times 10^4. \end{aligned}$$

Using Eqs. (4.56), (4.57), (4.62) and (4.63), the mean and the variance of X and Y are calculated in Table 4.4. Finally, the expected value of SINR can be calculated as

$$\begin{aligned} E[\gamma_u^m] &= E\left[10 \cdot \log_{10}\frac{X}{Y}\right] = m_x - m_y = 47.916 - 38.0576, \\ &= \mathbf{9.86}\ \text{dB}. \end{aligned}$$

Table 4.4: The mean and the variance of log-normally distributed random variables X and Y

Variable	Mean [dB]	Variance [dB]
X	$m_x = 47.92$	$\sigma_x^2 = 44.50$
Y	$m_y = 38.06$	$\sigma_y^2 = 26.43$

4.9 Radio Access Bearer Efficiency and Bit Rate Modelling

The Radio Access Bearer (RAB) is defined in the previous chapter (Chapter 3, Section 3.13). In general, the RAB efficiency of a user on subchannel r is estimated as [109]

$$\eta_{r,k} = CR_k \log_2(N_k), \tag{4.68}$$

where $\eta_{r,k}$ is RAB efficiency (bits/symbol) on subchannel r for the selected MCS k, CR_k is coding rate of the MCS k and N_k is the number of constellation points of the MCS k, where, $k \in \mathcal{K}$ represents a particular MCS as shown in Table 3.1 [77, 78].

Once an MCS is selected, the bit-rate of user u over subchannel r is modelled as [93]

$$BR_{u,r} = \eta_{r,k}\frac{N_r O_r}{\tau} = CR_k \frac{N_r O_r}{\tau}\log_2(N_k), \tag{4.69}$$

where $BR_{u,r}$ is the bit-rate (bits/sec), $N_r = 12$ is the number of sub-carriers in subchannel r, $O_r = 11$ is the number of OFDM data symbols (where $14-11 = 3$ are control symbols) in subchannel r in $\tau = 1$ ms duration of a subframe.

4.10 Throughput Modelling

Once the bit-rate is known, the throughput of user u connected to cell m on subchannel r can be modelled as [94]

$$\begin{aligned} T_u^m &= BR_{u,r}\left(1 - \varepsilon\left(\gamma_{u,r}^m, k\right)\right), \\ &= CR_k \frac{N_r O_r}{\tau}\log_2(N_k)\left(1 - \varepsilon\left(\gamma_{u,r}^m, k\right)\right), \end{aligned} \tag{4.70}$$

where T_u^m represents the throughput of the user u in subchannel r connected to cell m, $\varepsilon(\gamma_{u,r}^m, k)$ represents the BLER suffered by the user u connected to cell m on subchannel r and is a function of both SINR, $\gamma_{u,r}^m$, and MCS, k.

The average cell throughput is the sum of the throughput of all the active users present in the cell and is calculated as

$$\begin{aligned} T^m &= \sum_{\boldsymbol{n}\in\mathcal{S}} \sum_{k=0}^{s(\boldsymbol{n})\leq M} \sum_{u=1}^{E[n^m]} p_k \boldsymbol{\pi}(\boldsymbol{n}) T_u^m, \\ &= \sum_{\boldsymbol{n}\in\mathcal{S}} \sum_{k=0}^{s(\boldsymbol{n})\leq M} E[n^m] \binom{s(\boldsymbol{n})}{k} \left(\frac{1}{R}\right)^k \left(1-\frac{1}{R}\right)^{s(\boldsymbol{n})-k} \boldsymbol{\pi}(\boldsymbol{n}) T_u^m, \\ &= \sum_{\boldsymbol{n}\in\mathcal{S}} \sum_{k=0}^{s(\boldsymbol{n})\leq M} E[n^m] \binom{s(\boldsymbol{n})}{k} \left(\frac{1}{R}\right)^k \left(1-\frac{1}{R}\right)^{s(\boldsymbol{n})-k} \left[\prod_{m=1}^{M} \boldsymbol{\pi}^m(\boldsymbol{n}^m)\right] \\ &\quad \left[CR_k \frac{N_r O_r}{\tau} \log_2(N_k) \left(1-\varepsilon\left(\gamma_{u,r}^m, k\right)\right)\right], \end{aligned} \tag{4.71}$$

where $\binom{s(\boldsymbol{n})}{k} = s(\boldsymbol{n})!/(k!\,(s(\boldsymbol{n})-k)!)$ is the binomial coefficient, T^m is the average throughput of cell m, $\boldsymbol{n} \in \mathcal{S}$.

The system throughput, T^{sys}, is the sum of the throughput of all the cells in the system and is calculated as

$$T^{sys} = \sum_{m}^{M} T^m. \tag{4.72}$$

Numerically: A possible MCS assigned by the expected SINR can be obtained by the look-up table from the modulation and the coding scheme. By looking up Table 3.1 from Chapter 3, a suitable modulation and coding scheme acquired by the expected SINR $\gamma_u^m = 9.8584$ dB is 7^{th} channel quality indicator, i.e., 16-Quadrature Amplitude Modulation (QAM) with coding rate, $CR_7 = 1/3$. Then, the RAB efficiency, η_7, and the bit-rate, BR_7, can be calculated as

$$\begin{aligned} \eta_7 &= CR_7 \log_2 N_7 = \frac{1}{3}\log_2(16) = \frac{4}{3} = \mathbf{1.333}. \\ BR_7 &= \frac{4}{3}\frac{12\times 11}{1\times 10^{-3}} = \mathbf{176} \text{ kbps}. \end{aligned}$$

If the BLER suffered by the user is zero, then the average throughput can be achieved by the user is **176** kbps.

4.11 Summary

This chapter has been focused on developing a complete dynamic analytical model for the performance evaluation of CoMP joint transmission in LTE-A cellular networks. The model considers the dynamic nature of user arrival and departure, random location of users in a cell, distance of users from neighbour base stations, sectorial antenna gain at an arbitrary position, probability density of SINR, throughput modelling. The following are the main contributions made during the development of an analytical model:

- **Contribution 1**: Derivation of probabilistic and expected distance of a user in a cell.
- **Contribution 2**: Derivation of arbitrary and expected distance of a user in a cell from its neighbour base stations in the network.
- **Contribution 3**: Derivation of sectorial antenna gain at an arbitrary location from all base stations in the system.
- **Contribution 4**: Derivation of expected SINR under CoMP joint transmission.
- **Contribution 5**: Formulation of the user, the cell and the network throughput.

Table 4.3: Expected value of a function $f\{a,b\}$ and $g\{a,b\}$

Tier	eNB Index, h	User Distance d_u^h [m]	g_{tx}^m [dB]	a (Eq. (4.66)) [dB]	$f^h\{a,b\}$ (Eq. (4.54))	$g^h\{a,b\}$ (Eq. (4.55))
First Tier	1	178.26	12.738	40.9	67122	1295.8×10^8
	2	530.826	5.836	16.182	226	0
	3	340.151	7.316	24.929	1697	0.8×10^8
	4	340.151	7.316	24.929	1697	0.8×10^8
	5	530.826	5.836	16.182	226	0
	6	669.217	5.346	11.909	85	0
	7	669.217	5.346	11.909	85	0
Second Tier	8	1015.764	4.744	4.485	15	0
	9	784.667	5.082	9.04	44	0
	10	1015.764	4.744	4.485	15	0
	11	973.576	4.793	5.227	18	0
	12	1015.764	4.744	4.485	15	0
	13	784.667	5.082	9.04	44	0
	14	1015.764	4.744	4.485	15	0
	15	973.576	4.793	5.227	18	0
	16	1015.764	4.744	4.485	15	0
	17	784.667	5.082	9.04	44	0
	18	1015.764	4.744	4.485	15	0
	19	973.576	4.793	5.227	18	0

Chapter 5:

Performance of the Scheduling Algorithm under Intra-Site Homogeneous CoMP

In Chapter 3, a novel radio spectrum scheduling algorithm based on the maximum throughput in Coordinated Multi-Point (CoMP) Joint Transmission (JT) technique in an LTE-A system was proposed. Also, a design of an event-driven dynamic system-level simulator was formulated in order to evaluate the proposed algorithm. In Chapter 4, a complete dynamic analytical model for the throughput evaluation of such a system was developed.

In this chapter, the performance of the proposed resource scheduling algorithm is evaluated under an intra-site CoMP JT in a homogeneous network. The algorithm is evaluated for two different traffic behaviours under mobility and no mobility of users and under different criteria of cell-edge decisions.

5.1 Intra-Site CoMP Cluster Formation

The CoMP Cooperating Set (CCS) is a set of cells which take part in the coordination of scheduling and data transmission to UE. One of the main problems to determine a suitable CCS for a UE is which cells and how many cells should take part in a cooperation to serve this UE in order to achieve a maximum throughput performance. It is because too many cooperating cells in a CCS leads not only to complexity in terms of signalling and synchronisation,

they also impose a burden on the backhaul link since data and Channel State Information (CSI) are to be shared among all the coordinating cells.

Figure 5.1 shows an intra-site cluster with three cells of the same eNB participated in cooperation to schedule a particular UE. This type of cluster formation is considered as a *static cluster* since a UE has fixed cooperating cells all the time. For example, as shown in Fig. 5.1, the serving cell of UE 1 is Cell B, whereas, Cell A and Cell C are cooperating cells. This type of cluster formation does not have the problem of backhaul capacity since all the cooperating cells in a cluster are either co-located at the same eNB or located away from the eNB (in case of RRHs) and connected with high-speed optical fiber. Here, all three cooperating cells are co-located as shown in Fig. 5.1. In such a deployment scenario, the cooperating cells do not require any interface since all the co-operating cells are co-located, due to which the performance of CoMP would be faster.

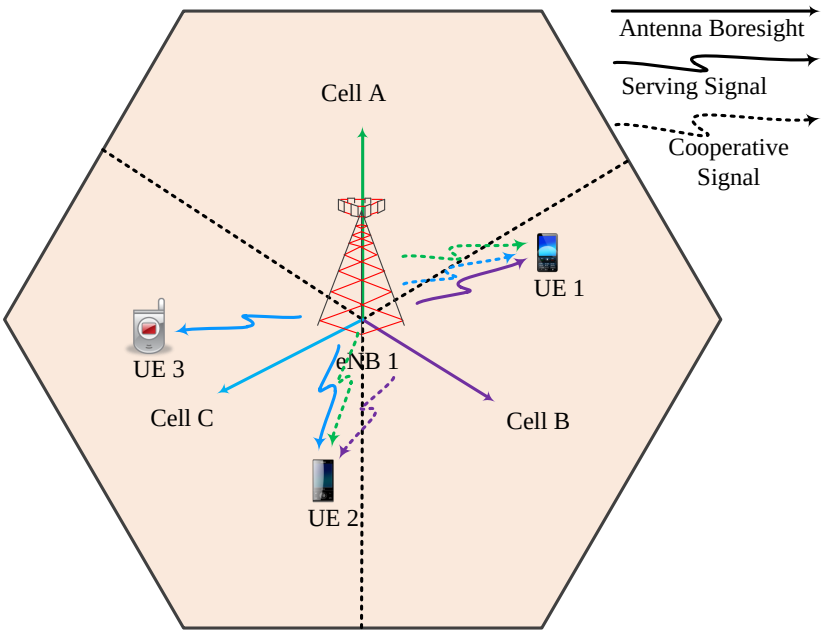

Figure 5.1: Intra-site CoMP cluster

5.2 Simulation Scenario Setup

A network of 19 tri-sectored eNBs (i.e., 57 cells in the network) has been considered as shown in Fig. 5.2. Users were uniformly distributed within the coverage area of each cell. Users arrive in a cell according to a Poisson process with inter-arrival time exponentially distributed with the mean arrival rate λ_u^m and leave the system after being served. The holding time is exponentially distributed with the mean μ_u^m. The network was implemented into the system level event-driven simulator as presented in Chapter 3. The path loss and antenna radiation pattern were modelled according to the models as presented in Chapter 3; the shadow fading was modelled using a log-normal shadowing with a standard deviation of 8 dB; and the flat fading due to multipath propagation was modelled as a Rayleigh fading model. To avoid base station tower shadow effects, users were distributed 35 metres away from the base station. Further details about the simulation parameters are presented in Table 5.1. Users suffered from outage if they fell in any of the following stages:

- *Blocked/No Resource*, which means all subchannels are already occupied when a user tries to access a subchannel to attach to the network.
- *No Coverage*, which means the user has accessed a subchannel but the received signal strength is less than the required receiver sensitivity.
- *No RAB*, which means the user has sufficient coverage but its SINR does not satisfy the minimum required SINR to access an MCS.

The simulation model to evaluate the performance of CoMP in an intra-site scenario is shown in Fig. 5.2. In this scenario, cooperating clusters are formed from the same eNB. A list of intra-cell clusters is shown in Table 5.2.

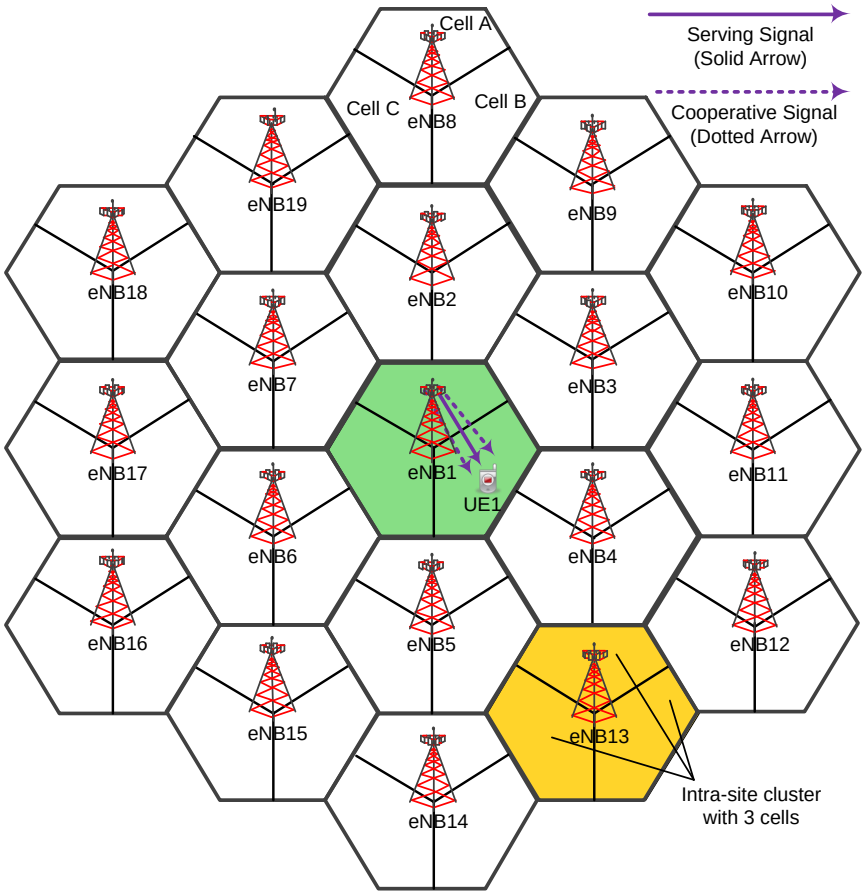

Figure 5.2: Network model for homogeneous intra-site CoMP simulation scenario

Table 5.1: Simulation parameters for a homogeneous CoMP

User distribution	Uniform
User generation process	Poisson, Fixed
User mean arrival rate (λ_u^m) for Poisson	0.2 users/s/cell
User mean holding time (μ_u^m)	30 s to 300 s in step of 30 s
User inter-arrival and holding time dist.	Exponential
Network layout	19 hexagonal sites with 3 cells
Carrier frequency/Subcarrier spacing	2 GHz/15 kHz
System bandwidth	10 MHz
Resource Block (RB) spacing	12×15 kHz = 180 kHz
Number of subchannels (R)	50
Data symbol per time slot (O_r)	11 OFDM data symbols
Frame duration (τ)	1 ms
Thermal noise density (σ)	-174 dBm/Hz
Thermal noise power	-121.4 dBm
Resource allocation	1 RB/user
eNB Tx power	46 dBm
eNB/UE antenna height (h_b/h_u)	32/1.5 m
eNB/UE antenna gain	18/0 dBi
UE noise figure	9 dB
UE receiver sensitivity	-95 dBm
eNB antenna boresight	0/120/240 degrees
eNB antenna pattern	3GPP Case1: 3D antenna pattern
Shadowing model	Gudmunson model
Shadowing standard deviation	8 dB
Correlation shadowing distance (d_{cor})	50 m
CoMP cluster type	intra/inter-site static cluster
CCS size (N)	2, 3
Scheduling algorithms	JPF, JMT, PF and MT

Table 5.2: List of intra-site clusters in a homogeneous network

Cluster Name	Cooperating Cells	Cluster Size
c1	{eNB1:CellA, eNB1:CellB, eNB1:CellC}	3
c2	{eNB2:CellA, eNB2:CellB, eNB2:CellC}	3
c3	{eNB3:CellA, eNB3:CellB, eNB3:CellC}	3
c4	{eNB4:CellA, eNB4:CellB, eNB4:CellC}	3
c5	{eNB5:CellA, eNB5:CellB, eNB5:CellC}	3
c6	{eNB6:CellA, eNB6:CellB, eNB6:CellC}	3
c7	{eNB7:CellA, eNB7:CellB, eNB7:CellC}	3
c8	{eNB8:CellA, eNB8:CellB, eNB8:CellC}	3
c9	{eNB9:CellA, eNB9:CellB, eNB9:CellC}	3
c10	{eNB10:CellA, eNB10:CellB, eNB10:CellC}	3
c11	{eNB11:CellA, eNB11:CellB, eNB11:CellC}	3
c12	{eNB12:CellA, eNB12:CellB, eNB12:CellC}	3
c13	{eNB13:CellA, eNB13:CellB, eNB13:CellC}	3
c14	{eNB14:CellA, eNB14:CellB, eNB14:CellC}	3
c15	{eNB15:CellA, eNB15:CellB, eNB15:CellC}	3
c16	{eNB16:CellA, eNB16:CellB, eNB16:CellC}	3
c17	{eNB17:CellA, eNB17:CellB, eNB17:CellC}	3
c18	{eNB18:CellA, eNB18:CellB, eNB18:CellC}	3
c19	{eNB19:CellA, eNB19:CellB, eNB19:CellC}	3

5.3 Performance Indicators and Simulation Parameter Tuning

5.3.1 Key Performance Indicators

The performance of the network was assessed through the following Key Performance Indicators (KPIs):

- *Generated users*, which represent the absolute total number of users generated during the entire simulation period.
- *Connected users*, which denote the average number of active users simultaneously connected to the network at any instant during the entire simulation period in the steady state.
- *Success users*, which denote the average number of active users successfully achieving the service during the entire simulation period in the steady state.
- *Outage users*, which represent the average number of outages incurred to users during the entire simulation period in the steady state. The possible reasons for user outage are either because of *No Coverage* or *No RAB*.
- *Cell activity*, which represents the percentage of a subchannel utilised by the network.
- *User throughput*, which indicates the average throughput of a user at any time during the entire simulation period in the steady state.
- *Cell-edge user throughput*, which indicates the average throughput of cell-edge users at any time during the entire simulation period in the steady state.

- *System throughput*, which indicates the average sum throughput obtained by the network at any time during the entire simulation period in the steady state,

5.3.2 Obtaining Various Traffic Load in the Network

In order to model the behaviour of dynamic incoming user data traffic or of dynamic user service occupancy time, and consequently obtain various traffic loads in the network, two different approaches have been implemented. In the first approach, the behaviour of the dynamic incoming user data traffic was modelled by generating users with different arrival rates and keeping their service holding time (i.e., service rate) fixed. While in the second approach, the behaviour of the dynamic users service rate was modelled by generating users with different service holding time and keeping their arrival rate fixed. The parameters for the users' arrival rate (λ_u^m) and their service rate (μ_u^m) were tuned, and these tuned parameters have been used in the relevant simulation.

An example of obtaining different system loads[a] by various simulations is summarised in Table 5.3. Referring to the table, suppose each user has a fixed service time (say 300 s), while their arrival rate is varied (the last column in the table). With these parameters, the system load reaches about 95 % just in the case of $\lambda_u^m = 0.2$ and then remains constant after the arrival rate, λ_u^m, is increased beyond 0.4. Therefore, with these selected traffic parameters, we are unable to obtain different loads in the network. Similar results can be seen by selecting a fixed arrival rate (say 1.0) and varying the service time (the last row in the table). Hence, in order to obtain the network performance under different traffic loads, we have to select a proper arrival rate and service time. For this reason, we can select either the fixed service time of 60 s (light-

[a]Here, system load means the subchannel utilisation because each user is allowed only one subchannel.

grey coloured-column in the table), while varying the arrival rate or a fixed arrival rate of 0.2 users per second (light-grey coloured-row in the table), while varying the service time. Note that, in either approache, our motive is to obtain different user loads in the network and select the one which will be used in the simulation work later in the thesis. An example of the system load versus simulation time under the selected traffic pattern is shown in Fig. 5.3.

Table 5.3: System loads under different traffic behaviour by simulation

System		**Service Time (s),** $t_u^m = 1/\mu_u^m$									
Load (%)		30	60	90	120	150	180	210	240	270	300
Arrival Rate (Users/s/cell), λ_u^m	0.1	5.96	11.92	17.64	24.12	30.34	36.64	40.92	48.07	54.11	58.88
	0.2	12.04	23.99	35.83	47.60	59.28	**71.24**	82.63	87.57	92.28	94.38
	0.3	17.99	35.73	54.41	72.26	85.42	91.43	94.94	96.18	97.08	97.75
	0.4	24.00	48.07	71.64	88.11	94.19	96.39	97.39	97.93	98.41	98.62
	0.5	29.97	59.91	85.39	94.20	96.65	97.69	98.26	98.64	98.86	99.03
	0.6	36.10	71.18	91.71	96.31	97.74	98.37	98.71	98.99	99.10	99.25
	0.7	42.24	82.05	94.87	97.47	98.32	98.70	99.00	99.15	99.31	99.40
	0.8	47.91	87.87	96.34	97.97	98.63	98.98	99.16	99.33	99.39	99.49
	0.9	54.23	92.08	97.07	98.35	98.86	99.17	99.31	99.40	99.50	99.54
	1.0	59.84	94.16	97.74	98.63	99.03	99.23	99.37	99.46	99.55	**99.59**

Verification: Now let us verify analytically whether the results of the system loads obtained from various simulations, as shown in Table 5.3, are correct or not. For example, consider a user arrival rate in a cell is $\lambda_u^m = 0.2$ users per second and its service time is $t_u^m = 180$ s. Therefore, the traffic intensity in the cell can be calculated as $A = \lambda_u^m/\mu_u^m = \lambda_u^m t_u^m = 0.2 \times 180 = 36$. Then, using the loss formula (Eq. 4.11 from Chapter 4), the blocking probability can be calculated as

$$\mathbb{P}_B = \frac{\frac{A^R}{R!}}{\sum_{r=0}^{R} \frac{A^r}{r!}} = \frac{\frac{(36)^{50}}{50!}}{\sum_{r=0}^{50} \frac{(36)^r}{r!}} = 0.0050.$$

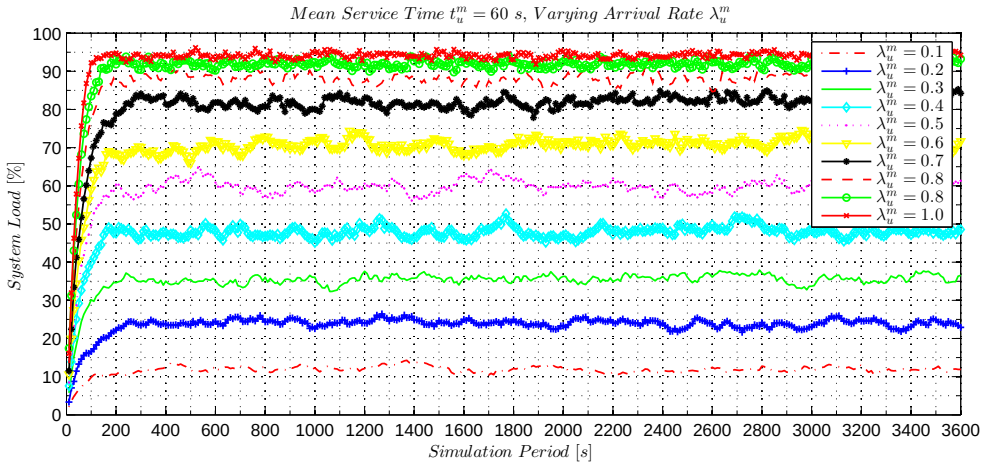

(a) Varying arrival rate (λ_u^m)

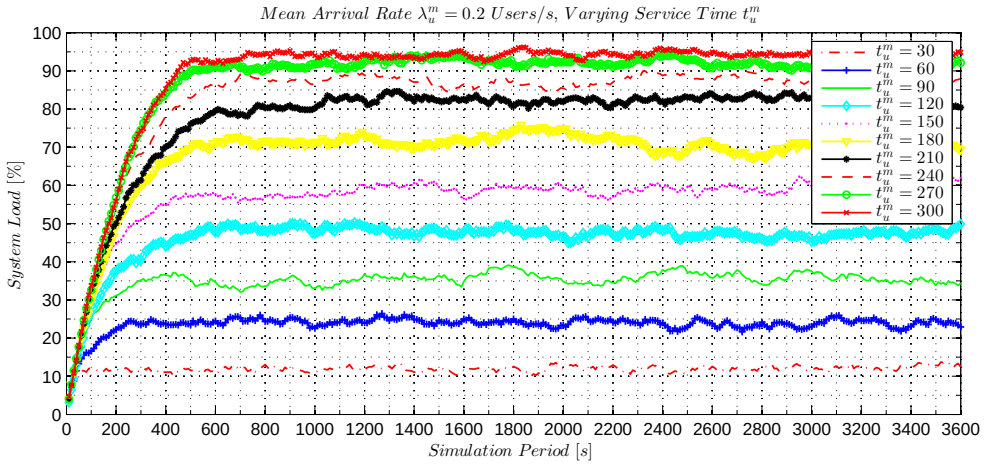

(b) Varying service rate ($\mu_u^m = 1/t_u^m$)

Figure 5.3: System loads under different traffic behaviour

Now, the average number of active users in the cell can be calculated by using Eq. 4.13 from Chapter 4 as

$$E[n^m] = A\,(1 - \mathbb{P}_B) = 36 \times (1 - 0.0050) = 35.8187.$$

Hence, the system load, i.e., the percentage of subchannel utilisation, can be calculated as $E[n^m]/R = 35.818/50 = 0.7164 =$ **71.64** %, which is nearly equal to the load obtained from simulation, i.e., **71.24** %.

Now, let us test another set of traffic parameters such as $\lambda_u^m = 1.0$ users per second and $\mu_u^m = 300$ s. Therefore, the traffic intensity is $A = \lambda_u^m t_u^m = 1.0 \times 300 = 300$. Then, the blocking probability can be calculated as

$$\mathbb{P}_B = \frac{\frac{(300)^{50}}{50!}}{\sum_{r=0}^{50} \frac{(300)^r}{r!}} = 0.8340.$$

Now, the average number of active users in the cell can be calculated as

$$E[n^m] = A\,(1 - \mathbb{P}_B) = 300 \times (1 - 0.8340) = 49.8019.$$

Hence, the percentage of subchannel utilisation can be calculated as $E[n^m]/R = 49.8019/50 = 0.9960 =$ **99.60** %, which is equal to the load obtained from the simulation, i.e., **99.59** %.

Three different ways to define the cell-centre and the cell-edge boundary, as described in Chapter 3 in Section 3.16, have been implemented. The threshold margin for the cell-edge decision play a key role in the network performance because it defines the cell-centre and the cell-edge boundary, which has the direct impact on the number of CEUs present in a cell. For example, if the threshold margins γ_{edge} and P_{edge} are too low, then the number of CEUs in a cell will be few and hence reserve less subchannels from the cooperating cells, which is an advantage in terms of the system capacity. However, if these threshold margins are too high, then the number of CEUs in the cell will be high and hence reserve more subchannels from the cooperating cells, which in turn, reduces the overall network capacity. Similarly, if threshold margin

d_{edge} is too low, then the number of CEUs in the cell will be high and hence consume more subchannels from the cooperating cells in order to serve CEUs as JT. Therefore, we need to tune the threshold margins for better network performance. In order to fine tune the threshold parameters (γ_{edge}, d_{edge} and P_{edge}), several simulations were run under the proposed scheduling algorithm and their performance results are highlighted as a summary in Tables 5.4, 5.5 and 5.6 for SINR based, distance based and RSRP based cell-edge decision, respectively.

Table 5.4 illustrates that $\gamma_{edge} = 1$ dB provides the best network performance. For instance, outage of users compared with other threshold values is lower, while the number of success of users is higher.

Table 5.4: Absolute Pilot SINR threshold, γ_{edge}, parameter tuning

System Performance for Different Pilot SINR Threshold, γ_{edge}, values									
γ_{edge}(dB)	-4	-3	-2	-1	0	1	2	3	4
Generated Users	41209	40875	41393	41399	41033	41158	41167	41175	41282
Outage Users	10661	10395	10275	9925	9736	**9647**	10397	11153	12250
Success Users	30548	30480	31118	31474	31297	**31511**	30770	30022	29032

Table 5.5 illustrates that d_{edge}= 225 m (which is 90% of ISD value) provides the best network performance in terms of less outage of users and high success of users compared with other sets of threshold values.

Table 5.5: Distance threshold, d_{edge}, parameter tuning

System Performance for Different Distance Threshold, d_{edge}, values					
d_{edge}(m)	150	175	200	225	250
Generated Users	41014	41209	40875	41393	41399
Outage Users	15059	13807	12565	**12092**	12206
Success Users	25955	27402	28310	**29301**	29193

Similarly, Table 5.6 illustrates that P_{edge}= 3 dBm provides the best network performance in terms of less outage of users and high success of users compared with other sets of threshold values.

Table 5.6: Relative RSRP threshold, P_{edge}, parameter tuning

System Performance for Different RSRP Threshold, P_{edge}, values									
P_{edge} (dBm)	-4	-3	-2	-1	0	1	2	3	4
Generated Users	41209	40875	41394	41401	41033	41150	41169	41177	41282
Outage Users	11076	10757	10631	10399	10264	9877	9937	**9818**	10117
Success Users	30133	30118	30763	31002	30769	31273	31232	**31359**	31165

Therefore, in the following simulations, the cell-centre and the cell-edge threshold boundary values will be used as d_{edge}= **225** m, γ_{edge} = **1** dB and P_{edge}= **3** dBm.

5.4 Performance of Scheduling Algorithm under Intra-Site CoMP and Poisson Traffic

Under Poisson traffic, the performance of the scheduling algorithms under intra-site CoMP scenario was evaluated. Users were generated as a Poisson random process with the mean arrival rate, λ_u^m= 0.2 calls per second, and the mean holding time t_u^m second. To model the dynamic behaviour of service time and thereby obtain different traffic intensities in the network, different sets of holding time from 30 s to 300 s were considered. Traffic intensity per subchannel is also known as the channel utilisation factor, i.e., the offered traffic per subchannel and is calculated as $\rho = A^m/R = (\lambda_u^m/\mu_u^m)/R$, where $A_u^m = \lambda_u^m/\mu_u^m$ is the offered traffic by user u in cell m and λ_u^m and μ_u^m are the user arrival and the service rate parameters, respectively. For example, if the user arrival rate is λ_u^m= 0.2 users per second and the service time (i.e.,

the holding time) is $t_u^m = 60$ s, i.e., the service rate $\mu_u^m = 1/t_u^m$, while the total number of subchannels in cell m is $R = 50$, then the traffic intensity per subchannel can be calculated as $\rho = (0.2 \times 60)/50 = 0.24 = 24\%$. The performance of the network was assessed under different situations such as users that were static, users who had mobility, the cell-edge decision based on the absolute distance from the serving base station, the cell-edge decision based on the relative pilot RSRP power and the cell-edge decision based on the absolute pilot SINR. Users' mobility was modelled as a random direction model as described in Chapter 3. The performance of the network was evaluated in terms of the mean number of success users, the mean outage users (no coverage and no RAB) and the mean cell activity. The cell activity, in other terms, is defined as the percentage of a subchannel utilised by the network. The detailed simulation parameters are listed in the previous section in Table 5.1. Figure 5.4 shows a tree diagram of performance evaluation of resource scheduling algorithms in intra-site CoMP under Poisson traffic.

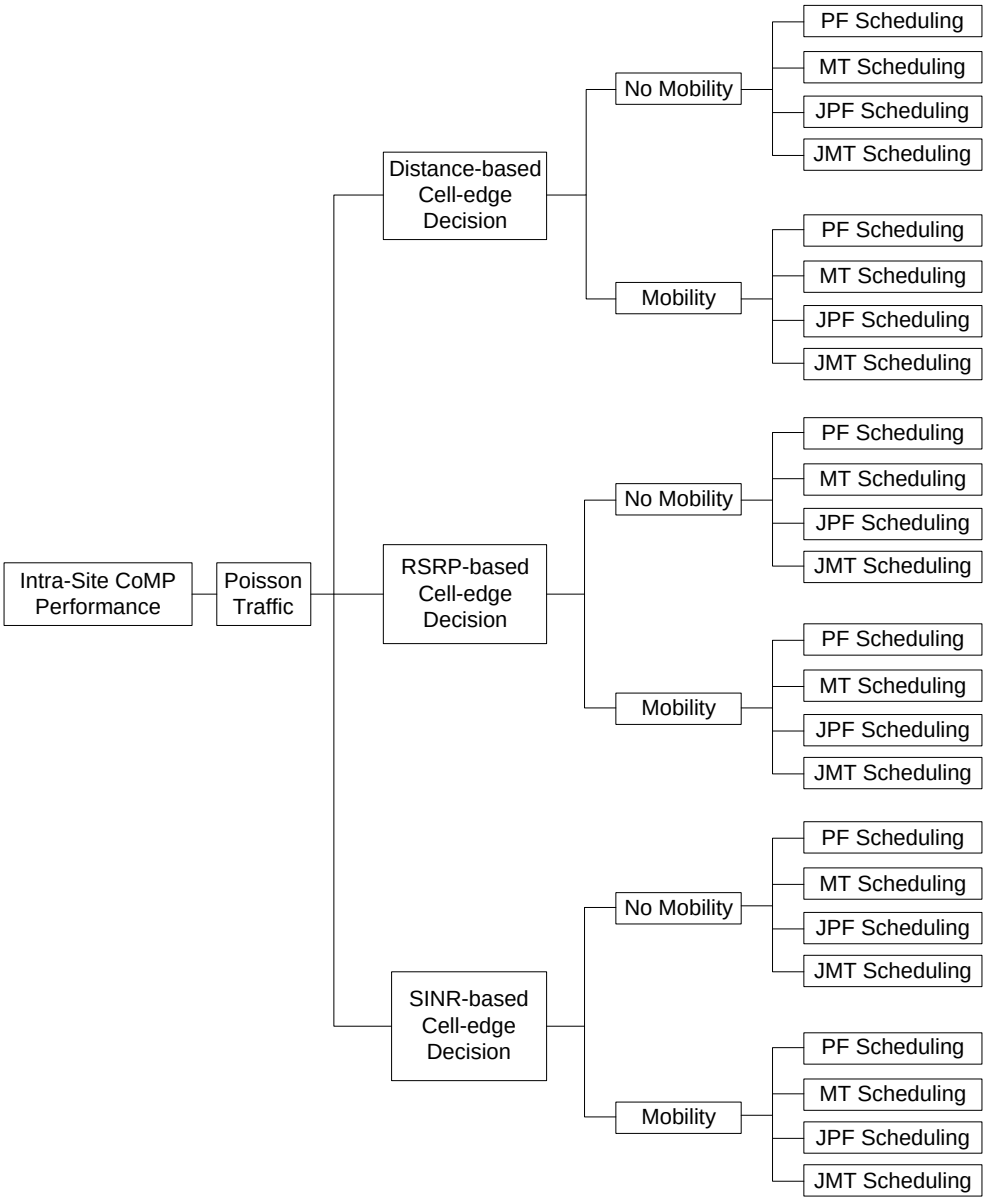

Figure 5.4: Tree diagram of performance evaluation of intra-site CoMP under Poisson traffic

5.4.1 Performance Results under a Distance based Cell-Edge

In this section, the performance of the network was evaluated considering cell-edge users based on their absolute distance from their serving base stations. The detail simulation results of the network-wide performance in terms of the mean number of success users, the mean outage users and the mean cell activity under no mobility and mobility conditions for various traffic intensities are shown in Appendix D in Table D.1. In the table, rows denote a KPIs performance for each o the four different scheduling algorithms, where scheduling algorithms Joint Maximum Throughput (JMT) and Joint Proportional Fairness (JPF) consider JT CoMP, while MT and PF consider without CoMP, i.e., Non-CoMP. The relative performance of the KPIs compared with the scheduling algorithm PF are calculated in Table 5.7. From these tables, it is noted that the cell activities of CoMP and Non-CoMP algorithms are inline with their counterpart both under no mobility and mobility conditions. For example, at the traffic intensity of 96 % under no mobility condition, the cell activity achieved by the CoMP algorithm JMT is 95.30 %, which is nearly equal to the 95.67 % as achieved by JPF. Similarly, the cell activity achieved by Non-CoMP algorithm MT is 87.25 %, which is nearly equal to 88.16 % as achieved by PF. This means, each algorithm utilised their available resources equally compared with their counter part algorithm.

Table 5.7: System level intra-site CoMP relative performance under distance based cell-edge and Poisson traffic

[a] **Relative (%) KPIs under Distance based Cell-edge and Poisson Traffic**											
KPIs ⇓	Sch. ⇓	Traffic Intensity per Subchannel									
		0.12	0.24	0.36	0.48	0.6	0.72	0.84	0.96	1.08	1.2
No Mobility											
Success UE	JMT	7.05	5.3	8	4.83	1.9	-6.15	-13.43	-19.75	-20.96	-20.66
	JPF	3.69	3.64	4.85	3.91	-1.82	-10.59	-18.1	-23.14	-24.84	-24.5
	MT	3.18	1.01	3.23	0.85	4.08	4.12	3.42	1.11	0.25	1.73
Outage UE	JMT	-27.29	-25.45	-27.11	-27.45	-29.34	-40.93	-49.78	-57.88	-58.91	-62.39
	JPF	-16.67	-15.52	-20.09	-19.02	-23.18	-32.39	-39.01	-45.67	-46.76	-49.08
	MT	-9.64	-6.93	-7.27	-9.58	-3.15	-4.96	-0.7	-8.72	-0.34	-2.95
Cell Activity	JMT	50.23	49.16	51.58	45.45	43.59	28.22	17.4	8.11	4.88	3.85
	JPF	48.88	49.99	50.04	48.29	40.08	27.72	16.96	8.52	4.83	3.51
	MT	0.82	-0.49	1.19	-1.23	2.68	2.25	2.56	-1.02	0.12	0.71
Mobility											
Success UE	JMT	13.05	20.68	15.14	7.94	-6.8	-13.5	-23.74	-26.43	-28.23	-28.4
	JPF	15.06	20.03	15.72	6.11	-8.5	-16.71	-26.12	-28.66	-29.83	-28.63
	MT	-0.27	5.93	-0.55	1.02	-2.54	2.48	-0.98	0.29	-0.56	1.35
Outage UE	JMT	-28.35	-27.67	-29.63	-32.48	-41.43	-49.6	-55.93	-58.32	-60.89	-61.29
	JPF	-23.85	-24.3	-26.61	-30.1	-40.67	-47.45	-54.18	-56.95	-58.08	-59.69
	MT	-2.51	-1.41	-2.95	1.33	-1.6	-1.63	-3.58	1.07	-0.19	-0.26
Cell Activity	JMT	85.87	95.31	86.4	75.11	48.91	32.75	15.64	9.28	4.87	3.46
	JPF	92.03	96.56	89.83	77.2	49.99	32.54	15.78	9.32	5.02	3.41
	MT	-1.05	3.19	-1.46	1.12	-2.19	0.89	-1.98	0.59	-0.41	0.71

[a]compared with PF scheduling

Figure 5.5 shows the performance of the network in terms of the mean number of success users. Under no mobility condition, it is noted that each algorithm has nearly similar performance until the traffic intensity of 60 %, as marked with a rectangle box in Fig. 5.5(a). As the traffic intensity increases beyond 60 %, the performance of CoMP algorithms (JMT and JPF) becomes lower than the performance of Non-CoMP algorithms (MT and PF). The reason is that, as the load in the network increases, new users may come to the cell-edge boundary and according to the cell-edge decision based on the absolute distance from the serving base station, a large number of users may be categorised as cell-edge users. Therefore, to improve the performance of such cell-edge users by the CoMP technique, more subchannels from the cooperating cells are used, due to which, the cooperating cells can not take more users because no further subchannels are available. From Fig. 5.6, it can be noted that the proposed CoMP algorithm (JMT) has less outage problem in terms of no coverage (Fig. 5.6(a)) and no RAB (Fig. 5.6(b)) compared with JPF under no mobility condition. For example, at the traffic intensity of 96 %, JMT has about 3.39 % higher success users (Fig. 5.5(b)), while about 15 % less coverage problem and about 10 % less RAB problem compared with JPF under no mobility condition.

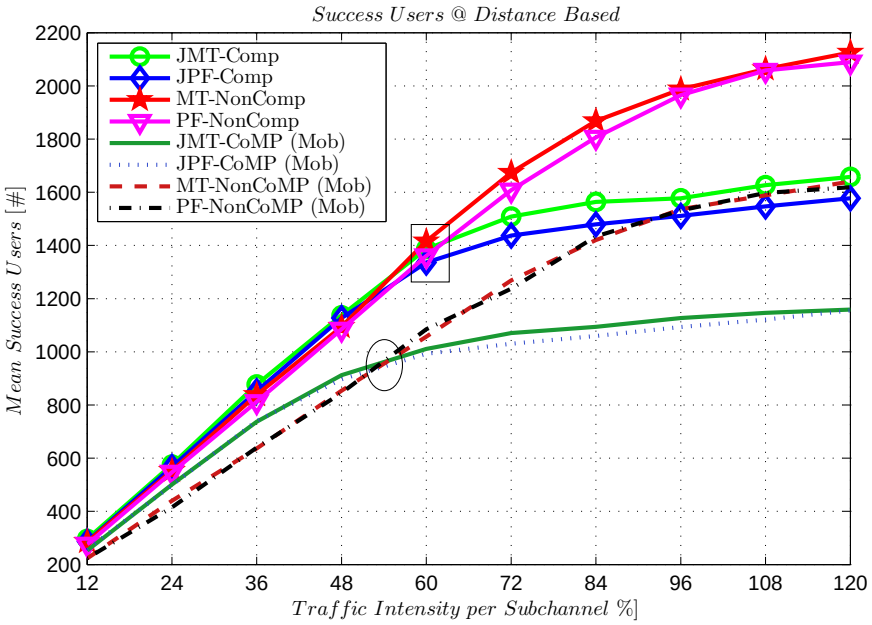

(a) Success users

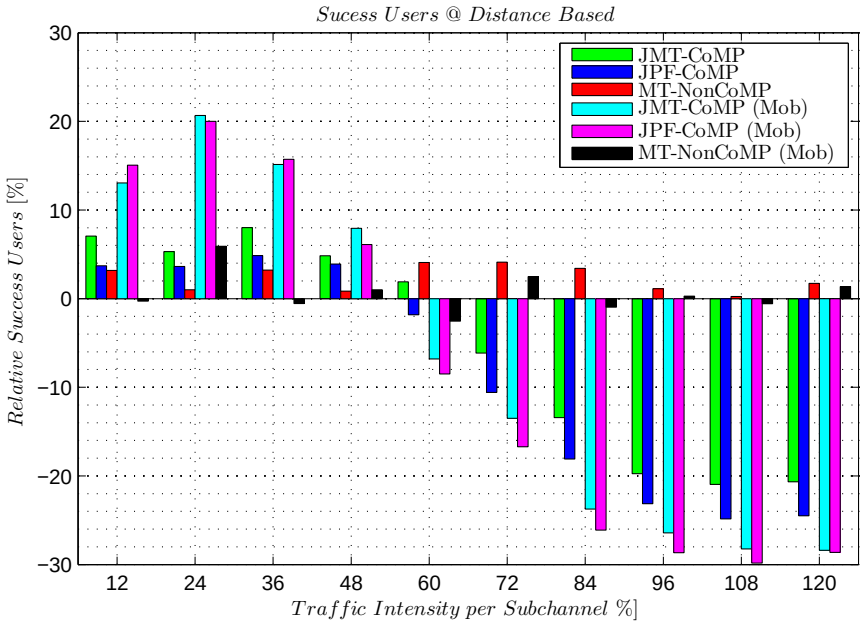

(b) Relative success users compared with PF

Figure 5.5: Intra-site CoMP performance in terms of success users under distance based cell-edge decision and Poisson traffic

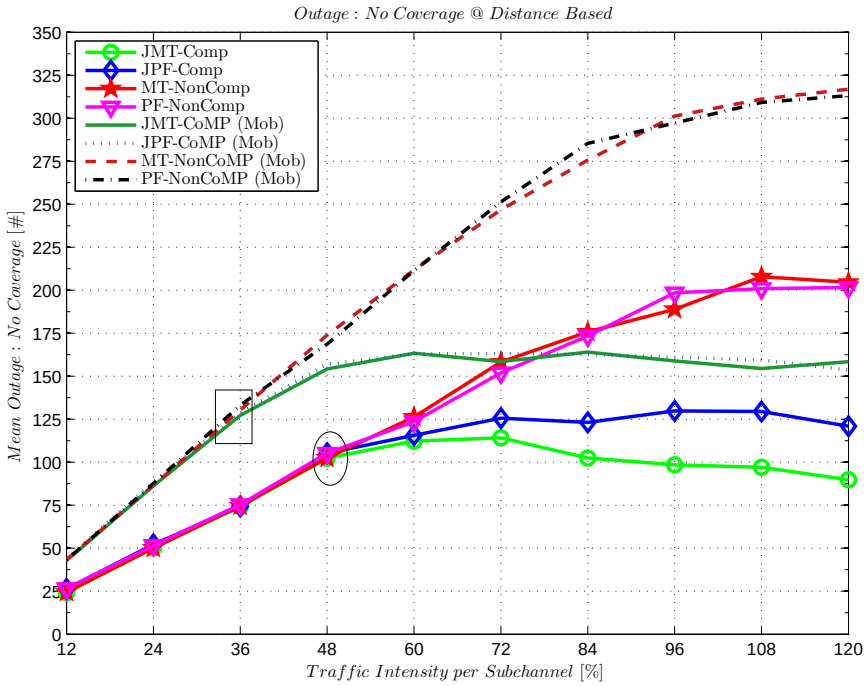

(a) Outage due to no coverage

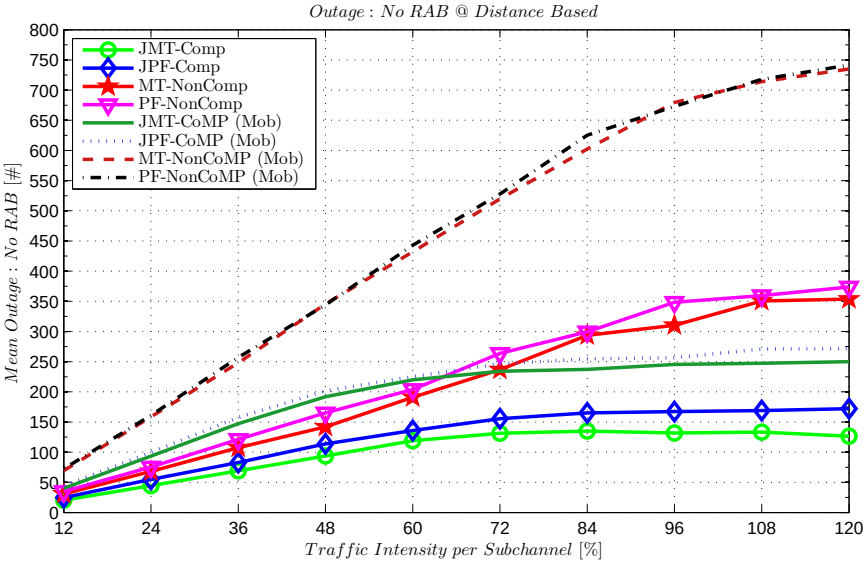

(b) Outage due to no RAB

Figure 5.6: Intra-site CoMP performance in terms of users outage under distance based cell-edge decision and Poisson traffic

Under mobility condition, the performance of CoMP algorithms (JMT and JPF) are higher than those of Non-CoMP algorithms (MT and PF) until the traffic intensity is around 55 % (marked as ellipse in Fig. 5.5(a)) and then decreases as the traffic intensity increases. It is also noted that the performance of each of the four algorithms under mobility is lower than those under no mobility. The reason is that under mobility, users may move away from the base station (i.e., towards the cell-edge boundary) and hence, according to the cell-edge decision based on the absolute distance, a large number of users may fall in the cell-edge criteria and therefore, more subchannels from the cooperating cells are used to improve the performance of such cell-edge users in a CoMP scenario, whereas a large number of outage occurs in Non-CoMP scenario due to a coverage lack problem, as shown in Fig. 5.6(a), because the received power at the cell-edge may be lower than the required receiver antenna sensitivity. From Fig. (5.6), it can also be noted that each algorithm under mobility condition has a nearly similar performance with their counter part in terms of no coverage and no RAB. For example, at the traffic intensity of 96 %, JMT has about 2.23 % higher success users (Fig. 5.5(b)), while about 0.74 % less coverage problem and about 1.64 % less RAB problem compared with JPF under mobility conditions.

5.4.2 Performance Results under RSRP based Cell-Edge

In this section, the performance of the network was evaluated considering cell-edge users based on their received pilot RSRP power from their serving base stations and compared with the strongest received interfering RSRP power. The detailed simulation results of the network-wide performance in terms of the mean number of success users, the mean outage users and the mean cell activity under no mobility and mobility conditions for various traffic intensities are shown in Appendix D in Table D.2. The relative performance of the KPIs compared with the scheduling algorithm PF are calculated in Table 5.8. From these tables, like in the previous section, it is noted that the cell activities of CoMP and Non-CoMP algorithms are inline with their counterpart both under no mobility and mobility conditions. For example, at the traffic intensity of 96 % under a no mobility condition, the cell activity achieved by the CoMP algorithm JMT is 90.08 %, which is nearly equal to 89.77 % as achieved by JPF. Similarly, the cell activity achieved by the Non-CoMP algorithm MT is 88.11 %, which is nearly equal to 88.35 % as achieved by PF. This means, each algorithm utilised their available resources equally compared with their counter part algorithm.

Table 5.8: System level intra-site CoMP relative performance under RSRP based cell-edge and Poisson traffic

[a]Relative (%) KPIs under RSRP based Cell-edge and Poisson Traffic											
KPIs ⇓	Sch. ⇓	Traffic Intensity per Subchannel (%)									
		12	24	36	48	60	72	84	96	108	120
No Mobility											
Success UE	JMT	6.56	12.55	10.78	5.5	-5.88	-15.32	-20.2	-24.03	-23.02	-22.4
	JPF	7.35	8.07	8.42	0.46	-13.77	-25.47	-33.9	-37.96	-39.06	-41.53
	MT	-0.14	5.21	3.26	3.43	2.25	-0.74	1.09	-0.12	1.47	0.83
Outage UE	JMT	-38.52	-38.41	-41.4	-46.07	-58.3	-68.63	-75.43	-78.41	-80.65	-82.43
	JPF	-33.28	-34.38	-35.94	-38.52	-47.96	-54.19	-60.22	-62.7	-64.17	-64.01
	MT	-7.87	-7.02	-7.4	-0.91	-4.39	-5.37	-8.09	-0.89	0.7	-3.15
Cell Activity	JMT	75.17	81.77	78.45	68.74	42.81	22.62	8.58	1.95	-0.17	-2.86
	JPF	77.64	77.58	78.05	66.99	43.07	22.66	8.72	1.6	-0.52	-3.05
	MT	-1.55	2.9	1.19	2.58	0.9	-1.68	-0.87	-0.28	1.3	-0.04
Mobility											
Success UE	JMT	23.11	32.71	23.7	10.75	-6.99	-14.54	-24.46	-26.43	-27.61	-28.21
	JPF	25.79	31.1	23.98	6.89	-11.87	-20.47	-29.67	-32.96	-34.68	-35.43
	MT	0.94	5.86	-0.58	1.2	-2.01	1.56	-1.23	0.37	0.76	0.36
Outage UE	JMT	-47.5	-48.14	-51.36	-60.62	-70.17	-75.71	-79.61	-81.78	-83.34	-83.95
	JPF	-44.32	-44.83	-50.18	-56.63	-66.68	-71.75	-75.88	-77.55	-79.16	-79.53
	MT	-4.91	-1.29	-2.92	0.99	-2.48	-0.17	-3.16	0.93	-2.21	1.27
Cell Activity	JMT	117.45	128.08	112.45	82.72	47.5	29.08	11.77	5.33	0.59	-0.77
	JPF	124.17	131.45	113.6	83.24	46.99	29.04	11.72	5.25	0.7	-0.96
	MT	-1.05	3.19	-1.46	1.12	-2.19	0.89	-1.98	0.59	-0.41	0.71

[a]compared with PF scheduling

Figure 5.7 shows the performance of the network in terms of the mean number of success users. Under a no mobility condition, it is noted that each algorithm has nearly similar performance until the traffic intensity of 48 %, as marked with a rectangle in Fig. 5.7(a). As the traffic intensity increases beyond 48 %, the performance of JMT and JPF becomes lower than the performance of Non-CoMP algorithms (MT and PF). The reason is that, as the load in the network increases, the interference level in the receiver increases. Therefore, to overcome the interference of cell-edge users by the CoMP technique, more subchannels from the cooperating cells are used, due to which, the cooperating cells cannot take more users because no further subchannels are available. It can also be noted that the proposed algorithm, JMT, has better performance compared with JPF and is increasing, while the performance of JPF becomes saturate although the cell activity is not reached to 100 %. The reason is that in the case of JPF, if a user's received signal strength is lower than that which is required to achieve a minimum MCS, the instantaneous bit rate is zero, which then means the estimation of aggregate bit rates over the considered time window in JPF becomes lower and hence the proportional weight becomes lower. At the traffic intensity of 96 %, JMT has about 13.92 % higher success users (Fig. 5.7(b)), while about 27 % less coverage problem (Fig. 5.8(a)) and about 9.7 % less RAB problem (Fig. 5.8(b)) compared with JPF under a no mobility condition. While, at the traffic intensity of 120 %, JMT has about 19 % higher success users, about 33.6 % lower coverage problem and about 10 % lower RAB problem compared with JPF.

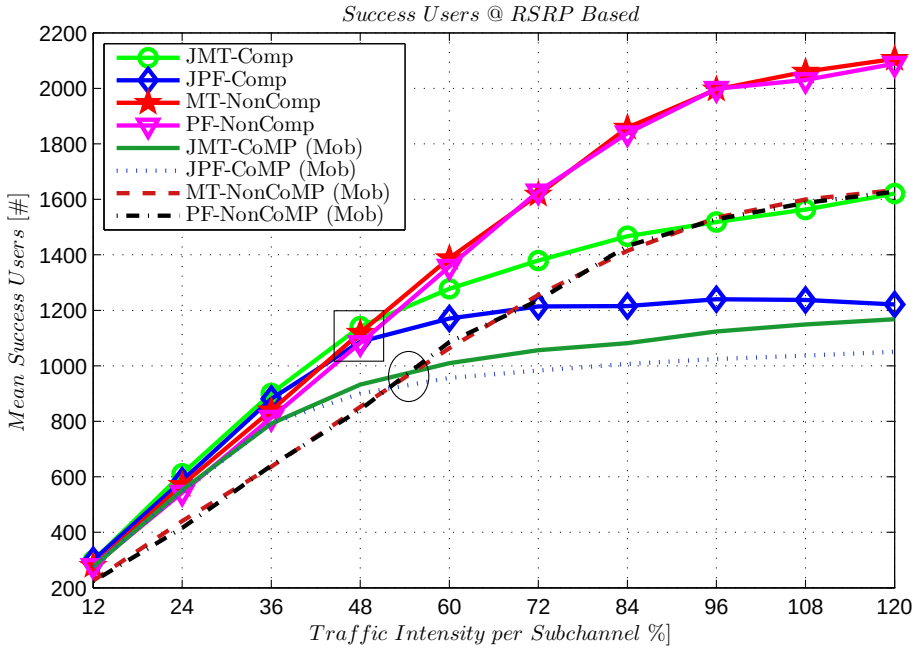

(a) Success users

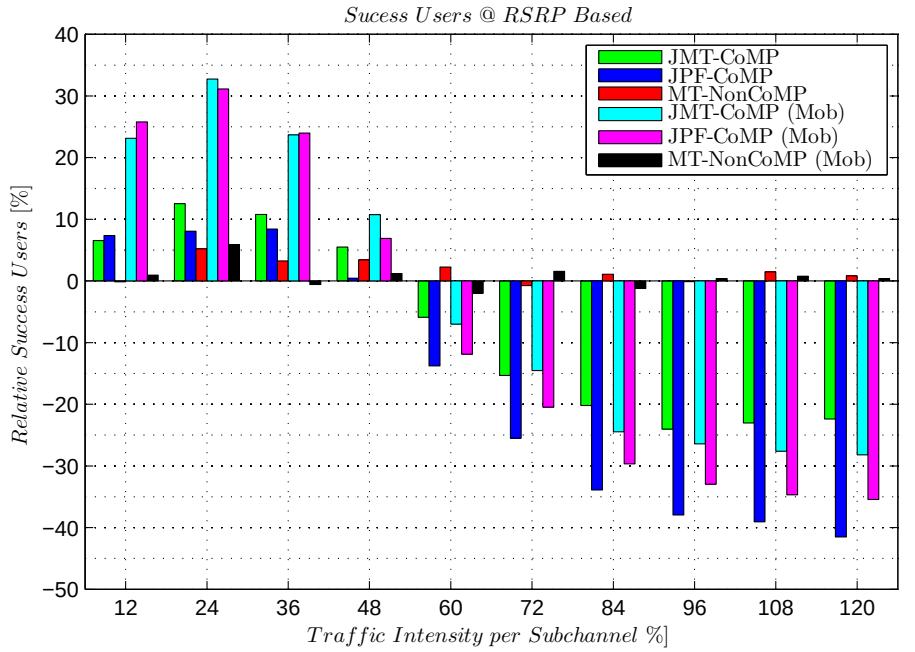

(b) Relative success users compared with PF

Figure 5.7: Intra-site CoMP performance in terms of success users under RSRP based cell-edge decision and Poisson traffic

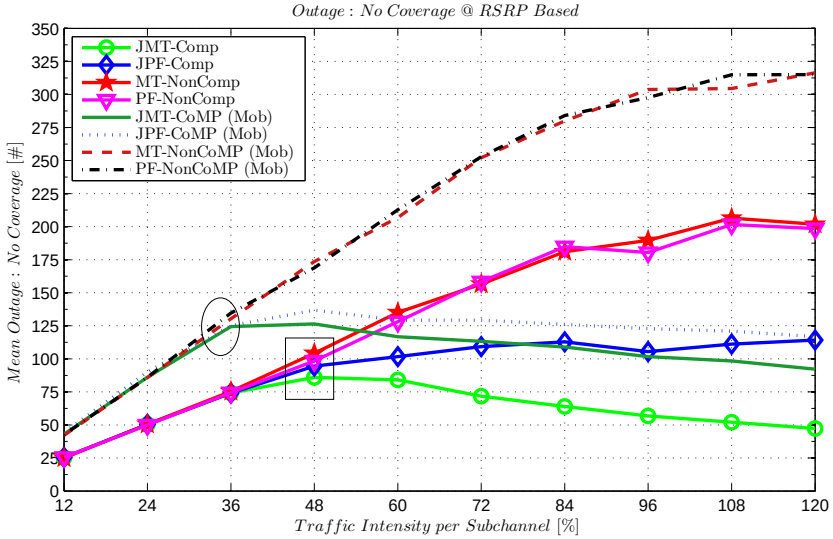

(a) Outage due to no coverage

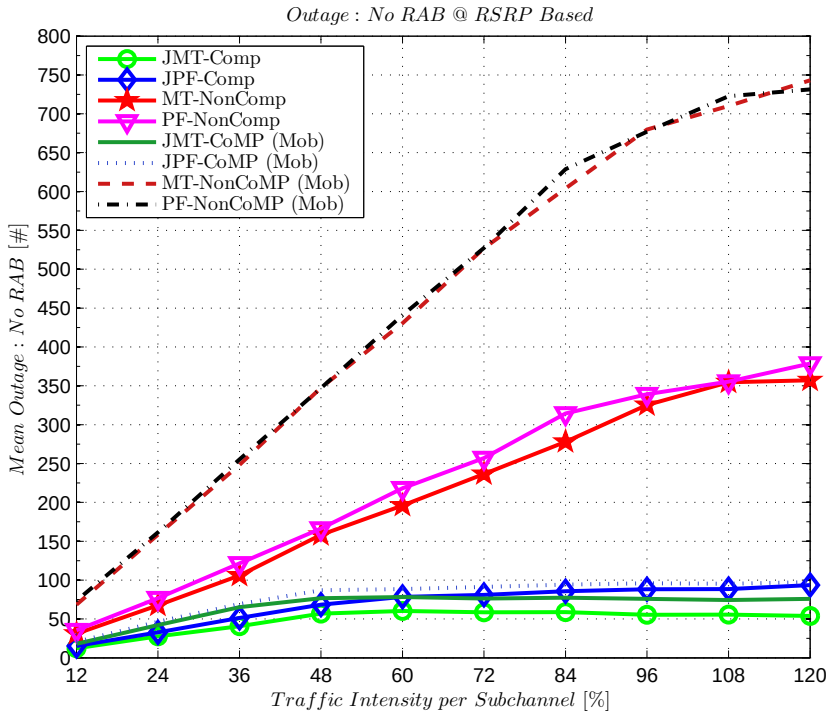

(b) Outage due to no RAB

Figure 5.8: Intra-site CoMP performance in terms of users outage under RSRP based cell-edge decision and Poisson traffic

Under mobility condition, the performance of CoMP algorithms (JMT and JPF) is higher than those of Non-CoMP algorithms (MT and PF) until the traffic intensity of around 55 % (marked as an ellipse in Fig. 5.7(a)) and then decreases as the traffic intensity further increases. It is also noted that the performance of each of the four algorithms under mobility condition are lower than those under no mobility. Compared with JPF, JMT has about 6.5 % higher success users, about 7 % less coverage problem and about 3 % less RAB problem at a traffic intensity of 96 %.

5.4.3 Performance Results under SINR based Cell-Edge

In this section, the performance of the network was evaluated considering cell-edge users based on pilot SINR. The detailed simulation results of the network-wide performance in terms of the mean number of success users, the mean outage users and the mean cell activity under no mobility and mobility conditions for various traffic intensities are shown in Appendix D in Table D.3. The relative performance of the KPIs compared with the scheduling algorithm PF are calculated in Table 5.9. Again, it is noted that the cell activities of the CoMP and the Non-CoMP algorithms are inline with their counterparts both under no mobility and mobility conditions. For example, at the traffic intensity of 96 % under no mobility condition, the cell activity achieved by the CoMP algorithm JMT is 89.74 %, which is nearly equal to 90.46 % as achieved by JPF. Similarly, the cell activity achieved by the Non-CoMP algorithm MT is 87.25 %, which is nearly equal to 88.16 % as achieved by PF. This means, each algorithm utilised their available resources equally compared with their counter part algorithm.

Table 5.9: System level intra-site CoMP relative performance under SINR based cell-edge and Poisson traffic

[a]Relative (%) KPIs under SINR based Cell-edge and Poisson Traffic											
KPIs ⇓	Sch. ⇓	Traffic Intensity per Subchannel (%)									
		12	24	36	48	60	72	84	96	108	120
No Mobility											
Success UE	JMT	10.01	8.81	10.86	3.1	-5.87	-14.43	-19.99	-24.46	-24.34	-22.88
	JPF	7.41	8.28	8.57	-0.81	-14.74	-26.84	-34.7	-40.98	-42	-43.14
	MT	3.18	1.14	3.18	0.66	4.39	4.19	3.74	1.04	0.47	1.66
Outage UE	JMT	-40.75	-40.12	-42.22	-49.24	-59.19	-69.57	-74.64	-79.04	-80.38	-82.07
	JPF	-33.55	-35.05	-37.12	-40.75	-47.77	-56.3	-60.23	-63.69	-64.89	-65.66
	MT	-9.98	-7.34	-6.99	-8.79	-4.34	-5.26	-1.88	-8.46	-1.12	-2.73
Cell Activity	JMT	81.61	82.08	81.88	65.76	45.07	24.33	12.06	1.8	-1.2	-2.69
	JPF	80.7	83	82.3	66.94	45.02	24.75	12.06	2.61	-1.04	-2.36
	MT	0.82	-0.49	1.19	-1.23	2.68	2.25	2.56	-1.02	0.12	0.71
Mobility											
Success UE	JMT	23.25	33.28	23.4	10.45	-7.65	-15.66	-24.83	-27.37	-28.37	-28.47
	JPF	22.8	33.59	23.98	7.1	-12.09	-21.28	-30.28	-34.79	-35.62	-35.58
	MT	0.8	5.96	-1.4	1.73	-3.17	0.9	-1.36	-0.04	-0.97	0.62
Outage UE	JMT	-48.31	-48.51	-52.43	-61.09	-70.21	-75.22	-79.57	-81.81	-83.5	-84.37
	JPF	-45.28	-47.23	-50.62	-58.28	-66.67	-71.69	-76.11	-77.3	-79.25	-79.95
	MT	-4.76	-1.41	-1.58	0.13	-0.57	0.9	-2.97	1.6	0.47	0.86
Cell Activity	JMT	119.85	130.24	113.04	82.59	47.59	29.4	12.18	5.53	0.88	-0.64
	JPF	122.06	133.05	115.63	83.08	47.81	29.47	12.2	5.36	1.1	-0.62
	MT	-1.05	3.19	-1.46	1.12	-2.19	0.89	-1.98	0.59	-0.41	0.71

[a]compared with PF scheduling

Figure 5.9 shows the performance of the network in terms of the mean number of success users. Under no mobility condition, it is noted that each algorithm has a nearly similar performance until the traffic intensity of 48 % is reached, as marked with a rectangle in Fig. 5.9(a). As the traffic intensity increases beyond 48 %, the performance of JMT and JPF becomes lower than the performance of the Non-CoMP algorithms (MT and PF). At the traffic intensity of 96 %, JMT has about 16.5 % higher success users (Fig. 5.9(b)), while about 28 % less coverage problem (Fig. 5.10(a)) and about 8 % less RAB problem (Fig. 5.10(b)) compared with JPF under a no mobility condition. At the traffic intensity of 120 %, JMT has about 20 % higher success users, about 30 % lower coverage problem and about 9 % lower RAB problem compared with JPF. It can also be seen that the network performance under the SINR based cell-edge and those under the RSRP based cell-edge are nearly similar. It is because the pilot SINR is estimated based on the pilot RSRP.

Under a mobility condition, the performance of the CoMP algorithms (JMT and JPF) is higher than those of the Non-CoMP algorithms (MT and PF) until the traffic intensity of around 55 % (marked as an ellipse in Fig. 5.9(a)) and then decreases as the traffic intensity further increases. It is also noted that the performance of each of the four algorithms under a mobility condition is lower than those under a no mobility. Compared to JPF, JMT has about 7.4 % higher success users, about 7.9 % less coverage problem and about 3 % less RAB problem at a traffic intensity of 96 % which are similar to the performance obtained in the case of RSRP based cell-edge decision.

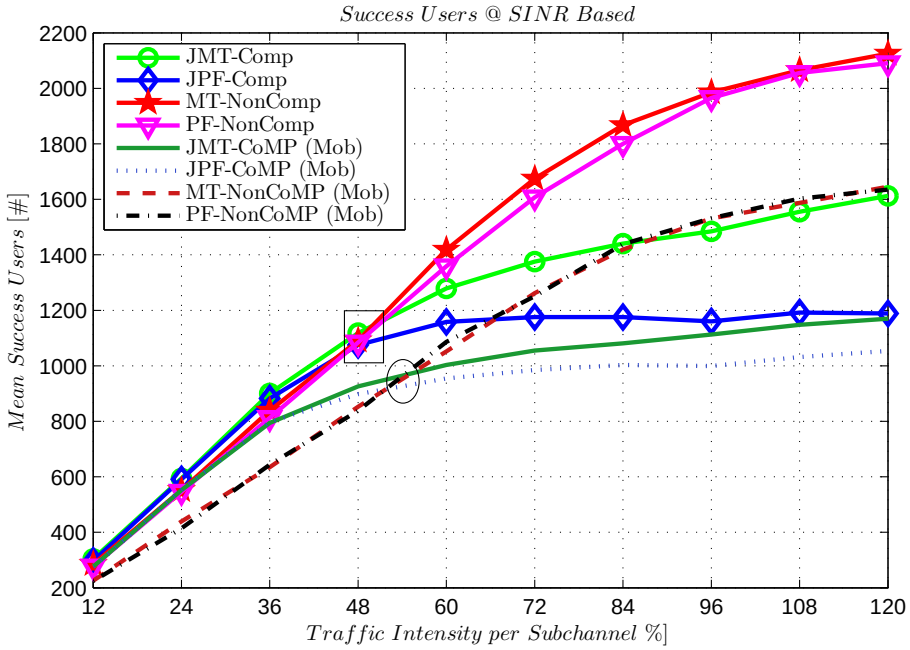

(a) Success users

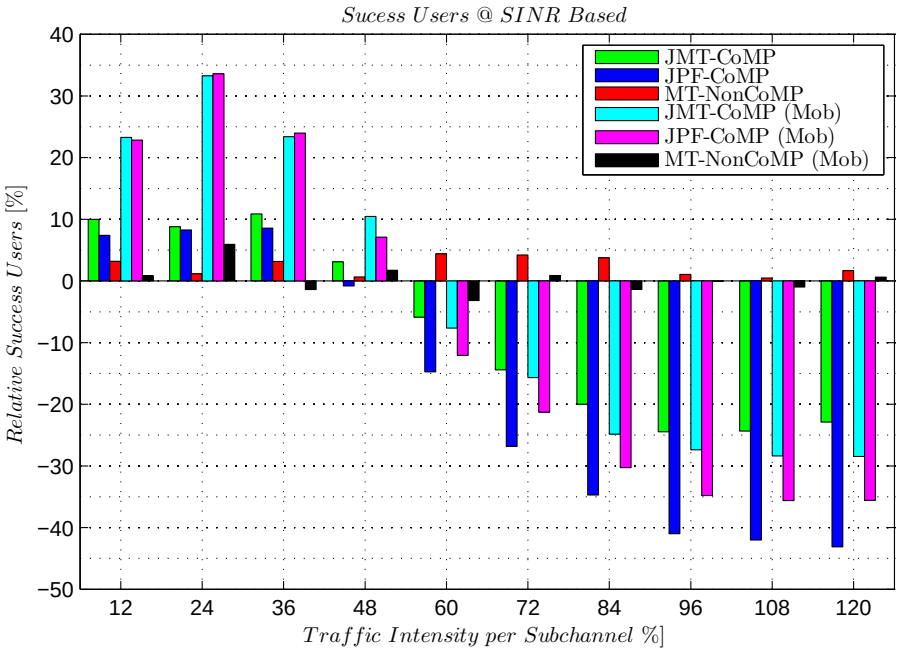

(b) Relative success users compared with PF

Figure 5.9: Intra-site CoMP performance in terms of success users under SINR based cell-edge decision and Poisson traffic

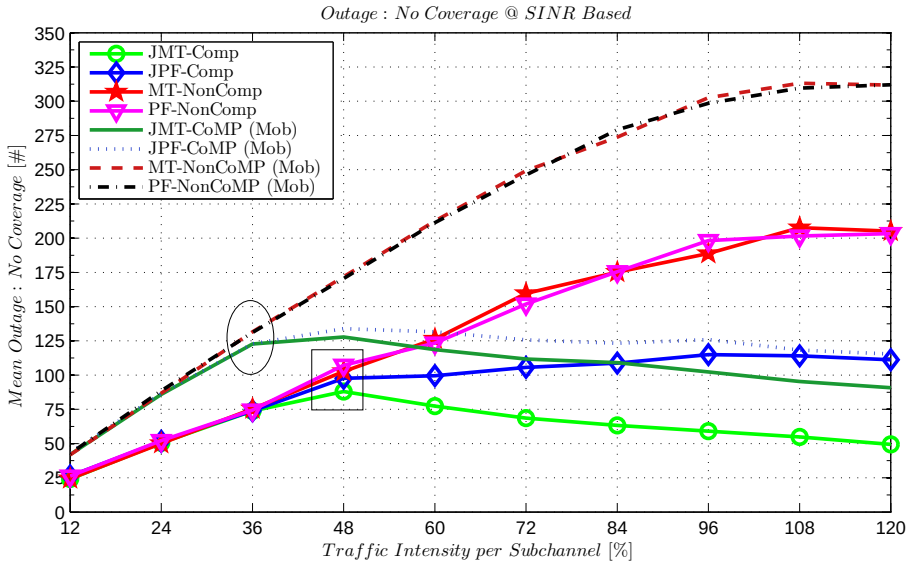

(a) Outage due to no coverage

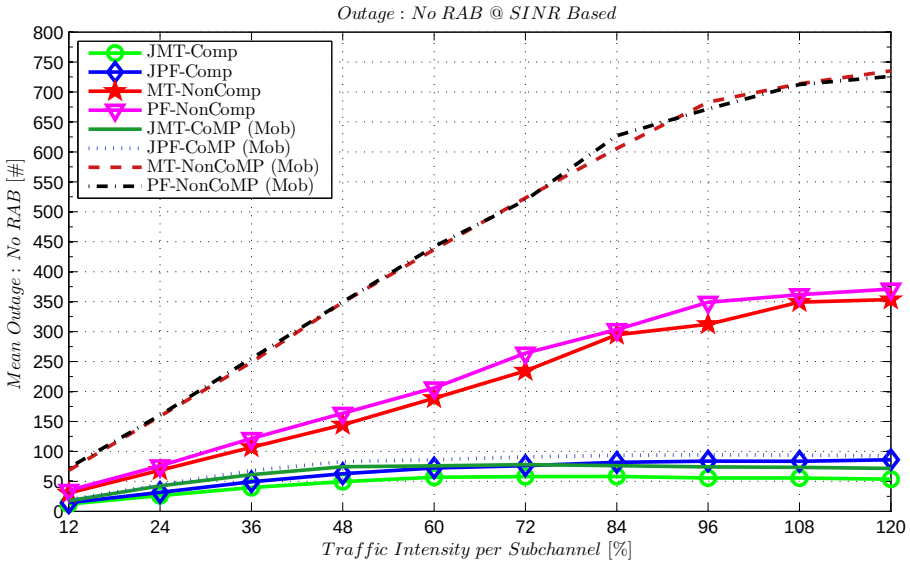

(b) Outage due to no RAB

Figure 5.10: Intra-site CoMP performance in terms of users outage under SINR based cell-edge decision and Poisson traffic

5.5 Performance of Scheduling Algorithm under Intra-Site CoMP and Fixed Traffic

Under fixed traffic, the performance of the scheduling algorithms in an intra-site CoMP scenario was evaluated for data service. A fixed number of users were uniformly distributed from 5 users per cell to 35 users per cell in step of 5 users, representing the traffic intensity per subchannel of 10 % to 70 %, respectively, and remain in the network during the entire simulation period as long as users are not lack of subchannels. For example, if the total number of users in a cell is 35, then the traffic intensity per subchannel is $\rho = 35/50 = 0.70 = 70$ %. A full-buffer of user data traffic model was used. Users suffered from outage due to no coverage and no RAB problem. The performance of the network was assessed under different situations such as: users under static, users under mobility, cell-edge decision based on the absolute distance from the serving base station, cell-edge decision based on the relative pilot RSRP power and cell-edge decision based on the absolute pilot SINR. Users' mobility was modelled as a random direction model as described in Chapter 3. The performance of the network was evaluated in terms of the mean connected users, the mean success users, the mean outage users (no coverage and no RAB), the mean cell activity, the mean user throughput, the mean cell-edge user throughput and the mean system throughput. Throughput of only successfully transmitted users were evaluated, which means, throughput of outage users were not considered during generating statistic log. Figure 5.11 shows a tree diagram of performance evaluation of resource scheduling algorithms in intra-site CoMP under fixed traffic.

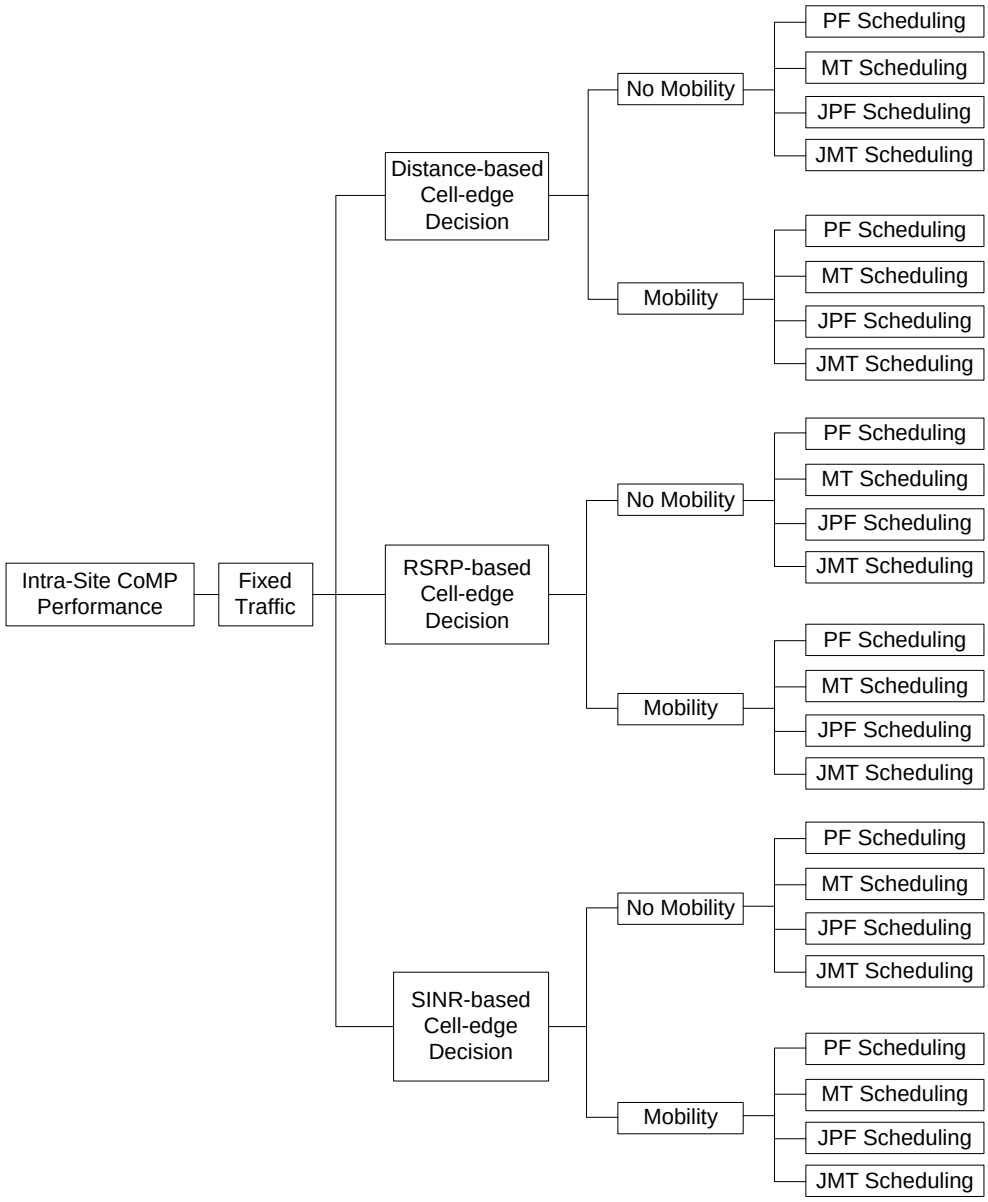

Figure 5.11: Tree diagram of performance evaluation of intra-site CoMP under Fixed traffic

5.5.1 Performance Results under Distance based Cell-Edge

In this section, the performance of the network was evaluated considering cell-edge users based on their absolute distance from their serving base stations. Table E.1 in Appendix E illustrates the network-wide performance for various KPIs for a different number of users per cell under no mobility and mobility conditions. Table 5.10 shows the relative performance of the scheduling algorithms compared with the PF algorithm.

Figure 5.12 shows the performance of the network in terms user throughput. It shows that as the number of users per cell increases, the average user throughput decreases. The reason is that in the presence of a large number of users, more subchannels are utilised in the neighbour cells and hence, the interference level from such cells increases weakening the signal quality and thereby not able to use the higher modulation and coding scheme which in turn decreases the downlink bit rate. It can be noted that under both no mobility and mobility conditions, the cell-edge user throughput and the average user throughput in the CoMP scenario are higher than the Non-CoMP scenario which is the ultimate goal of the CoMP technique. But JPF has better performance than JMT. For example, at 35 users per cell, JPF has about 5 % higher overall user throughput, while 5 % less cell-edge user throughput and about 2.7 % less success users compared with JMT, all under a no mobility condition. Under a no mobility condition, JPF has about 2 % higher system throughput than JMT at 35 users per cell. Figure 5.13 shows the throughput distribution at 35 users per cell.

Table 5.10: System level intra-site CoMP relative performance under distance based cell-edge in fixed traffic

[a]Relative (%) Performance under Distance based Cell-edge in Fixed Traffic								
KPIs ⇓	Sch. ⇓	Number of UE per Cell (#)						
		5	10	15	20	25	30	35
		Mobility Considered: No/Yes						
Conn. UE	JMT	0/0	0/0	0/0	0/0	0/-0.27	0/-4.11	-4.86/-15.96
	JPF	0/0	0/0	0/0	0/0	0/-0.01	-0.12/-4.15	-6.57/-16.75
	MT	0/0	0/0	0/0	0/0	0/0	0/0	0/0
Success UE	JMT	5.69/13.97	11.65/16.66	8.61/16.19	5.84/15.48	9.03/13.52	7.93/9.99	2.63/-4.8
	JPF	6.74/13.56	8.32/14.17	7.64/14.08	7.09/13.57	6.7/12.91	6.76/7.89	-0.1/-6.18
	MT	-3.35/-1.17	2.36/1.14	-0.66/1.31	-2.4/1.57	-0.2/-0.31	-0.11/0.17	-0.71/-1.18
Outage UE	JMT	-23.86/-30.86	-39.91/-34.81	-31.41/-32.79	-23.17/-31.47	-30.92/-28.52	-28.13/-33.36	-31.4/-39.36
	JPF	-28.05/-29.95	-28.49/-29.51	-27.87/-28.55	-28.18/-27.59	-22.94/-26.49	-24.53/-29.12	-29.49/-38.91
	MT	13.84/2.48	-8.07/-2.38	2.45/-2.69	9.55/-3.19	0.65/0.64	0.43/-0.36	2.5/2.5
Cell Activity	JMT	51.93/64.62	54.04/57.79	52.87/60.53	52.11/60.54	54.32/64.3	49.01/51.22	41.35/33.19
	JPF	40.7/63.99	50.88/57.4	48.19/59.71	50.53/58.57	49.68/56.5	50.18/51.68	39.65/31.3
	MT	0/0	0/0	0/0	0/0	0/0	0/0	0/0
UE Thrput.	JMT	18.05/17.46	14.17/13.91	13.93/13.91	15.88/11.53	9.51/10.97	9.49/10.19	6.75/8.15
	JPF	17.1/19.25	16.08/16.79	18.17/14.55	18.44/13.26	16.8/11.8	15.59/12.09	11.74/11.37
	MT	-1.32/-0.89	-1.62/0.75	1.11/2.04	2.8/0.43	-1.92/-1.31	-0.42/-0.95	-1.18/-2.27
CEU Thrput.	JMT	153.81/64.83	96.16/60.4	80.65/48.18	54.04/42.31	61.75/44.06	53.99/41.21	64.07/39.16
	JPF	139.59/56.63	80.07/55.85	80.73/50.22	66.82/42.44	61.82/40.27	60.06/38.06	54.86/39.16
	MT	23.35/1.31	8.66/7.89	-2.41/-0.26	-11.88/0.51	-3.86/-2.4	-6.68/1.48	7.52/1.34
Sys. Thrput.	JMT	24.8/33.87	27.5/32.91	23.76/32.4	22.66/28.78	19.37/25.91	18.15/21.16	9.56/2.97
	JPF	25.12/35.29	25.7/33.44	27.2/30.76	26.86/28.68	24.61/26.21	23.36/20.92	11.64/4.46
	MT	-4.57/-2.03	0.65/1.99	0.47/3.43	0.31/2.01	-2.14/-1.65	-0.53/-0.77	-1.88/-3.39

[a]compared with PF scheduling

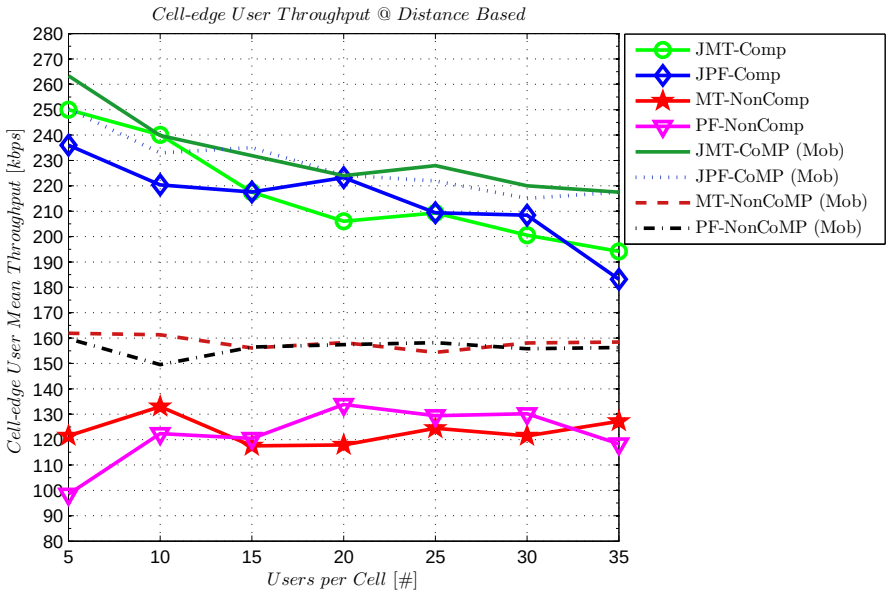

(a) Cell-edge user throughput

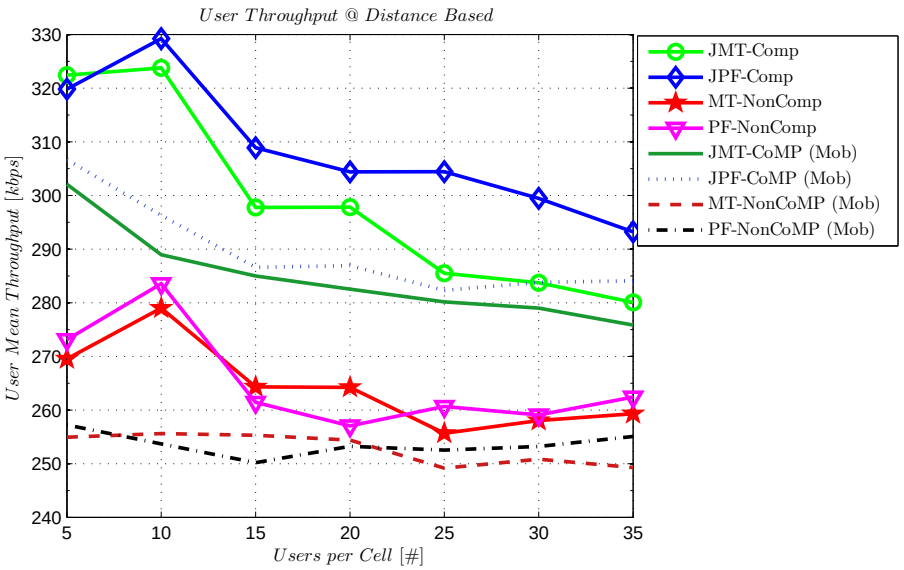

(b) User throughput

Figure 5.12: Intra-site CoMP performance in terms of user throughput under distance based cell-edge decision and fixed traffic

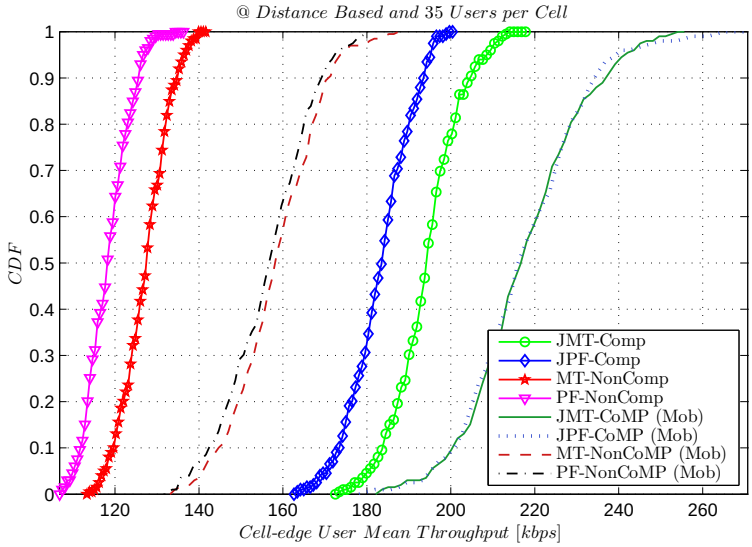

(a) Cell-edge user throughput distribution

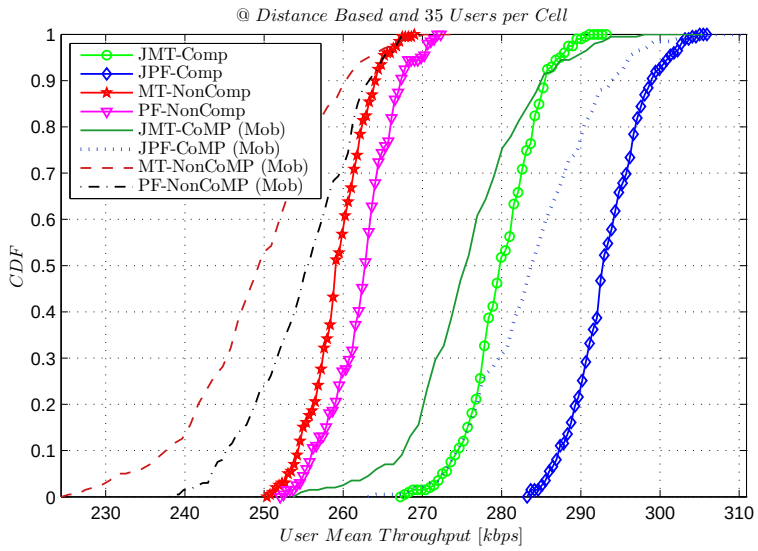

(b) User throughput distribution

Figure 5.13: Intra-site CoMP performance in terms of user throughput distribution at 35 users per cell under distance based cell-edge decision and fixed traffic

5.5.2 Performance Results under RSRP based Cell-Edge

Table E.1 in Appendix E illustrates the network-wide performance for various KPIs for a different number of users per cell under no mobility and mobility conditions. Table 5.11 shows their relative performance compared with the scheduling algorithm PF. From Fig. 5.14, it is noted that JMT has better performance than JPF in terms of the cell-edge user throughput and the overall user throughput under both no mobility and mobility conditions after the number of users per cell is greater than 20. For example, at 35 users per cell, JMT has 65.5 % higher cell-edge user throughput, 17.7 % higher user throughput and 30 % higher system throughput compared with JPF under a no mobility condition, while under mobility, it has 29 % higher cell-edge user throughput, 7.9 % higher user throughput and 15.7 % higher system throughput. Comparing between the CoMP and the Non-CoMP techniques, JMT provides 43.9 % higher user throughput and 21.2 % system throughput compared with MT under no mobility condition. But this is achieved at the cost of a 28 % loss of connected users and a 16 % loss of success users as shown in Fig. 5.18. It is because to improve the performance of cell-edge user throughput by the CoMP techniques, more subchannels are used from the cooperating cells and hence the cooperating cells lack sufficient subchannels. Figure 5.16, shows the throughput distribution at 35 users per cell.

Table 5.11: System level intra-site CoMP relative performance under RSRP based cell-edge in fixed traffic

[a]Relative (%) Performance under RSRP based Cell-edge in Fixed Traffic (%)								
KPIs ⇓	Sch. ⇓	Number of UE per Cell (#)						
		5	10	15	20	25	30	35
		Mobility Considered: No/Yes						
Conn. UE	JMT	0/0	0/0	0/0	0/-1.01	-6.91/-17.41	-18.45/-29.99	-28.56/-38.93
	JPF	0/0	0/0	0/0	0/-1.74	-9.24/-19.61	-22.9/-32.39	-34.42/-42.24
	MT	0/0	0/0	0/0	0/0	0/0	0/0	0/0
Success UE	JMT	15.18/23.34	11.43/27.29	13.24/25.72	13.54/25.34	6.24/3.13	-5.32/-10.73	-14.79/-21.5
	JPF	13.4/21.72	12.12/26.14	12.98/24.13	12.81/22.83	0.56/-1.95	-14.04/-16.19	-26.68/-28.31
	MT	3.33/-1.77	-2.31/0.39	0.79/0.17	0.23/0.35	0.16/-1.62	0.33/0.1	1.34/-0.33
Outage UE	JMT	-50.91/-52.69	-42.64/-54.77	-44.26/-54.04	-46.04/-54.13	-52.64/-61.17	-65.53/-69.65	-76.14/-75.43
	JPF	-44.66/-48.91	-45.22/-52.45	-43.3/-50.74	-43.54/-51.3	-43.28/-57.26	-54.68/-65.75	-61.19/-71.43
	MT	-11.13/4.11	8.65/-0.79	-2.64/-0.33	-0.77/-0.74	-0.53/3.45	-1.21/-0.2	-4.62/0.7
Cell Activity	JMT	69.71/101.03	79.97/100.08	78.25/99.67	79.37/98.94	62.58/64.47	36.93/37.43	16.72/18.07
	JPF	79.28/101.24	77.52/100.83	80.03/101.54	79.58/99.35	64.79/64.12	38.65/35.78	18.38/16.16
	MT	0/0	0/0	0/0	0/0	0/0	0/0	0/0
UE Thrput.	JMT	48.7/42.4	47.41/43.85	30.66/43.51	38.01/40.48	39.43/38.4	34.53/42.05	44.59/46.35
	JPF	42.93/40.55	40.75/43.46	40.43/41.88	39.95/39.2	27.59/35.39	22.44/36.29	26.87/38.45
	MT	11.47/-5	6.23/-1.96	-1.14/1.63	1.17/-1.27	2.75/-2.82	-1.73/-0.75	0.66/-0.99
CEU Thrput.	JMT	191.73/190.6	183.56/179.24	145.93/175.85	169.65/176.35	170.14/170	171.87/185.54	202.78/192.53
	JPF	173.74/174.16	153.88/171.69	171.07/165.61	167.19/170.01	143.36/159.33	133.62/160.5	137.33/163.48
	MT	9.08/0.08	-1.49/-1.19	-2.29/-1.5	-0.87/0.43	0.79/-3.08	0.94/-0.43	0.56/-2.35
Sys. Thrput.	JMT	71.43/75.64	64.33/83.03	47.96/80.42	56.68/76.02	48.14/42.73	27.36/26.84	23.22/14.94
	JPF	62.14/71.12	57.85/80.88	58.66/76.07	57.9/70.93	28.33/32.74	5.25/14.21	-6.96/-0.75
	MT	15.18/-6.68	3.82/-1.61	-0.35/1.75	1.4/-0.91	2.9/-4.38	-1.44/-0.63	2.01/-1.32

[a]compared with PF scheduling

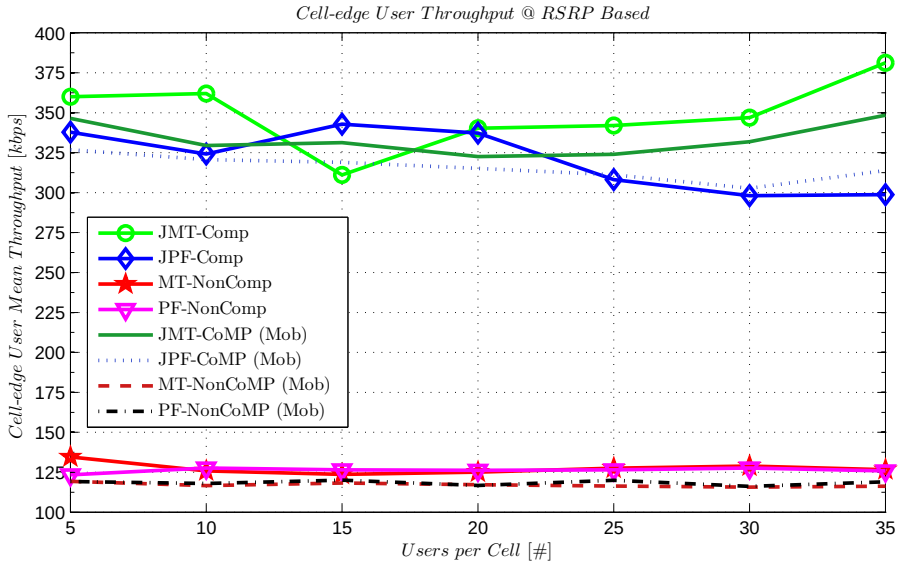

(a) Cell-edge user throughput

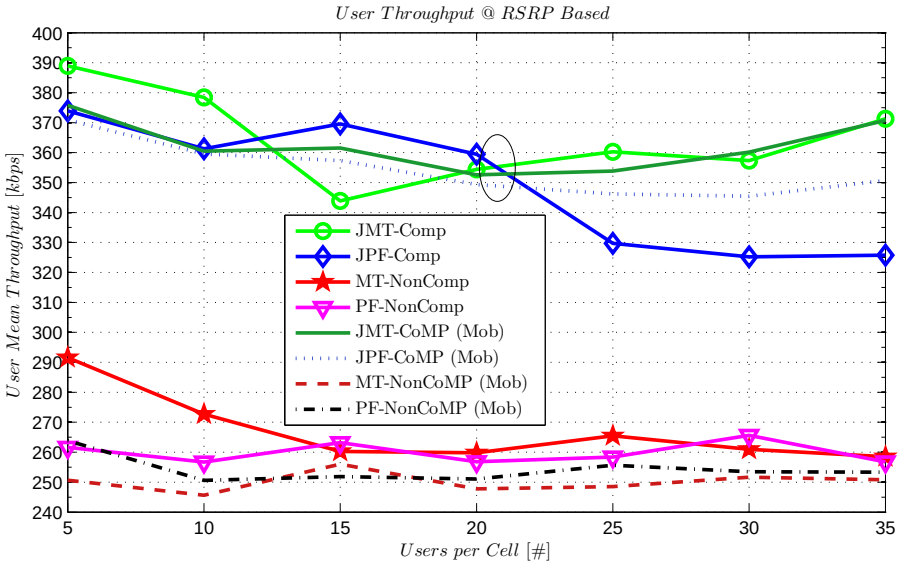

(b) User throughput

Figure 5.14: Intra-site CoMP performance in terms of user throughput under RSRP based cell-edge decision and fixed traffic

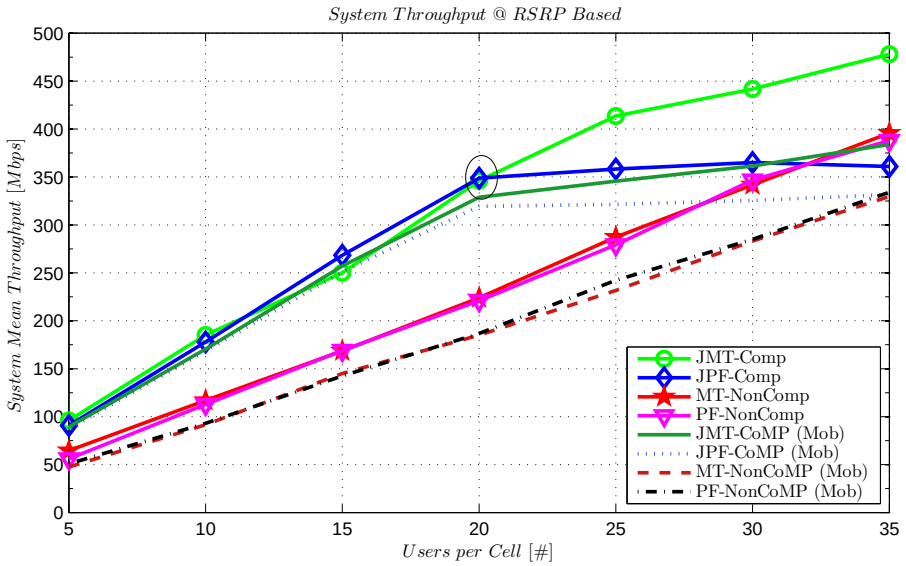

Figure 5.15: Intra-site CoMP performance in terms of system throughput under RSRP based cell-edge decision and fixed traffic

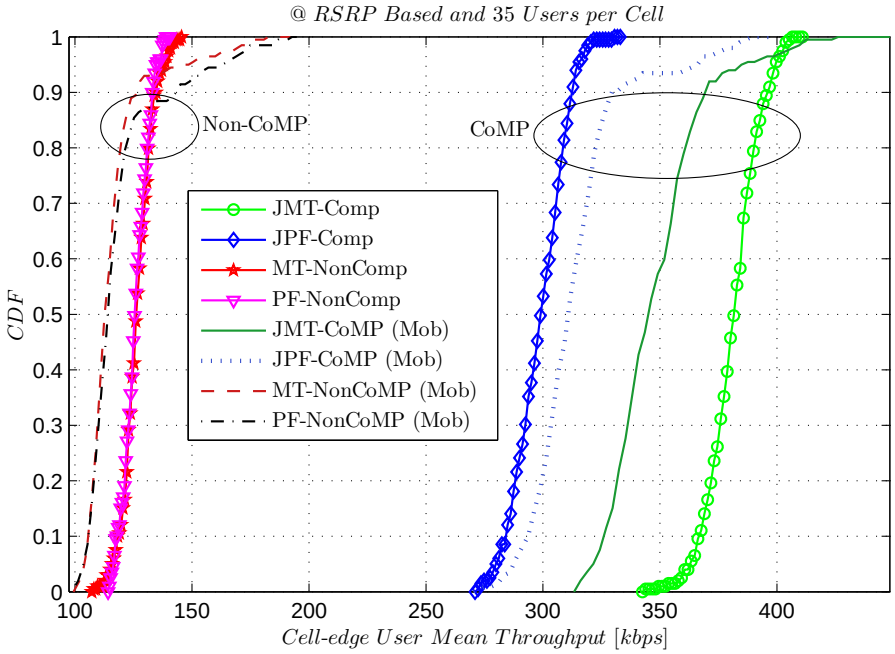

(a) Cell-edge user throughput distribution

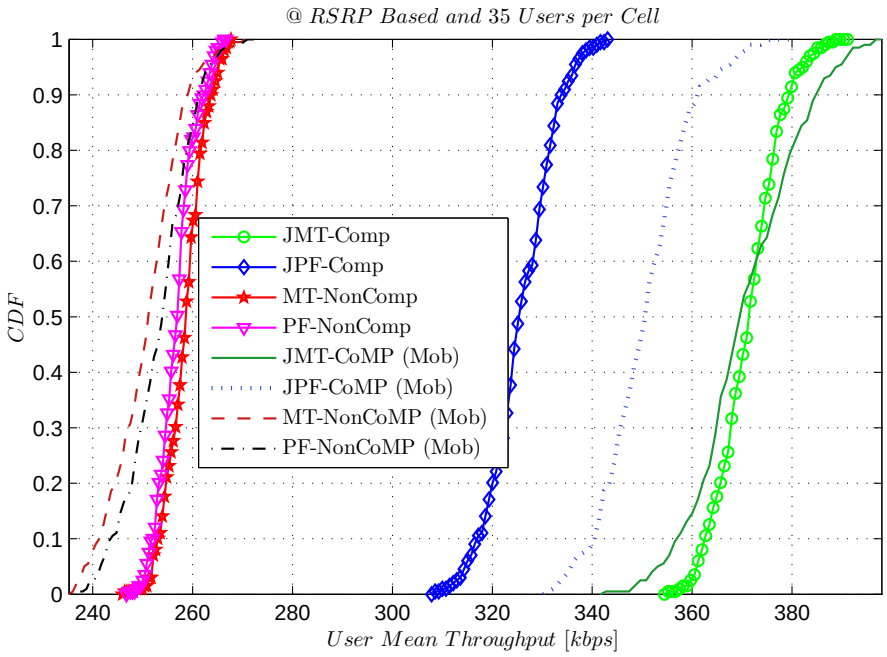

(b) User throughput distribution

Figure 5.16: Intra-site CoMP performance in terms of user throughput distribution at 35 users per cell under RSRP based cell-edge decision and fixed traffic

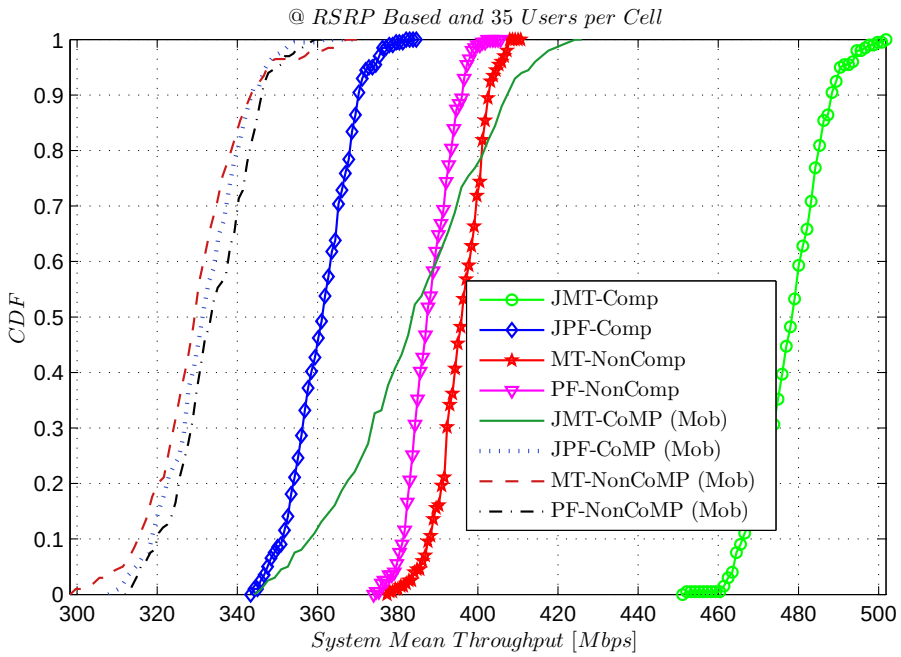

Figure 5.17: Intra-site CoMP performance in terms of system throughput distribution at 35 users per cell under RSRP based cell-edge decision and fixed traffic

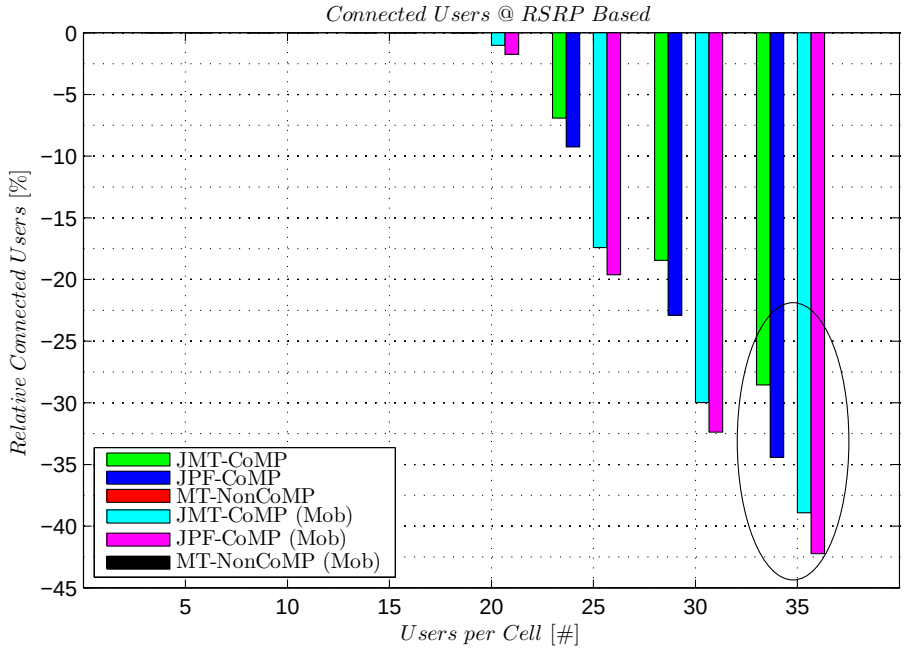

(a) Relative connected users compared with PF

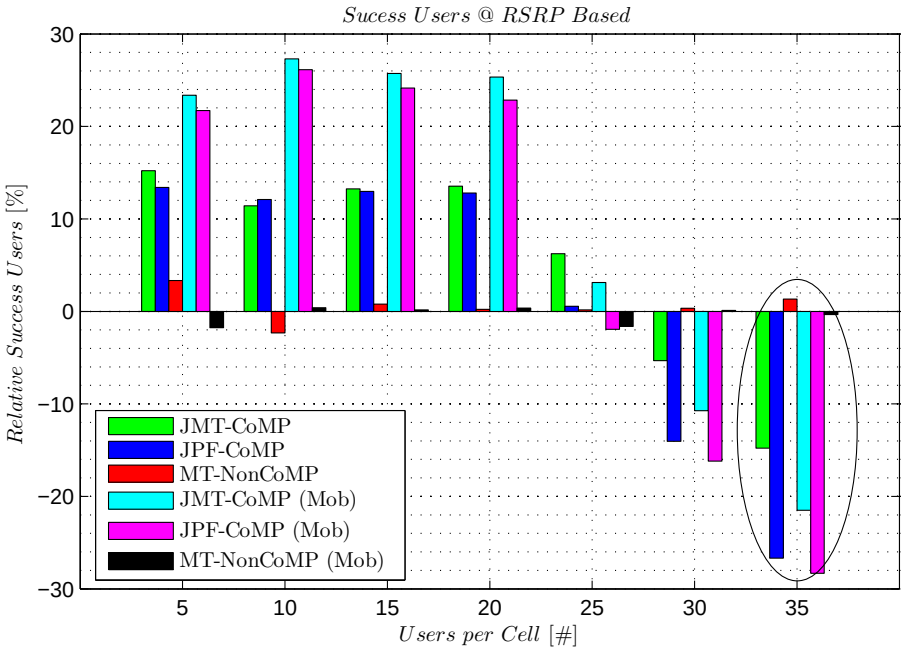

(b) Relative success users compared with PF

Figure 5.18: Intra-site CoMP performance in terms of connected and success users under RSRP based cell-edge decision and fixed traffic

5.5.3 Performance Results under SINR based Cell-Edge

Table E.3 in Appendix E illustrates the network-wide performance of various KPIs for a different number of users per cell under no mobility and mobility conditions. Table 5.12 shows their relative performance compared with the scheduling algorithm PF. From Fig. 5.19, it is noted that JMT has better performance than JPF in terms of the cell-edge user throughput and the overall user throughput under both no mobility and mobility conditions after the number of users per cell is greater than 20. For example, at 35 users per cell, JMT has 60 % higher cell-edge user throughput, 16.4 % higher user throughput and 27.5 % higher system throughput compared with JPF under a no mobility condition, while under mobility, it has 33.2 % higher cell-edge user throughput, 9.3 % higher user throughput and 16.6 % higher system throughput. Comparing between the CoMP and the Non-CoMP techniques, JMT provides 42.2 % higher user throughput and 20.5 % system throughput compared with MT under a no mobility condition. However, this is achieved at the cost of 28.9 % loss of connected users and 15.2 % loss of success users as shown in Fig. 5.23. It is because to improve the performance of cell-edge user throughput by CoMP techniques, more subchannels are used from the cooperating cells and hence the cooperating cells lack sufficient subchannels. Figure 5.21, shows the throughput distribution at 35 users per cell.

Table 5.12: System level intra-site CoMP relative performance under SINR based cell-edge in fixed traffic

[a]Relative (%) Performance under SINR based Cell-edge in Fixed Traffic (%)								
KPIs ⇓	Sch. ⇓	Number of UE per Cell (#)						
		5	10	15	20	25	30	35
		Mobility Considered: No/Yes						
Conn. UE	JMT	0/0	0/0	0/0	0/-2.29	-8.84/-18.32	-20.01/-30.42	-28.95/-40.18
	JPF	0/0	0/0	0/0	-0.04/-2.25	-10.76/-19.53	-25.36/-33.6	-34.96/-43.24
	MT	0/0	0/0	0/0	0/0	0/0	0/0	0/0
Success UE	JMT	9.11/24.99	14.4/27.57	12.48/25.37	10.16/25.02	4.87/3.39	-6.38/-11.2	-15.81/-22.77
	JPF	10.85/25.45	12.2/25.87	11.78/23.1	11.44/23.19	-0.47/0.35	-16.75/-17.69	-26.82/-29.51
	MT	-3.23/0	2.2/1.2	-0.55/-0.31	-2.59/1.48	-0.24/0.18	-0.05/0.59	-0.6/0.62
Outage UE	JMT	-37.41/-54.45	-49.19/-56.38	-45.67/-53.87	-40.55/-56.7	-55.83/-62.87	-68.39/-70.4	-75.46/-75.9
	JPF	-44.78/-55.46	-41.83/-52.86	-43.06/-49.09	-45.94/-52.94	-46.1/-60.28	-55.92/-66.73	-63.82/-71.42
	MT	13.31/0	-7.59/-2.4	2.01/0.66	10.43/-2.91	0.84/-0.34	0.16/-1.24	2.16/-1.27
Cell Activity	JMT	81.21/105.28	77.56/102.93	83.45/103.84	83.3/99.71	65.1/65.74	37.24/38.92	18.65/18.52
	JPF	76.46/101.39	80.89/106.44	80.86/106.46	79.21/102.6	66.22/65.49	38.55/36.38	19.07/17.74
	MT	0/0	0/0	0/0	0/0	0/0	0/0	0/0
UE Thrput.	JMT	38.88/46.49	31.2/42.8	38.22/44.3	38.58/42.51	36.69/43.11	39.94/44.65	40.72/48.22
	JPF	41.33/51.74	33.94/42.25	37.45/43.66	38.89/41.51	30.27/41.27	25.98/39.16	24.3/38.86
	MT	-1.64/0.27	-1.69/-0.94	1.03/2.15	2.95/0.72	-1.77/0.24	-0.42/0.72	-1.49/0.84
CEU Thrput.	JMT	156.33/195.61	168.32/181.64	157.49/176.91	153.74/176.19	160.65/175.04	173.57/181.09	185.55/191.32
	JPF	163.08/194.21	154.16/177.41	151.06/169.44	157.56/169.78	143.5/163.94	133.2/161.31	126.31/158.08
	MT	-5.08/2.81	4.64/0.34	-4.63/-2.04	-3.42/0.52	-2/-0.95	0.4/-0.09	0/-0.69
Sys. Thrput.	JMT	51.38/83.33	50.12/82.25	55.52/80.83	52.66/78.07	43.38/47.97	31.02/28.43	18.48/14.46
	JPF	56.59/90.53	50.37/79.2	53.71/76.83	54.76/74.23	29.67/41.76	4.91/14.5	-9.03/-2.17
	MT	-4.88/0.41	0.49/0.32	0.53/1.83	0.26/2.16	-2/0.39	-0.47/1.31	-2.08/1.46

[a]compared with PF scheduling

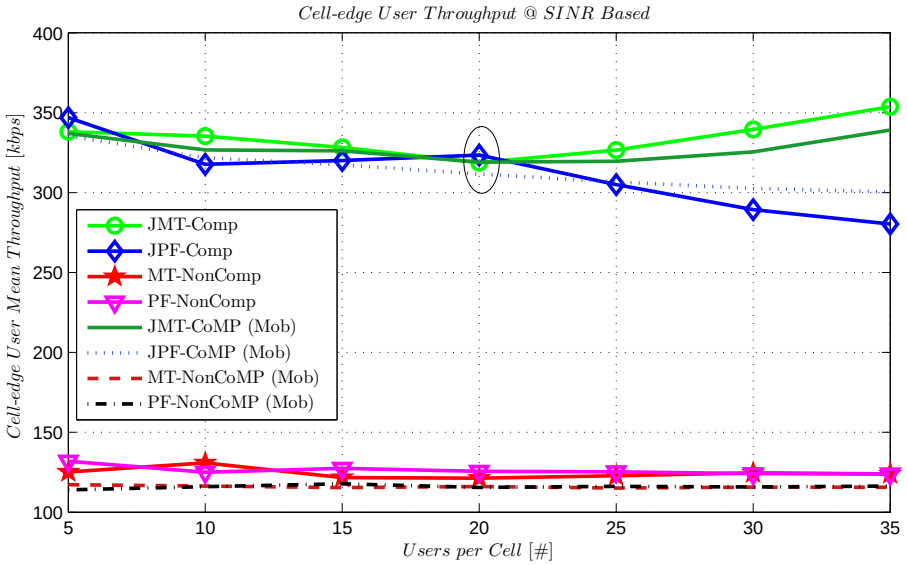

(a) Cell-edge user throughput

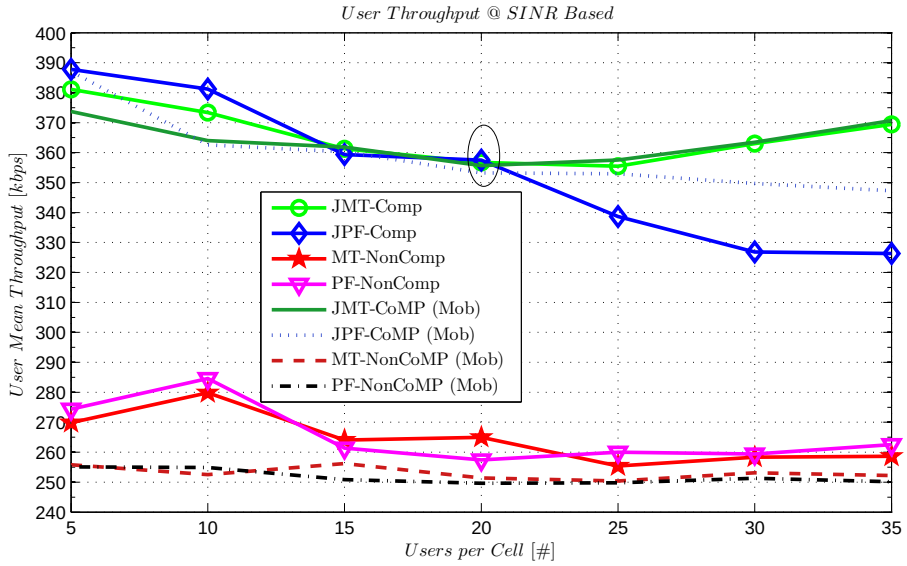

(b) User throughput

Figure 5.19: Intra-site CoMP performance in terms of user throughput under SINR based cell-edge decision and fixed traffic

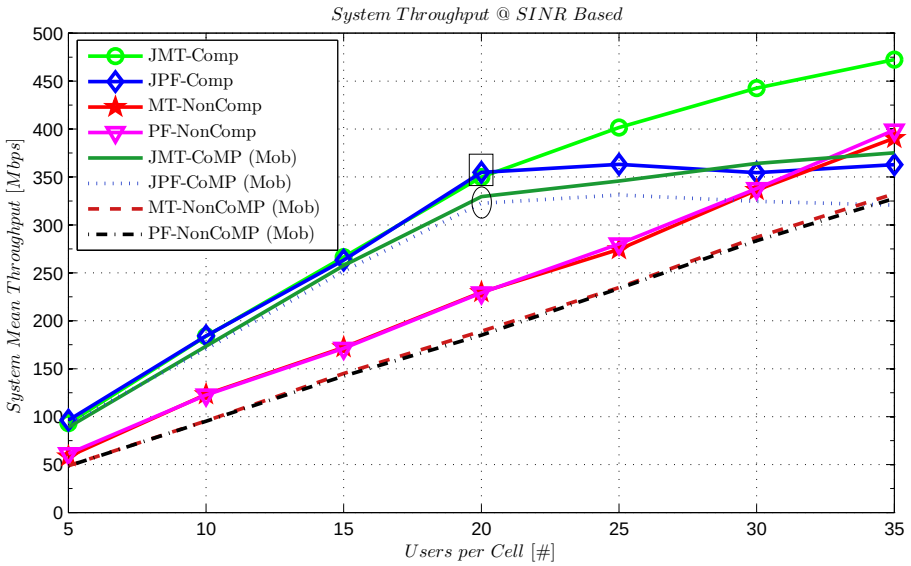

Figure 5.20: Intra-site CoMP performance in terms of system throughput under SINR based cell-edge decision and fixed traffic

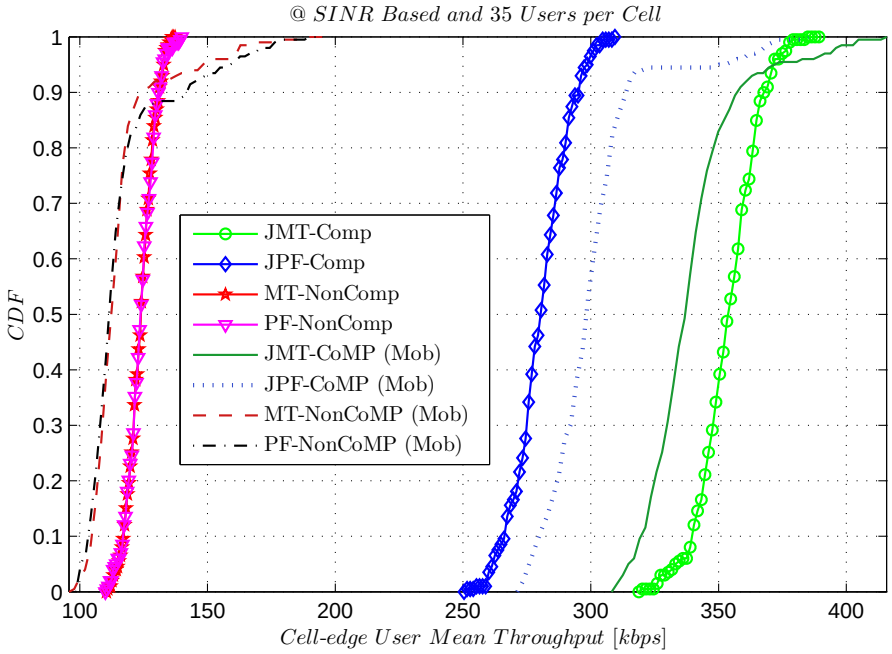

(a) Cell-edge user throughput distribution

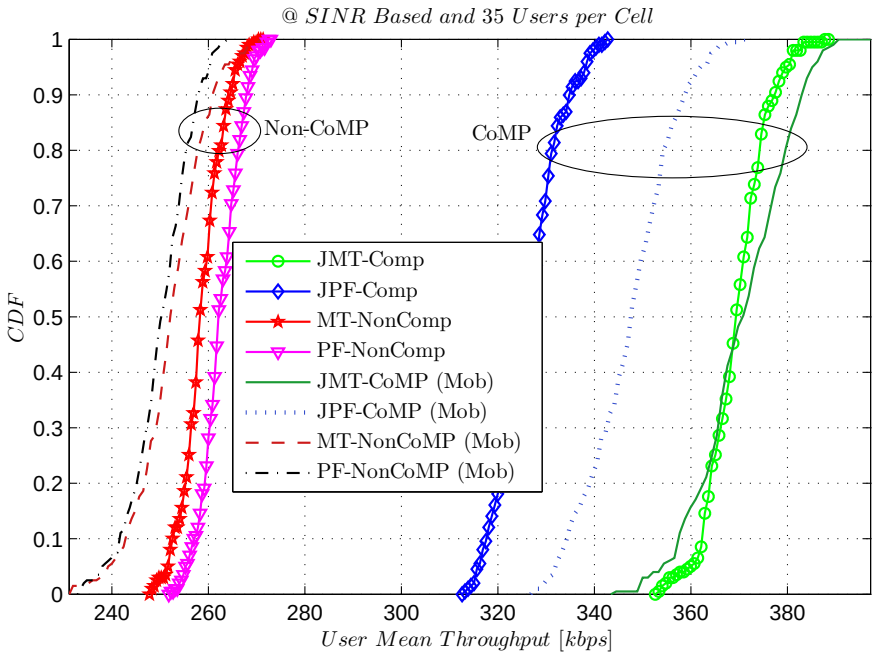

(b) User throughput distribution

Figure 5.21: Intra-site CoMP performance in terms of user throughput distribution at 35 users per cell under SINR based cell-edge decision and fixed traffic

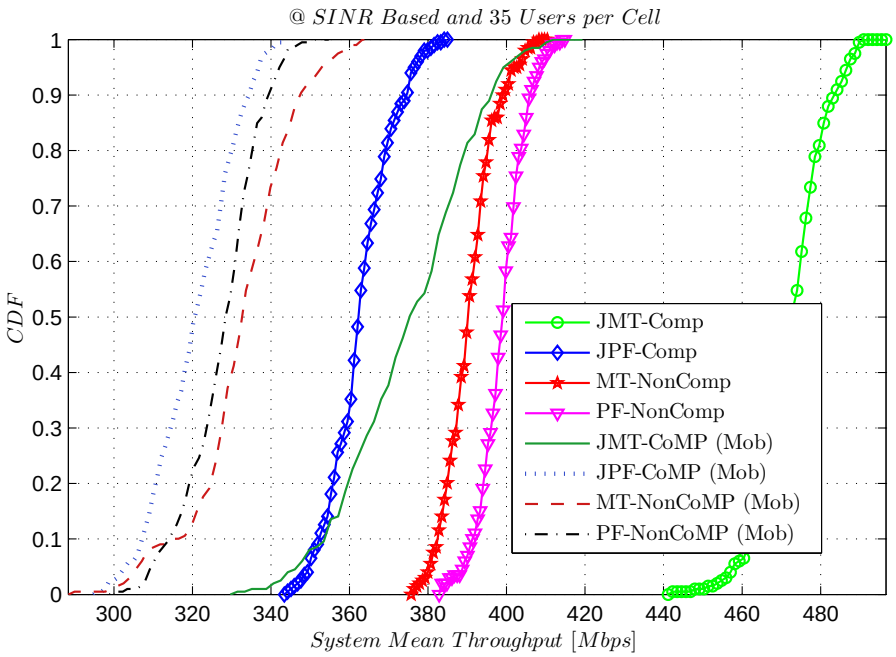

Figure 5.22: Intra-site CoMP performance in terms of system throughput distribution at 35 users per cell under SINR based cell-edge decision and fixed traffic

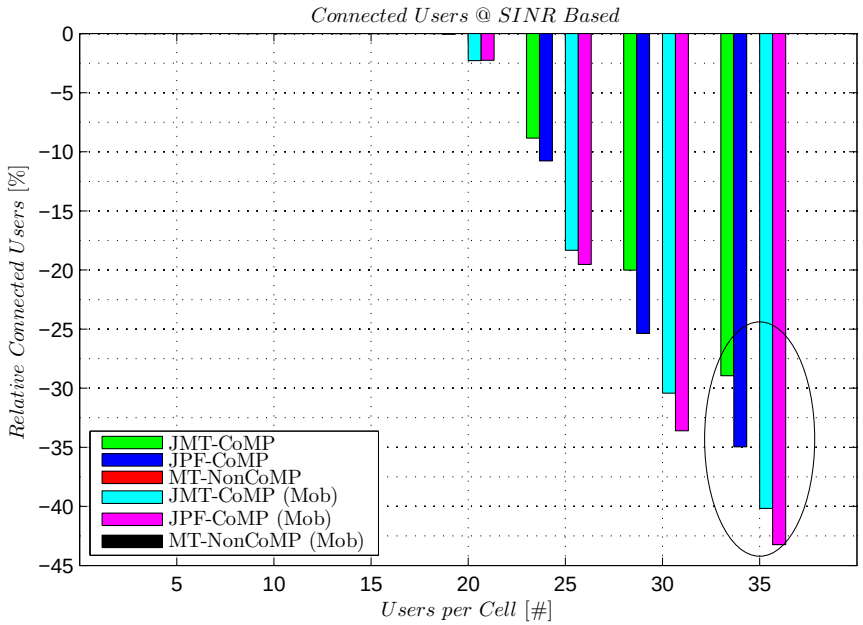

(a) Relative connected users compared with PF

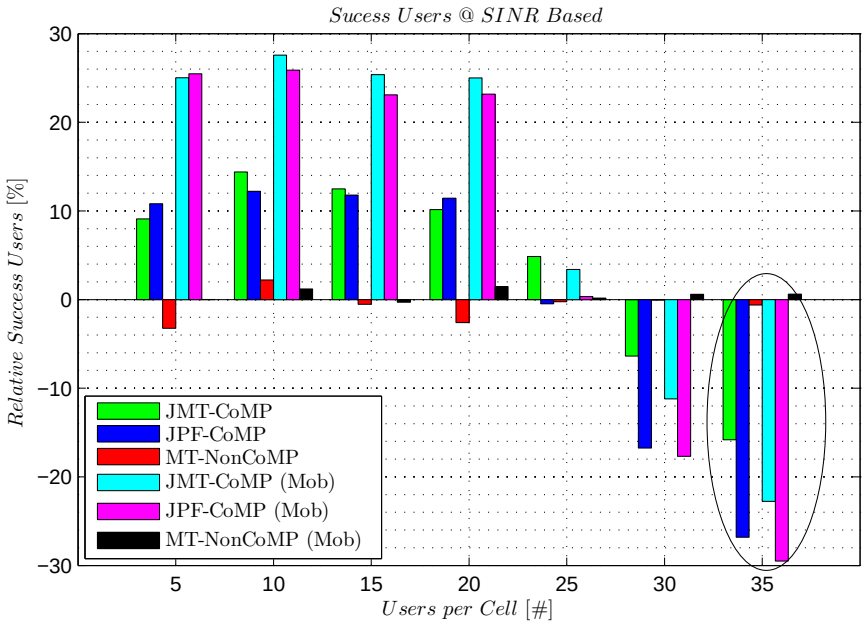

(b) Relative success users compared with PF

Figure 5.23: Intra-site CoMP performance in terms of connected and success users under SINR based cell-edge decision and fixed traffic

5.6 Summary

This chapter has evaluated the performance of the scheduling algorithms in intra-site CoMP scenario under different situations such as users under static, users in mobility, the cell-edge decision based on the absolute distance from the serving base station, the cell-edge decision based on the relative pilot RSRP power and the cell-edge decision based on the absolute pilot SINR. It has been noted that under Poisson traffic, both the Non-CoMP and the CoMP have almost similar performance until a traffic intensity of 55 % in all scenarios of cell-edge decision under a mobility condition. Whereas under a no mobility condition, the Non-CoMP and the CoMP have similar performance until a traffic intensity of 60 % in a scenario of the distance based cell-edge decision, while until the traffic intensity of 48 % in scenarios of RSRP and SINR based cell-edge decision. A summary of the KPIs performance compared between JMT and JPF algorithms, at 96 % of traffic intensity in the case of Poisson traffic and at 35 users per cell in the case of fixed traffic, is shown in Table 5.13.

Table 5.13: Summary of intra-site CoMP performance

Traffic	[a]KPIs (%)	Distance Based		RSRP Based		SINR Based	
		No Mobility	Mobility	No Mobility	Mobility	No Mobility	Mobility
Poisson	Success	JMT: + 3.4	JMT: + 2.23	JMT: + 13.92	JMT: + 6.5	JMT: + 16.5	JMT: + 7.4
	No Coverage	JMT: - 15	JMT: - 0.74	JMT: - 27	JMT: - 7	JMT: -28	JMT: - 7.9
	No RAB	JMT: - 10	JMT: -1.64	JMT: - 9.7	JMT: - 3	JMT: - 8	JMT: - 3
Fixed	CEU thr.	JMT: + 9.21	0	JMT: + 65.5	JMT: + 29	JMT: + 60	JMT: + 33.2
	UE Thr.	**JPF: + 5**	**JPF: + 3.22**	JMT: + 17.7	JMT: + 7.9	JMT: + 16.4	JMT: + 9.3
	Sys. Thr.	**JPF: + 2.08**	**JPF: + 1.49**	JMT: + 30	JMT: + 15.7	JMT: + 27.5	JMT: 16.6

[a]compared between JPF and JMT schedulings at 96 % of Poisson traffic intensity and 35 users per cell of fixed traffic

As shown in the table, it can be concluded that JMT has better perform-

ance for all scenarios except in the distance based cell-edge decision under fixed traffic, where JPF has better user and system throughput performance. For example, as shown in the table, under fixed traffic and the distance based cell-edge decision, JPF has 5 % and 3.22 % higher user throughput (UE. Thr.) under no mobility and mobility conditions, respectively, while it has 2.08 % and 1.49 % system throughput (Sys. Thr.) all compared with JMT.

Chapter 6:

Performance of the Scheduling Algorithm under Inter-Site Homogeneous CoMP

In Chapter 5, the performance of the scheduling algorithms in intra-site CoMP deployment of homogeneous networks was evaluated for two different traffic behaviours under user mobility and no mobility conditions. The performance was evaluated also for different cell-edge decision criteria. The cooperating cells in the CoMP cluster are formed from the same eNB.

In this chapter, the performance of the scheduling algorithms in inter-site CoMP deployment of homogeneous networks are evaluated, where the cooperating cells in the CoMP cluster comes from different eNBs.

6.1 Inter-Site CoMP Cluster Formation

In the inter-site of CoMP deployment scenario, as shown in Fig. 6.1, the co-operating cells in a CCS are formed from different eNBs. This type of cluster formation requires the backhaul capacity since eNBs are geographically located far from each other. It is because, a high capacity and low latency backhaul is required to share the scheduling information among the cooperating cells which serve a user simultaneously. The scheduling information, the CSI and the data for a UE are shared through an X2 interface. One of the cells in a cluster acts as a master cell (usually the serving cell) and the remaining cells

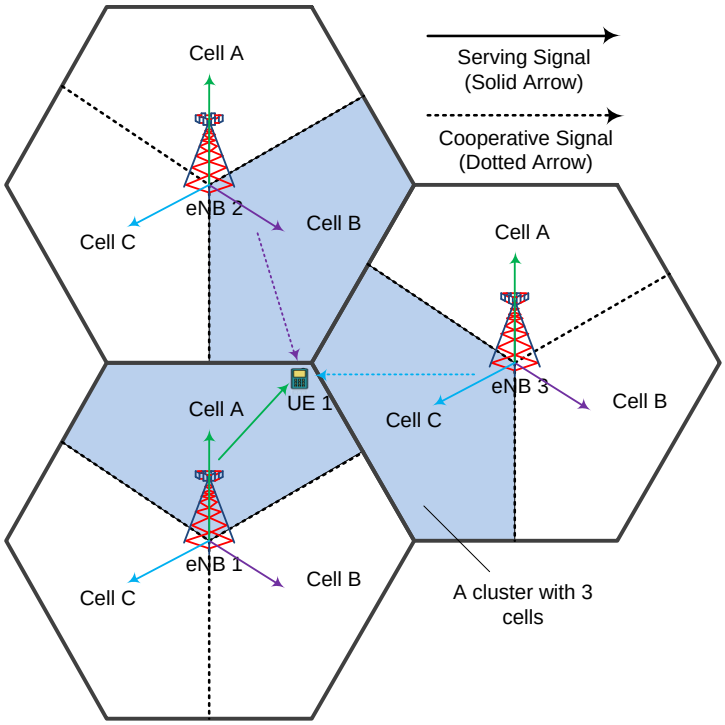

Figure 6.1: Inter-site CoMP cluster

act as cooperating cells. As shown in Fig. 6.1, Cell A of eNB1 acts as a master cell for the cluster, whereas Cell B of eNB 2 and Cell C of eNB 3 act as cooperating cells for UE 1.

6.2 Simulation Scenario Setup

The simulation setup and the simulation parameters are similar to the one used in intra-site CoMP performance except for the list of clusters. The simulation model to evaluate the performance of CoMP in inter-site scenario is shown in Fig. 6.2. Note that the colouring of the cells are just to distinguish from one cluster to another cluster. A list of inter-site clusters is shown in Table 6.1.

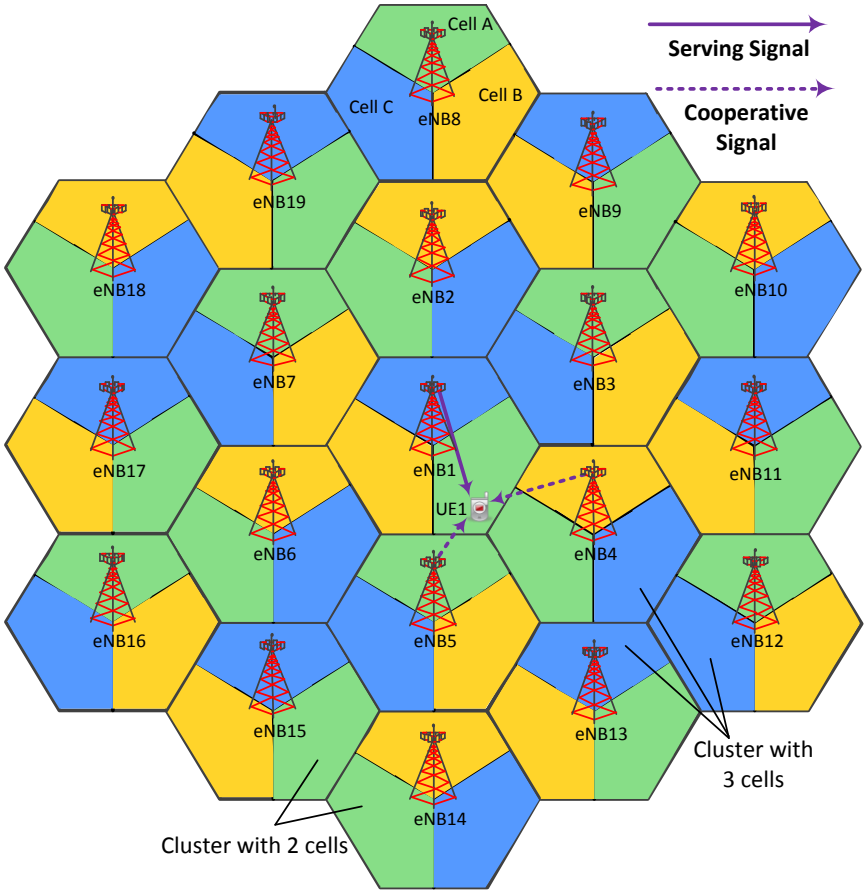

Figure 6.2: System model for homogeneous inter-site CoMP simulation scenario

Table 6.1: List of inter-site clusters in a homogeneous network

Cluster Name	Cooperating Cells	Cluster Size
c1	{eNB1:CellA, eNB2:CellB, eNB3:CellC}	3
c2	{eNB5:CellC, eNB15:CellA, eNB6:CellB}	3
c3	{eNB7:CellC, eNB17:CellA eNB18:CellB}	3
c4	{eNB4:CellB, eNB12:CellC, eNB13:CellA}	3
c5	{eNB1:CellB, eNB4:CellC, eNB5:CellA}	3
c6	{eNB6:CellC, eNB16:CellA, eNB17:CellB}	3
c7	{eNB2:CellC, eNB7:CellA, eNB19:CellB}	3
c8	{eNB3:CellA, eNB9:CellB, eNB10:CellC}	3
c9	{eNB2:CellA, eNB8:CellB, eNB9:CellC}	3
c10	{eNB3:CellB, eNB11:CellC, eNB4:CellA}	3
c11	{eNB5:CellB, eNB13:CellC, eNB14:CellA}	3
c12	{eNB1:CellC, eNB6:CellA, eNB7:CellB}	3
c13	{eNB8:CellC, eNB19:CellA}	2
c14	{eNB10:CellB, eNB11:CellA}	2
c15	{eNB11:CellB, eNB12:CellA}	2
c16	{eNB14:CellC, eNB15:CellB}	2
c17	{eNB15:CellC, eNB16:CellB}	2
c18	{eNB18:CellA, eNB19:CellC}	2

6.3 Performance of the Scheduling Algorithm under Inter-Site CoMP and Poisson Traffic

As in the intra-site scenario, the performance of the scheduling algorithms was evaluated in the inter-site CoMP scenario under Poisson process. The simulation parameters and the evaluation process are similar to the one used in the intra-site CoMP scenario except for the list of clusters.

6.3.1 Performance Results under Distance based Cell-Edge

In this section, the performance of the inter-site CoMP scenario was evaluated considering cell-edge users based on their absolute distance from their serving base stations. The network-wide performance in terms of the mean number of success users, the mean outage users and the mean cell activity under no mobility and mobility conditions for various traffic intensities are shown in Appendix F in Table F.1. Figure 6.3 shows the relative performance in terms of user outage due to no coverage and no RAB problem compared with the scheduling algorithm PF. It can be noted that user outage problem in JMT is relatively low compared to that in JPF. For example, at a traffic intensity of 96 %, JMT has 14.71 % less coverage problems and 15.74 % less RAB problems compared with JPF under a no mobility condition, while 4.44 % less RAB problems and nearly equal performance in coverage problems under a mobility condition. The reason is that JPF scheduling is based on the past performance of a user and if the user just arrives in the network, it has no record of its performance, therefore, its proportional fair weight is supposed to zero. Also, in the presence of a large number of users, more subchannels are utilised in the neighbour cells and hence, the interference level from such

cells increases weakening the signal quality and thereby not able to satisfy the minimum required received power or not able to use the minimum modulation and coding scheme.

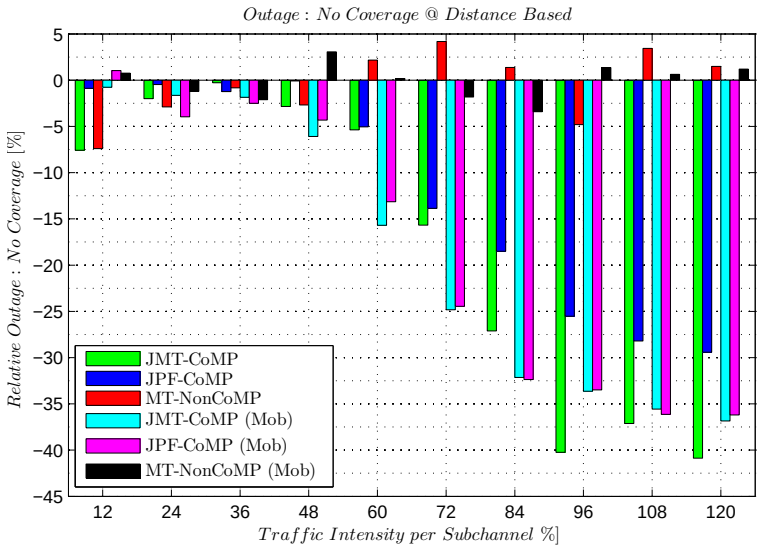

(a) Outage due to no coverage

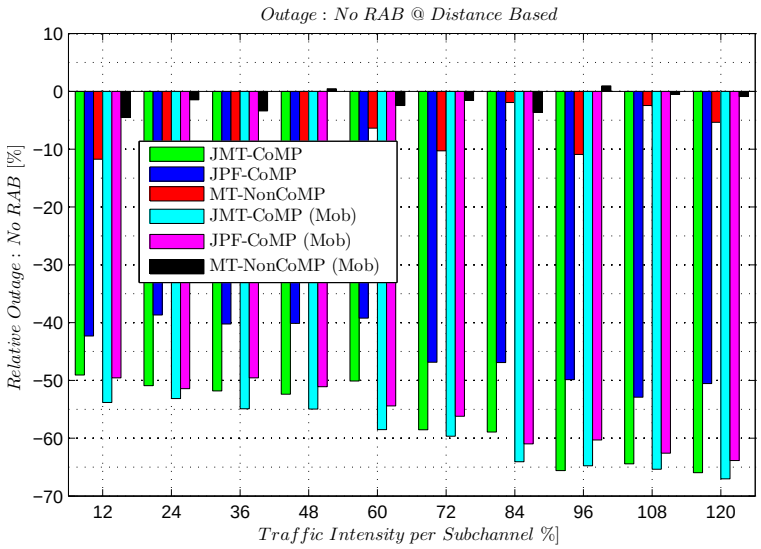

(b) Outage due to no RAB

Figure 6.3: Inter-site CoMP performance in terms of relative user outage compared with PF under distance based cell-edge decision and Poisson traffic

6.3.2 Performance Results under RSRP based Cell-Edge

In this section, the performance of the inter-site CoMP scenario was evaluated considering cell-edge users, based on their received pilot RSRP power from their serving base stations and compared with the strongest received interfering RSRP power. The network-wide performance in terms of the mean number of success users, the mean outage users and the mean cell activity under no mobility and mobility conditions for various traffic intensities are shown in Appendix F in Table F.2. Figure 6.4 shows the relative performance in terms of user outage due to no coverage and no RAB problem compared with the scheduling algorithm PF. It can be noted that the user outage problem in JMT is relatively low compared to that in JPF. For example, at a traffic intensity of 96 %, JMT has 14.46 % less coverage problems and 7.36 % less RAB problems compared with JPF under a no mobility condition, while, 5 % less coverage problems and 3 % less RAB problems under a mobility condition. Again, the reason is that JPF scheduling is based on the past performance of a user and if the user just arrives in the network, it has no record of its performance, therefore, its proportional fair weight is supposed to zero which affects the order of scheduling.

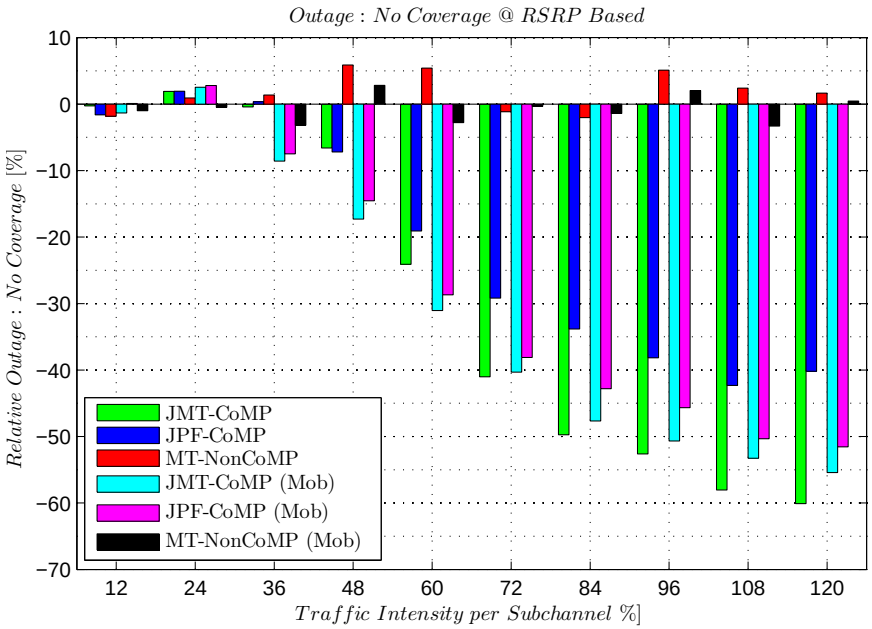

(a) Outage due to no coverage

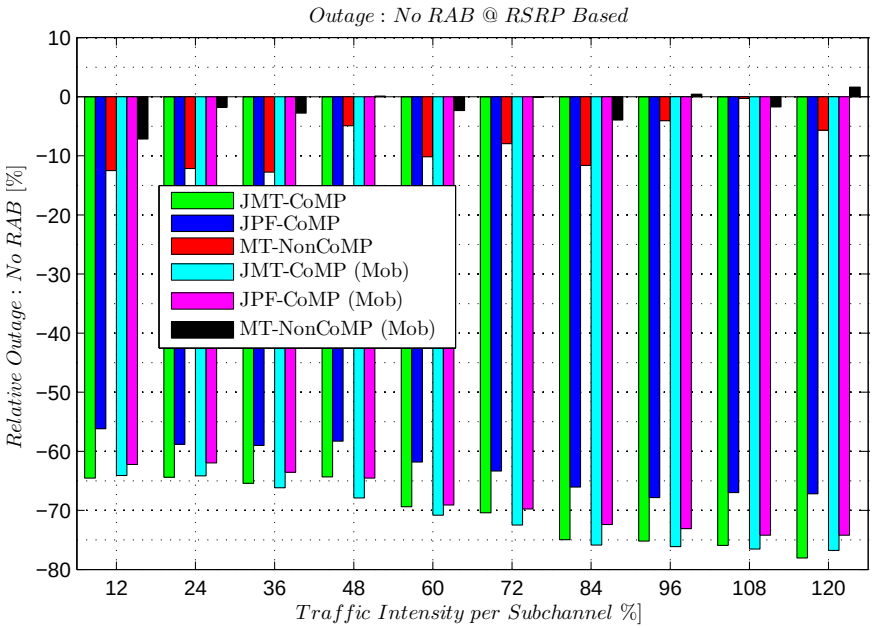

(b) Outage due to no RAB

Figure 6.4: Inter-site CoMP performance in terms of relative user outage compared with PF under RSRP based cell-edge decision and Poisson traffic

6.3.3 Performance Results under SINR based Cell-Edge

In this section, the performance of the inter-site CoMP was evaluated considering cell-edge users based on the pilot SINR. The network-wide performance in terms of the mean number of success users, the mean outage users and the mean cell activity under no mobility and mobility conditions for various traffic intensities are shown in Appendix F in Table F.3. Figure 6.5 shows the relative performance in terms of user outage due to no coverage and no RAB problems compared with the scheduling algorithm PF. It can be noted that user outage problem in JMT is relatively low compared to that in JPF. For example, at traffic intensity of 96 %, JMT has 14.46 % less coverage problems and 7.36 % less RAB problems compared with JPF under a no mobility condition, while 5 % less coverage problems and 3 % less RAB problems under a mobility condition. The reason is that JPF scheduling is based on the past performance of a user and if the user just arrives in the network, it has no record of its performance, therefore, its proportional fair weight is supposed to zero. Also, in the presence of a large number of users, more subchannels are utilised in the neighbour cells and hence, the interference level from such cells increases weakening the signal quality and thereby not able to satisfy the minimum required received power or not able to use the minimum modulation and coding scheme.

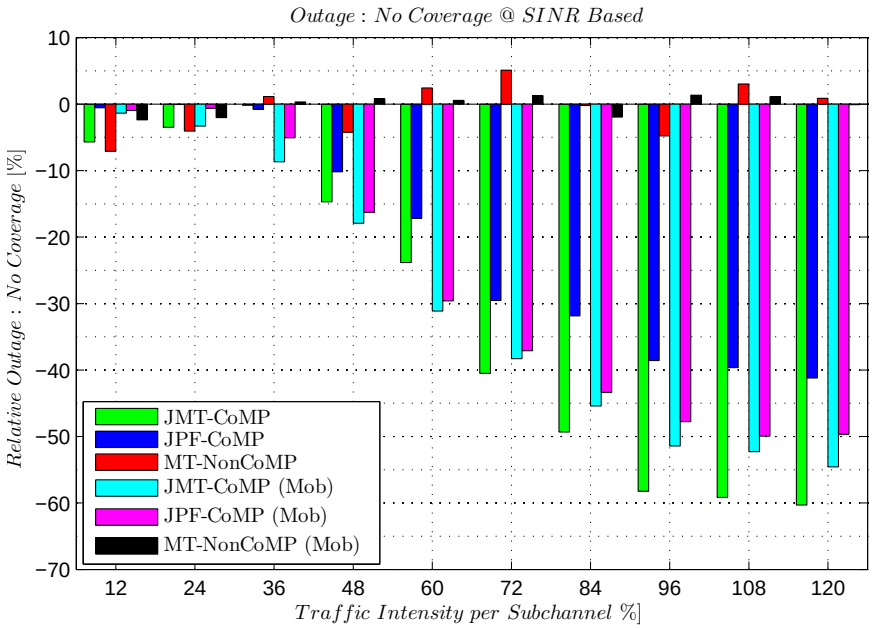

(a) Outage due to no coverage

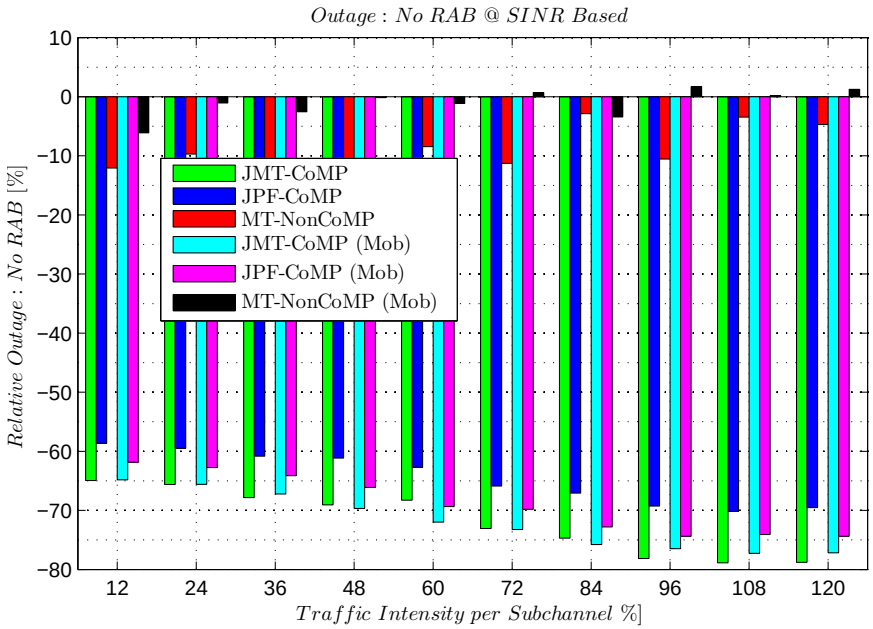

(b) Outage due to no RAB

Figure 6.5: Inter-site CoMP performance in terms of relative user outage compared with PF under SINR based cell-edge decision and Poisson traffic

6.4 Performance of the Scheduling Algorithm under Inter-Site CoMP and Fixed Traffic

Like the intra-site CoMP scenario, the performance of the scheduling algorithms in the inter-site CoMP scenario was evaluated. A fixed number of users were uniformly distributed from 5 users per cell to 35 users per cell in steps of 5 users, representing the the traffic intensity per subchannel of 10 % to 70 %, respectively, and remain in the network during the entire simulation period as long as users are lack of subchannels. The simulation parameters and the evaluation process are similar to the one used in the intra-site CoMP scenario, except the list of clusters.

6.4.1 Performance Results under Distance based Cell-Edge

The network-wide performance of various KPIs for different numbers of users per cell under no mobility and mobility conditions are shown in Appendix G in Table G.1. Figure 6.6 shows the performance in terms of cell-edge user mean throughput and user mean throughput. It can be noted that JPF has better performance than JMT under both no mobility and mobility conditions. For example, at 35 users per cell, JPF has a 32.1 % higher cell-edge user throughput and a 8.4 % higher user throughput compared with JMT under a no mobility condition, while an 11 % higher cell-edge user throughput and nearly equal performance of user throughput under a mobility condition. Figure 6.7 shows the user throughput distribution at 35 users per cell. It is noted that JPF provides higher throughput performance than JMT.

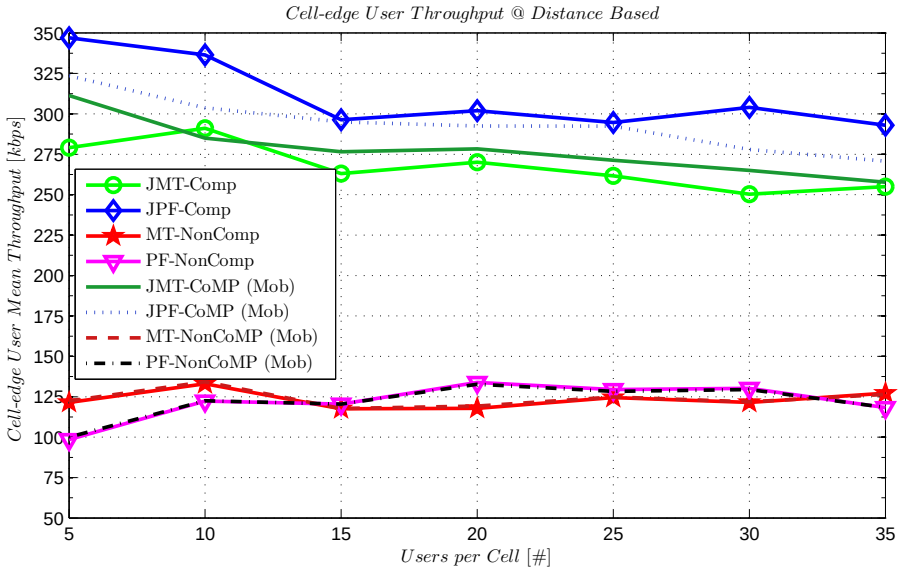

(a) Cell-edge user throughput

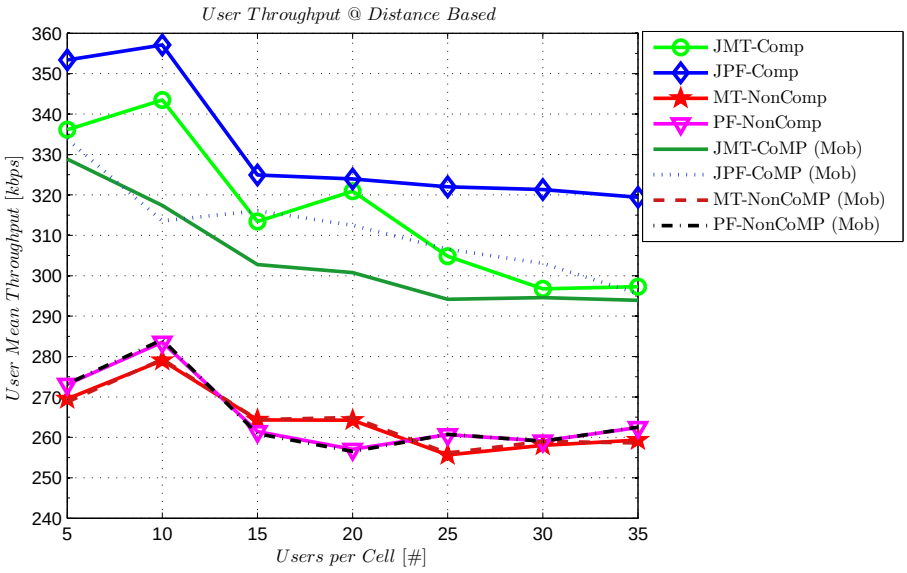

(b) User throughput

Figure 6.6: Inter-site CoMP performance in terms of user throughput under distance based cell-edge decision and fixed traffic

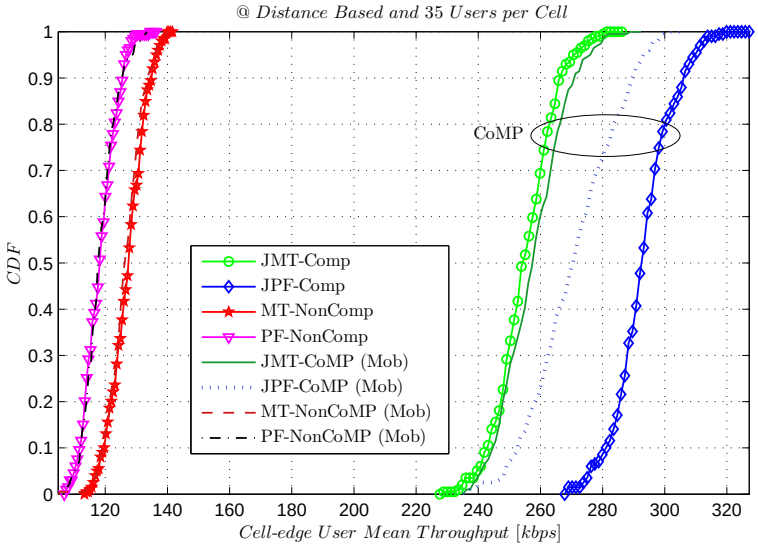

(a) Cell-edge user throughput distribution

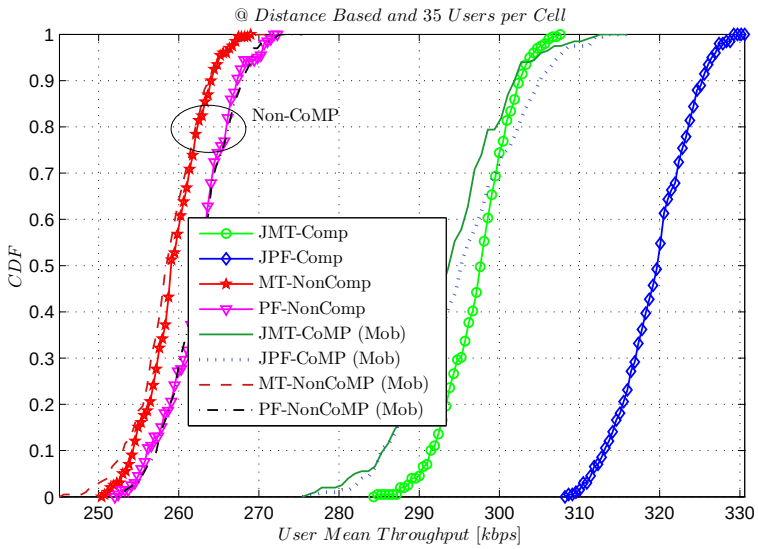

(b) User throughput distribution

Figure 6.7: Inter-site CoMP performance in terms of user throughput distribution at 35 users per cell under distance based cell-edge decision and fixed traffic

6.4.2 Performance Results under RSRP based Cell-Edge

The network-wide performance of various KPIs for a different number of users per cell under no mobility and mobility conditions are shown in Appendix G in Table G.2. Figure 6.8 shows the performance in terms of cell-edge user mean throughput and user mean throughput. It can be noted that JPF has better performance than JMT at a low number of users in a cell, while JMT has better performance than JPF at a high number of users in a cell under no mobility. At 35 users per cell, JMT has 18.92 % higher cell-edge user throughput and 7.07 % higher user throughput compared with JPF under a no mobility condition, while nearly equal performance under a mobility condition. Figure 6.9 shows the user throughput distribution at 35 users per cell. It is noted that JMT provides higher throughput performance than JPF.

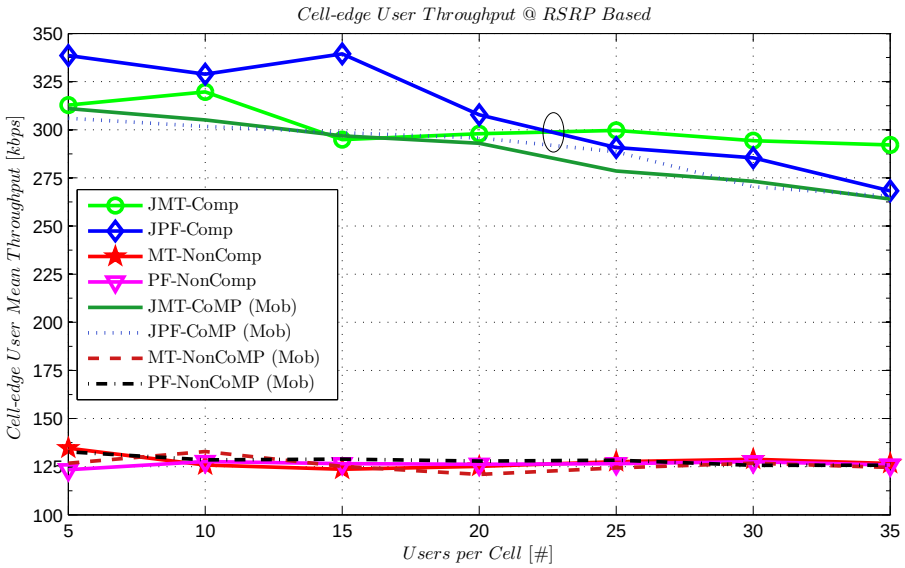

(a) Cell-edge user throughput

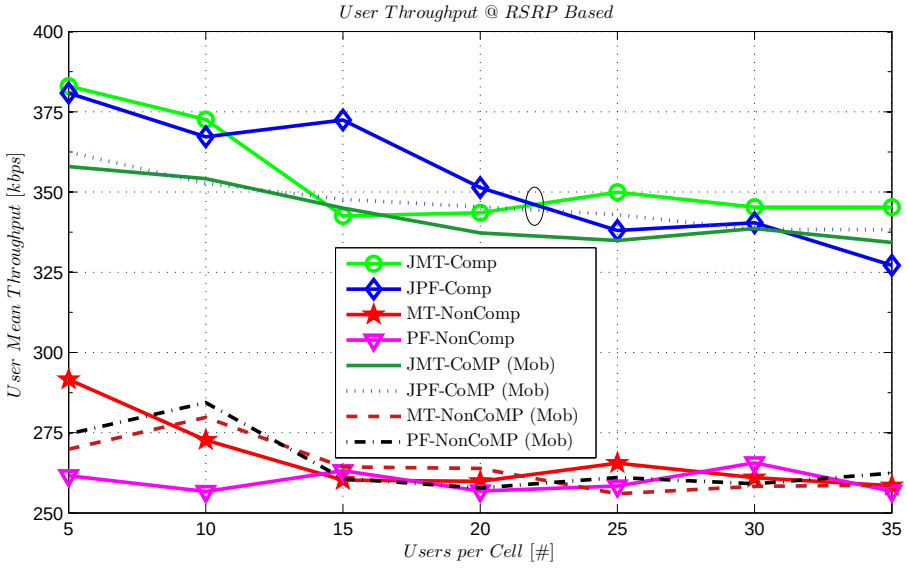

(b) User throughput

Figure 6.8: Inter-site CoMP performance in terms of user throughput under RSRP based cell-edge decision and fixed traffic

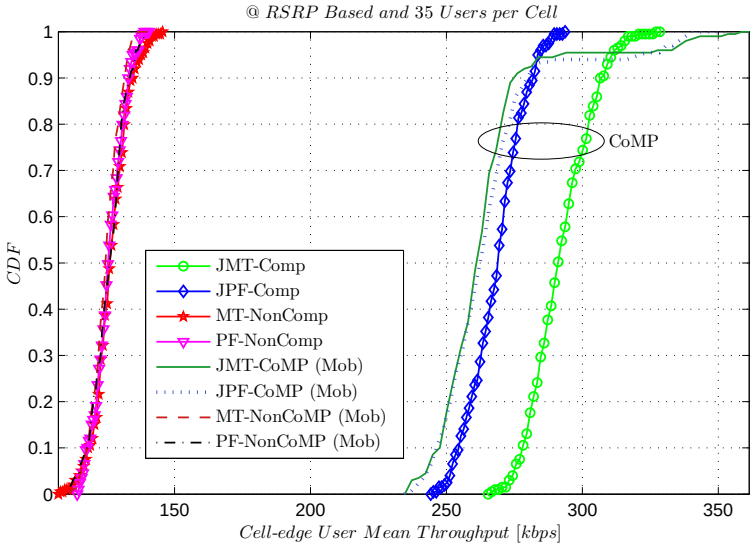

(a) Cell-edge user throughput distribution

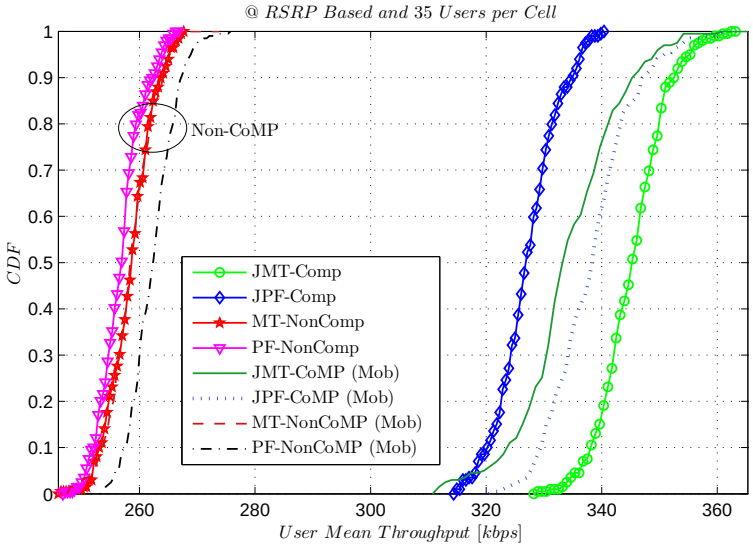

(b) User throughput distribution

Figure 6.9: Inter-site CoMP performance in terms of user throughput distribution at 35 users per cell under RSRP based cell-edge decision and fixed traffic

6.4.3 Performance Results under SINR based Cell-Edge

The network-wide performance of various KPIs for different numbers of users per cell under no mobility and mobility conditions are shown in Appendix G in Table G.3. Figure 6.10 shows the performance in terms of cell-edge user mean throughput and user mean throughput. At 35 users per cell, JMT has a 17.43 % higher cell-edge user throughput and a 5.48 % higher user throughput compared with JPF under a no mobility condition, while a 7.04 % higher cell-edge user throughput and nearly equal user throughput performance under a mobility condition. Figure 6.11 shows the user throughput distribution at 35 users per cell. It is noted that JMT provides higher throughput performance than JPF.

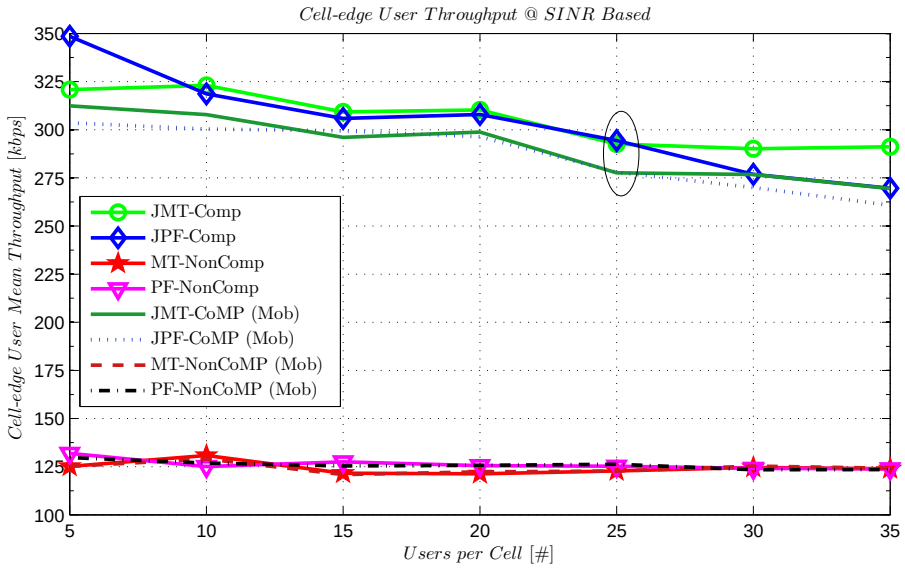

(a) Cell-edge user throughput

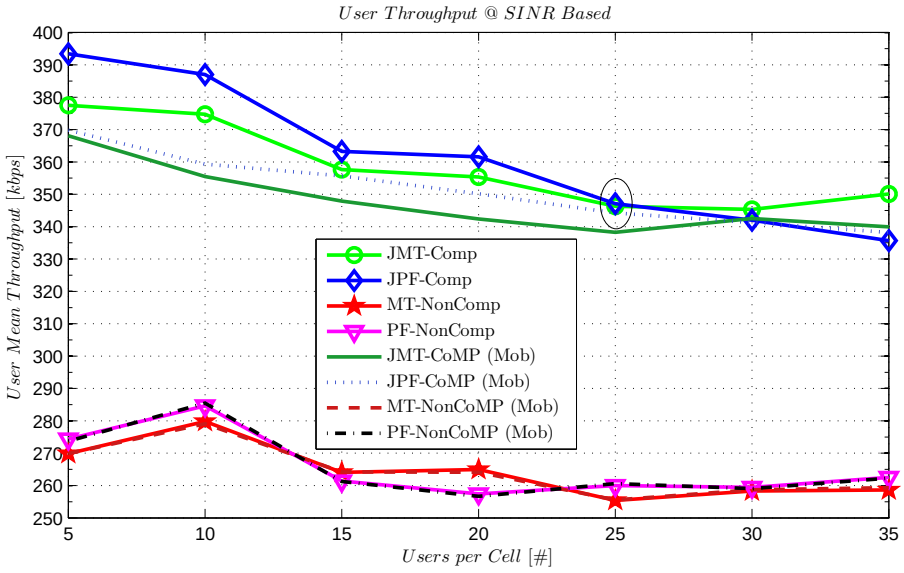

(b) User throughput

Figure 6.10: Inter-site CoMP performance in terms of user throughput under SINR based cell-edge decision and fixed traffic

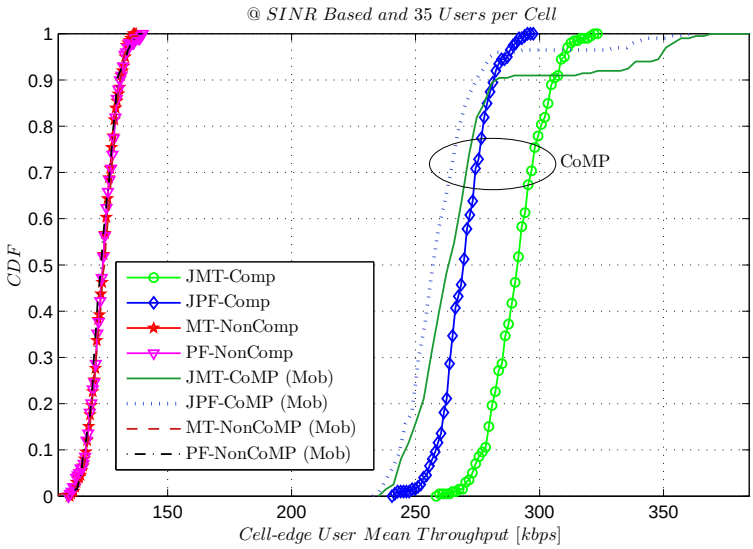

(a) Cell-edge user throughput distribution

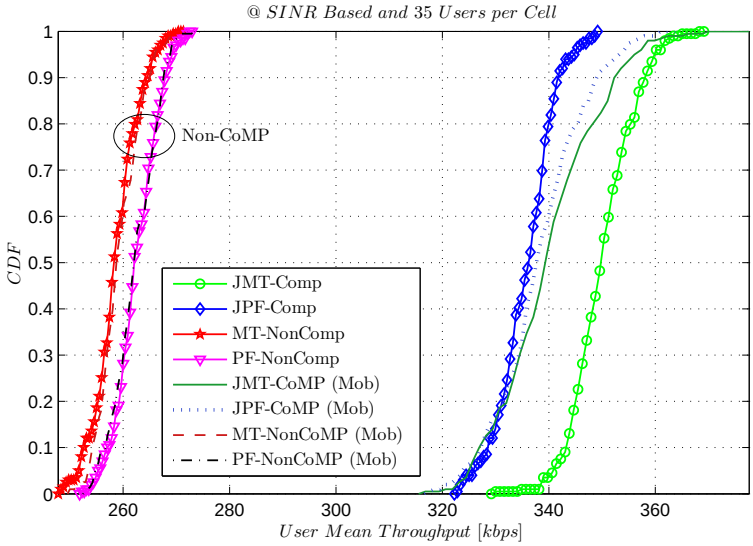

(b) User throughput distribution

Figure 6.11: Inter-site CoMP performance in terms of user throughput distribution at 35 users per cell under SINR based cell-edge decision and fixed traffic

6.5 Summary

This chapter has evaluated the performance of the scheduling algorithms in inter-site CoMP scenario under different situations such as users under static, users under mobility, cell-edge decision based on the absolute distance from the serving base station, cell-edge decision based on the relative pilot RSRP power and cell-edge decision based on the absolute pilot SINR. A summary of KPIs performance comparing JMT and JPF algorithms, at 96 % of traffic intensity in the case of Poisson traffic and at 35 users per cell in the case of fixed traffic, is shown in Table 6.2.

Table 6.2: Summary of inter-site CoMP performance

Traffic	[a]KPIs (%)	Distance Based		RSRP Based		SINR Based	
		No Mobility	Mobility	No Mobility	Mobility	No Mobility	Mobility
Poisson	Success	JMT: + 2.7	JMT: + 0.8	JMT: + 9.5	JMT: + 3.97	JMT: + 11.73	JMT: + 4
	No Coverage	JMT: - 14.71	JMT: -0.15	JMT: - 14.46	JMT: - 5	JMT: - 19.64	JMT: - 3.66
	No RAB	JMT: - 15.74	JMT: - 4.44	JMT: - 7.36	JMT: - 3.03	JMT: - 8.87	JMT: - 2.11
Fixed	CEU Thr.	**JPF: + 32.1**	**JPF: + 11.01**	JMT: + 18.92	JPF: + 1.11	JMT: + 17.43	JMT: + 7.05
	UE Thr.	**JPF: + 8.43**	JPF: + 0.62	JMT: + 7.07	JPF: + 1.53	JMT: + 5.48	JMT: 0.65
	Sys. Thr.	**JPF: + 6.65**	**JPF: - 2.63**	JMT: + 17.18	JMT: + 2.66	JMT: + 13	JMT: + 2.89

[a]compared between JPF and JMT schedulings

As shown in the table, it can be concluded that JMT has better performance for all scenarios except in the distance based cell-edge decision under fixed traffic, where JPF has better throughput performance under both no mobility and mobility conditions. For example, as shown in the table, under fixed traffic and the distance based cell-edge decision, JPF has 32.1 %, 8.43 % and 6.65 % higher cell-edge user throughput (CEU Thr.), user throughput (UE Thr.) and system throughput (Sys. Thr.), respectively, under no mobility compared with JMT; while under a mobility condition, it has 11.01 % higher cell-edge user throughput and 2.63 % less system throughput compared with JMT.

Chapter 7:

Hybrid Model: Combination of Analytic and Simulation Approach

In Chapter 3, a design of an event-driven dynamic system level simulator was formulated for the downlink communication of OFDMA based networks, i.e., LTE-A. In Chapter 4, a complete dynamic analytic model for the throughput evaluation of such a system was developed.

In this chapter, a hybrid model combining analytic and simulation approaches is developed. The hybrid model has the advantage that an individual inter-mediate call state of a network can be evaluated.

7.1 Hybrid Model

This model combines an analytic and a simulation approach. The probability of call distribution being in a particular state in the system is obtained from the analytic expressions (Chapter 4, Eqs. (4.3) to (4.7)) and is used as input to the simulation to estimate the throughput of a cell. The average throughput for a cell m is expressed as

$$\sum_{\boldsymbol{n}\in\mathcal{S}}\sum_{u=1}^{U^m}[\boldsymbol{\pi}^m(\boldsymbol{n}^m)\ \underbrace{T^m_{u,r}}_{sim.\ thr.}\ ], \tag{7.1}$$

where

- $\boldsymbol{n} \in \mathcal{S}$ is the possible call configurations in the system and $\mathcal{S}$ is the state space of users in the system,

- $\sum_{u=1}^{U^m}$ represents the number of users in cell m,
- $\boldsymbol{\pi}^m(\boldsymbol{n}^m)$ represents the probability that there are $\boldsymbol{n}^m$ calls in cell m,
- $T_{u,r}^m$ is the average throughput of a user u on subchannel r in cell m obtained from event-driven simulation (Chapter 3) for a particular state of call in the system.

The average throughput for the system is expressed as

$$\sum_{\boldsymbol{n}\in\mathcal{S}}[\boldsymbol{\pi}(\boldsymbol{n}) \underbrace{T}_{sim.\ thr.}], \tag{7.2}$$

where

- $\boldsymbol{\pi}(\boldsymbol{n})$ represents the probability of the state space $\boldsymbol{n}$ in the system,
- T is the average system throughput (sim. thr.) obtained from the simulation for a particular call configuration in the system.

7.2 System Model and Simulation Configuration

In order to evaluate the performance of the system and validate our proposed hybrid model, an event-driven dynamic SLS tool was used. The network model considered to evaluate the hybrid model is shown in Fig. 7.1, where each hexagonal cell-site is divided into three cells: Cell A, Cell B and Cell C. Each cell is equipped with 1 transmit antenna and each user equipment has 1 receive antenna. Each user is allowed only one subchannel of a 1 ms time slot. The traffic was modelled as a homogeneous Poisson random process in each cell. To account for the dynamic behaviour of the incoming traffic pattern or of the service time, and to obtain various traffic loads in the network, we have implemented two approaches. In the first approach, the mean holding time of users is fixed and the inter-arrival time is varied, which models the dynamic

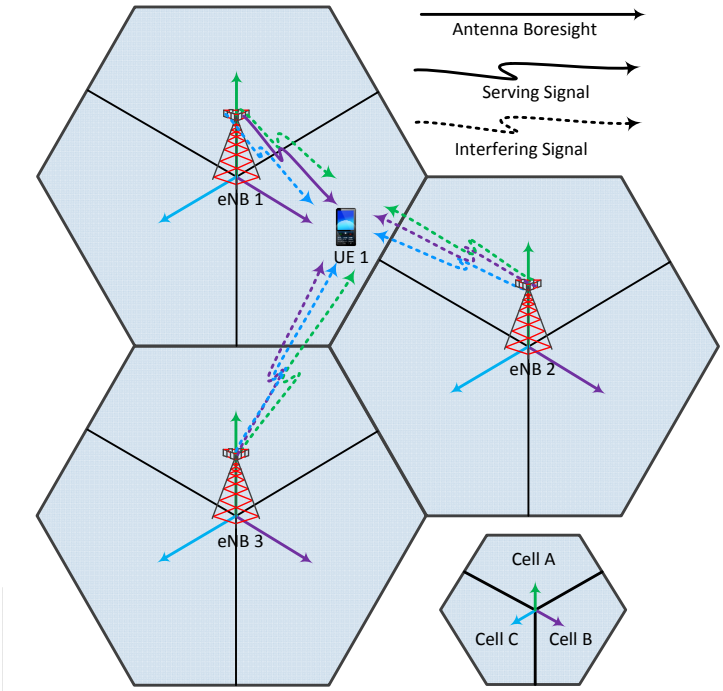

Figure 7.1: The complete model used for the performance evaluation consists of 3 cell-sites

behaviour of the incoming traffic into the system. In the second approach, the inter-arrival time is fixed and the mean holding time is varied, which models the dynamic behaviour of the service time by each user in the system. The simulation is based on the event-driven simulation; an event occurs when:

a) a user arrives and accesses a subchannel to connect to the network,

b) the user moves position randomly,

c) the user leaves the network and the subchannel is freed,

d) the system triggers to log the simulator status indicator.

The logged data of users such as SINR and throughput are obtained on a regular basis. The wireless channel for a user from a BS is selected randomly

from available subchannels and remains the same as long as the user stays in the network. A different level of adaptive modulation and coding scheme is selected from Table 3.1 when mapping the user SINR to its achievable data throughput. The parameters in the simulation are consistent with the LTE downlink, and are listed in Table 7.1.

The process for evaluating the performance of the system in the hybrid model is described as follows:

1) calculate the probability of the system being in a particular call configuration from the statistically stationary distribution of calls using expressions (4.3) to (4.7).

2) run the event-driven simulation for this particular configuration only, and change the user position during the simulation (thus accounting for the effect of different locations when estimating the average throughput).

3) multiply the simulated throughput for this particular configuration obtained from the simulation with the probability calculated analytically for the system in a specific configuration.

4) repeat the simulation for all possible configurations of calls in the system.

5) sum the throughput for all the possible configurations for the overall system throughput.

7.3 Configuration and Validation

To validate the simulation, we have tested the results of probability of call distribution and probability of call blocking obtained from the simulation with that obtained by analysis for different traffic intensities. Figure 7.2 shows that both the probability of call distribution for the highest possible call state and

Table 7.1: Simulation parameters for hybrid model evaluation

Call distribution	Uniform
Call generation process	Poisson
Call mean arrival rate (λ_u^m)	0.1, 0.2, 0.3, 0.4, 0.5, 0.6, 0.7, 0.8, 0.9, 1.0 calls/min/cell
Call mean holding time (μ_u^m)	0.5, 1, 1.5, 2.0, 2.5, 3.0, 3.5, 4.0, 4.5, 5.0 min
Call inter-arrival and holding time dist.	Exponential
Site layout	1 hexagonal site with 3 cells
Carrier frequency/Subcarrier spacing	2 GHz/15 kHz
Resource Block (RB) spacing	12×15 kHz = 180 kHz
Number of subchannels (R)	2, 3, 4, 5
Data symbols per time slot (O_r)	11 OFDM data symbols
Frame duration (τ)	1 ms
Thermal noise density (σ)	-174 dBm/Hz
Thermal noise power	-121.4 dBm
Resource allocation	1 RB/user
eNB Tx power	46 dBm
eNB/UE antenna height	32/1.5 m
eNB/UE antenna gain	18/0 dBi
UE noise figure	9 dB
UE receiver sensitivity	-95 dBm
eNB antenna boresight	0/120/240 degrees
eNB antenna pattern	3GPP Case1: 3D antenna pattern
Shadowing model	Gudmunson model
Shadowing standard deviation	8 dB
Correlation shadowing distance (d_{cor})	50 m

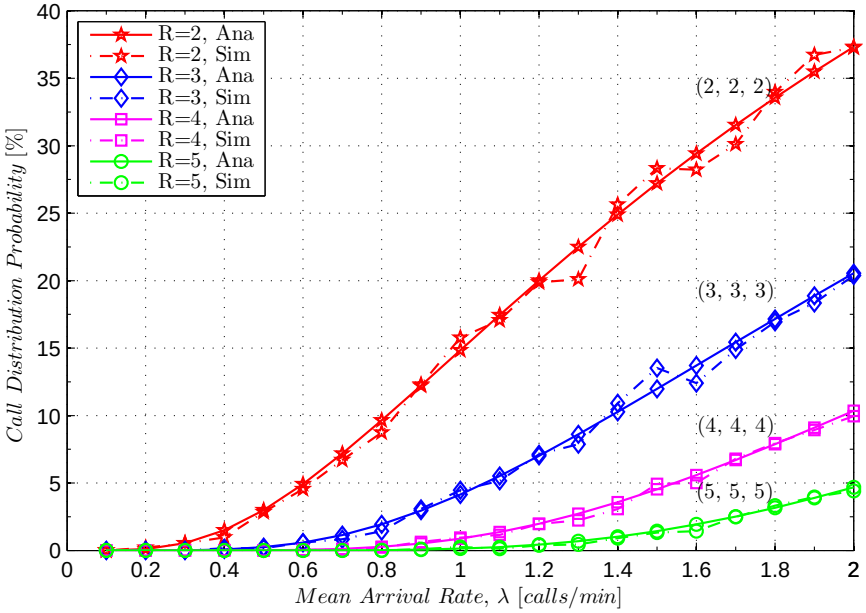

(a) Call distribution probability

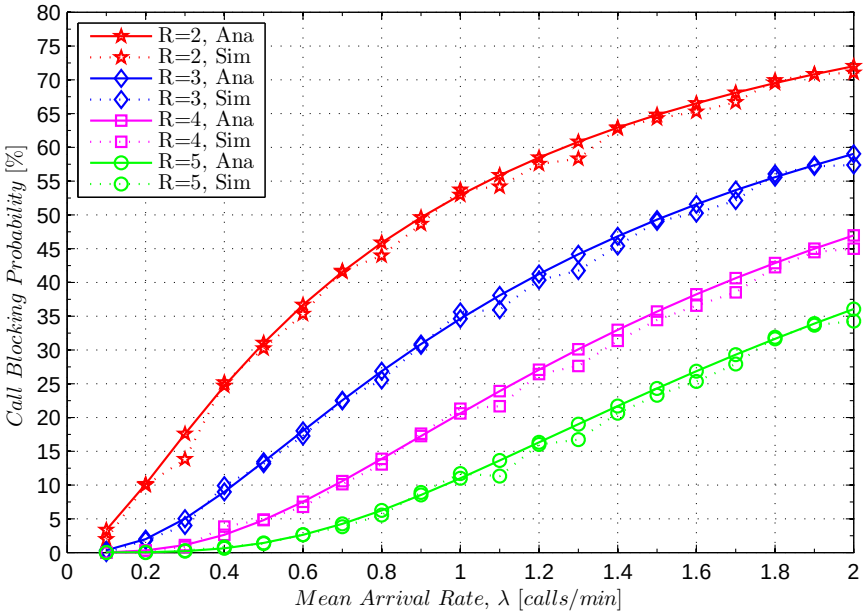

(b) Call blocking probability

Figure 7.2: Probability comparison between simulation and analysis at mean holding time, $1/\mu^m = 3$ min, in terms of a) probability of highest possible call state, i.e., (R, R, R) and b) probability of call blocking

the probability of call blocking obtained by simulation are inline with those obtained by analysis for different traffic intensities and different numbers of users. The performance of the system throughput obtained by our hybrid model was evaluated for different scenarios of traffic behaviour by changing the mean arrival rate, the mean holding time and the number of subchannels.

7.3.1 Arrival Rate

In this case, the performance of the system was evaluated for different call arrival rates for different numbers of subchannels to account for the variation of inter-arrival traffic, while the mean holding time remained fixed. Figure 7.3 shows the performance of the average system throughput for different arrival rates. The detail result is shown in Appendix H in Table H.1. It is noted that the system throughput performance by the hybrid model is similar to the simulation for all arrival traffic patterns. The mean of the throughput error between the two methods is found to be -0.878 % for $R = 2$, -7.60 % for $R = 3$, -0.356 % for $R = 4$ and -0.205 % for $R = 5$.

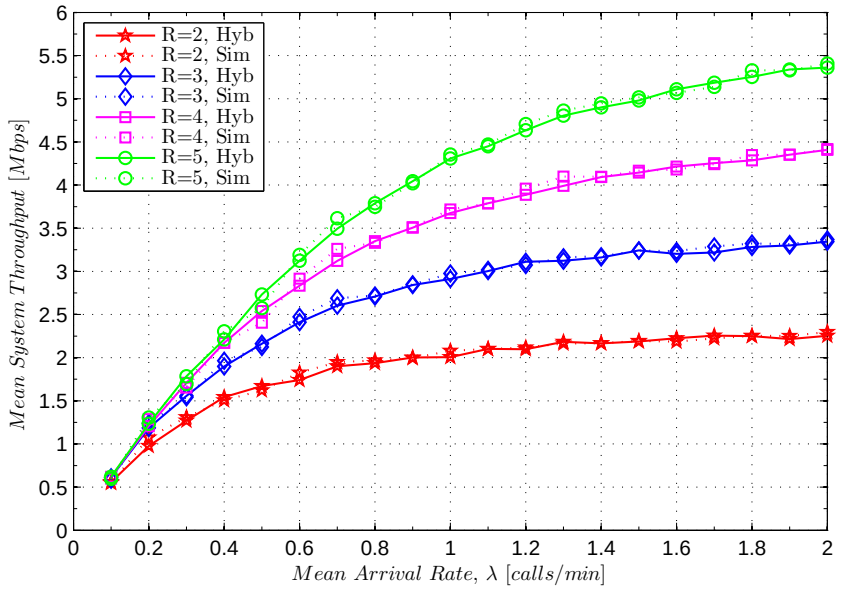

Figure 7.3: System throughput performance in hybrid model with mean holding time, $1/\mu^m = 3$ min

7.3.2 Holding Time

In this case, the performance of the system was evaluated for different mean holding times and for different numbers of subchannels to account for the variation of service-time, while the mean arrival rate remained fixed. Figure 7.4 shows the performance of the average system throughput for a range of mean holding times. The detail result is shown in Appendix H in Table H.2. It is noted that the system throughput performance by the hybrid model is similar to the simulation for all arrival traffic patterns. The mean of the throughput error between the two methods is found to be 0.943 % for $R = 2$, -1.059 % for $R = 3$, -0.666 % for $R = 4$ and -0.663 % for $R = 5$.

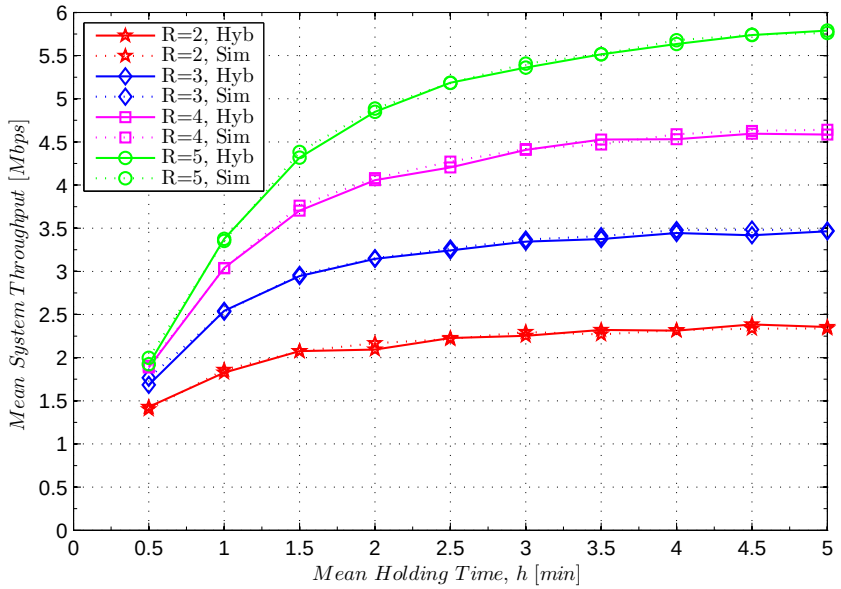

Figure 7.4: System throughput performance in hybrid model with mean arrival rate, $\lambda^m = 2$ calls/min

7.4 Summary

A hybrid model consisting of analysis and simulation for the evaluation of average system data throughput is proposed. The model allows throughput of intermediate call states to be evaluated as well as the overall network throughput. To evaluate the performance of the hybrid model, a detailed probability of call distribution in the system is first obtained from analytical expressions of a statistically stationary distribution, which are used as an input to the simulator to calculate the system throughput. We compared the results of the hybrid model with those obtained from simulation. We tested the model for different parameters of user arrival rates, their mean holding time and a different number of radio subchannels in the network. It has been found that the results of the hybrid model are in line with the simulation based results. The max-

imum difference of the mean throughput error performance between the hybrid model and the simulation is found to be in the interval of $(0.043\%, 1.059\%)$ for different call arrival rates, mean holding times and number of subchannels in the system. It was noted that for a large number of cells and users, the number of possible call configurations in the system is very large. With such a large possible number of call configurations, it is difficult to evaluate the system throughput by the hybrid model from a user point of view because we need to evaluate the throughput for all possible call configurations. But there may be a case where we need to know the throughput of any particular call configuration in the system from a user point of view. The simulation does not provide the throughput of any intermediate call state because it does not log the call state. The benefit of the hybrid model is that the throughput of any possible call state can be evaluated.

Chapter 8:

Empirical Indoor-to-Outdoor Path Loss Modelling

In this chapter, the results are presented from a study of radio propagation behaviour for an indoor-to-outdoor urban environment in a residential area for two different ranges of frequencies, together with empirical path loss models that were developed based on measurement data. In a heterogeneous network, small cells such as femtocells create severe interference to macrocell users. In order to estimate the level of interference coming from the femtocells, it is necessary to have a suitable propagation model, and this chapter focuses on the development of an empirical path loss model for this purpose.

8.1 Motivation and Objectives

Emerging small cells such as femtocells are interference-limited and the interfering power depends on the geometry of the scenario. Various models of indoor-to-outdoor propagation are available in the literature but each one has its own limitation due to the constraint of the environment or frequency range.

The objective of the propagation modelling campaign was to characterise the behaviour of the radio propagation in indoor-to-outdoor scenarios and to develop empirical path loss models based on measurement data. The measurements were done by a colleague [110] for four different carrier frequencies 900 MHz, 2 GHz, 2.5 GHz and 3.5 GHz, but in this thesis models have been developed based on the carrier frequencies 900 MHz and 2 GHz.

8.2 Related Works

Various empirical path loss models for indoor-to-outdoor environments can be found in the literature, such as in [111–119]. However, each model has its own restriction in terms of frequency range or modelling approach. For example, the path loss model developed in [111] is suitable for the frequency range 5-6 GHz. Dohler, in his Master's thesis [112], has studied path loss in outdoor-to-indoor propagation at the frequencies of 2.4 GHz, 5.2 GHz and 60 GHz, which is not suitable for indoor-to-outdoor scenarios because the radio propagation inside a building behaves differently due to the multiple reflections from walls and objects. Rose *et al.* in [113] have carried out exhaustive measurements to study indoor-to-outdoor propagation of LTE femtocells at 800 MHz and 2600 MHz frequencies, but the paper has not mentioned any analytical model. In [114], the WINNER project studied propagation behaviour under various scenarios in a University area. The measurements were done for the frequency ranges 2-6 GHz; and the indoor-to-outdoor path loss models can be found in pages 39-44 in [114]. However, the lower frequencies such as 900 MHz have not been considered. Linares, in his Master's thesis [115], has developed an empirical path loss model in a Femto-to-Macro indoor-to-outdoor scenario under a 2.4 GHz carrier frequency. In [116], an analytical expression for the additional losses at the indoor/outdoor interface were developed based on the statistics extracted from ray-tracing simulations, and it has not been validated by measurements. The ITU - Radiocommunication Sector (ITU-R) in Recommendation [117] has provided guidance on indoor propagation over the frequency range from 900 MHz to 100 GHz. This recommendation considers only indoor propagation and not indoor-to-outdoor. Corre and Stephan in [118] have proposed two different indoor-to-outdoor path loss models at a frequency of 2.1 GHz, which are not suitable for 900 MHz frequency.

From the literature review, it is noted that many of the papers have studied propagation behaviour in indoor-to-outdoor environments for higher frequencies but have not considered lower frequencies such as 900 MHz, which is under trials for LTE-A in some countries according to a blog [120]. Valcarce, in [119], has developed an empirical indoor-to-outdoor path loss model for the frequency ranges 900 MHz to 3.5 GHz. The model is a general expression in terms of frequency and the number of walls. However, the propagation attenuation inside the building is not considered.

8.3 Measurement Campaign

Various experiments of continuous wave (CW) power measurements were done by a [a]colleague [110] during his PhD study.

8.3.1 Measurements Equipment

The equipment used for the measurement are shown in Fig. 8.1 and described in brief as follows.

Antennas

The antennas used in the transmitter and the receiver were slim flexible dipoles of the SVD2 series from *Cobham* manufacturing [121], similar to those usually used in Wireless Fidility (WiFi) access points and Femtocells [110]. The antennas had onmi-directional radiation patterns in azimuth, with a wide vertical beamwidth and are vertically polarised with a maximum gain of 2 Decibel Isotropic (dBi) in the horizontal direction; their characteristics at different frequencies are summarised in Table 8.1 [110].

[a]Note that the measurement was carried by a colleague Valcarce, and for clarity Section 8.3 describes the procedure followed by him during the measurement campaign.

(a) Signal generator

(b) Spectrum analyser

Figure 8.1: Measurement equipments

Table 8.1: Antenna characteristics

Freq. Range	Part No.	Max. Gain	Vert. HPBW	Max. VSWR
870 - 960 MHz	SVD2 - 915/432	2 dBi	80°	2:1
2.38 - 2.61 GHz	SVD2 - 2500/869	2 dBi	80°	2:1
3.40 - 3.65 GHz	SVD2 - 3450/426	2 dBi	80°	2:1

Vector Signal Generator

A Vector Signal Generator from Anritsu of model MG3700A, as shown in Fig. 8.1(a), was used as a transmitter to generate unmodulated Continuous Wave (CW) signals under different frequencies of interest. This signal generator supports a frequency modulation range between 250 kHz and 6 GHz.

Spectrum Analyser

A Spectrum Analyser from Anritsu of type MS2721B, as shown in Fig. 8.1(b), and was used as a receiver to measure the received power. This is a portable device with a Global Positioning System (GPS) module which was used to record the location of each measurement.

8.3.2 Measurement Environment and Scenarios

The measurements were done in a residential environment of a medium-size British town called Luton. Two residential sites were chosen for the measurement: Russell Rise (RR) and Stockwood Crescent (SC) streets, where each house has 2-3 floors. Both sites are in a close proximity of 500 m. The houses are typically made of brick, plaster and wood. The measurements were done on the road as a concept of measuring the leakage power from a Femtocell placed inside a nearby house, which causes interference to the nearby macrocell users in the environment. The weather condition was sunny and dry. An arial view of the measurement sites using the Google Earth tool is shown in Fig. 8.2 and a closer view of each measurement site is shown in Fig. 8.3.

Figure 8.2: An ariel view of the measurement sites (©Bluesky International Ltd, 2013)

(a) Site 1: Russell Rise (RR) street

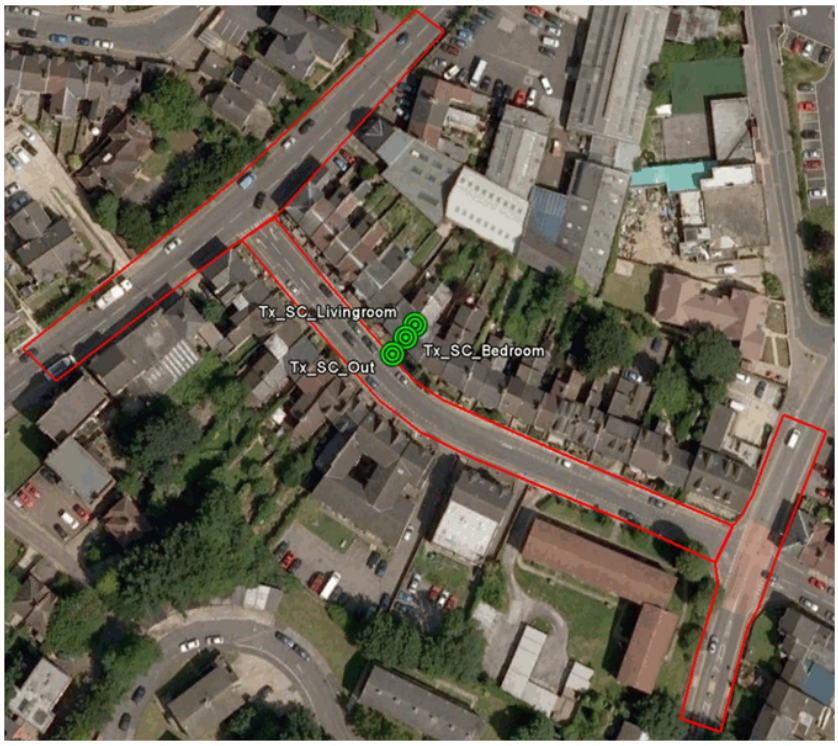

(b) Site 2: Stockwood Crescent (SC) street

Figure 8.3: A closer view of the measurement sites (©Bluesky International Ltd, 2013)

Three different scenarios of transmitter locations were chosen in each site, which are described as follows.

- Scenario 1: The transmitter was located outside and in front of the building near the edge of the road.
- Scenario 2: The transmitter was located inside the building in the first room (called Bedroom (BR)) from the road, where the direct radio path between the transmitter and the road includes one wall.
- Scenario 3: The transmitter was located inside the building in the second room (called Livingroom (LR)) from the road, where the direct radio path between the transmitter and the road includes two walls.

The zoom view of the transmitter locations are shown in Fig. 8.4. The parameters of measurements settings are listed in Table 8.2.

(a) Site 1: RR (b) Site 2: SC

Figure 8.4: A closer view of transmitter locations (©Bluesky International Ltd, 2013)

Table 8.2: Parameters for measurement settings

Measurement Parameters	Value
Carrier frequencies	0.9, 2.0 GHz
Transmitter output power	19 dBm
Transmitter/Receiver antenna's gain	2 dBi
Transmitter antenna height from the floor	1 m
Receiver height	$\approx$ 1.2 m above the street

8.3.3 Measurement Methodology

The measurements were carried out for each location on a frequency sweep of 1 kHz band centred at the carrier frequency of interest. The measurement device was carried by hand and the data was recorded while walking to reduce small-scale fading effects and the locations of the measurements were resolved using a GPS receiver [110].

8.4 Measurement Postprocessing

These types of measurements are subject to random fading phenomena and in particular to small-scale fading. Therefore, in order to use the measured data to model empirical path loss, the data must first be treated by postprocessing where the outliers and fading effects in the data are removed.

8.4.1 Bad GPS Positioning

The locations of outdoor measurement points were obtained by using GPS coordinates, which are eventually subject to error. An example of error due to bad GPS positioning is highlighted in Fig. 8.5. It was noted that in the Site 2 (SC) measurement, GPS positioning had been badly affected, as shown in Fig. 8.5; whereas in Site 1 (RR), it was less affected in comparison to the Site

2 measurement.

8.4.2 Removal of 'Outlier' Data

Any measurement data subject to location error, such as badly positioned GPS coordinates, coordinates inside a building, no GPS coverage or coordinates outside of the scenario, were removed with the help of GPS Track Maker [122] tool. The following process was followed to correct the outlier data:

- Firstly, an assumption was made that the measurement path had been taken following a similar route for all of the scenarios in a site.
- Then an approximate track of the measurement route was traced over the pedestrian pavement with the help of the Google Earth tool. This approximation is in line with reality because pedestrians walk on the side of the road occasionally but not in the middle of the road.
- The receiver coordinates (GPS value) were plotted over the Google Earth display using a kml file format.
- A screenshot of the plotted receiver coordinates over the Google Earth display was taken.
- Finally, with the help of the GPS Track Maker tool, all the badly shifted receiver coordinates were brought towards the traced route using common sense as no one tends to walk in the middle of the road or on the roofs of houses.

8.5 Empirical Path Loss Modelling

After receiving and post-processing the measured channel power data, it was fitted to develop an empirical path loss model. From the measurement of the

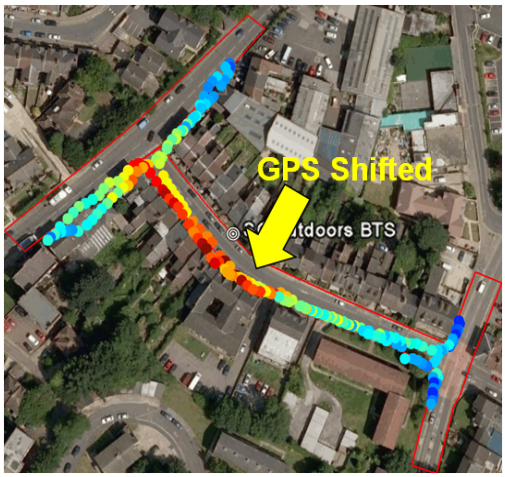

(a) GPS shifted

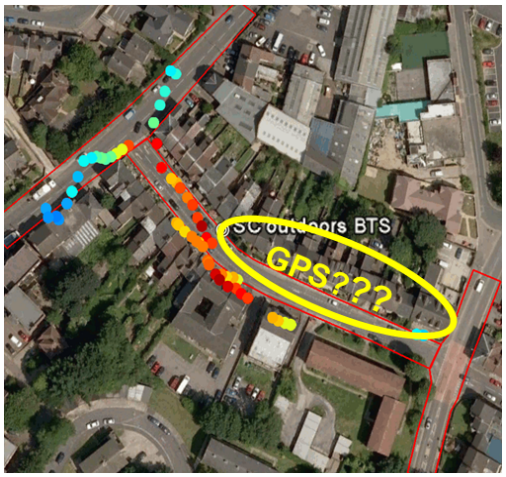

(b) GPS missed

(c) GPS highly shifted

Figure 8.5: An example of outliers data or erroneous data due to GPS positioning (©Bluesky International Ltd, 2013)

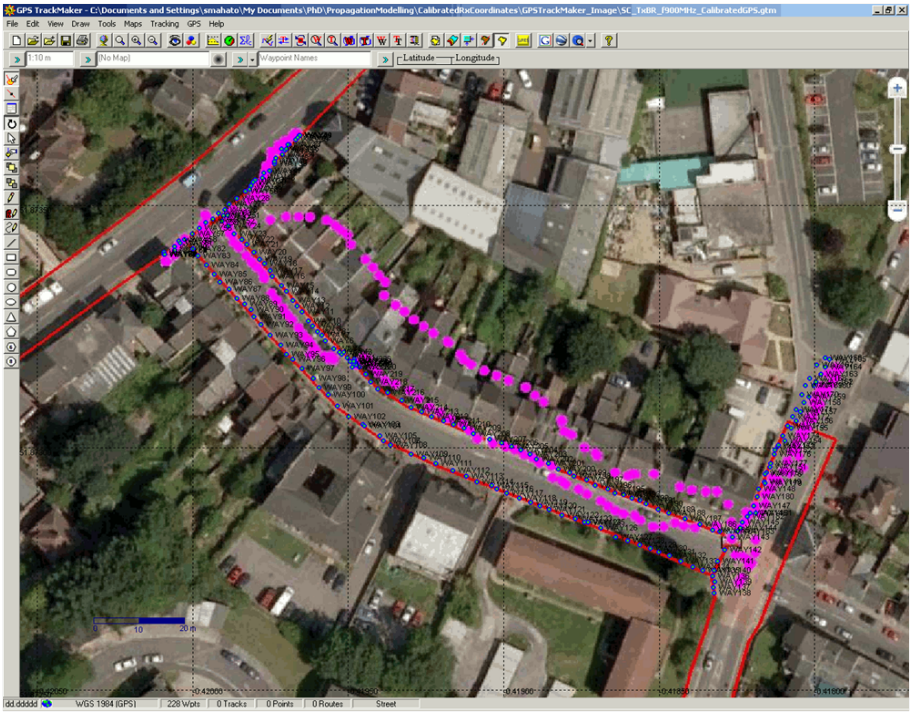

Figure 8.6: A snapshot of GPS coordinates corrected (©Bluesky International Ltd, 2013)

received power data, the path loss, L, can be calculated as

$$L = P_{tx} + G_{tx} + G_{rx} - P_{rx}, \qquad [\text{dB}] \tag{8.1}$$

where $P_{tx} = 19$ Decibel Milliwatts (dBm) is the transmitter power, $G_{tx} = 2$ dBi is the gain of the transmitter antenna, $G_{tx} = 2$ dBi is the gain of the receiver antenna and P_{rx} is the received power as measured. The process of modelling the calculated path loss data is described in the following subsections.

8.5.1 Modelling Methodology

The methodology used to analyse the measured data and to fit it into an empirical path loss model is described as follows.

- Firstly, the Line-Of-Sight (LOS) data was separated from the Non-LOS (NLOS) data. This was done by inspecting the measurement path and

removing those measurement points which were outside of the LOS path, as illustrated in Fig. 8.7, where the measurement points inside the LOS region are represented by Cyan colour, while the NLOS points are represented by Blue colour.

- Only LOS data was considered for the modelling.
- A Linear Least-Square fit with the help of Singular Value Decomposition (SVD) algorithm [123–125] was used to fit the measurement data. According to the SVD algorithm,

$$\boldsymbol{L} = \boldsymbol{D}\boldsymbol{C} + \boldsymbol{e}, \tag{8.2}$$

where $\boldsymbol{L}$ is an $n \times 1$ vector of the calculated path loss from the measurement data where n represents the number of measurement points, $\boldsymbol{D}$ is an $n \times m$ design matrix for a model where m represents the number of the modelled parameters, $\boldsymbol{C}$ is an $m \times 1$ vector of unknown coefficients (i.e., the modelled parameters) of the model and $\boldsymbol{e}$ is an $n \times 1$ vector of the residual path loss data obtained from the measurement data and the fitted model.

- The solution of the unknown coefficients is obtained by the SVD algorithm as

$$\boldsymbol{C} = (\boldsymbol{D}^\top \boldsymbol{D})^{-1} \boldsymbol{D}^\top \boldsymbol{L}, \tag{8.3}$$

where $(\cdot)^\top$ represents the transpose of the matrix, while $(\cdot)^{-1}$ represents the inverse.

- The residual path loss data from the measured data and the fitted model can be obtained as

$$\boldsymbol{e} = (\boldsymbol{I} - \boldsymbol{H})\boldsymbol{L}, \tag{8.4}$$

$$\boldsymbol{H} = \boldsymbol{D}(\boldsymbol{D}^\top \boldsymbol{D})^{-1} \boldsymbol{D}^\top, \tag{8.5}$$

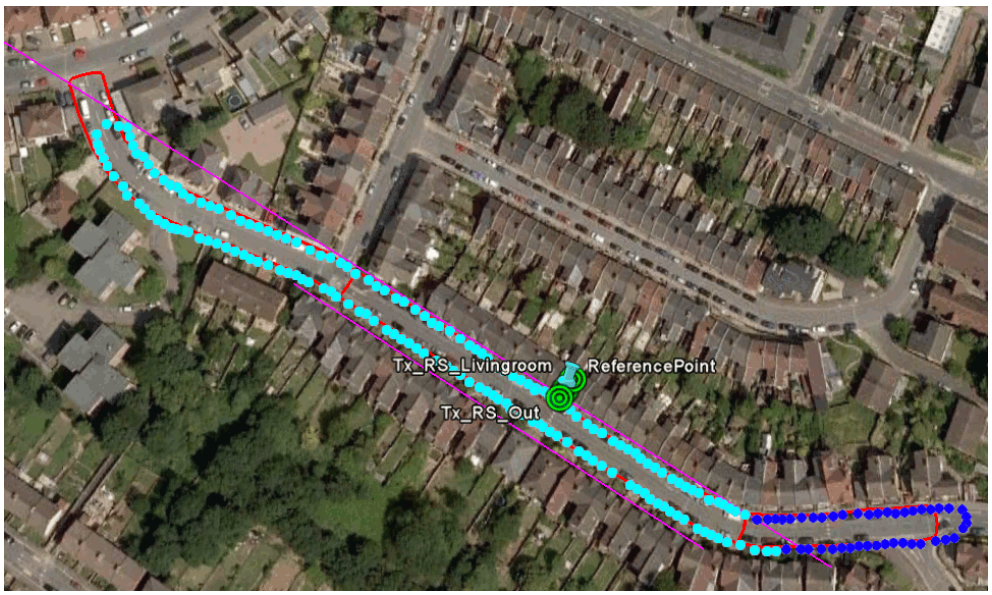

(a) Line-of-sight data of Site 1

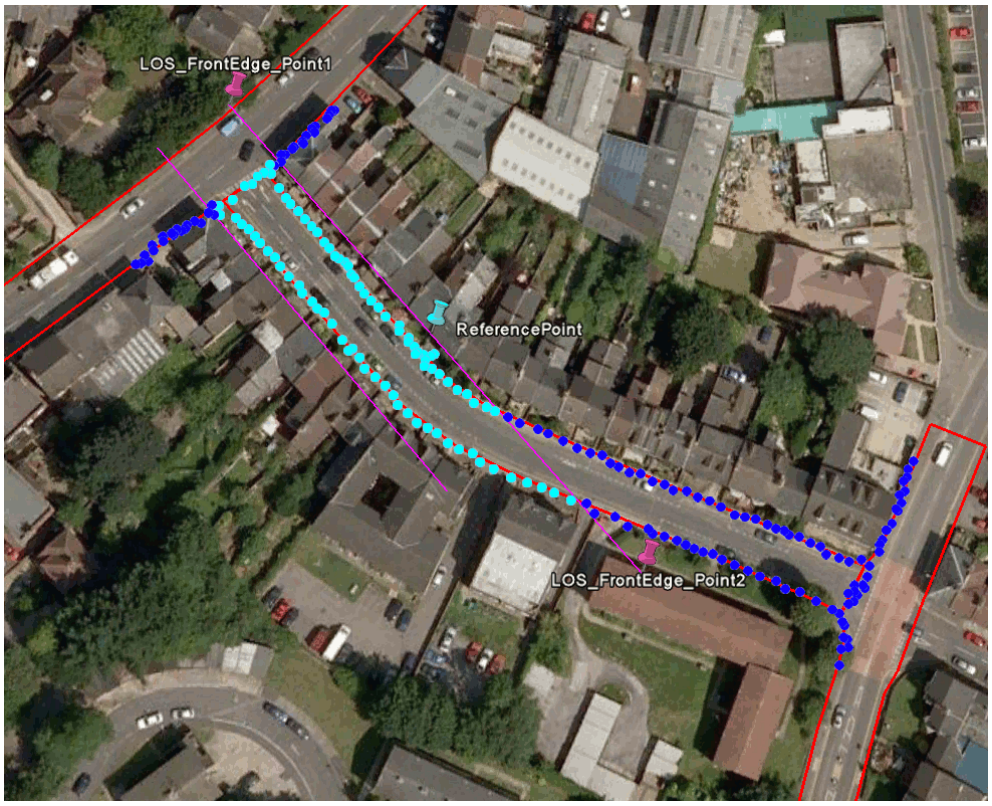

(b) Line-of-sight data of Site 2

Figure 8.7: Illustration of line-of-sight data extraction (©Bluesky International Ltd, 2013)

where $\boldsymbol{I}$ represents $n \times m$ identity matrix, e represents $n \times 1$ vector of the residual data obtained from the measurement data and the fitted model, and $\boldsymbol{H}$ comes in $n \times m$ matrix form.

- The residual path loss data was analysed with the Minimum Root Mean Square Error (MRMSE) as

$$\sigma = \sqrt{\frac{\boldsymbol{e}^\top \boldsymbol{e}}{n}}, \tag{8.6}$$

where σ is the standard deviation of the residual path loss data in dB which is the Root Mean Square Error (RMSE) value as described later in the thesis.

The estimated path loss data was modelled in two different ways called *Model A* and *Model B*, and are described as follows.

8.5.2 Path Loss Model A

In this model, the estimated path loss data was modelled with a simple pathloss model as

$$L = \alpha + 10\beta \log_{10}(d) + \sigma, \tag{8.7}$$

where L is the path loss in dB, α is a constant in dB, β is the path loss exponent, d is the distance between the transmitter and the receiver; and σ represents the standard deviation in dB of the log-normal shadow fading. Remember that in the case of the transmitter placed inside the building, the losses due to walls are considered in α. In this model, the modelled parameters are α and β; and the design matrix and the coefficient vector for Model A in the SVD algorithm can be expressed as

$$\boldsymbol{D} = \begin{bmatrix} 1 & 10\log_{10}(d_1) \\ 1 & 10\log_{10}(d_2) \\ \vdots & \vdots \\ 1 & 10\log_{10}(d_n) \end{bmatrix} \text{ and } \boldsymbol{C} = \begin{bmatrix} \alpha \\ \beta \end{bmatrix}, \tag{8.8}$$

where d_n represents the distance between the transmitter and the receiver at the measurement position n.

8.5.3 Path Loss Model B

In this model, the measurement data of Scenario 1 (Tx Outside) waw modelled according to Model A, while the measurement data from Scenario 2 (Tx in BR) and Scenario 3 (Tx in LR) were modelled in two steps. In the first step, the modelled parameters, α and β, from Scenario 1 (Tx Outside) were used to calculate the path loss between the front face of the building and the receiver position. In the second step, the excess path loss data was calculated by subtracting the calculated path loss from the measured path loss of Scenario 2 (Tx in BR) and Scenario 3 (Tx in LR) respectively. Then, the excess path loss data was modelled as a loss due to walls and the propagation inside of the building.

- Path loss outside:

$$L_{out} = \alpha + 10\beta \log_{10}(d_{ref-rx}), \tag{8.9}$$

  where L_{out} is the path loss outside of the building, d_{ref-rx} is the distance between the reference point (i.e., the front face of the building) and the receiver location.

- Path loss inside:

$$L_{in} \;=\; L_{meas} - L_{out} = \gamma w + \delta d_{in}, \tag{8.10}$$

  where L_{in} is the path loss inside the building in dB including walls, L_{meas} is the path loss measured in the case of the transmitter placed inside, γ is the attenuation coefficient in dB per wall, w is the number of walls, δ is the distance attenuation coefficient in dB per metre distance inside of the building and d_{in} is the propagation distance inside of the building.

Therefore, the combined path loss in the case of a transmitter placed inside of the building can be written as

$$L_{inside} = L_{out} + L_{in}. \tag{8.11}$$

The modelled parameters are α, β, γ and δ; and the design matrix and the coefficient vector for Model B in the SVD algorithm are expressed as

- Path loss outside:

$$\boldsymbol{D} = \begin{bmatrix} 1 & 10\log_{10}(d_{ref-rx_1}) \\ 1 & 10\log_{10}(d_{ref-rx_2}) \\ \vdots & \vdots \\ 1 & 10\log_{10}(d_{ref-rx_n}) \end{bmatrix} \text{ and } \boldsymbol{C} = \begin{bmatrix} \alpha \\ \beta \end{bmatrix}. \tag{8.12}$$

- Path loss inside:

$$\boldsymbol{D} = \begin{bmatrix} w & d_{in} \\ w & d_{in} \\ \vdots & \vdots \\ w & d_{in} \end{bmatrix} \text{ and } \boldsymbol{C} = \begin{bmatrix} \gamma \\ \delta \end{bmatrix}. \tag{8.13}$$

8.6 Results and Analysis

The modelled parameters of the path loss Model A are summarised in Table 8.3 for Site 1 and in Table 8.4 for Site 2. Since the measurement sites are in close proximity (500 m) and the environment around both measurement sites are quite similarl, we can assume that the propagation behaves similarly at both sites. Assuming this, we can estimate an average for the modelled parameters from both sites and the average values are summarised in Table 8.5.

Table 8.3: Modelled parameters of Model A in site 1

Modelled Parameters ⇓	Measurement Site 1: RS Road					
	Tx Outside		Tx in BR ($w = 1$)		Tx in LR ($w = 2$)	
	2 GHz	900 MHz	2 GHz	900 MHz	2 GHz	900 MHz
α (dB)	50.33	39.62	49.29	45.61	57.80	40.61
β	2.31	2.98	3.29	3.26	3.23	3.77
RMSE (dB)	9.12	6.79	7.72	7.02	7.90	5.26

Table 8.4: Modelled parameters of Model A in site 2

Modelled Parameters ⇓	Measurement Site 2: SC Road					
	Tx Outside		Tx in BR ($w = 1$)		Tx in LR ($w = 2$)	
	2 GHz	900 MHz	2 GHz	900 MHz	2 GHz	900 MHz
α (dB)	61.07	45.50	41.30	27.78	54.82	28.03
β	1.25	2.36	3.98	4.41	3.59	4.63
RMSE (dB)	10.57	9.01	8.68	7.25	8.98	6.46

Table 8.5: Average value of the modelled parameters for Model A

Modelled Parameters	Tx Outside		Tx in BR ($w = 1$)		Tx in LR ($w = 2$)	
	2 GHz	900 MHz	2 GHz	900 MHz	2 GHz	900 MHz
α (dB)	58.41	43.49	46.92	42.67	56.56	37.83
β	1.78	2.67	3.64	3.84	3.41	4.20
RMSE (dB)	9.90	8.04	8.23	7.13	8.47	5.90

The modelled parameters of Model B for path loss outside the building are summarised in Table 8.6 and the path loss inside the building are summarised in Table 8.7.

Figure 8.8 shows the measured path loss and its fit by Model A. Figure 8.9 shows a normal distribution fit of the residual path loss obtained from measurement and fitted by Model A, Fig. 8.10 shows their probability density plot.

Table 8.6: Modelled parameters for Model B for outside path loss

Modelled Parameters	Site 1: RS		Site 2: SC		Average Value	
	2 GHz	900 MHz	2 GHz	900 MHz	2 GHz	900 MHz
α (dB)	50.33	39.61	61.071	45.50	58.41	43.49
β	2.31	2.98	1.25	2.36	1.78	2.67
RMSE (dB)	9.12	6.79	10.57	9.01	9.90	8.04

Table 8.7: Average value of the modelled parameters for Model B

Modelled Parameters	Average Value	
	2 GHz	900 MHz
γ (dB)	18.32	6.51
δ	4.62	1.63
RMSE (dB)	9.35	7.24

It has been noted that the residual path loss data follows normal distribution with a mean 0 dB and a standard deviation equal to a RMSE value. Figure 8.11 and Fig. 8.12 show the cumulative distribution of the residual data for Site 1 and Site 2 respectively. It has been noted that the variation of signal from the mean path loss is larger in a higher frequency (2 GHz) than of 900 MHz.

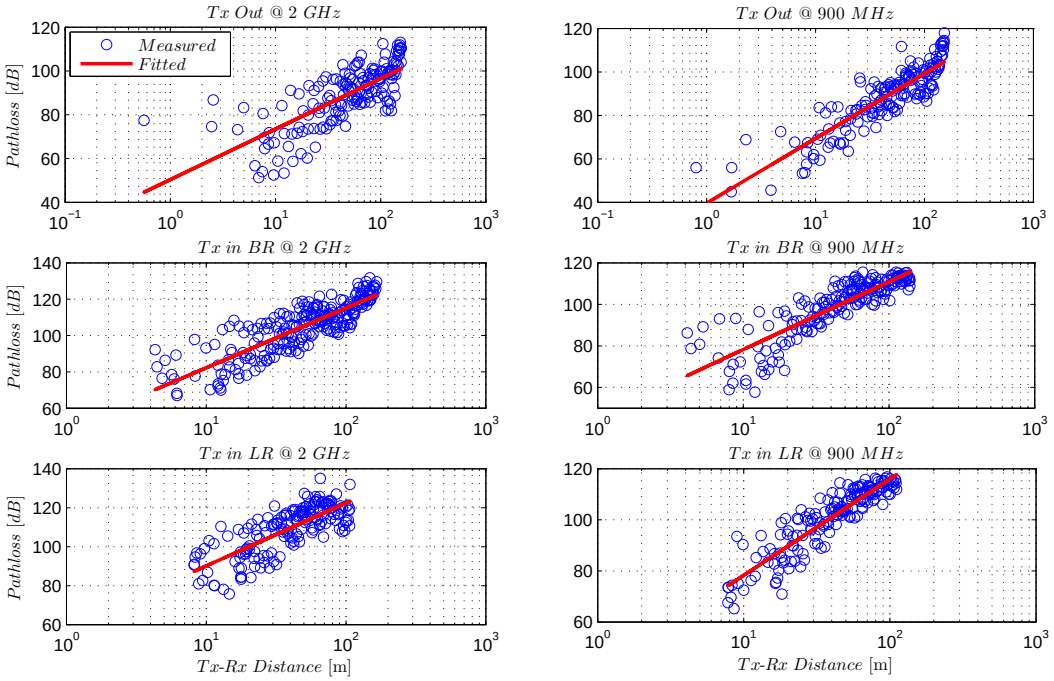

Figure 8.8: Fitted path loss according to Model A

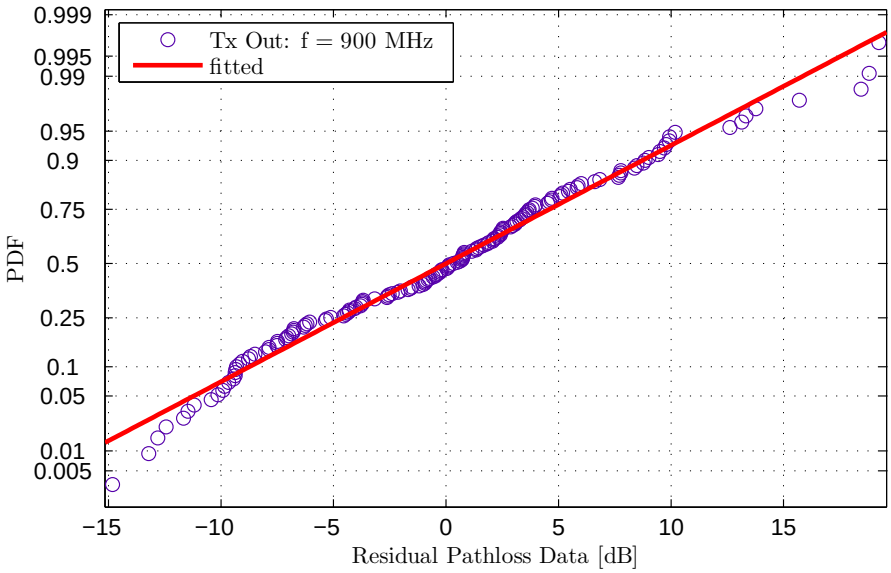

(a) Tx Outside

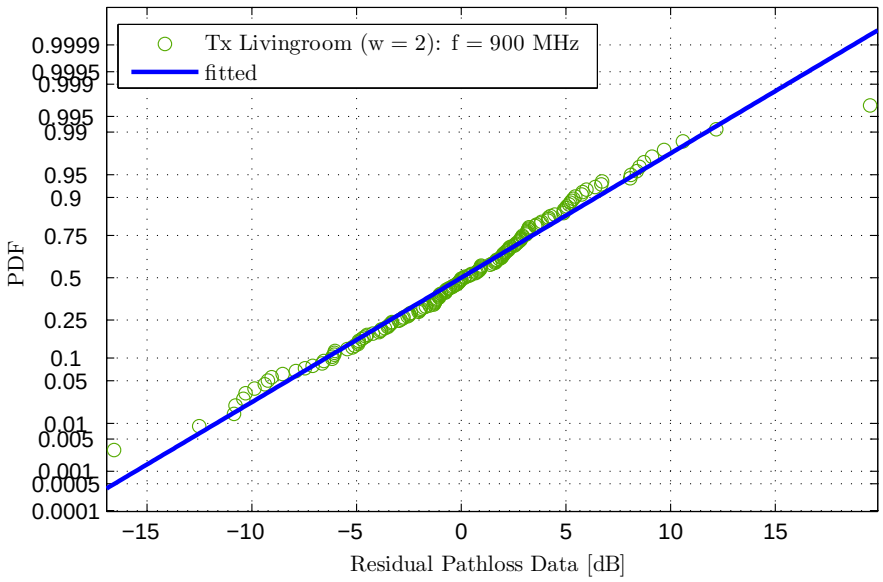

(b) Tx in Livingroom

Figure 8.9: Residual pathloss fit

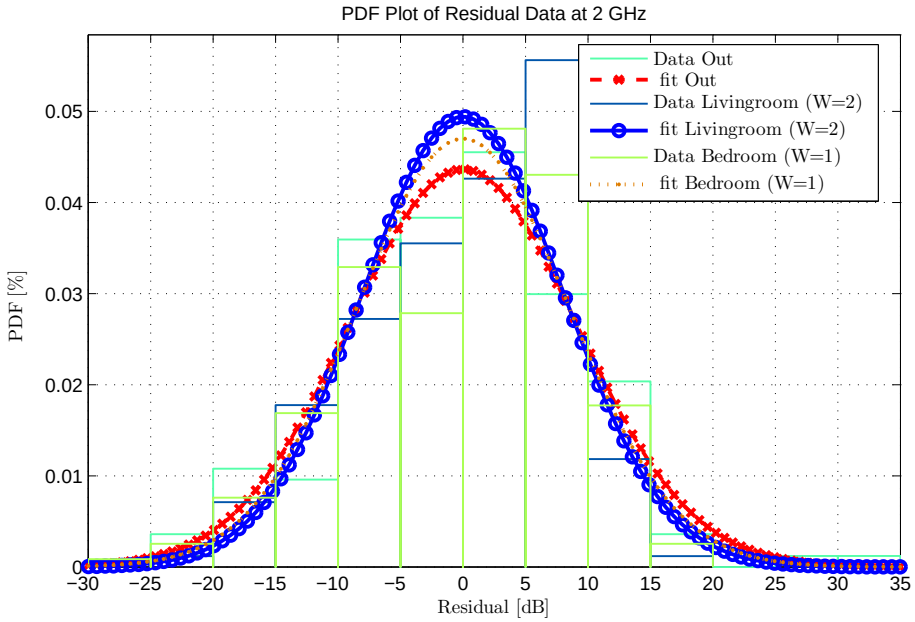

(a) Residual at 2 GHz

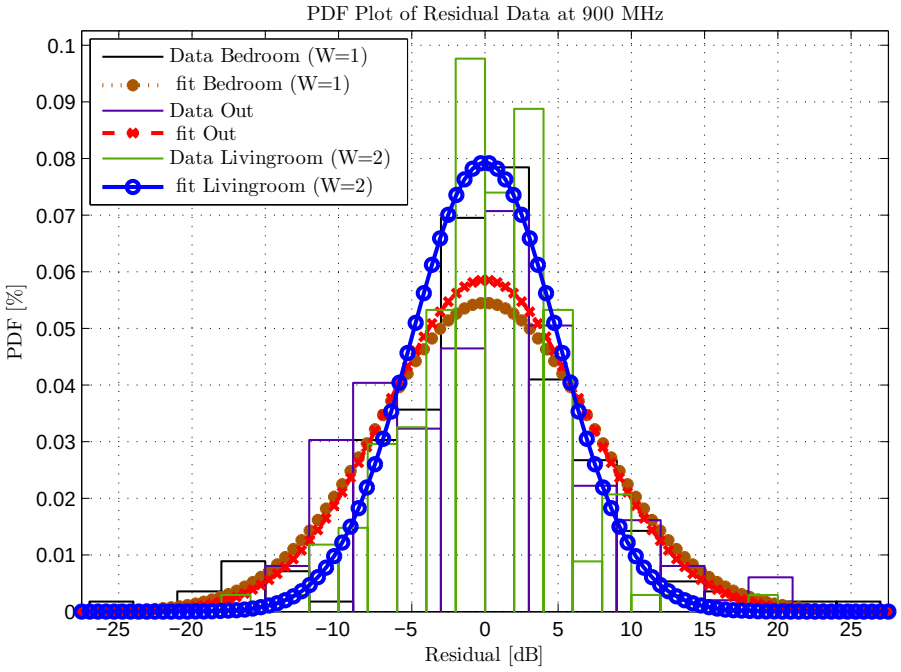

(b) Residual at 900 MHz

Figure 8.10: Distribution of error from the pathloss fit

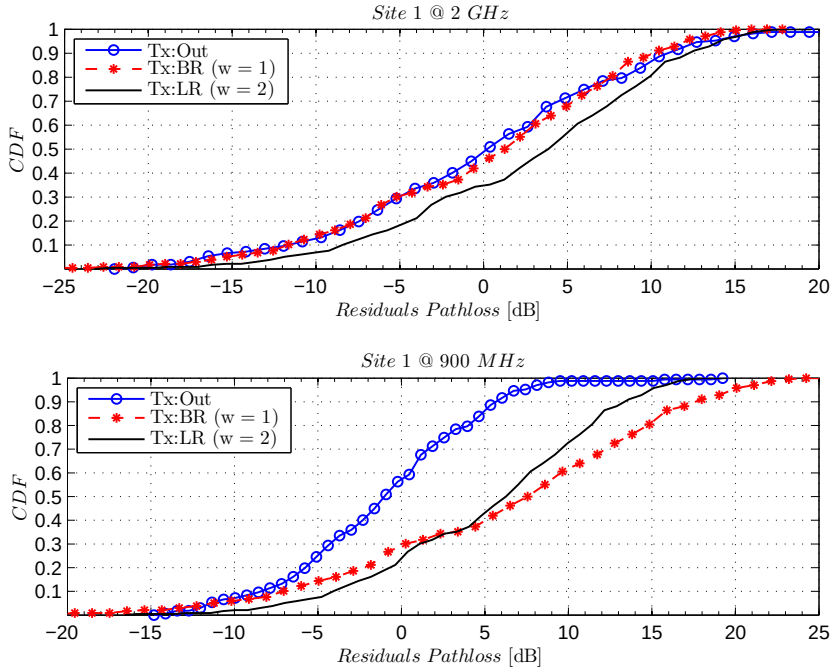

Figure 8.11: CDF plot of residual pathloss from the fit in Site 1

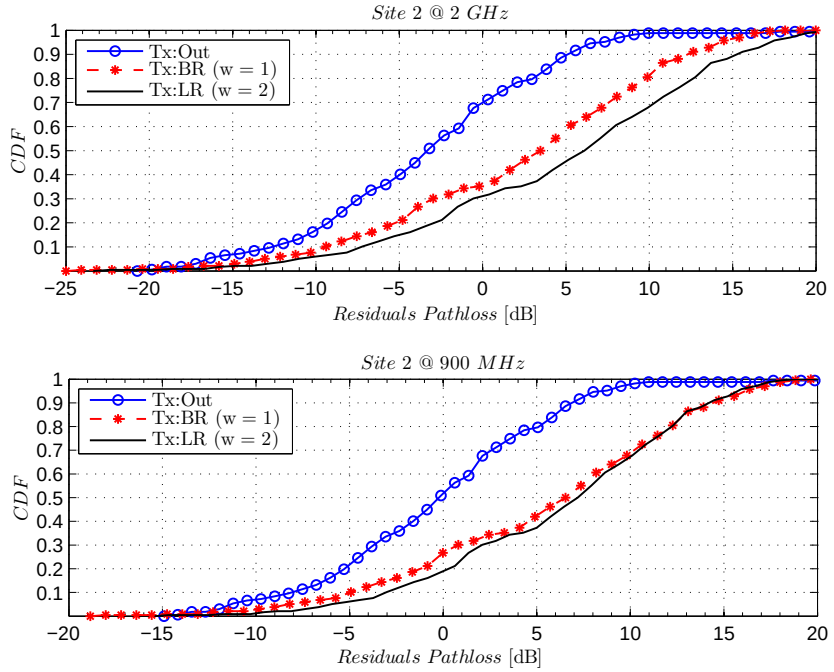

Figure 8.12: CDF plot of residual pathloss from the fit in Site 2

The accuracy of the model is evaluated using the RMSE. For comparison, the RMSE value, which is the standard deviation of shadow fading, of Model A is compared with one obtained in Valcarce's model [119]. Table 8.8 shows that the RMSE value obtained from our model is comparable with the RMSE obtained by Valcarce's model. There is a good reason behind the difference, this is because the modelled approaches used are different. From the comparison of the RMSE value, it is concluded that the proposed model can be used as an analytical model to estimate the path loss or in a simulation to evaluate the interference level coming from an indoor femtocell in a heterogeneous network.

Table 8.8: Comparison of the RMSE value with Valcarce's Model

Site	Path Loss Model ⇓	RMSE Value in dB of the Path Loss Model					
		Tx Outside		Tx in BR ($w = 1$)		Tx in LR ($w = 2$)	
		2 GHz	900 MHz	2 GHz	900 MHz	2 GHz	900 MHz
Site 1	Valcarce's Model	10.7	8.7	9.5	8.4	9.7	6.3
	Model A	9.1	6.8	7.7	7.0	7.9	5.3
Site 2	Valcarce's Model	9.7	9.6	11.5	9.2	11.1	11.4
	Model A	10.6	9.0	8.7	7.3	9.0	6.5

8.7 Summary

This chapter has focused on understanding an indoor-to-outdoor radio propagation behaviour for different carrier frequencies under a femtocell network in an urban residential environment and on developing empirical path loss models based on the measurement of the received channel power. A measurement campaign was conducted by a colleague in two streets of an urban residential environment for different carrier frequencies under three different scenarios of transmitter locations: a transmitter outside a building, a transmitter inside a bedroom where the direct path in between the transmitter and a receiver on the street interfaces one wall, and a transmitter inside a livingroom where the direct path in between the transmitter and a receiver on the street interfaces two walls. Based on the measurement data, two empirical path loss models have been developed. Only LOS data has been used for the modelling. The LOS data was modelled with the help of a Singular Value Decomposition (SVD) algorithm and the error from the fit was analysed with a minimum root mean square error. It has been found that the residual path loss obtained from the measurement data and the fit follows a log-normal distribution with a 0 dB mean and a root mean square error value as the standard deviation. The models can be used as analytical expressions to estimate the level of interference by a femtocell to a macrocell user in a link-level simulation.

Chapter 9:

Conclusions and Future Work

This thesis presented a novel radio resource allocation algorithm in CoMP joint transmission of future networks. In addition to the algorithm, a complete analytical model for CoMP performance, a hybrid model consisting of simulation and analysis and empirical path loss models of indoor-to-outdoor scenarios have been presented.

This chapter summarises the research work and draws conclusions. Firstly, the summary of the thesis is provided. Secondly, the conclusions of the thesis are discussed. Lastly, a list of future work is described.

9.1 Summary

To satisfy the needs of the ever increasing demand of high data rate services, cellular providers are forced to use their available spectrum smartly and efficiently in their upgraded cellular networks because, being scarce, the radio spectrum is highly valued. CoMP has been considered as a tool to improve the performance of users especially close to a cell-edge boundary by turning the strongest interfering signal coming from neighbouring cells into a useful signal in a coordinated way. This thesis has evaluated the performance of the proposed radio resource allocation in intra-site and inter-site CoMP of a homogeneous network. Two types of traffic patterns: Poisson process and fixed traffic are considered. Various traffic loads in the network from around 10 % to 97 % under user mobility and no mobility conditions have been considered. Three ways of cell-edge user decision criteria have been implemented. From

various simulation results, it has been seen that the Joint Maximum Throughput (JMT) scheduling algorithm has better performance than the Joint Proportional Fairness (JPF) algorithm under RSRP and SINR based cell-edge decision.

The major contributions of the thesis are structured as follows:

- Chapter 3 presented a novel radio resource allocation algorithm in CoMP joint transmission based on the joint maximum throughput. The modelling of a dynamic simulation tool developed during the research was presented.
- Chapter 4 presented a complete dynamic analytical model for performance of CoMP evaluation. This model can be used by network planners to dimension a network by estimating the average performance of a network under the CoMP technique. The model has considered a real scenario by considering sectorial antenna, shadow fading, a random location inside a cell, and steady state distribution of users in the network.
- Chapter 5 has evaluated the performance of CoMP in an intra-site deployment scenario under various traffic loads, different criteria of cell-edge decision, users under static and in mobility.
- Chapter 6 has evaluated the performance of CoMP in an inter-site deployment under various traffic loads, different criteria of cell-edge decision, users under static and in mobility.
- Chapter 7 presented a hybrid model consisting of simulation and analysis under Non-CoMP transmission. It has been concluded that with the hybrid model, the throughput of any possible call state in the system can be evaluated.
- In Chapter 8, empirical path loss models in indoor-to-outdoor scenario have been modelled based on the data from a measurement campaign.

Although, the developed model has not been used in the CoMP performance, the initial planning of the path loss modelling was to to be included in the performance evaluation of heterogeneous CoMP. The modelled path loss equations will be used in future work considering heterogeneous networks.

9.2 Conclusions

The following conclusions are drawn from the research of the thesis:

- The proposed radio resource scheduling algorithm based on the joint maximum throughput in CoMP joint transmission provides better performance in terms of users's and network's throughput as compared with the joint proportional fair scheduling algorithm.
- The RSRP and the SINR based cell-edge decisions have nearly the same CoMP performance. It is because SINR has been evaluated using pilot RSRP. Hence, either RSRP or SINR can be used for a cell-edge decision.
- The performance of CoMP is affected by the mobility of users.
- The proposed JMT algorithm is suitable for a centralised scheduling based on a static cluster, where one of the cells from the cooperating set, usually the serving cell, acts as a master cell and the remaining cells in the set cooperate with this serving cell.
- The main limitation of the proposed scheduling algorithm is the fairness. It does not consider the history of users' performance. It allocates the resource to the user who provides the best performance in terms of throughput from the network and the spectral efficiency point of view.
- The complete dynamic analytical model has features of random arrivals and departures of users, random locations of users in a cell, distance of

users from neighbour base stations, sectorial antenna gain at arbitrary positions, probability density of SINR and throughput modelling under CoMP joint transmission. The model can be used to estimate an average throughput of a user without simulation.

- The hybrid model can be used to estimate the throughput of any possible call state in the network under Non-CoMP transmission.

9.3 Future Work

In order to extend the present work, the following research directions are considered for future work:

- **Heterogeneous CoMP:** Due to random appearance of small cells, such as Femtocells, in a cellular network, interference is a big problem. A CoMP technique will be used to mitigate such interference. However, CoMP represents a challenge from the coordination view point since at present there is no direct interface between a femtocell and a macrocell.
- **Dynamic cluster:** To consider the best performance, an algorithm of dynamic cluster formation will be developed in future. In a heterogeneous network, a random appearance and disappearance of Femtocells creates a challenging task in the formation of a dynamic cluster.
- **Handover in CoMP:** Handover is a mechanism that transfers an ongoing call or data session from one base station to another base station (known as hard handover) or one cell to another cell in the same base station (known as soft handover). An ordinary handover algorithm is not suitable in a CoMP technique, because users at the cell-edge boundary are in connection with multiple cells at a given time. Hence, to consider a successful handover in a CoMP technique, a suitable handover algorithm

should be implemented. Future work will be focused on developing a handover algorithm in a CoMP technique.

References

[1] T. S. Rappaport, *Wireless Communications Principles and Practice*, 2nd ed. Prentice Hall, Jan. 2002, p. 736, ISBN 978-0130422323.

[2] L. D. Olavarrieta and A. A. Nava, "Wireless Commuications: A Bird's Eye View of an Emerging Technology," in *IEEE International Symposium on Commnications and Information Technology (ISCIT)*, vol. 1, Oct. 2004, pp. 541–546.

[3] A. Kumar, Y. Liu, J. Sengupta, and Divya, "Evolution of Mobile Communication Networks: 1G to 4G," *International Journal of Electronics & Communication Technology*, vol. 1, no. 1, Dec. 2010.

[4] OECD, "Mobile Cellular Communication: Pricing Strategies and Competition, ICCP No. 39," in *OECD Digital Economy Papers*. OECD Publishing, Jun. 1996, no. 23, http://dx.doi.org/10.1787/237304123855.

[5] *ETSI GSM Specifications*, ETSI Series 01-12.

[6] GSM Association, "trial," http://www.gsma.com/aboutus/history/.

[7] A. Eisenblatter, "Frequency Assignment in GSM Networks: Models, Heuristics and Lower Bounds," Ph.D. Dissertation, Technische Universitat Berlin, Fachbereich Mathematik, Berlin, Germany, 2001.

[8] H. Holma and A. Toskala, *WCDMA for UMTS: Radio Access for Third Generation Mobile Communications*, 3rd ed. John Wiley & Sons, Ltd, 2004, p. 478, ISBN 978-0470870969.

[9] ITU-R M.1645, "Framework and Overall Objectives of the Future Development of IMT-2000 and Systems Beyond IMT-2000," ITU-R, Recommendation, Jun. 2003.

[10] ITU-R 57, "Principles for the Process of Development of IMT-Advanced," ITU, Resolutions Radio Communication Assembly (RA-07), Oct. 2007.

[11] IMT-ADV/1-E, "Background on IMT-Advanced," ITU, Tech. Rep., Mar. 2008.

[12] Cisco, "Cisco Visual Networking Index: Global Mobile Data Traffic Forecast Update, 2012-2017," White Paper, Feb. 2013.

[13] P. E. Mogensen, T. Koivisto, K. I. Pedersen, I. Z. Kovacs, B. Raaf, K. Pajukoski, and M. J. Rinne, "LTE-Advanced: The Path towards Gigabit/s in Wireless Mobile Communications," in *Wireless Communication, Vehicular Technology, Information Theory and Aerospace & Electronic Systems Technology (Wireless VITAE)*, May 2009, pp. 147–151.

[14] Ericsson, "5G Radio Access," Ericsson White Paper, Jun. 2013, http://www.ericsson.com/res/docs/whitepapers/wp-5g.pdf.

[15] A. Osseiran, V. Braun, T. Hidekazu, P. Marsch, H. Schotten, H. Tullberg, M. A. Uusitalo, and M. Schellman, "The Foundation of the Mobile and Wireless Communications System for 2020 and beyond Challengers, Enablers and Technology Solutions," in *VTC Spring 2013*, Jun. 2-5 2013.

[16] University of Surrey, "The University of Surrey Secures £35 M For New 5G Research Centre," University News, 8 Oct. 2012.

[17] BBC, "5G Research Centre Gets Major Funding Grant," BBC News, 8 Oct. 2012, http://www.bbc.co.uk/news/technology-19871065.

[18] 3GPP TS 36.201, *Evolved Universal Terrestrial Radio Access (E-UTRA); LTE Physical Layer - General Description (Release 8)*, 3GPP TSG RAN Std. v.8.3.0, Mar. 2009.

[19] 3GPP TS 36.211, *Evolved Universal Terrestrial Radio Access (E-UTRA); Physical Channels and Modulation (Release 10)*, 3GPP TSG RAN Std. v.10.5.0, Jun. 2012.

[20] E. Dahlman, S. Parkvall, J. Skold, and P. Beming, *3G Evolution: HSPA and LTE for Mobile Broadband*, 2nd ed. ELSEVIER, 2008, p. 648, ASIN B002ZJSVW8.

[21] M. Rahman and H. Yanikomeroglu, "Enhancing Cell-Edge Performance: A Downlink Dynamic Interference Avoidance Scheme with Inter-Cell Coordination," *IEEE Transactions on Wireless Communications*, vol. 9, pp. 1414–1425, Apr. 2010.

[22] Samsung R1-082886, "Inter-Cell Interference Mitigation Through Limited Coordination," 3GPP, Jeju, Korea, TSG RAN WG1 Meeting #54, Aug. 2008.

[23] R. Bosisio and U. Spagnolini, "Interfernece Coordination vs. Interference Randomization in Multicell 3GPP LTE System," in *Wireless Communications and Networking Coneference (WCNC, IEEE)*, 31 Mar.-3 Apr. 2008, pp. 824–829.

[24] 3GPP TR 25.912, "Feasiblility Study for Evolved Universal Radio Access (UTRA) and Universal Terrestrial Radio Access Network (Release 9)," 3GPP TSG RAN, Tech. Rep. v.9.0.0, Sep. 2009.

[25] 3GPP TR 25.814, "Physical Layer Aspects for Evolved Universal Terrestrial Radio Access (UTRA) (Release 7)," 3GPP TSG RAN, Tech. Rep. v.7.1.0, Sep. 2006.

[26] G. Fodor, C. Koutsimanis, A. Racz, N. Reider, A. Simonsson, and W. Muller, "Intercell Interference Coordination in OFDMA Networks and in the 3GPP Long Term Evolution System," *Journal of Communicstions*, vol. 4, no. 4, pp. 445–453, Aug. 2009.

[27] Hitachi R1-083689, "Inter Cell Interference Coordination Scheme for CoMP," 3GPP, Prague, Czech Republic, TSG RAN WG1 Meeting #54bis, 29 Sep.-3 Oct. 2008.

[28] ST-Ericsson R1-094279, "Extended ICIC - A Rel-10 CoMP Scheme," 3GPP, Miyazaki, Japan, TSG RAN WG1 Meeting #57, Oct. 2009.

[29] 3GPP TR 36.814, "Evolved Universal Terrestrial Radio Access (E-UTRA); Further Advancements for E-UTRA Physical Layer Aspects (Release 9)," 3GPP TSG RAN, Tech. Rep. v.9.0.0, Mar. 2010.

[30] Ofcom, "Ofcom Announces Winners of the 4G Mobile Acution," News, Feb. 2013, http://media.ofcom.org.uk/2013/02/20/ofcom-announces-winners-of-the-4g-mobile-auction/.

[31] S. E. Elayoubi, O. B. Haddada, and B. Fourestie, "Performance Evaluation of Frequency Planning Schemes in OFDMA-based Networks," *IEEE Transactions on Wireless Communications*, vol. 7, no. 5, pp. 1623–1633, May 2008.

[32] N. Saquib, E. Hossain, and D. Kim, "Fractional Frequency Reuse for Interference Management in LTE-Advanced HetNets," *IEEE Wireless Communications*, vol. 20, no. 2, pp. 113–122, Apr. 2013.

[33] Z. Xu, G. Y. Li, C. Yang, and X. Zhu, "Throughput and Optimal Threshold for FFR Schemes in OFDMA Cellular Networks," *IEEE Transactions on Wireless Communications*, vol. 11, no. 8, pp. 2776–2785, Aug. 2012.

[34] R. Ghaffar and R. Knopp, "Interference Suppression Strategy for Cell-Edge Users in the Downlink," *IEEE Transactions on Wireless Communications*, vol. 11, no. 1, pp. 154–165, Jan. 2012.

[35] L.-C. Wang and C.-J. Yeh, "3-Cell Network MIMO Architectures with Sectorization and Fractional Frequency Reuse," *IEEE Transactions on Selected Areas in Communications*, vol. 29, no. 6, pp. 1185–1199, Jun. 2011.

[36] L. Liu, G. Zhu, and D. Wu, "A Novel Fractional Frequency Reuse Structure Based on Interference Avoidance Scheme in Multi-cell LTE Networks," in *International Conference on Communications and Networking in China (CHINACOM, ICST 6th)*, Aug. 2011, pp. 551–555.

[37] H. Xiao and Z. Feng, "A Novel Fractional Frequency Reuse Architecture and Interference Coordination Scheme for Multi-Cell OFDMA Networks," in *IEEE Vehicular Technology Conference (VTC2010-Spring, IEEE 71st)*, May 2010, pp. 1–5.

[38] Y. Yu, E. Dutkiewicz, X. Huang, M. Mueck, and G. Fang, "Performance Analysis of Soft Frequency Reuse for Inter-cell Interference Coordination in LTE Networks," in *Communications and Information Technologies (ISCIT), International Symposium*, Tokyo, Japan, Oct. 2010, pp. 504–509.

[39] Samsung RP-101425, "Revised SID Proposal: Coordinated Multi-Point Operation for LTE," 3GPP, Istanbul, Turkey, TSG RAN Meeting #50, Dec. 2010.

[40] R1-110611, "Final Report of 3GPP TSG RAN WG1 #63 BIS," 3GPP TSG RAN WG1 Meeting #64, Taipei, Taiwan, Tech. Rep. v.1.0.0, Feb. 2011.

[41] ZTE R1-110814, "Further Consideration for CoMP Scenarios," 3GPP, Taipei, Taiwan, TSG RAN WG1 Meeting #64, Feb. 2011.

[42] ST-Ericsson R1-110650, "On Simulations Assumptions for Phase 2 CoMP Evaluations," 3GPP, Taipei, Taiwan, TSG RAN WG1 Meeting #64, Feb. 2011.

[43] R1-110973, "Clarifications and Design Requirements for CoMP Scenarios 1-3," Intel Corporation, Taipei, Taiwan, 3GPP TSG RAN WG1 Meeting #64, Feb. 2011.

[44] ETSI MCC RP-121389, "Report of 3GPP TSG RAN Meeting #56," 3GPP TSG RAN Meeting #57, Ljublijana, Slovenia, Tech. Rep., Jun. 2012.

[45] 3GPP Work Programme, http://www.3gpp.org/ftp/Specs/html-info/GanttChart-Level-2.htm.

[46] Q. Cui, S. Yang, Y. Xu, X. Tao, and B. Liu, "An Effective Inter-Cell Interference Coordination Scheme for Downlink CoMP in LTE-A Systems," in *IEEE Vehicular Technology Conference (VTC2011-Fall, IEEE 74th)*, Sep. 2011, pp. 1–5.

[47] R. Irmer, H. Droste, P. Marsch, M. Grieger, G. Fettweis, S. Brueck, H. P. Mayer, L. Thiele, and V. Jungnickel, "Coordinated Multi-Point:

Concepts, Performance, and Field Trial Results," *IEEE Communications Magazine*, vol. 49, no. 2, pp. 102–111, Feb. 2011.

[48] Z. Feng, W. Muqing, and L. Huixin, "Coordinated Multi-Point Transmission and Reception for LTE-Advanced," in *International Conference on Wireless Communications, Networking and Mobile Computing (WiCom, 5th)*, Beijing, Sep. 2009, pp. 1–4.

[49] Q. Wang, D. Jiang, G. Liu, and Z. Yan, "Coordinated Multiple Points Transmission for LTE-Advanced Systems," in *International Conference on Wireless Communications, Networking and Mobile Computing (WiCom, 5th)*, Beijing, Sep. 2009, pp. 1–4.

[50] 3GPP TR 36.819, "Coordinated Multi-Point Operation for LTE Physical Layer Aspects (Release 11)," 3GPP TSG RAN, Tech. Rep. v.11.1.0, Dec. 2011.

[51] Q. Li, Y. Yang, S. Fang, and G. Wu, "Coordinated Beamforming in Downlink CoMP Transmission System," in *Communications and Networking in China (CHINACOM)*, Beijing, Aug. 2012, pp. 1–5.

[52] U. Jang, K.-Y. Lee, K.-S. Cho, and W. Ryu, "Transmit Beamforming Based Inter-Cell Interference Alignment and User Selection with CoMP," in *Vehicular Technology Conference Fall (VTC2010-Fall, IEEE 72nd)*, Sep. 2010, pp. 1–5.

[53] HTC R1-110180, "Views of Schemes for CoMP," 3GPP, Dublin, Ireland, TSG RAN WG1 Meeting #63bis, Jan. 2011.

[54] J. Zhao and Z. Lei, "Clustering Methods for Base Station Cooperation," in *Wireless Communications and Networking Conference (WCNC, IEEE)*, Shanghai, China, Apr. 2012, pp. 946–951.

[55] F. Huang, Y. Wang, J. Geng, M. Wu, and D. Yang, "Clustering Approach in Coordinated Multi-Point Transmission/Reception System," in *IEEE Vehicular Technology Conference Fall (VTC2010-Fall, IEEE 72nd)*, Sep. 2010, pp. 1–5.

[56] A. Papadogiannis, D. Gesbert, and E. Hardouin, "A Dynamic Clustering Approach in Wireless Networks with Multi-Cell Cooperative Processing," in *IEEE International Conference on Communications (ICC)*, Beijing, China, May 2008, pp. 4033–4037.

[57] W. Xiaoyi, K. Mingyan, and Q. Xin, "Downlink System Performance of Cooperative Multiple Points Transmission with Realistic RRM Structure," in *Computer Modeling and Simulation (ICCMS)*, vol. 4, Sanya, Hainan, Jan. 2010, pp. 467–470.

[58] R. Weber, A. Garavaglia, M. Schulist, S. Brueck, and A. Dekorsy, "Self-Organizing Adaptive Clustering for Cooperative Multipoint Transmission," in *IEEE Vehicular Technology Conference (VTC2011-Spring, IEEE 73rd)*, Yokohama, Japan, May 2011, pp. 1–5.

[59] ZTE R1-110573, "Views on Rel-11 CoMP," 3GPP, Dublin, Ireland, TSG RAN WG1 Meeting #63bis, Jan. 2011.

[60] ZTE R1-111139, "Initial CoMP Evaluation for Homogeneous Network with High Tx Power RRHs," 3GPP, Taipei, Taiwan, TSG RAN WG Meeting #64, Feb. 2011.

[61] M. Feng, X. She, L. Chen, and Y. Kishiyama, "Enhanced Dynamic Cell Selection with Muting Scheme for DL CoMP in LTE-A," in *IEEE Vehicular Technology Conference (VTC2010-Spring, IEEE 71st)*, Taipei, May 2010, pp. 1–5.

[62] M. Zhou and L. Wan, "Analysis into Timing Advance Issue in CoMP Systems," in *IEEE Vehicular Technology Conference (VTC2009-Fall, IEEE 70th)*, Sep. 2009, pp. 1–5.

[63] A. Papadogiannis, H. J. Bang, D. Gesbert, and E. Hardouin, "Efficient Selective Feedback Design for Multicell Cooperative Networks," *IEEE Transactions on Vehicular Technology*, vol. 60, no. 1, pp. 196–205, Jan. 2011.

[64] Motorola R1-110871, "CoMP Schemes with Backhaul Constraints and the Modeling," 3GPP, Taipei, Taiwan, TSG RAN1 Meeting #64, Feb. 2011.

[65] H. M. Soliman, A. A. Naguib, O. A. Nasr, M. M. Khairy, and K. Elsayed, "Joint Power and Backhaul Bits Allocation for Coordinated Multi-Point Transmission," in *Wireless Communication Systems (ISWCS, 8th International Symbosium)*, 2011, pp. 76–80.

[66] Q. Zhang, C. Yang, and A. F. Molisch, "Cooperative Downlink Transmission Mode Selection under Limited-Capacity Backhaul," in *Wireless Communications and Networking Conference (WCNC, IEEE)*, Shanghai, Apr. 2012, pp. 1082–1087.

[67] C.-C. Lin, K. Sandrasegaran, and S. Reeves, "Handover Algorithm with Joint Processing in LTE-advanced," in *Electrical Engineering/Electronics, Computer, Telecommunications and Information Technology (ECTI-CON), 9th International Conference*, May 2012, pp. 1–4.

[68] C.-C. Lin, K. Sandrasegaran, X. Zhu, and Z. Xu, "Performance Evaluation of Capacity based CoMP Handover Algorithm for LTE-Advanced," in *Wireless Personal Multimedia Communications (WPMC), 15th International Symposium*, Sept. 2012, pp. 236–240.

[69] Intel Corporation R1-110251, "Coordinated Multi-Point Schemes with Centralized and Distributed Scheduling," 3GPP, Dublin, Ireland, TSG RAN WG1 Meeting #63bis, Jan. 2011.

[70] Mitsubishi Electric R1-110977, "Considerations on Control Schemes for CoMP Scheduling," 3GPP, Taipei, Taiwan, TSG WG1 Meeting #64, Feb. 2011.

[71] S. Brueck, L. Zhao, J. Giese, and M. A. Amin, "Centralized Scheduling for Joint Transmission Coordinated Multi-Point in LTE-Advanced," in *International ITG Worshop on Smart Antennas (WSA)*, Feb. 2010, pp. 177–184.

[72] Samsung R1-090613, "Discussions on CoMP SU-MIMO," 3GPP, Athens, Greece, TSG RAN WG1 Meeting #56, Feb. 2009.

[73] Potevio R1-091415, "Further Discussion of Frequency Plan Scheme on CoMP-SU-MIMO," 3GPP, Seoul Korea, TSG RAN WG1 Meeting #56 bis, Mar. 2009.

[74] J. Li, H. Zhang, X. Xu, X. Tao, T. Svensson, C. Botella, and B. Liu, "A Novel Frequency Reuse Scheme for Coordinated Multi-Point Transmission," in *IEEE Vehicular Technology Conference (VTC2010-Spring, IEEE 71st)*, Taipei, May 2010, pp. 1–5.

[75] J. Liu, Y. Chang, Q. Pan, X. Zhang, and D. Yang, "A Novel Transmission Scheme and Scheduling Algorithm for CoMP-SU-MIMO in LTE-A System," in *IEEE Vehicular Technology Conference (VTC2010-Spring, IEEE 71st)*, Taipei, May 2010, pp. 1–5.

[76] A. Haider and R. Harris, "A Novel Proportional Fair Scheduling Algorithm for HSDPA in UMTS Networks," in *Wireless Broadband and Ul-*

tra Wideband Communications (AusWireless 2007), Sydney, Australia, Aug. 2007, pp. 43–50.

[77] 3GPP TS 36.213, *Evolved Universal Terrestrial Radio Access (E-UTRA); Physical layer procedures (Release 10)*, 3GPP TSG RAN Std. v.10.4.0, Dec. 2011.

[78] D. Lopez-Perez and X. Chu, "Inter-Cell Interference Coordination for Expanded Region Picocells in Heterogeneous Networks," in *International Conference on Computer Communications and Networks (ICCCN, 20th) Proceedings*, Hawaii, USA, 31 Jul.-4 Aug. 2011, pp. 1–6.

[79] T. Girici, C. Zhu, J. R. Agre, and A. Ephremides, "Proportional Fair Scheduling Algorithm in OFDMA-Based Wireless Systems with QoS Constraints," *Journal of Communications and Networks*, vol. 12, no. 1, pp. 30–42, Feb. 2010.

[80] H. Kim and Y. Han, "A Proportional Fair Scheduling for Multicarrier Transmission Systems," *IEEE Communications Letters*, vol. 9, no. 3, pp. 210–212, Mar. 2005.

[81] T. B. Sorensen and M. R. Pons, "Performance Evalaution of Proportional Fair Scheduling Algorithm with Measured Channels," in *IEEE Vehicular Technology Conference (VTC2005-Fall, IEEE 62nd)*, vol. 4, 2005, pp. 2580–2585.

[82] S. Mahato, B. Allen, E. Liu, and J. Zhang, "Performance Evaluation of Maximum Throughput Based Scheduling of OFDMA LTE Networks," in *Wireless Advanced (WiAd, IEEE 8th)*, London, UK, Jun. 2012, pp. 1–5.

[83] A. Pablo, Y. Wang, J. Navarro-Ortiz, , P. E. Mogensen, and J. M. Lopez-Soler, "Traffic Models Impact on OFDMA Scheduling Design," *EURASIP Journal on Wireless Communications and Networking*, vol. 2012, no. 1, p. 61, 2012.

[84] D. Lopez-Perez, "Practical Models and Optimisation Methods for Inter-Cell Interference Coordination in Self-organising Cellular Networks," PhD Thesis, University of Bedfordshire, Luton, UK, Mar. 2011.

[85] R. Kwan, C. Leung, and J. Zhang, "Multiuser Scheduling on the Downlink of an LTE Cellular System," *Research Letters in Communications*, vol. 2008, no. Article ID 323048, p. 4, 2008.

[86] B. Gloss, M. Scharf, and D. Neubauer, "A More Realistic Random Direction Mobility Model," COST 290, Wurzburg, Germany, 4th Management Committee Meeting TD (05) 052, OCt. 2005.

[87] R. C. French, "The Effect of Fading and Shadowing on Channel Reuse in Mobile Radio," *IEEE Transactions on Vehicular Technology*, vol. 28, no. 3, pp. 171–181, Aug. 1979.

[88] Y. S. Yeh and S. C. Schwartz, "Outage Probability in Mobile Telephony Due to Multiple Log-Normal Interferers," *IEEE Transactions on Communications*, vol. 32, no. 4, pp. 380–388, Apr. 1984.

[89] K. W. Sowerby and A. G. Williamson, "Outage Probability Calculations for a Mobile Radio System Having Multiple Rayleigh Interferers," *Electronics Letters*, vol. 23, no. 11, pp. 600–601, May 1987.

[90] M. Gudmundson, "Correlation Model for Shadow Fading in Mobile Radio Systems," in *Electronics Letters*, vol. 27, no. 23, Nov. 1991, pp. 2145–2146.

[91] J. Monserrat, R. Fraile, N. Cardona, and J. Gozalvez, "Effect of Shadowing Correlation Modeling on the System Level Performance of Adaptive Radio Resource Management Techniques," in *IEEE International Symposium on Wireless Communication Systems, 2nd*, Sep. 2005, pp. 460–464.

[92] I. K. Fu, C. F. Li, T. C. Song, and W. H. Sheen, "Correlation Models for Shadow Fading Simulation," IEEE 802.16, Orland, USA, TGm Evaluation Methodology Development IEEE S802.16m-07/060, Mar. 2007.

[93] H. Holma and A. Toskala, *WCDMA for UMTS - HSPA Evolution and LTE*, 4th ed. John Wiley & Sons, Ltd, 2007, p. 572, ISBN 978-0-470-31933-8.

[94] D. Lopez-Perez, A. Ladanyi, A. Juttner, and J. Zhang, "OFDMA femtocells: A self-organizing approach for frequency assignment," in *IEEE International Symposium on Personal, Indoor and Mobile Radio Communications (PIMRC, IEEE 20th)*, Sep. 2009, pp. 2202–2207.

[95] G. Haring, R. Marie, R. Puigjaner, and K. Trivedi, "Loss Formulas and Their Application to Optimization for Cellular Networks," *IEEE Transactions on Vehicular Technology*, vol. 50, no. 3, pp. 664–672, May 2001.

[96] V. Sarangan, D. Ghosh, N. Gautam, and R. Acharya, "Steady State Distribution for Stochastic Knapsack with Bursty Arrivals," *IEEE Communications Letters*, vol. 9, no. 2, pp. 187–189, Feb. 2005.

[97] X. Chao and W. Li, "Performance Analysis of a Cellular Network with Multiple Classes of Calls," *IEEE Transactions on Communications*, vol. 53, no. 9, pp. 1542–1550, Sep. 2005.

[98] S. Dharmaraja, K. S. Trivedi, and D. Logothetis, "Performance Modeling of Wireless Networks with Generally Distributed Handoff Interarrival Times," *Elsevier Journal of Computer Communications*, vol. 26, no. 15, pp. 1747–1755, Sep. 2003.

[99] Y. Zhang and B.-H. Soong, "Handoff Dwell Time Distribution Effect on Mobile Network Performance," *IEEE Transactions on Vehicular Technology*, vol. 54, no. 4, pp. 1500–1508, Jul. 2005.

[100] A. E. Xhafa and O. K. Tonguz, "Handover Performance of Priority Schemes in Cellular Networks," *IEEE Transactions on Vehicular Technology*, vol. 57, no. 1, pp. 565–577, Jan. 2008.

[101] W. Li, Y. Fang, and R. R. Henry, "Actual Call Connection Time Characterization for Wireless Mobile Networks Under a General Channel Allocation Scheme," *IEEE Transactions on Wireless Communications*, vol. 1, no. 4, pp. 682–691, Oct. 2002.

[102] F. P. Kelly, *Reversibility and Stochastic Networks*. Cambridge University Press, 2011, p. 238, ISBN 978-1107401150.

[103] D. Gross, J. F. Shortle, J. M. Thompson, and C. M. Harris, *Fundamentals of Queueing Theory*, 4th ed. John Willey & Sons, 2008, p. 528, ISBN 978-0471791270.

[104] R. B. Cooper, *Introduction to Queing Theory*, 2nd ed. North Holland, 1981, p. 347, ISBN 9780444010650.

[105] Y. Zhuang, Y. Luo, L. Cai, and J. Pan, "A Geometric Probability Model for Capacity Analysis and Interference Estimation in Wireless Mobile Cellular Systems," in *IEEE Global Telecommunications Conference (GLOBECOM)*, Dec. 2011, pp. 1–6.

[106] M. H. Ismail and M. M. Matalgah, "Complete Analytical Framework for Throughput Calculation in WCDMA Downlink TDD Mode," in *IEEE Wireless Communications and Networking Conference*, vol. 1, Mar. 2005, pp. 212–217.

[107] L. F. Fenton, "The Sum of Log-Normal Probability Distributions in Scatter Transmission Systems," *IRE Transactions on Communications Systems*, vol. 8, no. 1, pp. 57–67, Mar. 1960.

[108] I. Koo, Y. Lee, and K. Kim, "Performance Analysis of CDMA Systems with Adapative Modulation Scheme," *IEICE Transaction on Communications*, vol. E86-B, no. 1, pp. 79–87, Jan. 2003.

[109] J. G. Andrews, A. Ghosh, and R. Muhamed, *Fundamentals of WiMAX*, 3rd ed., T. S. Rappaport, Ed. United States: Prentice Hall, Oct. 2007.

[110] A. Valcarce, "Applying the Finite-Difference Time-Domain to the Modelling of Large-Scale Radio Channels," PhD Thesis, University of Bedfordshire, Luton, UK, Aug. 2010.

[111] G. D. Durgin, T. S. Rappaport, and H. Xu, "Partition-Based Path Loss Analysis for In-Home and Residential Areas at 5.85 GHz," in *Global Telecommunications Conference (GLOBECOM, IEEE)*, vol. 2, 1998, pp. 904–909.

[112] M. Dohler, "An Outdoor-Indoor Interface Model for Radio Wave Propagation for 2.4, 5.2 and 60 GHz," Master's Thesis, King's College, University of London, London, UK 1999.

[113] D. M. Rose, T. Jansen, and T. Kurner, "Indoor to Outdoor Propagation - Measuring and Modeling of Femto Cells in LTE Networks at 800 and

2600 MHz," in *GLOBECOM Workshops (GC Wkshps, IEEE)*, Dec. 2011, pp. 203–207.

[114] P. Kyösti *et al.*, "WINNER II Channel Models Part II Radio Channel Measurement and Analysis Results," WINNER II Public Deliverables, Sep. 2007.

[115] L. A. Linares and J. G. Sanchez, "Empirical Modeling of Femtocell Path Loss in a Femto-to-Macro Indoor-to-Outdoor Interference Scenario," Long Master Thesis, University of Aalborg, Aalborg, Denmark, May 2011.

[116] Ofcom, "Predicting Coverage and Interference Involving the Indoor-Outdoor Interface," Ofcom Project SES-2005-08 Final Report v.1.0, Jan. 2007.

[117] ITU-R P.1238, "Propagation Data and Prediction Methods for the Planning of Indoor Radiocommunication Systems and Radio Local Area Networks in the Frequency Range 900 MHz to 100 GHz," ITU, Recommendation ITU-R P Series Radiowave Propagation, Feb. 2012.

[118] Y. Corre, J. Stephan, and Y. Lostanlen, "Indoor-to-Outdoor Path-Loss Models for Femtocell Predictions," in *Personal Indoor and Mobile Radio Communications (PIMRC, IEEE 22nd)*, Sep. 2011, pp. 824–828.

[119] A. Valcarce and J. Zhang, "Empirical Indoor-to-Outdoor Propagation Model for Residential Areas at 09.-3.5 GHz," *IEEE Antennas and Wireless Propagation Letters*, vol. 9, pp. 682–685, 2010.

[120] R. LeMay, "Telstra adds 900Mhz 4G band, trials LTE-A," Blog, Telecommunications, Feb. 2013, http://delimiter.com.au/2013/02/20/telstra-adds-900mhz-4g-band-trials-lte-a/.

[121] Cobham, "Cobham Antenna Systems," Feb. 2010, http://www.european-antennas.co.uk/.

[122] GPS TrackMaker, http://www.trackmaker.com/index.php.

[123] K. Baker, "Singular Value Decomposition Tutorial," Ohio State University, Jan. 2013, http://www.ling.ohio-state.edu/~kbaker/pubs/Singular_Value_Decomposition_Tutorial.pdf.

[124] Y.-B. Jia, "Singular Value Decomposition (Comp S 477/577 Notes)," Iowa State University, Sep. 2012, http://www.cs.iastate.edu/~cs577/handouts/svd.pdf.

[125] M. W. Berry, D. Mezher, B. Philippe, and A. Sameh, *Chapter 4: Parallel Algorithms for the Singular Value Decomposition, Book: Handbook of Parallel Computing and Statistics*, E. J. Kontoghiorghes, Ed. Chapman and Hall/CRC, Dec. 2005, p. 552, ISBN 978-0824740672.

[126] F. Khan, *LTE for 4G Mobile Broadband: Air Interface Technologies and Performance*, 1st ed. Cambridge University Press, Apr. 2009, p. 506, ISBN 9780521882217.

Appendix A:

Resource Scheduling Algorithms Used for Comparison

PF Based Scheduling Algorithm

The concept of PF scheduling is described in Chapter 3 in Section 3.2.2. The PF based scheduling algorithm implemented in the simulator as Non-CoMP transmission scheme is shown in Algorithm 2.

MT Based Scheduling Algorithm

The concept of MT scheduling is described in Chapter 3 in Section 3.2.3. The MT based scheduling algorithm implemented in the simulator as Non-CoMP transmission scheme is shown in Algorithm 3.

JPF Based Scheduling Algorithm

The concept behind JPF scheduling [75] is that both the CCUs and CEUs have equal opportunities to transmit in every subchannel. The JPF based scheduling algorithm implemented in the simulator as a CoMP transmission scheme is shown in Algorithm 4.

Algorithm 2 PF based scheduling algorithm under Non-CoMP transmission

1. For a subhcannel $r \in \mathcal{R}$ in a cell m, calculate the instantaneous throughput, $T^m_{u,r}(t)$, for all UE in the cell.
2. Then calculate the proportional fair on subchannel r for all UE in the cell m as
$$\left\{ \frac{T^m_{u,r}(t)}{\tilde{T}^m_u(t-1)} : u \in \mathcal{U}^m \right\}.$$
3. Sort and select the UE which provides the highest proportional fair value. That is, UE u is scheduled on subchannel r as
$$\{u, r\} \leftarrow \arg \max_{1 \le u \le U^m} \left\{ \frac{T^m_{u,r}(t)}{\tilde{T}^m_u(t-1)} \right\}.$$
4. Update the average throughput of the scheduled UE u as
$$\tilde{T}^m_u(t) \leftarrow \left(1 - \frac{1}{t_a}\right) \tilde{T}^m_u(t-1) + \frac{1}{t_a} T^m_{u,r}(t).$$
5. Remove the scheduled UE u and the subchannel r from their available list as
$$\mathcal{U}^m = \mathcal{U}^m - \{u\} \text{ and } \mathcal{R} = \mathcal{R} - \{r\}.$$
6. Repeat the above steps from 1 to 6 for scheduling the remaining UE on the available subchannels.
7. Stop if either $\mathcal{U}^m \to \emptyset$ or $\mathcal{R} \to \emptyset$; and update the average throughput of the unscheduled UE, if it happens, as
$$\tilde{T}^m_u(t) \leftarrow \left(1 - \frac{1}{t_a}\right) \tilde{T}^m_u(t-1).$$

Algorithm 3 MT based scheduling algorithm under Non-CoMP transmission

1. For a subhcannel $r \in \mathcal{R}$ in a cell m, calculate the throughput, $T^m_{u,r}$, for all UE in the cell.
2. Sort the calculated throughput and select the UE which provides the highest throughput on subchannel r. That is, UE u is scheduled on subchannel r as
$$\{u, r\} \leftarrow \arg \max_{1 \leq u \leq U^m} \left\{T^m_{u,r}\right\}.$$
3. Remove the scheduled UE u and the subchannel r from their available list as
$$\mathcal{U}^m = \mathcal{U}^m - \{u\} \text{ and } \mathcal{R} = \mathcal{R} - \{r\}.$$
4. Repeat the above steps from 1 to 4 for scheduling the remaining UE on the available subchannels.
5. Stop if either $\mathcal{U}^m \rightarrow \emptyset$ or $\mathcal{R} \rightarrow \emptyset$.

Algorithm 4 JPF based scheduling algorithm under CoMP transmission

1: **for** a cluster $c \in \mathcal{C}$ **do**,

2: categorise all UE of cell $m \in c$ as CCUs and CEUs as follows

- if the cell-edge decision is based on the pilot absolute SINR:

$$\mathcal{U}^m_{ccu} = \{u : \gamma^m_u > \gamma_{th}\} \quad \text{and} \quad \mathcal{U}^m_{ceu} = \{u : \gamma^m_u \leq \gamma_{th}\},$$

- if the cell-edge decision is based on the pilot relative RSRP:

$$\mathcal{U}^m_{ccu} = \{u : P_s - P_n > P_{edge}\} \quad \text{and} \quad \mathcal{U}^m_{ceu} = \{u : P_s - P_n \leq P_{edge}\},$$

- if the cell-edge decision is based on the absolute distance:

$$\mathcal{U}^m_{ccu} = \{u : d^m_u < d_{edge}\} \quad \text{and} \quad \mathcal{U}^m_{ceu} = \{u : d^m_u \geq d_{edge}\}.$$

3: **for** a subchannel $r \in \mathcal{R}$ **do**,

4: initialize the sets: $\mathcal{F}^m_{ccu} \leftarrow \emptyset$ and $\mathcal{F}^c_{ceu} \leftarrow \emptyset, \quad \forall m \in c$.

5: estimate the throughput, $T^m_{u,r}(t)$, of each CCU u in the cluster c on the subchannel r at scheduling time t.

6: estimate the proportional fair throughput of each CCU u in the cluster c and store as

$$\mathcal{F}^m_{ccu} \leftarrow \mathcal{F}^m_{ccu} \cup \left\{ \frac{T^m_{u,r}(t)}{T^m_u(t-1)} \right\}, \quad \forall u \in \mathcal{U}^m_{ccu} \text{ and } \forall m \in c.$$

7: estimate the throughput, $T^m_{u,r}(t)$, of each CEU u in the cluster c on the subchannel r at scheduling time t.

8: estimate the proportional fair throughput of each CEU u in the cluster c and store as

$$\mathcal{F}^c_{ceu} \leftarrow \mathcal{F}^c_{ceu} \cup \left\{ \frac{T^m_{u,r}(t)}{T^m_u(t-1)} \right\}, \quad \forall u \in \mathcal{U}^m_{ceu} \text{ and } \forall m \in c.$$

9: choose one best CCU from each cell in the cluster c as

$$\left\{ \frac{T^m_{u,r}(t)}{T^m_u(t-1)} \right\} \leftarrow \max(\mathcal{F}^m_{ccu}), \quad \forall m \in c, u \in \mathcal{U}^m_{ccu}.$$

10: choose one best CEU from the cluster c as

$$\frac{T^i_{u,r}(t)}{T^m_u(t-1)} \leftarrow \max(\mathcal{F}^c_{ceu}), \quad i \in c, u \in \mathcal{U}^i_{ceu}.$$

Algorithm 4 JPF based scheduling algorithm under CoMP transmission (continued)

if $N \cdot \dfrac{T^i_{u,r}(t)}{T^m_u(t-1)} \geq \displaystyle\sum_{m \in c, u \in \mathcal{U}^m_{ccu}} \dfrac{T^m_{u,r}(t)}{T^m_u(t-1)}$, where $N = \|c\|$ **then**

schedule CEU u from cell i on subchannel r under CoMP transmission scheme, where all cells in the cluster c serve this user.

update the average throughput of the scheduled UE u as

$$\tilde{T}^m_u(t) \leftarrow \left(1 - \frac{1}{t_a}\right) \tilde{T}^m_u(t-1) + \frac{1}{t_a} \sum_{i \in c} T^i_{u,r}(t).$$

remove the scheduled UE u from the set as

$$\mathcal{U}^i_{ceu} \leftarrow \mathcal{U}^i_{ceu} - u,$$

else

each cell in the cluster c schedule its own CCU u on the subchannel r independently under Non-CoMP transmission scheme.

remove the scheduled UE from the sets as

$$\mathcal{U}^m_{ccu} \leftarrow \mathcal{U}^m_{ccu} - \{u\}, \quad \forall m \in c.$$

end if

remove the scheduled subchannel r from the set as

$$\mathcal{R} \leftarrow \mathcal{R} - \{r\}.$$

if $\mathcal{R} \neq \emptyset$ **then**

repeat from step 3 for the remaining UE in the cluster c.

else

repeat from step 1 for remaining clusters in the system.

end if

end for ▷ end for subchannel loop

end for ▷ end for cluster loop

Appendix B:

Probability Calculation of Call Distribution

Consider there are 3 cells in the network, i.e., $M = 3$. Assume 2 subchannels in each cell, i.e., $R = 2$, then the maximum number of calls in each cell is 2. Suppose each cell has only one type of user service, i.e., voice. Then the state space, $\mathcal{S}$, of the network consists of all possible vectors, $\boldsymbol{n}$ ($\boldsymbol{n} = (\boldsymbol{n}^1, \boldsymbol{n}^2, \boldsymbol{n}^3)$, $\boldsymbol{n}^m = (n_1^m)$).

The possible configurations of calls in the network are as follows:

- $(\boldsymbol{n} = ((0), (0), (0)) \Longrightarrow$ no calls in the system,
- $(\boldsymbol{n} = ((1), (0), (0)) \Longrightarrow$ 1 call in cell 1,
- $(\boldsymbol{n} = ((2), (0), (0)) \Longrightarrow$ 2 calls in cell 1,
- $(\boldsymbol{n} = ((0), (1), (0)) \Longrightarrow$ 1 call in cell 2,
- $(\boldsymbol{n} = ((0), (2), (0)) \Longrightarrow$ 2 calls in cell 2,
- $(\boldsymbol{n} = ((0), (0), (1)) \Longrightarrow$ 1 call in cell 3,
- $(\boldsymbol{n} = ((0), (0), (2)) \Longrightarrow$ 2 calls in cell 3,
- $(\boldsymbol{n} = ((1), (1), (0)) \Longrightarrow$ 1 call in cell 1 and 1 call in cell 2,
- $(\boldsymbol{n} = ((1), (1), (1)) \Longrightarrow$ 1 call in each cell,
- $(\boldsymbol{n} = ((2), (1), (0)) \Longrightarrow$ 2 calls in cell 1 and 1 call in cell 2,
- . . . . . .
- $(\boldsymbol{n} = ((2), (2), (2)) \Longrightarrow$ 2 calls in each cell, which is the highest possible state in the system.

The number of possible configurations is $3 \times 3 \times 3 = 27$. If $R = 3$, the number of possible configurations is $4 \times 4 \times 4 = 64$, etc. In general, the number of possible configurations can be written as $(R+1)^M$. It should be noted that if the number of cells is large, let us say 7, and the number of calls in each cell is 10, then the number of possible configurations is too large, i.e., $(10+1)^7 = 19487171$. Hence, it is difficult to evaluate the system performance by simulation for each possible configuration from a user point of view.

Since for this analysis, there is only one type of user service, the subscript of user type can be dropped. The normalisation constant of Eq. (4.7) can then be simplified as

$$\begin{aligned} G &= \sum_{n^m \leq R} \prod_{l=1}^{n^m} \frac{\lambda^m}{l\mu^m}, \quad m = 1, \ldots, M \\ &= \sum_{n^m \leq R} \frac{(\frac{\lambda^m}{\mu^m})^{n^m}}{n^m!}. \end{aligned} \tag{B.1}$$

Arbitrarily, assume the state of the system at a particular time is ($\boldsymbol{n} = ((1),(2),(1))$, $\lambda^m = 1.5$ calls/min and $\mu^m = 1$ calls/min. Since $R = 2$, the possible number of calls in a cell would be $0, 1, \ldots, R-1, R$. The normalisation constant can be calculated as $G = (\lambda/\mu)^0/0! + (\lambda/\mu)^1/1! + (\lambda/\mu)^2/2! = 3.625$. To check the summation of probabilities in a cell (say, cell 1), we can write Eq. (4.5) as

$$\begin{aligned} \sum_{n^1=0}^{2} \boldsymbol{\pi}^1(\boldsymbol{n}^1) &= \pi^1(0) + \pi^1(1) + \pi^1(2) \\ &= \frac{1}{G}\left[\left(\frac{\lambda}{\mu}\right)^0/0! + \left(\frac{\lambda}{\mu}\right)^1/1! + \left(\frac{\lambda}{\mu}\right)^2/2!\right] \\ &= \frac{1}{3.625}\left[1 + 1.5 + 1.125\right] \\ &= 1. \end{aligned} \tag{B.2}$$

Using Eq. (4.4), we can calculate the probability of corresponding calls in each cell as

- $\pi^1(1) = (\frac{\lambda}{\mu})^1/1!/G = 0.41379 = 41.379\%$,
- $\pi^2(2) = (\frac{\lambda}{\mu})^2/2!/G = 0.31034 = 31.034\%$,
- $\pi^3(1) = (\frac{\lambda}{\mu})^1/1!/G = 0.41379 = 41.379\%$.

Hence, we can easily calculate the probability of the system in the state space ($\boldsymbol{n} = ((1), (2), (1))$ using Eq. (4.3) as

$$\pi(n) = \prod_{m=1}^{3} \pi^m(n^m) = \pi^1(1)\pi^2(2)\pi^3(1) = 0.053137 = 5.314\%.$$

The probability 5.314 % is for one possible call configuration in the system. If we sum the probability of all possible call configurations, we will get 100 % according to Eq. (4.6).

Appendix C:

Traffic Model

Best Effort FTP Traffic Model

An FTP session is a sequence of file transfers separated by reading times and is considered as the best effort traffic [126]. There are two main FTP session parameters: the size S of a file to be transferred and the reading time D, i.e., the time interval between the end of the download of the previous file and the user request for the next file. An example of FTP traffic model parameters is shown in Table C.1 [126].

Table C.1: FTP traffic model parameters

Parameter	Statistical Characterisation
File size	Truncated lognormal distribution with mean = 2 MBytes, standard deviation = 0.772 MBytes, maximum file size = 5 MBytes (before truncation) PDF: $f_x = \frac{1}{\sqrt{2\pi}\sigma x} e^{\frac{-(\ln x - \mu)^2}{2\sigma^2}}, x > 0, \sigma = 0.35, \mu = 14.45$
Reading time	Exponential distribution with mean = 180 seconds PDF: $f_x = \lambda e^{-\lambda x}, x \geq 0, \lambda = 0.006$

Web Browsing HTTP Traffic Model

A typical HTTP web browsing session of a packet trace is shown in Fig. C.1 [126], which is divided into active and inactive periods representing web-page

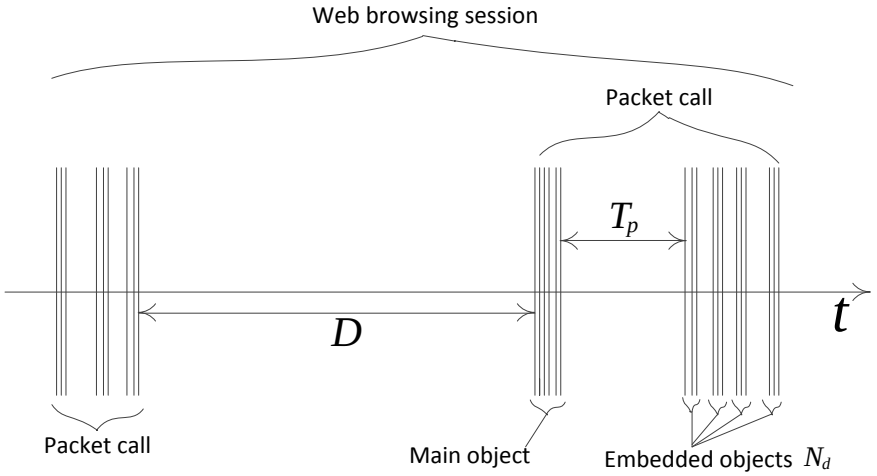

Figure C.1: Packet trace of a web-browsing session

downloads and the intermediate reading times. The web-page downloads are generally referred to as packet calls which represent a web user's request for information; and the reading time identifies the time required to digest the web-page. A packet call is divided into active/inactive periods which are attributed to machine interaction rather than human interaction. A web-browser will begin serving a user's request by fetching the initial HTML page using an HTTP GET request. The retrieval of the initial page and each of the embedded objects (e.g. pictures, advertisements, etc.) is represented by the active period within the packet call while the parsing time and protocol overhead are represented by the inactive periods within a packet call. The parsing time refers to the time the browser spends in parsing for the embedded objects in the packet call or the web-page [126].

The main parameters to characterise for the web-browsing traffic are the main object size S_M, the size of an embedded object in a web-page S_E, the number of embedded objects N_D, reading time D and parsing time T_p which are are given in Table C.2 [126].

Table C.2: HTTP traffic model parameters

Parameter	Statistical Characterisation
Main object size S_M	Truncated lognormal distribution with mean = 10710 Bytes, standard deviation = 25032 Bytes, minimum = 100 Bytes, maximum = 2 MBytes (before truncation) PDF: $f_x = \frac{1}{\sqrt{2\pi}\sigma x} e^{\frac{-(\ln x - \mu)^2}{2\sigma^2}}, x > 0, \sigma = 1.37, \mu = 8.37$
Embedded object size S_E	Truncated lognormal distribution, mean = 7758 Bytes, standard deviation = 126168 Bytes, minimum = 50 Bytes, maximum = 2 Bytes (before truncation) PDF: $f_x = \frac{1}{\sqrt{2\pi}\sigma x} e^{\frac{-(\ln x - \mu)^2}{2\sigma^2}}, x > 0, \sigma = 2.36, \mu = 6.17$
Number of embedded objects per page N_D	Truncated Pareto distribution, mean = 5.64, maximum = 53 (before truncation) PDF: $f_x = \frac{\alpha_k^\alpha}{\alpha + 1}, k \leq x < m, f_x \left(\frac{k}{m}\right)^\alpha, x = m, \alpha = 1.1, k = 2, m = 55$ Note: subtract k from the generated random value to obtain N_D
Reading time D	Exponential distribution with a mean = 30 seconds PDF: $f_x = \lambda e^{-\lambda x}$, $x \geq 0, \lambda = 0.033$
Parsing time T_p	Exponential distribution with mean = 0.13 seconds PDF: $f_x = \lambda e^{-\lambda x}$, $x \geq 0, \lambda = 7.69$

Video Streaming Traffic Model

It is assumed that each frame of a video data arrives at a regular interval T determined by the number of frames per second and each video frame is decomposed into a fixed number of slices which is transmitted as a single packet. The size of these packets/slices is modelled as a truncated Pareto distribution. The video encoder introduces encoding delay intervals between the packets of a frame and these intervals are also modelled by a truncated Pareto distribution. An example of a video streaming traffic model parameters are shown in Table C.3 [126].

Table C.3: Video streaming traffic model parameters

Parameter	Statistical Characterisation
Inter-arrival time between the beginning of each frame	Deterministic at 100 ms (10 frames per sec)
Number of packets (slices) in a frame	Deterministic, 8 packets per frame
Packet (slice) size	Truncated Pareto distribution with mean = 10 Bytes, maximum = 250 Bytes (before truncation) PDF: $f_x = \frac{\alpha_k^\alpha}{\alpha+1}, k \leq x < m, f_x \left(\frac{k}{m}\right)^\alpha$ $x = m, \alpha = 1.1, k = 2$
Inter-arrival time between packets (slices) in a frame	Truncated Pareto distribution with mean = m = 6 ms, maximum = 12.5 ms (before truncation) PDF: $f_x = \frac{\alpha_k^\alpha}{\alpha+1}, k \leq x < m, f_x \left(\frac{k}{m}\right)^\alpha$ $x = m, \alpha = 1.1, k = 2$

Appendix D:

Results of Intra-Site CoMP under Poisson Traffic

In this appendix, the simulation results of the network-wide performance of intra-site CoMP scenario under Poisson traffic are presented in Table D.1 for distance-based cell-edge decision, Table D.2 for RSRP-based cell-edge decision and Table D.3 for SINR-based cell-edge decision.

Appendix D. Results of Intra-Site CoMP under Poisson Traffic

Table D.1: System level intra-site CoMP performance under distance based cell-edge and Poisson traffic

KPIs under Distance based Cell-edge and Poisson Traffic											
KPIs ⇓	Sch. ⇓	Traffic Intensity per Subchannel (%)									
		12	24	36	48	60	72	84	96	108	120
No Mobility											
Mean Success UE (#)	JMT	296.1	576.1	877.1	1137.1	1386.5	1508.7	1563.6	1577.5	1627	1657.8
	JPF	286.8	567	851.5	1127.1	1335.9	1437.4	1479.2	1510.9	1547.1	1577.4
	MT	285.4	552.6	838.3	1093.9	1416.1	1673.8	1867.9	1987.5	2063.6	2125.5
	PF	276.6	547.1	812.1	1084.7	1360.6	1607.6	1806.2	1965.7	2058.5	2089.4
Mean Outage UE (#)	JMT	44.5	94.6	143.3	196.1	231.4	245.5	237.4	230.3	230.2	216.4
	JPF	51	107.2	157.1	218.9	251.6	281	288.3	297.1	298.3	293
	MT	55.3	118.1	182.3	244.4	317.2	395	469.4	499.1	558.4	558.4
	PF	61.2	126.9	196.6	270.3	327.5	415.6	472.7	546.8	560.3	575.4
Mean Cell Activity (%)	JMT	17.81	35.28	53.65	69.15	85.05	91.03	93.87	95.30	96.37	97.10
	JPF	17.65	35.48	53.10	70.50	82.97	90.67	93.52	95.67	96.33	96.78
	MT	11.95	23.54	35.81	46.96	60.82	72.59	82.01	87.25	92.00	94.17
	PF	11.85	23.65	35.39	47.54	59.23	70.99	79.96	88.16	91.89	93.50
Mobility											
Mean Success UE (#)	JMT	253	500.7	736.8	912.3	1011	1070.3	1093.7	1127.2	1146.6	1159
	JPF	257.5	498	740.5	896.8	992.6	1030.6	1059.5	1093	1121.1	1155.4
	MT	223.2	439.5	636.4	853.8	1057.2	1268.1	1420.1	1536.5	1588.7	1640.6
	PF	223.8	414.9	639.9	845.2	1084.8	1237.4	1434.1	1532.1	1597.7	1618.8
Mean Outage UE (#)	JMT	82.9	179.8	274.5	346.2	383.2	392.7	401.3	404.4	401.7	408.3
	JPF	88.1	188.2	286.3	358.4	388.2	409.4	417.2	417.7	430.5	425.1
	MT	112.8	245.1	378.6	519.5	643.8	766.4	878	980.7	1025.1	1052
	PF	115.7	248.6	390.1	512.7	654.3	779.1	910.6	970.3	1027	1054.7
Mean Cell Activity (%)	JMT	22.14	45.47	67.36	83.43	90.87	93.92	95.13	95.95	96.58	97.06
	JPF	22.87	45.76	68.60	84.43	91.52	93.78	95.25	95.99	96.72	97.01
	MT	11.79	24.02	35.61	48.18	59.68	71.38	80.64	88.32	91.71	94.48
	PF	11.91	23.28	36.14	47.65	61.02	70.75	82.27	87.80	92.09	93.81

Table D.2: System level intra-site CoMP performance under RSRP based cell-edge and Poisson traffic

KPIs under RSRP based Cell-edge and Poisson Traffic											
KPIs ⇓	Sch. ⇓	Traffic Intensity per Subchannel (%)									
		12	24	36	48	60	72	84	96	108	120
No Mobility											
Mean Success UE (#)	JMT	297.4	610.9	900.4	1141.5	1277.6	1379.2	1466.9	1518.2	1562.9	1620.8
	JPF	299.6	586.6	881.2	1087	1170.5	1213.8	1215.1	1239.9	1237.2	1221.3
	MT	278.7	571.1	839.3	1119.1	1387.9	1616.7	1858.2	1996.1	2060.1	2106
	PF	279.1	542.8	812.8	1082	1357.4	1628.7	1838.2	1998.5	2030.2	2088.7
Mean Outage UE (#)	JMT	37.5	78.1	114.8	142.8	144.4	130.3	122.7	112.2	107.8	101.4
	JPF	40.7	83.2	125.5	162.8	180.2	190.3	198.6	193.8	199.6	207.7
	MT	56.2	117.9	181.4	262.4	331.1	393.1	458.9	515	561	558.9
	PF	61	126.8	195.9	264.8	346.3	415.4	499.3	519.6	557.1	577.1
Mean Cell Activity (%)	JMT	20.90	42.71	63.16	79.74	85.37	87.95	89.06	90.08	90.62	90.87
	JPF	21.20	41.72	63.02	78.91	85.53	87.98	89.17	89.77	90.31	90.69
	MT	11.75	24.18	35.81	48.47	60.32	70.52	81.30	88.11	91.96	93.50
	PF	11.93	23.50	35.39	47.26	59.78	71.72	82.02	88.35	90.78	93.54
Mobility											
Mean Success UE (#)	JMT	274.9	552.2	791.7	932.5	1009.5	1056.5	1081.6	1124	1148.9	1168.2
	JPF	280.9	545.5	793.5	900	956.6	983.1	1007	1024.3	1036.7	1050.7
	MT	225.4	440.5	636.3	852.1	1063.6	1255.5	1414.2	1533.6	1599.3	1633
	PF	223.3	416.1	640	842	1085.4	1236.2	1431.8	1527.9	1587.2	1627.2
Mean Outage UE (#)	JMT	61	128.3	189.7	203.2	195	189.5	186.1	177.6	172.8	167.9
	JPF	64.7	136.5	194.3	223.8	217.8	220.4	220.2	218.8	216.2	214.2
	MT	110.5	244.2	378.6	521.1	637.5	779	884	983.6	1014.5	1059.6
	PF	116.2	247.4	390	516	653.7	780.3	912.8	974.5	1037.4	1046.3
Mean Cell Activity (%)	JMT	25.90	53.10	76.78	87.06	90.01	91.33	91.95	92.48	92.63	93.08
	JPF	26.70	53.88	77.19	87.31	89.69	91.30	91.91	92.41	92.74	92.91
	MT	11.79	24.02	35.61	48.18	59.68	71.38	80.64	88.32	91.71	94.48
	PF	11.91	23.28	36.14	47.65	61.02	70.75	82.27	87.80	92.09	93.81

Table D.3: System level intra-site CoMP performance under SINR based cell-edge and Poisson traffic

KPIs under SINR based Cell-edge and Poisson Traffic											
KPIs ⇓	Sch. ⇓	Traffic Intensity per Subchannel (%)									
		12	24	36	48	60	72	84	96	108	120
No Mobility											
Mean Success UE (#)	JMT	304.5	594	900.7	1117.6	1279	1375.3	1440.2	1484.6	1555.2	1612.3
	JPF	297.3	591.1	882.1	1075.2	1158.4	1175.9	1175.4	1160	1192.2	1188.8
	MT	285.6	552.1	838.3	1091.2	1418.3	1674.7	1867.5	1985.8	2065.2	2125.3
	PF	276.8	545.9	812.5	1084	1358.7	1607.3	1800.1	1965.3	2055.6	2090.6
Mean Outage UE (#)	JMT	36.2	76.7	113.3	137.5	134.4	126.6	121.4	114.7	110.5	103
	JPF	40.6	83.2	123.3	160.5	172	181.8	190.4	198.7	197.7	197.2
	MT	55	118.7	182.4	247.1	315	394.1	469.8	500.9	556.8	558.6
	PF	61.1	128.1	196.1	270.9	329.3	416	478.8	547.2	563.1	574.3
Mean Cell Activity (%)	JMT	21.53	43.07	64.37	78.81	85.93	88.26	89.61	89.74	90.79	90.99
	JPF	21.42	43.28	64.52	79.37	85.89	88.57	89.60	90.46	90.93	91.29
	MT	11.95	23.54	35.81	46.96	60.82	72.59	82.01	87.25	92.00	94.17
	PF	11.85	23.65	35.39	47.54	59.23	70.99	79.96	88.16	91.89	93.50
Mobility											
Mean Success UE (#)	JMT	276.2	552.3	794.1	925.7	1002.8	1055.1	1081.2	1112.8	1148	1169.8
	JPF	275.2	553.6	797.8	897.6	954.6	984.8	1002.8	999.1	1031.8	1053.6
	MT	225.9	439.1	634.5	852.6	1051.5	1262.2	1418.8	1531.6	1587.1	1645.6
	PF	224.1	414.4	643.5	838.1	1085.9	1251	1438.3	1532.2	1602.7	1635.4
Mean Outage UE (#)	JMT	59.7	128.2	183.8	202.3	194.6	189.7	185.2	176.5	168.6	162.3
	JPF	63.2	131.4	190.8	216.9	217.7	216.7	216.5	220.2	212	208.1
	MT	110	245.5	380.3	520.6	649.5	772.3	879.4	985.6	1026.7	1047
	PF	115.5	249	386.4	519.9	653.2	765.4	906.3	970.1	1021.9	1038.1
Mean Cell Activity (%)	JMT	26.19	53.60	76.99	87.00	90.06	91.55	92.29	92.66	92.90	93.21
	JPF	26.45	54.25	77.93	87.24	90.20	91.60	92.31	92.51	93.11	93.23
	MT	11.79	24.02	35.61	48.18	59.68	71.38	80.64	88.32	91.71	94.48
	PF	11.91	23.28	36.14	47.65	61.02	70.75	82.27	87.80	92.09	93.81

Appendix E:

Results of Intra-Site CoMP under Fixed Traffic

In this appendix, the simulation results of the network-wide performance of intra-site CoMP scenario under Fixed traffic are presented in Table E.1 for distance-based cell-edge decision, Table E.2 for RSRP-based cell-edge decision and Table E.3 for SINR-based cell-edge decision.

Table E.1: System level intra-site CoMP performance under distance based cell-edge in fixed traffic

KPIs under Distance based Cell-edge in Fixed Traffic								
KPIs ⇓	Sch. ⇓	Number of UE per Cell (#)						
		5	10	15	20	25	30	35
		Mobility Considered: No/Yes						
Mean Connected UE (#)	JMT	285/285	570/570	855/855	1140/1140	1425/1421.2	1710/1639.7	1898/1676.5
	JPF	285/285	570/570	855/855	1140/1140	1425/1424.8	1708/1639	1864/1660.9
	MT	285/285	570/570	855/855	1140/1140	1425/1425	1710/1710	1995/1995
	PF	285/285	570/570	855/855	1140/1140	1425/1425	1710/1710	1995/1995
Mean Success UE (#)	JMT	243.2/223.6	492.6/449.5	729/665.1	964/882.4	1202.5/1087.1	1440.3/1269.2	1596.5/1285.8
	JPF	245.6/222.8	477.9/439.9	722.5/653	975.4/867.8	1176.8/1081.2	1424.7/1244.9	1554.1/1267.2
	MT	222.4/193.9	451.6/389.7	666.8/579.9	888.9/776.1	1100.7/954.6	1333/1155.9	1544.5/1334.7
	PF	230.1/196.2	441.2/385.3	671.2/572.4	910.8/764.1	1102.9/957.6	1334.5/1153.9	1555.6/1350.7
Mean Outage UE (#)	JMT	41.8/61.4	77.4/120.4	126/190	176.1/257.6	222.5/334.1	269.8/370.5	301.5/390.7
	JPF	39.5/62.2	92.1/130.2	132.5/202	164.6/272.2	248.2/343.6	283.3/394.1	309.9/393.6
	MT	62.5/91	118.4/180.3	188.2/275.1	251.1/363.9	324.2/470.4	377/554	450.5/660.4
	PF	54.9/88.8	128.8/184.7	183.7/282.7	229.2/375.9	322.1/467.4	375.4/556	439.5/644.3
Mean Cell Activity (%)	JMT	15.19/16.46	30.81/31.56	45.86/48.16	60.84/64.22	77.16/82.151	89.40/90.73	98.95/93.23
	JPF	14.07/16.40	30.17/31.48	44.46/47.91	60.21/63.43	74.84/78.25	90.10/91.01	97.75/91.91
	MT	10/10	20/20	30/30	40/40	50/50	60/60	70/70
	PF	10/10	20/20	30/30	40/40	50/50	60/60	70/70
UE Mean Thrput. (kbps)	JMT	322.4/302.1	323.8/289	297.8/285	297.8/282.5	285.5/280.2	283.7/279	280.1/275.9
	JPF	319.8/306.7	329.2/296.3	308.9/286.6	304.4/286.9	304.5/282.3	299.5/283.8	293.2/284.1
	MT	269.5/254.9	279/255.6	264.3/255.3	264.2/254.4	255.7/249.2	258/250.8	259.3/249.3
	PF	273.1/257.2	283.6/253.7	261.4/250.2	257/253.3	260.7/252.5	259.1/253.2	262.4/255.1
CEU Mean Thrput. (kbps)	JMT	250/263.4	240.1/239.8	217.5/231.9	206.1/224	209.3/227.9	200.5/220	194.1/217.5
	JPF	236/250.3	220.4/233	217.6/235.1	223.2/224.2	209.4/221.9	208.4/215.1	183.2/217.5
	MT	121.5/161.9	133/161.3	117.5/156.1	117.9/158.2	124.4/154.4	121.5/158.1	127.2/158.4
	PF	98.5/159.8	122.4/149.5	120.4/156.5	133.8/157.4	129.4/158.2	130.2/155.8	118.3/156.3
System Mean Thrput. (Mbps)	JMT	76.5/66	155.8/126.8	212/185.1	280.4/243.4	335.2/297.4	399/345.8	436.7/346.5
	JPF	76.7/66.7	153.6/127.3	217.9/182.8	290/243.2	349.9/298.1	416.6/345.1	445/351.5
	MT	58.5/48.3	123/97.3	172.1/144.6	229.3/192.8	274.8/232.3	335.9/283.2	391.1/325.1
	PF	61.3/49.3	122.2/95.4	171.3/139.8	228.6/189	280.8/236.2	337.7/285.4	398.6/336.5

Table E.2: System level intra-site CoMP performance under RSRP based cell-edge in fixed traffic

KPIs under RSRP based Cell-edge in Fixed Traffic								
KPIs ⇓	Sch. ⇓	Number of UE per Cell (#)						
		5	10	15	20	25	30	35
		Mobility Considered: No/Yes						
Mean Connected UE (#)	JMT	285/285	570/570	855/855	1140/1128.5	1326.5/1176.9	1394.5/1197.2	1425.3/1218.4
	JPF	285/285	570/570	855/855	1140/1120.2	1293.3/1145.5	1318.4/1156.2	1308.3/1152.4
	MT	285/285	570/570	855/855	1140/1140	1425/1425	1710/1710	1995/1995
	PF	285/285	570/570	855/855	1140/1140	1425/1425	1710/1710	1995/1995
Mean Success UE (#)	JMT	252.7/243.6	501.1/484.1	745.1/728.3	1000.2/955.1	1175.6/1000.3	1265.9/1027.7	1318.5/1060.2
	JPF	248.8/240.4	504.2/479.7	743.4/719.1	993.7/936	1112.7/951	1149.3/964.8	1134.6/968.3
	MT	226.7/194	439.3/381.8	663.2/580.3	882.9/764.7	1108.3/954.2	1341.4/1152.4	1568.1/1346.1
	PF	219.4/197.5	449.7/380.3	658/579.3	880.9/762	1106.5/969.9	1337/1151.2	1547.4/1350.6
Mean Outage UE (#)	JMT	32.2/41.4	69/85.8	109.8/126.7	139.8/173.4	150.8/176.7	128.6/169.6	106.8/158.3
	JPF	36.3/44.7	65.9/90.2	111.7/135.8	146.3/184.1	180.6/194.5	169.1/191.4	173.7/184.1
	MT	58.3/91.1	130.7/188.2	191.8/274.8	257.1/375.2	316.7/470.8	368.6/557.7	426.9/648.9
	PF	65.6/87.5	120.3/189.7	197/275.7	259.1/378	318.4/455.1	373.1/558.8	447.6/644.4
Mean Cell Activity (%)	JMT	16.97/20.10	35.99/40.02	53.47/59.90	71.75/79.57	81.29/82.24	82.16/82.46	81.70/82.65
	JPF	17.93/20.12	35.50/40.16	54.01/60.46	71.83/79.74	82.40/82.06	83.19/81.47	82.86/81.31
	MT	10/10	20/20	30/30	40/40	50/50	60/60	70/70
	PF	10/10	20/20	30/30	40/40	50/50	60/60	70/70
UE Mean Thrput. (kbps)	JMT	389/375.8	378.4/360.5	343.9/361.5	354.4/352.6	360.3/353.9	357.3/360.1	371.3/370.7
	JPF	373.9/370.9	361.3/359.5	369.6/357.4	359.4/349.4	329.7/346.2	325.2/345.5	325.8/350.7
	MT	291.6/250.7	272.7/245.7	260.2/256	259.8/247.8	265.5/248.5	261/251.6	258.5/250.8
	PF	261.6/263.9	256.7/250.6	263.2/251.9	256.8/251	258.4/255.7	265.6/253.5	256.8/253.3
CEU Mean Thrput. (kbps)	JMT	360/346.4	362.1/329.5	311.1/331.3	340.3/322.5	342/324	346.9/331.8	381.2/348.4
	JPF	337.8/326.8	324.2/320.6	342.9/319	337.2/315.1	308.1/311.2	298.1/302.7	298.8/313.8
	MT	134.6/119.3	125.8/116.6	123.6/118.3	125.1/117.2	127.6/116.3	128.8/115.7	126.6/116.3
	PF	123.4/119.2	127.7/118	126.5/120.1	126.2/116.7	126.6/120	127.6/116.2	125.9/119.1
System Mean Thrput. (Mbps)	JMT	96/89.4	185.2/170.4	250.2/257.1	346.1/328.8	413.6/345.7	441.7/361.5	478.1/384
	JPF	90.8/87.1	177.9/168.4	268.3/250.9	348.8/319.3	358.3/321.5	365/325.5	361/331.6
	MT	64.5/47.5	117/91.6	168.5/145	224/185.1	287.3/231.6	341.8/283.2	395.8/329.7
	PF	56/50.9	112.7/93.1	169.1/142.5	220.9/186.8	279.2/242.2	346.8/285	388/334.1

Table E.3: System level intra-site CoMP performance under SINR based cell-edge in fixed traffic

KPIs under SINR based Cell-edge in Fixed Traffic								
KPIs ⇓	Sch. ⇓	Number of UE per Cell (#)						
		5	10	15	20	25	30	35
		Mobility Considered: No/Yes						
Mean Connected UE (#)	JMT	285/285	570/570	855/855	1140/1113.9	1299/1163.9	1367.8/1189.9	1417.5/1193.5
	JPF	285/285	570/570	855/855	1139.5/1114.3	1271.6/1146.7	1276.3/1135.4	1297.5/1132.4
	MT	285/285	570/570	855/855	1140/1140	1425/1425	1710/1710	1995/1995
	PF	285/285	570/570	855/855	1140/1140	1425/1425	1710/1710	1995/1995
Mean Success UE (#)	JMT	250.3/244.1	504.5/488.2	755.1/728.9	1004.4/949	1157.1/990.4	1248.9/1025.6	1309.7/1036
	JPF	254.3/245	494.8/481.7	750.4/715.7	1016.1/935.1	1098.2/961.3	1110.5/950.7	1138.5/945.6
	MT	222/195.3	450.7/387.3	667.6/579.6	888.2/770.3	1100.8/959.6	1333.3/1161.8	1546.3/1349.7
	PF	229.4/195.3	441/382.7	671.3/581.4	911.8/759.1	1103.4/957.9	1334/1155	1555.7/1341.4
Mean Outage UE (#)	JMT	34.8/40.9	65.6/81.7	99.8/126.2	135.6/164.9	142/173.4	118.9/164.3	107.8/157.5
	JPF	30.7/40	75.1/88.3	104.6/139.3	123.3/179.2	173.3/185.5	165.8/184.7	158.9/186.8
	MT	63/89.8	119.3/182.8	187.4/275.4	251.9/369.7	324.2/465.4	376.7/548.2	448.7/645.3
	PF	55.6/89.8	129.1/187.3	183.7/273.6	228.1/380.8	321.5/467	376.1/555.1	439.2/653.6
Mean Cell Activity (%)	JMT	18.12/20.53	35.51/40.59	55.03/61.15	73.32/79.89	82.55/82.87	82.34/83.35	83.05/82.96
	JPF	17.65/20.14	36.18/41.29	54.26/61.94	71.68/81.04	83.11/82.74	83.13/81.83	83.35/82.42
	MT	10/10	20/20	30/30	40/40	50/50	60/60	70/70
	PF	10/10	20/20	30/30	40/40	50/50	60/60	70/70
UE Mean Thrput. (kbps)	JMT	381.1/373.7	373.4/364	361.3/361.9	356.7/355.7	355.4/357.5	363/363.5	369.4/370.7
	JPF	387.8/387.1	381.2/362.6	359.3/360.3	357.5/353.2	338.7/352.9	326.8/349.7	326.3/347.3
	MT	269.9/255.8	279.8/252.5	264.1/256.2	265/251.4	255.4/250.4	258.3/253.1	258.6/252.2
	PF	274.4/255.1	284.6/254.9	261.4/250.8	257.4/249.6	260/249.8	259.4/251.3	262.5/250.1
CEU Mean Thrput. (kbps)	JMT	338.1/337	335.4/326.7	328.3/326.2	318.7/319	326.6/319.6	339.5/325.5	353.8/339.1
	JPF	347/335.4	317.7/321.8	320.1/317.4	323.5/311.6	305.1/306.7	289.4/302.6	280.4/300.4
	MT	125.2/117.2	130.8/116.4	121.6/115.4	121.3/116.1	122.8/115.1	124.6/115.7	123.9/115.6
	PF	131.9/114	125/116	127.5/117.8	125.6/115.5	125.3/116.2	124.1/115.8	123.9/116.4
System Mean Thrput. (Mbps)	JMT	93.1/89.1	183.9/173.5	266.4/257.5	349.9/329.6	401.6/345.8	442.7/364.1	472.5/375.1
	JPF	96.3/92.6	184.2/170.6	263.3/251.8	354.7/322.5	363.2/331.3	354.5/324.6	362.8/320.6
	MT	58.5/48.8	123.1/95.5	172.2/145	229.8/189.1	274.5/234.6	336.3/287.2	390.5/332.5
	PF	61.5/48.6	122.5/95.2	171.3/142.4	229.2/185.1	280.1/233.7	337.9/283.5	398.8/327.7

Appendix F:

Results of Inter-Site CoMP under Poisson Traffic

In this appendix, the simulation results of the network-wide performance of inter-site CoMP scenario under Poisson traffic are presented in Table F.1 for distance-based cell-edge decision, Table F.2 for RSRP-based cell-edge decision and Table F.3 for SINR-based cell-edge decision.

Appendix F. Results of Inter-Site CoMP under Poisson Traffic

Table F.1: System level inter-site CoMP performance under distance based cell-edge and Poisson traffic

KPIs under Distance based Cell-edge and Poisson Traffic											
KPIs ⇓	Sch. ⇓	Traffic Intensity per Subchannel (%)									
		12	24	36	48	60	72	84	96	108	120
No Mobility											
Mean Success UE (#)	JMT	298.4	583.2	886.8	1153.5	1444.4	1606.5	1698.8	1774.2	1807.9	1861.2
	JPF	291.6	576.6	861.8	1146.7	1385.3	1564.2	1644.8	1721.1	1793.8	1820.4
	MT	285.4	552.6	838.3	1093.9	1416.1	1673.8	1867.9	1987.5	2063.6	2125.5
	PF	276.6	547.1	812.1	1084.7	1360.6	1607.6	1806.2	1965.7	2058.5	2089.4
Mean Outage UE (#)	JMT	42.2	87.6	133.5	180.8	218.7	237.5	249.3	238.4	254.1	246.5
	JPF	46.3	97.6	146.8	204	241.2	271	300.2	322.4	313.5	327.2
	MT	55.3	118.1	182.3	244.4	317.2	395	469.4	499.1	558.4	558.4
	PF	61.2	126.9	196.6	270.3	327.5	415.6	472.7	546.8	560.3	575.4
Mean Cell Activity (%)	JMT	15.99	31.6	48.13	62.41	78.39	86.23	90.63	93.12	95.06	96.2
	JPF	15.98	31.7	47.57	63.68	75.96	85.9	90.46	93.63	95.21	95.98
	MT	11.95	23.54	35.81	46.96	60.82	72.59	82.01	87.25	92	94.17
	PF	11.85	23.65	35.39	47.54	59.23	70.99	79.96	88.16	91.89	93.5
Mobility											
Mean Success UE (#)	JMT	259.6	518.9	766	983.9	1139	1258	1309.6	1365.5	1389.2	1406.1
	JPF	261.5	499	767.4	954.3	1113	1221.6	1284.3	1353.3	1379.7	1393.2
	MT	223.2	439.5	636.4	853.8	1057.2	1268.1	1420.1	1536.5	1588.7	1640.6
	PF	223.8	414.9	639.9	845.2	1084.8	1237.4	1434.1	1532.1	1597.7	1618.8
Mean Outage UE (#)	JMT	76.3	161.6	246.5	313.3	362	401.8	418.3	434.5	447.8	442.2
	JPF	80.2	162.4	259.4	329.6	385.5	420.9	436.9	464.8	465.9	467.8
	MT	112.8	245.1	378.6	519.5	643.8	766.4	878	980.7	1025.1	1052
	PF	115.7	248.6	390.1	512.7	654.3	779.1	910.6	970.3	1027	1054.7
Mean Cell Activity (%)	JMT	18.99	38.85	58.36	73.54	83.76	89.22	91.78	94.28	95.64	96.35
	JPF	19.5	38.11	58.62	72.77	83.22	88.77	91.6	93.7	95.34	96.31
	MT	11.79	24.02	35.61	48.18	59.68	71.38	80.64	88.32	91.71	94.48
	PF	11.91	23.28	36.14	47.65	61.02	70.75	82.27	87.8	92.09	93.81

Table F.2: System level inter-site CoMP performance under RSRP based cell-edge and Poisson traffic

KPIs under RSRP based Cell-edge and Poisson Traffic											
KPIs ⇓	Sch. ⇓	Traffic Intensity per Subchannel (%)									
		12	24	36	48	60	72	84	96	108	120
No Mobility											
Mean Success UE (#)	JMT	296.8	610.8	902.3	1152.7	1353.3	1478	1609.2	1683.8	1742.7	1791
	JPF	299.7	587.2	883	1121.3	1266.6	1383.3	1448.8	1493.8	1499.4	1502.6
	MT	278.7	571.1	839.3	1119.1	1387.9	1616.7	1858.2	1996.1	2060.1	2106
	PF	279.1	542.8	812.8	1082	1357.4	1628.7	1838.2	1998.5	2030.2	2088.7
Mean Outage UE (#)	JMT	38.1	78.3	116.1	151.2	164.1	169.4	171.7	169.6	170.1	162.3
	JPF	40.7	82.6	124.4	160.7	187	206.3	229	220.7	233.6	242.9
	MT	56.2	117.9	181.4	262.4	331.1	393.1	458.9	515	561	558.9
	PF	61	126.8	195.9	264.8	346.3	415.4	499.3	519.6	557.1	577.1
Mean Cell Activity (%)	JMT	18.55	38.17	56.26	71.47	80.11	84.18	87.82	89.78	90.83	91.59
	JPF	18.81	37.08	55.89	70.57	79.05	84.54	88.4	89.5	90.58	91.67
	MT	11.75	24.18	35.81	48.47	60.32	70.52	81.3	88.11	91.96	93.5
	PF	11.93	23.5	35.39	47.26	59.78	71.72	82.02	88.35	90.78	93.54
Mobility											
Mean Success UE (#)	JMT	267.4	534.3	779.3	959.2	1078.5	1179.9	1233.6	1291.1	1316.2	1349.3
	JPF	267.9	535.1	788.3	940.7	1055.5	1151.6	1183.4	1230.3	1262	1281.5
	MT	225.4	440.5	636.3	852.1	1063.6	1255.5	1414.2	1533.6	1599.3	1633
	PF	223.3	416.1	640	842	1085.4	1236.2	1431.8	1527.9	1587.2	1627.2
Mean Outage UE (#)	JMT	68.5	146.1	209.4	251	275.4	296	300.4	308.5	316.7	310.3
	JPF	70.5	149.9	217.6	267.4	288	316	336	343.9	342.7	341.2
	MT	110.5	244.2	378.6	521.1	637.5	779	884	983.6	1014.5	1059.6
	PF	116.2	247.4	390	516	653.7	780.3	912.8	974.5	1037.4	1046.3
Mean Cell Activity (%)	JMT	21.94	45.19	65.18	77.06	83.57	87.85	89.75	91.64	92.88	93.3
	JPF	22.13	45.83	66.04	77.61	83.46	87.93	89.95	91.65	92.68	93.03
	MT	11.79	24.02	35.61	48.18	59.68	71.38	80.64	88.32	91.71	94.48
	PF	11.91	23.28	36.14	47.65	61.02	70.75	82.27	87.8	92.09	93.81

Table F.3: System level inter-site CoMP performance under SINR based cell-edge and Poisson traffic

KPIs under SINR based Cell-edge and Poisson Traffic											
KPIs ⇓	Sch. ⇓	Traffic Intensity per Subchannel (%)									
		12	24	36	48	60	72	84	96	108	120
No Mobility											
Mean Success UE (#)	JMT	303.6	594.3	903	1130.6	1357.6	1494.6	1583.2	1662.2	1732.4	1806.3
	JPF	297.3	591.2	885.5	1115.9	1275.3	1366	1396.1	1431.8	1482.2	1476.2
	MT	285.6	552.1	838.3	1091.2	1418.3	1674.7	1867.5	1985.8	2065.2	2125.3
	PF	276.8	545.9	812.5	1084	1358.7	1607.3	1800.1	1965.3	2055.6	2090.6
Mean Outage UE (#)	JMT	37	76.4	113.5	142	159.3	161.6	165.7	159	158.6	159.4
	JPF	40.5	82.9	121.6	159.8	179.1	197.2	219.4	229	229.5	232.6
	MT	55	118.7	182.4	247.1	315	394.1	469.8	500.9	556.8	558.6
	PF	61.1	128.1	196.1	270.9	329.3	416	478.8	547.2	563.1	574.3
Mean Cell Activity (%)	JMT	19.14	38.08	57.49	70.52	80.57	85.3	87.73	89.29	90.82	91.86
	JPF	19.08	38.48	57.13	71.38	80.3	84.93	87.93	90.06	91.06	91.66
	MT	11.95	23.54	35.81	46.96	60.82	72.59	82.01	87.25	92	94.17
	PF	11.85	23.65	35.39	47.54	59.23	70.99	79.96	88.16	91.89	93.5
Mobility											
Mean Success UE (#)	JMT	268.2	539.6	785	954.5	1074.8	1178.9	1219.8	1284.7	1323.5	1357.2
	JPF	268.3	537.3	785.3	950.2	1055.4	1154.5	1193.4	1223.1	1266	1265.4
	MT	225.9	439.1	634.5	852.6	1051.5	1262.2	1418.8	1531.6	1587.1	1645.6
	PF	224.1	414.4	643.5	838.1	1085.9	1251	1438.3	1532.2	1602.7	1635.4
Mean Outage UE (#)	JMT	67.7	140.8	203.5	245.8	269.3	290.9	304.2	303	309.6	307.5
	JPF	70	147.8	216	261.1	284.3	311.6	328.7	328.1	339.5	343
	MT	110	245.5	380.3	520.6	649.5	772.3	879.4	985.6	1026.7	1047
	PF	115.5	249	386.4	519.9	653.2	765.4	906.3	970.1	1021.9	1038.1
Mean Cell Activity (%)	JMT	22.17	45.41	65.31	77.18	83.67	87.97	89.95	91.9	93.07	93.66
	JPF	22.36	46.07	66.4	77.95	83.57	88.25	90.2	91.09	92.75	93.07
	MT	11.79	24.02	35.61	48.18	59.68	71.38	80.64	88.32	91.71	94.48
	PF	11.91	23.28	36.14	47.65	61.02	70.75	82.27	87.8	92.09	93.81

Appendix G:

Results of Inter-Site CoMP under Fixed Traffic

In this appendix, the simulation results of the network-wide performance of inter-site CoMP scenario under Fixed traffic are presented in Table G.1 for distance-based cell-edge decision, Table G.2 for RSRP-based cell-edge decision and Table G.3 for SINR-based cell-edge decision.

Table G.1: System level inter-site CoMP performance under distance based cell-edge in fixed traffic

KPIs under Distance based Cell-edge in Fixed Traffic								
KPIs ⇓	Sch. ⇓	Number of UE per Cell (#)						
		5	10	15	20	25	30	35
		Mobility Considered: No/Yes						
Mean Connected UE (#)	JMT	285/285	570/570	855/855	1140/1140	1425/1424	1710/1663.4	1933/1814.6
	JPF	285/285	570/570	855/855	1140/1140	1425/1425	1707/1667.6	1905/1803.2
	MT	285/285	570/570	855/855	1140/1140	1425/1425	1710/1710	1995/1995
	PF	285/285	570/570	855/855	1140/1140	1425/1425	1710/1710	1995/1995
Mean Success UE (#)	JMT	245.9/230.7	498.9/459.2	738.6/679.1	986.2/906.1	1219.1/1124.1	1459.1/1314	1656.5/1440.5
	JPF	250.2/226.8	485.5/450.8	729.4/673.2	989.5/896.9	1200.2/1122.1	1446.8/1305	1626.8/1396.2
	MT	222.4/222	451.6/450.5	666.8/667	888.9/889.7	1100.7/1100.2	1333/1332.3	1544.5/1547.9
	PF	230.1/229.7	441.2/442.5	671.2/673.1	910.8/911.4	1102.9/1101.9	1334.5/1334.2	1555.6/1555.5
Mean Outage UE (#)	JMT	39.1/54.3	71.1/110.8	116.3/175.8	153.8/234	205.9/299.9	250.9/349.5	276.5/374.1
	JPF	34.8/58.3	84.5/119.2	125.6/181.8	150.5/243.1	224.9/302.9	260.3/362.6	278.2/407
	MT	62.5/63	118.4/119.5	188.2/188	251.1/250.4	324.2/324.8	377/377.7	450.5/447.1
	PF	54.9/55.3	128.8/127.5	183.7/181.9	229.2/228.6	322.1/323.1	375.4/375.8	439.5/439.6
Mean Cell Activity (%)	JMT	13.86/14.7	27.79/28.4	40.81/42.28	55.47/56.82	68.77/71.65	80.42/82.3	91.16/87.31
	JPF	13.05/14.29	27.58/28.7	39.75/43.41	53.33/57.46	67.26/71.3	80.56/82.59	90/87.24
	MT	10/10	20/20	30/30	40/40	50/50	60/60	70/70
	PF	10/10	20/20	30/30	40/40	50/50	60/60	70/70
UE Mean Thrput. (kbps)	JMT	336.1/328.9	343.5/317.4	313.4/302.8	320.9/300.8	304.8/294.2	296.8/294.6	297.3/293.9
	JPF	353.4/333.8	357.1/313.6	324.9/316.1	324/312.5	322/306.6	321.3/303	319.4/295.5
	MT	269.5/268.8	279/279.3	264.3/264.4	264.2/264.9	255.7/256.1	258/259	259.3/258.6
	PF	273.1/273.2	283.6/284.2	261.4/260.9	257/256.5	260.7/260.8	259.1/259.1	262.4/262.5
CEU Mean Thrput. (kbps)	JMT	279/311.4	291/285	263/276.6	270.1/278.4	261.7/271.3	250.3/265	255/257.7
	JPF	347/323.5	336.4/303.8	296.3/295	301.9/292.4	294.7/292.4	304/278	293/270.7
	MT	121.5/122.4	133/134.3	117.5/117.7	117.9/119.2	124.4/124.8	121.5/121.9	127.2/126.4
	PF	98.5/100	122.4/122.5	120.4/120.4	133.8/132.7	129.4/128.4	130.2/129.5	118.3/118.4
System Mean Thrput. (Mbps)	JMT	80.7/74.1	167.3/142.3	226/200.8	309/266.2	362.9/322.9	422.8/378	480.9/413.4
	JPF	86.3/73.9	169.3/138	231.4/207.8	313/273.7	377.4/335.9	454/386.2	507.4/403
	MT	58.5/58.2	123/122.9	172.1/172.2	229.3/230.1	274.8/275.1	335.9/336.9	391.1/390.9
	PF	61.3/61.3	122.2/122.8	171.3/171.5	228.6/228.3	280.8/280.6	337.7/337.5	398.6/398.8

Table G.2: System level inter-site CoMP performance under RSRP based cell-edge in fixed traffic

KPIs under RSRP based Cell-edge in Fixed Traffic								
KPIs ⇓	Sch. ⇓	Number of UE per Cell (#)						
		5	10	15	20	25	30	35
		Mobility Considered: No/Yes						
Mean Connected UE (#)	JMT	285/285	570/570	855/855	1140/1128.7	1348.8/1266.5	1503/1373	1611.1/1443.2
	JPF	285/285	570/570	855/855	1140/1125.1	1333.4/1259.5	1481.5/1358.9	1531.4/1412.2
	MT	285/285	570/570	855/855	1140/1140	1425/1425	1710/1710	1995/1995
	PF	285/285	570/570	855/855	1140/1140	1425/1425	1710/1710	1995/1995
Mean Success UE (#)	JMT	251.9/240.4	501.2/485.4	746.3/723	997.6/951.3	1190.4/1072.3	1344.1/1167.3	1459.4/1221.8
	JPF	249.1/240.9	505/476.8	746/713.9	990.4/940.7	1153.6/1049.7	1298.1/1132.5	1331.7/1175.5
	MT	226.7/222	439.3/450.8	663.2/666.5	882.9/888.9	1108.3/1100.7	1341.4/1333.8	1568.1/1546.7
	PF	219.4/229.3	449.7/442	658/673	880.9/912.8	1106.5/1101.7	1337/1334.7	1547.4/1555.5
Mean Outage UE (#)	JMT	33.1/44.6	68.8/84.6	108.7/131.9	142.4/177.4	158.5/194.3	158.9/205.7	151.7/221.3
	JPF	35.9/44	65/93.2	109/141.2	149.6/184.5	179.8/209.8	183.4/226.4	199.6/236.7
	MT	58.3/63	130.7/119.1	191.8/188.5	257.1/251.1	316.7/324.3	368.6/376.3	426.9/448.2
	PF	65.6/55.7	120.3/127.9	197/182	259.1/227.2	318.4/323.3	373.1/375.3	447.6/439.5
Mean Cell Activity (%)	JMT	15.22/17.59	31.78/34.71	47.43/52	63.43/69.12	73.19/74.49	78.2/79.15	81.07/81.7
	JPF	16.05/17.41	31.22/34.97	48.2/52.74	63.36/68.85	73.43/74.96	78.76/78.9	81.13/80.68
	MT	10/10	20/20	30/30	40/40	50/50	60/60	70/70
	PF	10/10	20/20	30/30	40/40	50/50	60/60	70/70
UE Mean Thrput. (kbps)	JMT	383/357.9	372.6/354.2	342.5/345	343.6/337.3	350/334.9	345.3/338.6	345.3/334.3
	JPF	380.8/362.5	367.2/352.7	372.4/347.7	351.4/345.4	338/342.9	340.4/338.3	327.1/338.3
	MT	291.6/269.9	272.7/279.8	260.2/264.3	259.8/263.9	265.5/256	261/258.3	258.5/258.7
	PF	261.6/274.6	256.7/284.4	263.2/260.7	256.8/257.8	258.4/261	265.6/259.1	256.8/262.4
CEU Mean Thrput. (kbps)	JMT	312.8/311	319.6/305.1	294.9/296.8	297.9/292.9	299.6/278.5	294.3/273.2	292.1/264
	JPF	338.6/306	328.8/301.7	339.4/298.5	307.8/295.7	290.8/288.6	285.4/270.4	268.3/265.4
	MT	134.6/126.8	125.8/132.9	123.6/125.1	125.1/121	127.6/124.4	128.8/126.8	126.6/124.6
	PF	123.4/132.7	127.7/128.5	126.5/128.9	126.2/127.9	126.6/128.4	127.6/125.7	125.9/125.8
System Mean Thrput. (Mbps)	JMT	94.2/84	182.3/167.9	249.7/243.6	334.7/313.3	406.8/350.7	453.2/386.1	492.1/398.9
	JPF	92.6/85.3	181.1/164.2	271.3/242.4	339.9/317.3	380.8/351.5	431.5/374.2	425.4/388.3
	MT	64.5/58.5	117/123.2	168.5/172	224/229	287.3/275.1	341.8/336.4	395.8/390.7
	PF	56/61.5	112.7/122.7	169.1/171.3	220.9/229.8	279.2/280.8	346.8/337.7	388/398.6

Table G.3: System level inter-site CoMP performance under SINR based cell-edge in fixed traffic

KPIs under SINR based Cell-edge in Fixed Traffic								
KPIs ⇓	Sch. ⇓	Number of UE per Cell (#)						
		5	10	15	20	25	30	35
		Mobility Considered: No/Yes						
Mean Connected UE (#)	JMT	285/285	570/570	855/855	1140/1124.3	1342.2/1257.5	1481.1/1363.8	1585.5/1422.5
	JPF	285/285	570/570	855/855	1140/1116.3	1324.6/1251.3	1435.5/1353.8	1523.2/1407.6
	MT	285/285	570/570	855/855	1140/1140	1425/1425	1710/1710	1995/1995
	PF	285/285	570/570	855/855	1140/1140	1425/1425	1710/1710	1995/1995
Mean Success UE (#)	JMT	250.9/244.6	505.8/483	758.5/724.6	1009.1/951.4	1188.3/1063.8	1329.2/1159.9	1440.8/1205.7
	JPF	255.9/243.9	498.7/481.7	751.4/723.3	1015.8/936.8	1157.2/1051.1	1262.5/1129.9	1344.5/1176.9
	MT	222/222	450.7/450	667.6/668.7	888.2/888.4	1100.8/1100.5	1333.3/1332.2	1546.3/1545.7
	PF	229.4/229.2	441/441.8	671.3/673	911.8/912.5	1103.4/1102.9	1334/1334.3	1555.7/1556.5
Mean Outage UE (#)	JMT	34.1/40.4	64.3/87	96.5/130.4	130.9/172.8	153.9/193.7	151.9/204	144.7/216.8
	JPF	29.2/41	71.3/88.3	103.6/131.7	124.3/179.6	167.4/200.2	173/224	178.7/230.8
	MT	63/63	119.3/120	187.4/186.3	251.9/251.6	324.2/324.5	376.7/377.8	448.7/449.3
	PF	55.6/55.8	129.1/128.2	183.7/182	228.1/227.6	321.5/322.1	376.1/375.7	439.2/438.6
Mean Cell Activity (%)	JMT	16.28/17.78	31.73/35.6	48.5/53.59	65.16/69.8	74.66/75.61	78.28/79.55	81.2/81.66
	JPF	15.76/17.38	32.08/35.47	47.97/52.61	63.44/69.86	74.36/75.69	79.05/79.88	81.63/80.96
	MT	10/10	20/20	30/30	40/40	50/50	60/60	70/70
	PF	10/10	20/20	30/30	40/40	50/50	60/60	70/70
UE Mean Thrput. (kbps)	JMT	377.5/368.1	374.7/355.5	357.6/347.9	355.4/342.4	346.3/338.3	345.3/342.5	350.1/339.9
	JPF	393.4/369.8	387/359.3	363.2/355.7	361.6/350.2	347.1/344.2	342/341.2	335.7/338.2
	MT	269.9/269.9	279.8/279.1	264.1/264.2	265/264.1	255.4/255.6	258.3/258.7	258.6/259.4
	PF	274.4/273.7	284.6/285.5	261.4/261.3	257.4/256.7	260/260.6	259.4/259.1	262.5/262.3
CEU Mean Thrput. (kbps)	JMT	320.9/312.4	323/307.8	309.2/296	310.3/298.8	292.6/277.6	290.1/276.8	291.2/269.5
	JPF	348.5/303.6	318.7/300.4	305.9/299.4	307.9/296.3	294.4/277.9	276.8/270	269.6/260.8
	MT	125.2/125.2	130.8/129	121.6/120.9	121.3/122.3	122.8/122.7	124.6/125.3	123.9/124.2
	PF	131.9/129.7	125/126.8	127.5/125.4	125.6/125.7	125.3/126.2	124.1/123.4	123.9/123.5
System Mean Thrput. (Mbps)	JMT	92.5/87.9	185.1/167.6	264.9/246.2	350.2/318.1	401.9/351.4	448.3/387.9	492.6/400.3
	JPF	98.3/88.1	188.5/169	266.6/251.2	358.6/320.3	392.2/353.3	421.7/376.5	440.8/388.7
	MT	58.5/58.5	123.1/122.7	172.2/172.5	229.8/229.1	274.5/274.6	336.3/336.5	390.5/391.5
	PF	61.5/61.2	122.5/123.2	171.3/171.7	229.2/228.7	280.1/280.7	337.9/337.6	398.8/398.7

Appendix H:

Results of Hybrid Model

In this appendix, the simulation results of the hybrid model are presented in Table H.1 for varying arrival rate and Table H.2 for varying holding time.

Table H.1: System throughput performance with mean holding time, $1/\mu^m = 3\ min$

Arrival Rate (calls/min)	Average System Throughput (Mbps)								Percentage Throughput Error (%)			
	R = 2		R = 3		R = 4		R = 5					
	Sim	Hyb	Sim	Hyb	Sim	Hyb	Sim	Hyb	R = 2	R = 3	R = 4	R = 5
0.1	0.548	0.557	0.586	0.613	0.597	0.618	0.595	0.618	1.532	4.626	3.654	3.933
0.2	1.075	0.977	1.239	1.186	1.288	1.205	1.306	1.233	-9.121	-4.294	-6.436	-5.574
0.3	1.310	1.270	1.541	1.557	1.652	1.708	1.694	1.785	-2.986	0.993	3.347	5.360
0.4	1.504	1.543	1.964	1.898	2.173	2.172	2.304	2.211	2.539	-3.335	-0.037	-4.032
0.5	1.621	1.670	2.123	2.161	2.404	2.541	2.574	2.732	3.048	1.804	5.691	6.138
0.6	1.826	1.741	2.473	2.411	2.914	2.833	3.191	3.123	-4.650	-2.483	-2.783	-2.122
0.7	1.949	1.901	2.689	2.603	3.261	3.120	3.616	3.493	-2.453	-3.199	-4.320	-3.396
0.8	1.968	1.936	2.720	2.708	3.330	3.350	3.746	3.788	-1.631	-0.441	0.619	1.132
0.9	1.993	2.002	2.850	2.842	3.512	3.506	4.020	4.045	0.426	-0.284	-0.154	0.624
1	2.079	2.006	2.975	2.912	3.717	3.675	4.353	4.307	-3.540	-2.108	-1.133	-1.057

Table H.2: System throughput performance with mean arrival rate, $\lambda^m = 2\ calls/min$

Mean Holding Time (min)	Average System Throughput (Mbps)								Percentage Throughput Error (%)			
	R = 2		R = 3		R = 4		R = 5					
	Sim	Hyb	Sim	Hyb	Sim	Hyb	Sim	Hyb	R = 2	R = 3	R = 4	R = 5
0.5	1.402	1.430	1.766	1.684	1.905	1.885	1.998	1.924	2.033	-4.649	-1.034	-3.748
1	1.859	1.826	2.532	2.542	3.036	3.040	3.353	3.376	-1.754	0.383	0.122	0.689
1.5	2.073	2.075	2.960	2.945	3.761	3.703	4.384	4.318	0.068	-0.517	-1.540	-1.503
2	2.167	2.094	3.153	3.144	4.080	4.057	4.887	4.848	-3.391	-0.289	-0.554	-0.796
2.5	2.215	2.226	3.264	3.242	4.271	4.204	5.183	5.184	0.515	-0.680	-1.587	0.023
3	2.297	2.254	3.368	3.345	4.417	4.407	5.407	5.360	-1.876	-0.695	-0.229	-0.858
3.5	2.270	2.320	3.408	3.375	4.469	4.528	5.517	5.515	2.207	-0.963	1.325	-0.047
4	2.320	2.313	3.478	3.443	4.589	4.530	5.678	5.633	-0.267	-0.992	-1.275	-0.791
4.5	2.334	2.385	3.484	3.417	4.627	4.595	5.743	5.737	2.189	-1.923	-0.685	-0.101
5	2.338	2.355	3.473	3.463	4.641	4.585	5.762	5.790	0.710	-0.271	-1.207	0.500